

DISSERTATION

DEVELOPMENT OF MASS SPECTROMETRY TECHNIQUES FOR ANALYSIS OF
BIOMEDICAL SYSTEMS

Submitted by

Jesus B. Tapia

Department of Chemistry

In partial fulfillment of the requirements

For the Degree of Doctor of Philosophy

Colorado State University

Fort Collins, Colorado

Spring 2020

Doctoral Committee:

Advisor: Melissa M. Reynolds

Charles S. Henry

Delphine K. Farmer

Matthew J. Kipper

Joseph M. Zadrozny

Copyright by Jesus B. Tapia 2020

All Rights Reserved

ABSTRACT

DEVELOPMENT OF MASS SPECTROMETRY TECHNIQUES FOR ANALYSIS OF BIOMEDICAL SYSTEMS

The advances of modern mass spectrometry (MS) have allowed MS to become one of the essential analytical tools for biological and biomedical research. Mass spectrometry's ability to provide rapid and sensitive analysis of many types of analytes made it an excellent candidate to study the polysaccharide dextran, biodegradable poly(organophosphazene) and polyester derived polymers, as well as interfering species in commonly used cell viability studies. Electrospray ionization time-of-flight mass spectrometry (ESI-TOF MS) was used to analyze the polysaccharide dextran. Polysaccharides, including dextran, are difficult to ionize due to their inherent neutrality. Ionization efficiency is poor in negative polarity ESI because they lack acidic groups typically needed for proton abstraction, and ionization efficiency in positive polarity ESI is poor because polysaccharides have low proton affinity. In efforts to circumvent the issue of low ionization efficiency, dextran was derivatized to try mimicking protein-like ionization. Dextran was derivatized using a one-pot derivatization procedure with ethylenediamine, thus, giving dextran free terminal amine groups. The derivatization procedure attached up to four ethylenediamine groups and allowed dextran to have up to four protonations (or positive charges). The ability to carry up to four charges shifted the molecular weight of dextran to a lower m/z , similar to protein supercharging ionization. Mass spectrometric analysis was successfully applied to identify potential degradation products during the catalytic release of nitric oxide (NO) from *S*-nitrosoglutathione (GSNO) when it was exposed to metal-organic frameworks (MOFs) embedded

onto chitosan polymer support systems. Oxidized glutathione (GSSG) was confirmed to be the reaction byproduct of the release of NO from GSNO, and glucosamine and *N*-acetylglucosamine were identified as the degradation products from the chitosan polymer support system. In a similar use of MS, potential interferences in the commonly used CellTiter Blue and MTT cell viability assays were studied. When the UV-vis spectroscopic assays suggested interferences or produced inconclusive results, mass spectrometric analyses accurately determined whether selected small molecules were responsible for conversion of resazurin to resorufin, MTT to formazan, or if they were responsible for severe signal suppression on the UV-vis spectroscopic assays. MS was also successfully used to study the biodegradable poly(phosphazene), polyester polymers and their nitrosated analogues. The purpose of the studies was to investigate the potential degradation products from the degradation of these polymers. In-depth understanding of the degradation products from these polymers may aid in determining potential unwanted side effects that may render the polymeric devices unusable. A combination of direct flow injection MS, liquid chromatography mass spectrometry (LC-MS), and tandem mass spectrometry (LC-MS/MS) were successfully applied to identify the degradation products from each polymer system investigated. Identification of each degradation product from these polymers strongly suggests the implementation of LC-MS/MS when biodegradable polymers are developed for biomedical applications. Particularly because these methods can be used when a device intended for medical use undergoes the ISO 10993 series Biological Evaluation of Medical Devices. Additionally, in a highly collaborative effort, a chiral metal-organic framework (MOF) was used as a chiral stationary phase (CSP) for chiral resolution. The chiral-MOF (TAMOF-1) was packed in-house into an empty HPLC column and successfully used to resolve chiral compounds efficiently using normal and reversed phase solvent systems, highlighting the versatility of the chiral-MOF.

ACKNOWLEDGEMENTS

First, I would like to thank my advisor Dr. Melissa M. Reynolds for giving me the amazing opportunity of being part of her group at CSU. I will forever be grateful for her guidance and support throughout my graduate career. I am thankful to Dr. Kimberly Pacheco for making my decision to pursue my PhD in Chemistry at CSU one of the best decisions of my life and for always being my inspiration to be a better chemist. I wish to thank the members of my dissertation committee Dr. Delphine Farmer, Dr. Chuck Henry, Dr. Jamie Neilson, Dr. Matt Kipper, Dr. Ketul Popat and Dr. Joe Zadrozny for agreeing to be part of my committee, their time and support during my PhD journey. I am thankful to Dr. Claudia Boot, Dr. Karolien Deneff, Dr. Chris Rithner and the entire Central Instrument Facility for giving me the opportunity to be part of the CIF and for their constant support throughout the years. I would like to thank the current and previous members of the Reynolds group with whom I worked, had collaborative projects, and shared the great and tough times. I miss going to hang out at the Ramskeller, Krazy Karls, playing Pokémon Go, the amazing and supportive triad, and spending lots of quality time at the office “always” talking about science. I would also like to thank my family for their support throughout my entire graduate experience, from earning my M.S. at UNC, to working on my PhD at CSU. My biggest thanks to Danae Burgess for always being there for me throughout the great and difficult times. I know it was especially difficult for her to deal with my anxiety, stress and overall not-so-joyful attitude at times, so I am extremely thankful that she didn’t give up on me. My thanks to Josh Harrelson and Mile High Labs for giving me the amazing opportunity of landing my dream job on the first try and for letting me work at MHL while finishing up at CSU.

Thank you all for making a great impact on my life and for being part of this journey!

TABLE OF CONTENTS

ABSTRACT	ii
ACKNOWLEDGEMENTS.....	iv
CHAPTER 1 – INTRODUCTION	1
1.1 Mass Spectrometry	1
1.1.1 Ion Sources/Methods of Ionization	1
1.1.2 Mass Analyzers	4
1.1.3 Tandem mass spectrometry	6
1.2 Mass Spectrometry Application to Polysaccharides.....	7
1.2.1 Polysaccharides	7
1.2.2 Mass Spectrometric Analysis of Polysaccharides.....	9
1.3 Mass Spectrometry Application to Biodegradable Polymers	12
1.3.1 Biodegradable Polymers.....	12
1.3.2 Characterization of Biodegradable Polymers	12
1.4 Metal Organic Frameworks.....	13
1.4.1 Metal-Organic Frameworks as Chiral Stationary Phases (CSP).....	14
1.5 Dissertation Outline	15
CHAPTER 1 – REFERENCES	20
CHAPTER 2 – DERIVATIZATION OF DEXTRAN TO IMPROVE ELECTROSPRAY IONIZATION TIME-OF-FLIGHT MASS SPECTROMETRIC ANALYSIS OF POLYSACCHARIDES	29
2.1 Background	29
2.2 Introduction	30
2.2.1 Dextran	31
2.2.2 Dextran Uses and Applications.....	33
2.2.3 Current Methods for Dextran Analysis	34
2.2.4 Derivatization Method for Dextran to Achieve Improved Ionization Efficiency	35
2.3 Experimental	36
2.3.1 Chemicals	36
2.3.2 Derivatization Procedure.....	36
2.3.3 General Characterization Techniques.....	37
2.3.4 Mass Spectrometry.....	37
2.3.5 Data Analysis.....	38
2.4 Results and Discussion	38
2.4.1 Initial derivatization techniques for dextran.....	38
2.4.2 Characterization of dextran and EDA-dextran.....	41
2.4.3 ESI-TOF MS Analysis of dextran T1 and EDA-dex-T1	43
2.4.4 ESI-MS/MS of dextran T1 and EDA-dex-T1 Trisaccharides.....	48
2.5 Conclusions	51
CHAPTER 2 – REFERENCES.....	52
CHAPTER 3 – DEVELOPMENT OF MASS SPECTROMETRIC METHODS TO IDENTIFY UNKNOWN COMPOUNDS AND REACTION PRODUCTS IN COMPLEX SYSTEMS.....	57

3.1 Background	57
3.2 Introduction	59
3.2.1 Chitosan-MOF composites	60
3.2.2 Cell viability studies	61
3.2.3 Goals for this chapter.....	63
3.3 Experimental	64
3.3.1 Materials and Methods	64
3.4 Results.....	66
3.4.1 Chitosan-MOF membranes.....	66
3.4.2 Cell viability studies.....	68
3.4 Conclusions	79
CHAPTER 3 – REFERENCES	80
CHAPTER 4 – MASS SPECTROMETRIC METHODS FOR ANALYSIS OF DEGRADATION PRODUCTS FROM POLYPHOSPHAZENE AND POLYESTER BIODEGRADABLE POLYMERS	83
4.1 Background	83
4.2 Introduction	84
4.3 Experimental	88
4.3.1 Polyphosphazene Degradation.....	88
4.3.2 Biodegradable Polyester Degradation	89
4.4 Results.....	91
4.4.1 Mass Spectrometric Identification of Degradation Products.....	91
4.4.2 Liquid Chromatography-Mass Spectrometric Analysis	106
4.4.3 LC-MS/MS Structural Elucidation of Degradation Products	109
4.5 Conclusions	112
CHAPTER 4 - REFERENCES.....	114
CHAPTER 5 – METAL-ORGANIC FRAMEWORK AS A STATIONARY PHASE FOR CHIRAL LIQUID CHROMATOGRAPHIC SEPARATIONS	117
5.1 Background	117
5.2 Introduction	118
5.3 Experimental	121
5.3.1 Materials	121
5.3.2 Methods	121
5.4 Results.....	122
5.4.1 Initial column packing	122
5.4.2 Chromatographic resolution of <i>trans</i> -2,3-diphenyloxirane	123
5.4.3 Application of TAMOF-1 column to other chiral compounds	126
5.5 Conclusions	129
CHAPTER 5 – REFERENCES	130
CHAPTER 6 – CONCLUSIONS AND FUTURE DIRECTIONS	133
6.1 Conclusions	133
6.2 Future Directions	134
6.2.1 Improvements for ionization of dextran and applications to larger polysaccharides.....	134
6.2.2 Mass spectrometry application for degradation profiling of polymeric devices.....	135

6.2.3 Continuous use of mass spectrometry for analysis of reaction products....	136
6.2.4 Chiral chromatography using chiral metal-organic frameworks	136
APPENDIX A.....	139
APPENDIX B.....	149
APPENDIX C.....	156
APPENDIX D.....	162
APPENDIX E.....	168
APPENDIX F.....	174
APPENDIX G.....	180
APPENDIX H.....	188

CHAPTER 1
INTRODUCTION

1.1 Mass Spectrometry

Mass spectrometry is an analytical technique used to determine the mass of molecules of interest¹. By determining the mass of a molecule, the molecular formula can be calculated to confirm the identity of the molecule of interest or to identify an unknown molecule². Mass spectrometry takes place in a mass spectrometer, an instrument made up of an ion source, a mass analyzer, a detector and a computer system²⁻⁴. For analysis using mass spectrometry to take place, the molecule of interest must first be ionized in the ion source, then transported into the mass analyzer to measure its mass, detected, and recorded in a data form in a computer system (Figure 1.1)¹⁻⁴.

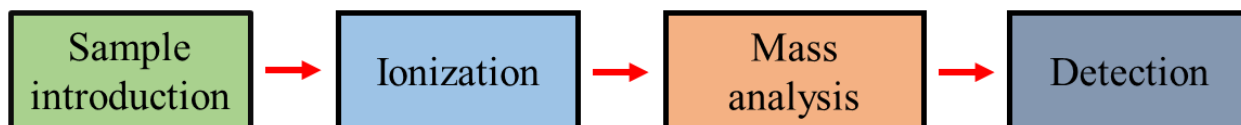


Figure 1.1 Block diagram of a mass spectrometer

1.1.1 Ion Sources/Methods of Ionization

The ionization stage has the function of generating ions that will be transferred into the mass analyzer. Multiple ionization techniques have been developed over time, but their purpose is the same: generate ions by addition of energy (electrons, electric fields, photons) or additives (adducted cations or anions)⁵. Ions can be formed *in vacuo* inside the mass spectrometer or outside at atmospheric pressure. Examples of ionization under vacuum are electron ionization (EI)⁶, chemical ionization (CI), and matrix-assisted laser desorption/ionization (MALDI)⁷. Examples of atmospheric pressure ionization (API) include electrospray ionization (ESI)⁸, atmospheric pressure chemical ionization (APCI)⁹ and desorption electrospray ionization (DESI)¹⁰.

Each method of ionization has advantages and disadvantages when used to generate ions. These will depend on the polarity and size of the analyte, and the amount of energy applied to the analyte. Depending on the amount of energy added during the ionization process, the structure of the analyte molecule ion generated will either remain intact or fragment into smaller ions. For example, EI is the most energetic type of ionization and ions will most likely fragment making EI an example of hard ionization^{6,11}. An example of soft ionization is ESI^{8,12,13}, which will typically preserve the analyte intact. The order of the amount of energy applied from most to least is

$$EI > CI \approx APCI \approx APPI > MALDI \approx ESI$$

A similar order applies to the size and polarity of molecules. Small molecules and non-polar molecules are typically ionized using EI, whereas ESI ionizes efficiently only polar compounds and imparts minimal energy to the analyte. Both ESI and MALDI are the preferred ionization methods to ionize large molecules. These relationships are shown in Figures 1.2 and 1.3 and for the work presented in this dissertation, ESI was the main ionization method used¹⁴.

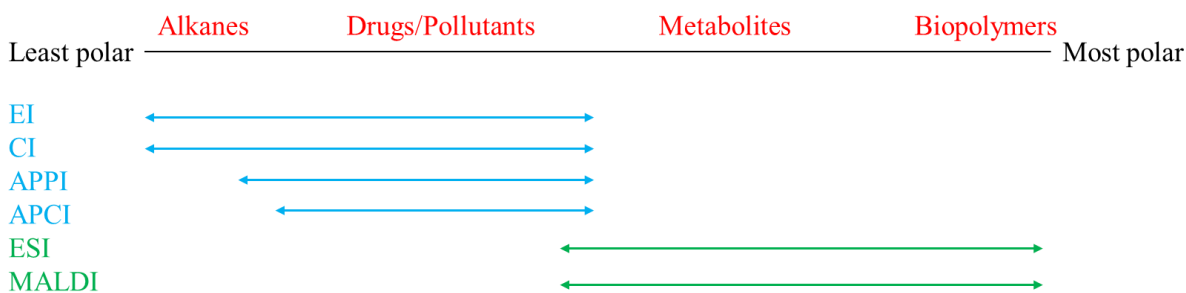


Figure 1.2 Ionization methods according to polarity of analytes

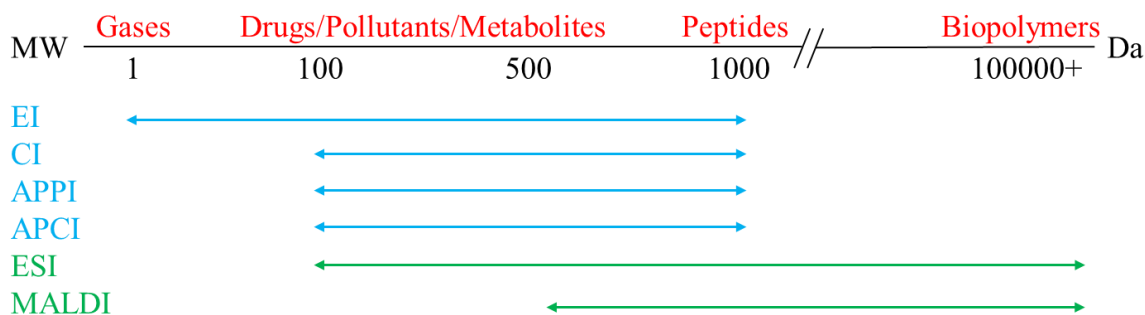


Figure 1.3 Mass ranges for each type of ionization

Electrospray ionization is a method by which analytes present in solution are transferred to into the gas phase as ions. ESI can ionize analytes such as polymers, nucleic acids, and proteins that may have very high molecular mass up to megadaltons for proteins^{15–17}. The analytes in solution may be present as ions (dissociated metal ions M^{n+} , protonated amines, deprotonated carboxylic acids, sulfates, alcohols, dissociated halides X^{n-} , and so on). Analytes of interest may also be neutral in solution, which are charged as they are sprayed by adduct formation^{12,18}.

Ionization by ESI takes place following three major steps: (1) charged droplets are produced at the ES tip; (2) the charged droplets shrink by evaporating the solvent leading to very small highly charged droplets; (3) production of the gas-phase ions ejected from the highly charged droplets^{13,14,19}. The process is driven by an imposed electric field into the liquid being sprayed which creates a Taylor cone and a jet charged by excess of positive or negative ions. The jet splits into droplets charged with an excess of positive or negative ions, and as the solvent evaporates, the shrinking of the droplets brings the charges closer together. The increasing Coulombic repulsion destabilizes the droplets leading them to emit smaller daughter droplets until free gas-phase ions form (Figure 1.4)¹⁹.

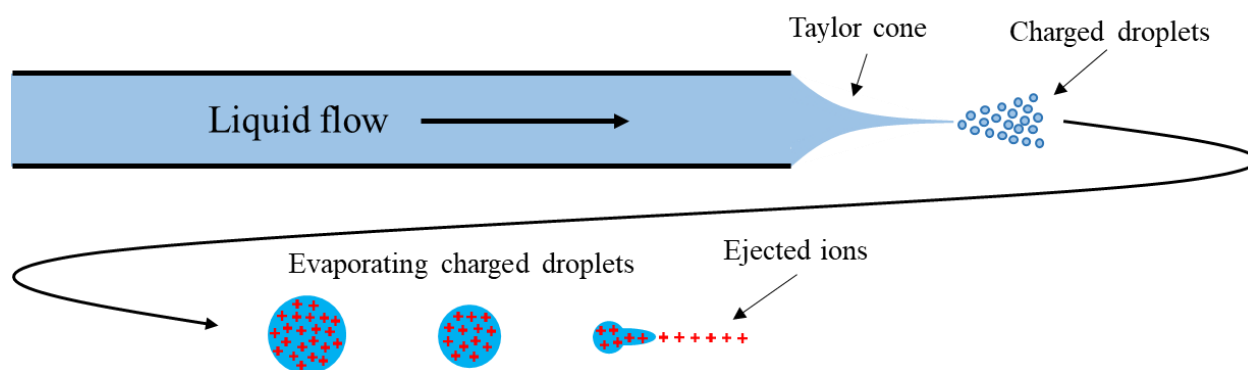


Figure 1.4 Electrostatic spray ionization source. (1) the nebulizer delivers the analyte(s) of interest (Liquid flow) which produces charged droplets at the nebulizer tip; (2) the charged droplets shrink by evaporation of the solvent (done by drying gas and in some cases a sheath gas); (3) ions are ejected from the highly charged, shrunk droplets.

1.1.2 Mass Analyzers

Following the formation of ions, the ions are separated according to their m/z ratios using a *mass analyzer*. There are several types of mass analyzers (Table 1.1) including the quadrupole (Q), quadrupole ion traps (QIT, LIT)^{20,21}, Fourier transform ion cyclotron resonance (FT-ICR)²², orbitrap²³ and time-of-flight (TOF)^{24,25}. Of all these mass analyzers, TOF was the mass analyzer used for the bulk of the work presented in this dissertation.

Table 1.1 Types of mass analyzers

Analyzer Type	Resolution	m/z range	Mass Accuracy (ppm)
Quadrupole	Up to 2000	4000	50 - 100
Time of Flight	Up to 30000	Unlimited	2 - 50
Orbitrap	Up to 150000	6000	2 - 5
FT-ICR	Up to 1000000	6000	< 2

14

Time of flight mass analyzers determine the mass of analytes by measuring the time it takes the ions of interest to arrive from a starting position, the ion pulser, to a detector (Figure 1.5). The mass can be determined because the flight time for each mass is unique. This process starts when a high voltage pulse is applied to the ions of interest at the ion pulser, the ions travel through the time of flight tube, and the ions strike the detector (Figure 1.5). The flight time (t) is determined by the energy (E) to which an ion is accelerated, the distance (d) it travels and its mass, specifically its mass to charge ratio (m/z)^{24,25}.

Two main equations apply to time-of-flight mass analysis. The first one is the formula for kinetic energy:

$$E = \frac{1}{2}mv^2 \quad \text{Eq. 1}$$

in which E stands for kinetic energy, m for mass and v for velocity and when it is solved for mass (m):

$$m = \frac{2E}{v^2} \quad \text{Eq. 2}$$

and further solved for velocity (v):

$$v = \sqrt{\frac{2E}{m}} \quad \text{Eq. 3}$$

By solving the equation for kinetic energy, it is observable that smaller masses will have larger velocities, and larger masses will have smaller velocities. This phenomenon is observed in the time-of-flight mass spectrometer, ions with lower masses arrive at the detector earlier, and ions with higher masses arrive at the detector later (Figure 1.5)²⁵. Since time-of-flight is what is measured, the second equation is:

$$v = \frac{d}{t} \quad \text{Eq. 4}$$

in which v stands for velocity, d for distance and t for time. When equations 2 and 4 are combined the following equation is obtained:

$$m = \left(\frac{2E}{d^2}\right) t^2 \quad \text{Eq. 5}$$

With equation 5, a basic time-of-flight relationship is established. For any given energy (E) and distance (d), the mass is proportional to the square of the flight time of the ion. In the final design of a time-of-flight tube, the energy applied and traveled distance of the ions is kept constant, so that the measurement of flight time is measured accurately to give an accurate mass value. Since the terms are kept constant, energy and distance are combined into a single variable giving equation 6, which is the generalized equation used to measure the mass (m/z) of ions of interest²⁶.

$$m = At^2 \quad \text{Eq. 6}$$

Most current TOF tubes are designed with an ion mirror or reflectron as shown in Figure 1.5. The purpose of using a reflectron is to mitigate potential problems caused by different initial kinetic energies after ions are accelerated by the ion pulser^{11,14}. Ions with higher kinetic energy penetrate more deeply than ions with lower kinetic energy before leaving the reflectron. Total

flight time corrections occur using the reflectron because ions with higher energy of a given m/z enter sooner, penetrate more deeply, spend more time in the mirror and exit later than the lower energy ions of the same m/z . Ion reflection takes place because there is a potential hill in the ion mirror leading to a time shift as the ions enter the mirror, are decelerated, turn around at an angle, and are accelerated in the opposite direction toward the detector^{11,26–28}. The correction can be seen in the Ion Mirror inset in Figure 1.5. Implementation of ion mirrors lead to high resolving power since it allows all ions of the same m/z to arrive at the detector at exactly the same time^{25,27,28}.

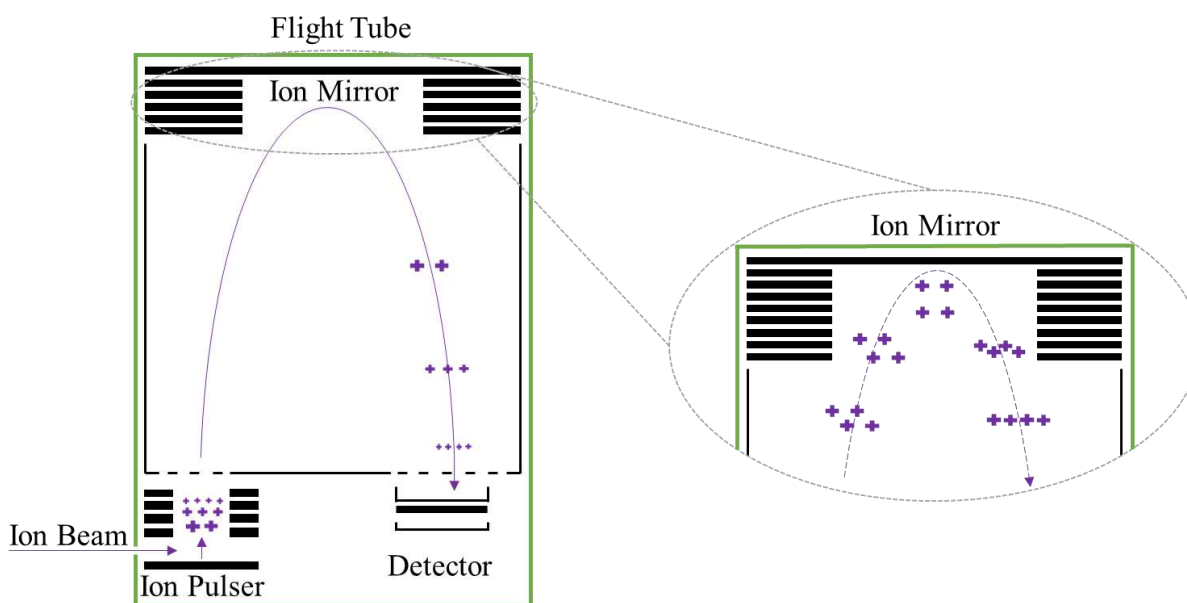


Figure 1.5 Schematic of time of flight mass analyzer. As the ions arrive to the TOF tube, an ion pulser pushes the ions towards the ion mirror and eventually the detector.

1.1.3 Tandem mass spectrometry

While efficient ionization and accurate mass measurements of analytes of interest can be readily achieved, no structural information is provided. When structural information is also desired, particularly when an unknown analyte is being analyzed, tandem mass spectrometry (MS/MS) is performed²². Combinations of quadrupole, ion trap, and TOF analyzers are MS/MS systems that are used. In MS/MS systems, the first analyzer usually selects an ion of interest that is then passed, with or without fragmentation, into a second analyzer. Between the first and second

analyzers, there is a collision cell that can be used to induce fragmentation. Once a selected ion is fragmented, the fragment ions can be used to determine the structure of an unknown to confirm its identity²⁹.

1.2 Mass Spectrometry Application to Polysaccharides

1.2.1 Polysaccharides

Carbohydrates are central players in several biological processes and play both a functional and structural role in nature. Usually classified as monosaccharides, oligosaccharides or polysaccharides (Figure 1.6), they are involved in molecular recognition, cellular signaling, cell adhesion, energy generation as well as being structural components³⁰.

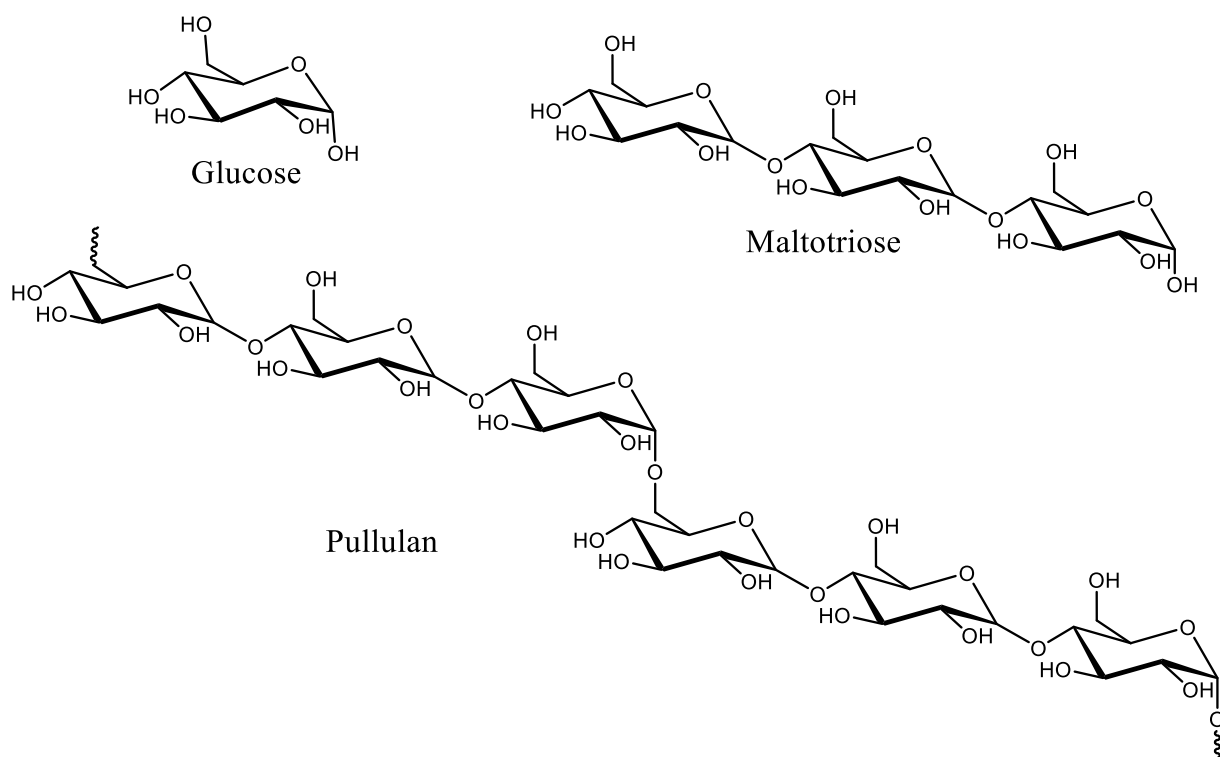


Figure 1.6 Examples of a monosaccharide (glucose), oligosaccharide (maltotriose) and polysaccharide (pullulan).

In contrast with nucleic acids and proteins, the biosynthesis of carbohydrates is not template-driven, leading polysaccharides to exist in nature as heterogeneous mixtures, often of high complexity with up to millions of monosaccharide units³¹. The possibility of substitution at

different positions in the monosaccharide units makes the primary structure of carbohydrates more complex than proteins, that have well-defined amide bond forming a linear structure³¹⁻³³. Additionally, increased complexity arises from the possibility of α - or β -configuration at the anomeric carbon of the monosaccharide units. For example, amylose in starch consists of α -1,4-linked glucose residues while cellulose in plants consists of β -1,4-linked glucose residues (Figure 1.7)³⁴.

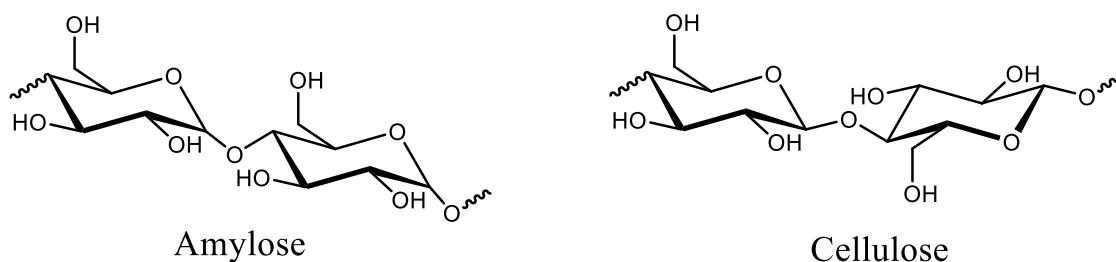


Figure 1.7 Amylose and cellulose representations of α -1,4- and β -1,4-glucose linkage configurations.

The different stereochemistry of the glycosidic linkages give amylose and cellulose very different properties. Additionally, due to the possibility of substitution at any of the positions of glucose monosaccharides, the monomer units can be linked to more than two other units, giving the possibility for polysaccharides to be branched (Figure 1.8)^{31,35,36}.

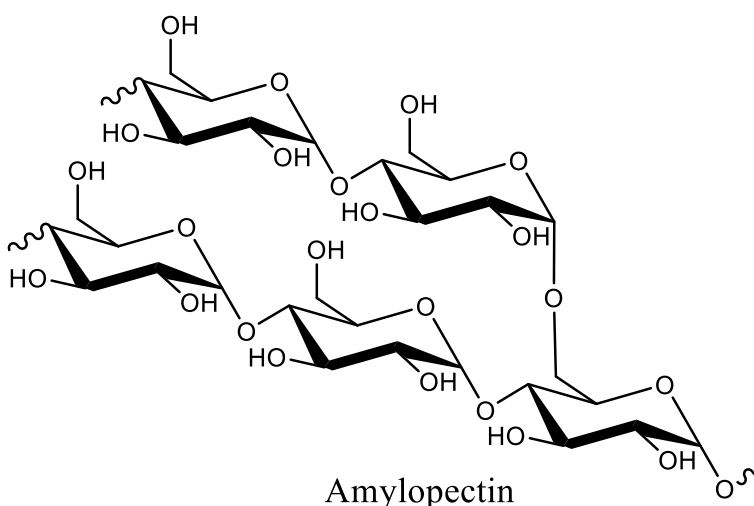


Figure 1.8 Structure of amylopectin, primarily composed of α -1,4-linkages with branches at the α -1,6-positions.

1.2.2 Mass Spectrometric Analysis of Polysaccharides

Compared to advances in protein analysis, progress in the application of mass spectrometry to carbohydrates has evolved somewhat slowly, mostly because carbohydrates are a more challenging set of analytes for structural characterization. Unlike proteins, there is no database containing an extensive set of sequences representing all possible carbohydrate structures^{31,33}. Therefore, characterization of carbohydrates relies upon obtaining the full details of structure from a collected mass spectrum³¹.

A fundamental flaw that limits mass spectrometric analysis of polysaccharides is their poor ionization due to their neutrality. Nevertheless, MALDI and ESI are still the predominant methods of ionization for polysaccharides. Unfortunately, the absence of basic sites in neutral polysaccharides inhibits protonation in MALDI and ESI mass spectrometry. Instead, polysaccharides most often ionize by adduction of metal ion, usually sodium cation, with comparatively low efficiency^{30,36,37}. Additionally, the absence of acidic sites in neutral polysaccharides inhibits deprotonation in MALDI and ESI mass spectrometry. To date, the majority of polysaccharide studies have focused on the positive-ion mode, done by metal cation adduction^{33,38}.

Despite the limitations in both MALDI and ESI, work has been done to analyze native oligosaccharides and polysaccharides and their derivatives. Mock³⁹ and coworkers reported the measurement of underivatized mannose oligosaccharides with MALDI-TOF MS with molecular mass of up to 2395 Da as $[M+Na]^+$ cations. Stahl⁴⁰ and coworkers also reported the measurement of the underivatized oligosaccharides maltodextrin and dextran using MALDI-TOF MS with molecular mass measurements of up to 3500 and 7000 Da respectively. Hsu⁴¹ and coworkers reported the molecular weight measurement of dextran up to 8000 Da using MALDI-TOF MS.

Using ESI-TOF MS, Ghiulai³⁶ and coworkers reported the analysis of underivatized dextrans with molecular mass of up to 5500 Da.

Despite the successful analysis of polysaccharides with molecular mass of up to 8000 Da, dextran, a polysaccharide with clinical and pharmaceutical applications requires a high molecular mass of between 40 and 70 kDa to have antithrombic effects. Interest in molecular mass and structural information for dextran 40 – 70 is therefore not attainable with the current MALDI-TOF and ESI-TOF techniques. Derivatization treatment of polysaccharides and glycans such as permethylation can improve MS sensitivity and the range of measurement to approximately 15 kDa³⁶.

These limitations contrast with the highly successful analysis of protein by both MALDI-TOF and ESI-TOF MS. Proteins can routinely be analyzed using both techniques and largest protein reported by Bahr⁴² and coworkers was the trimer of urease at 272000 Da. This substantial mass range is possible due to the ability of proteins to get multiply charged. For example, if a hypothetical protein has a molecular mass of 40 kDa, the hypothetical mass spectrum shown in Figure 1.9 shows the effects of multiple charges.

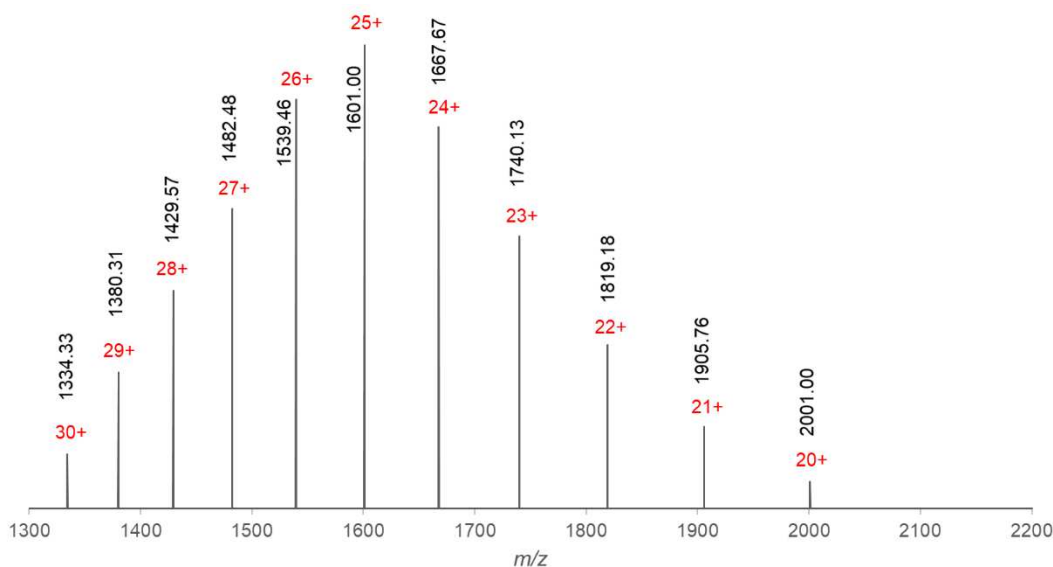


Figure 1.9 Multiple charging of a hypothetical 40 kDa protein.

This molecular mass measurement extends beyond typical TOF mass spectrometers. For example, the Agilent 6224 TOF operates at the 100 – 3200 m/z range in high accuracy mode and at the 100 – 20000 m/z range in extended mass mode. If the protein was to be analyzed by single charging, it would not be measurable in either mode. However, due to multiple charging^{14,43}, the protein should be accurately measured in the high accuracy mode that covers the 100 – 3200 m/z range. When an MS pattern like that shown in Figure 1.9 is obtained, and it is suspected that multiple charging is occurring, the spectra can be deconvoluted to obtain the actual mass of the protein using the following equations:

$$z = \frac{(m/z)_1 - x}{(m/z)_2 - (m/z)_1} \quad \text{Eq. 7}$$

$$M = z((m/z)_2 - x) \quad \text{Eq. 8}$$

where m/z is the mass of each peak on the mass spectrum and x is the mass of the adduct. In the case of proteins, the adduct is typically a proton with the exact mass of 1.0073.

Equation 7 is used to determine the number of charges found by using two adjacent peaks. For example, using the peaks 1334.33 and 1380.31 the number of charges for the peak at 1380.31 can be calculated:

$$z = \frac{(m/z)_1 - x}{(m/z)_2 - (m/z)_1} = \frac{1334.33 - 1.0073}{1380.31 - 1334.33} = 28.99$$

Therefore, the number of protonations (charges) on the ion found at 1334.33 is 29. The next step is to deconvolute the actual mass of the protein, using equation 8:

$$M = z((m/z)_2 - x) = 29 \times (1380.31 - 1.0073) = 39999.78$$

The same process is performed for all the peaks found in the mass spectrum until all the charges are found and the masses deconvoluted.

The ability of proteins to hold multiple charges is of great interest since applying this concept to polysaccharides would greatly extend their measurable range using mass spectrometry. Multiple charging of polysaccharides should in theory, shift the large molecular mass of polysaccharides toward a lower m/z range for accurate mass spectrometric analysis.

1.3 Mass Spectrometry Application to Biodegradable Polymers

1.3.1 Biodegradable Polymers

Biodegradable polymers are defined as degradable materials for which the degradation is a result from the action of microorganisms and ultimately the polymer is converted to water, carbon dioxide (aerobic degradation) and/or methane (anaerobic degradation)⁴⁴⁻⁴⁶. Biodegradable polymers include polysaccharides and other biopolymers, polyesters produced by microorganisms, synthetic polyesters, among others⁴⁷. The majority of biodegradable polymers belong to the polyester group (Figure 1.10).

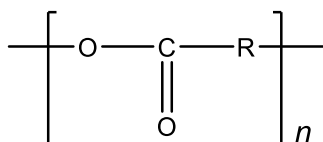


Figure 1.10 Polyester general structural features.

Polyesters can be easily broken down by hydrolysis, making them excellent candidates to be used to develop biomedical devices^{48,49}. Biodegradable polyesters can be used to develop devices capable of drug delivery, for tissue engineering and wound dressings.^{50,51}

1.3.2 Characterization of Biodegradable Polymers

Current techniques used to determine the biodegradation of a device over time are gravimetric analysis, Fourier transform infrared spectroscopy (FT-IR), nuclear magnetic resonance spectroscopy (NMR), scanning electron microscopy (SEM), high-performance liquid chromatography (HPLC) and mass spectrometry (MS). For example, the degradation mechanism

of acrylate-derivatized poly(ethylene glycol) (PEGDA) hydrogels was determined by tracking the cleavage of networked groups that result in a reduced crosslink density over time. The changes in crosslink density were monitored by measuring the swelling ratio and/or modulus of the hydrogel⁵². Another example follows the oxidative degradation of poly(carbonate urethanes) (PCU) that was tracked using FT-IR by monitoring selected functional groups over time. Additionally, SEM was used to track surface damage of the PCUs over time⁵³. A different study developed an HPLC method to track the degradation of implanted medical devices by determining acrylic monomers and degradation products⁵⁴. The degradation of poly(5-hydroxy-trimethylene carbonate) in aqueous environment was monitored using ¹H-NMR and the main degradation products were identified with electrospray ionization mass spectrometry (ESI-MS)⁵⁵.

The advantages of soft ionization mass spectrometry have further advanced the routine use of mass spectrometry for characterization of biodegradable polymers beginning with their design and synthesis all the way to investigation of their degradation products^{15,56-58}. Accurate knowledge of the degradation products of biodegradable polymers is highly desirable when they are used to develop biomedical devices. The importance of mass spectrometric implementation toward analysis of biopolymer degradation is highlighted when a biodegradable device must undergo biological evaluation for release as a medical device. While mass spectrometric identification of biodegradation products cannot determine the whole extent of a device's biological compatibility, it is an important addition for the fulfillment of the widely accepted standards for device evaluation under the ISO 10993 series (Biological Evaluation of Medical Devices).

1.4 Metal Organic Frameworks

Metal-organic frameworks (MOFs) are an extensive class of crystalline materials with ultrahigh porosity (up to 90% free volume) and ultrahigh surface areas, exceeding 6000 m²g⁻¹⁵⁹.

These hybrid inorganic-organic materials are constructed by joining metal-containing units with organic linkers to form open crystalline structures with permanent porosity^{60,61}. The flexibility with which the metal-containing units and organic linkers can be varied has led to many MOFs being prepared for highly specific applications. Potential applications include gas storage, separations, catalysis and biomedical applications⁶²⁻⁶⁴. The extraordinary degree of variability for both the organic and inorganic components, as well as the synthetic procedure can have a strong influence on the formation of the MOF and the pore size^{59,65}. An example is the design of MOFs with applications as antibacterial agents, drug delivery systems, and for catalytic release of therapeutic gases such as nitric oxide (NO)^{64,66-68}. MOFs designed for separations include gas-phase adsorptive separations, liquid-phase adsorptive separations and membrane-based separations^{63,69}. A particularly interesting type of separation falls under liquid-phase separations is the ability for MOFs to be designed for enantio-separation⁷⁰⁻⁷³.

1.4.1 Metal-Organic Frameworks as Chiral Stationary Phases (CSP)

Enantio-separation continues to be a substantial challenge in the modern pharmaceutical industry. Most of the produced drugs and natural products exhibit chirality, however, in most cases only one of the enantiomers has the desired specific biological activity and the other enantiomer has the potential for undesired effects. Since it is possible for one of the enantiomers to have undesirable effects, chiral drug molecules require stereoselective syntheses or challenging separations to purify one single enantiomer⁷⁴. Despite the crucial requirement of chiral separations in the pharmaceutical industry, it remains an expensive and complex challenge. Current chiral separations are performed using chiral chromatography which primarily depends on polysaccharide and cyclodextrin based chiral stationary phases (CSPs) with some chiral separations performed using protein, ligand, ion exchange and macrocyclic antibiotic CSPs⁷⁵.

Typically, these CSPs are poorly robust, expensive to manufacture and often too specific, lacking desirable versatility across multiple different chiral analytes^{75,76}. To circumvent these shortcomings, the use of MOFs is gaining attention for their potential use as CSPs. Examples of chiral MOFs have been synthesized using enantiopure organic linkers and have been used for chiral separations or asymmetric catalysis.

1.5 Dissertation Outline

The dissertation presented herein utilizes mass spectrometry as an analytical tool in a variety of systems to help answer a series of analytical questions:

Chapter 2. Derivatization techniques are investigated with the purpose of inducing ionization of dextran by means of multiple charges. Most polysaccharides, including dextran, are difficult to ionize due to their inherent neutrality. Ionization efficiency is poor in negative mode ESI because they lack acidic groups typically needed for proton abstraction, and ionization efficiency in positive mode ESI because they have low proton affinity. The goal for this project was to find a derivatization technique that would allow dextran to carry multiple charges. If successful, more charges would allow the molecular mass of dextran to be measured in a lower m/z region, similar to the supercharging of proteins with large molecular mass that allows them to be measured. **To encourage ionization of dextran by means of multiple proton adducts for ESI-TOF MS analysis, a one pot derivatization technique using ethylenediamine was used. We were able to successfully attach up to four ethylenediamine groups onto dextran allowing for up to four protonations. The ability of derivatized dextran to hold up to 4 charges by means of protonation is the first time a polysaccharide has been multiply charged by multiple protonations.** The progress made suggests that derivatization can allow for large and otherwise neutral polysaccharides be measured using mass spectrometry.

Chapter 3. The third chapter of this dissertation focuses the application of mass spectrometry to answer a series of analytical questions: to confirm the hypothesized reaction byproducts produced during the catalytic release of nitric oxide (NO) from *S*-nitrosoglutathione (GSNO) when exposed to metal-organic frameworks (MOFs) embedded onto chitosan polymer support systems. Simultaneously, the degradation products from the chitosan-MOF composite were studied to probe for the potential decomposition of the MOF by searching for the starting ligand. **With the use of mass spectrometry, oxidized glutathione (GSSG) was confirmed to be the reaction byproduct of the release of NO from GSNO. Additionally, the hydrolytic degradation of chitosan produced the anticipated glucosamine and *N*-acetylglucosamine as the degradation products. But most importantly, within the same mass spectrometric analyses, H₃BTTri, the ligand used to synthesize the MOF was not detected, indicating no decomposition of the MOF over time.**

In a second application of mass spectrometry, my colleague Bella H. Neufeld raised awareness regarding the potential chemical transformation of cell viability assays in the absence of cells. To investigate potential interferences and their effects, the CellTiter Blue (resazurin → resorufin) and MTT (MTT → formazan) cell viability assays were tested against selected small molecules. **When the UV-vis spectroscopic assays suggested interferences or produced inconclusive results, mass spectrometric analysis allowed for the accurate determination of resazurin/formazan or MTT/formazan presence and whether the selected small molecule was responsible for false positives/negatives or severe signal suppression.** Our findings strongly suggest that whenever the CellTiter Blue or MTT assays are used, the selected therapeutic should always first be tested for its effects on the assay first and the best way to do this is to run the assays in the absence of cells and confirm whether transformation has occurred using mass

spectrometry. This proved to be of great importance since even when appropriate control studies are performed, the typical user of this assays does not perform a thorough examination of the full UV-vis spectroscopic measurements which may still lead to inconclusive results regarding potential interferences.

Chapter 4. The importance of using mass spectrometry coupled with a pre-separation step is emphasized in Chapter 4 for analysis of polymer degradation products. Polymer systems based on poly(phosphazene) and polyester structures synthesized in our lab were degraded over time by hydrolytic degradation. The implementation of routine direct flow injection mass spectrometric analysis helped with the identification of the major degradation products from each polymer. However, a polyester based polymer with promising properties for biomedical applications was further studied for its decomposition over time to assess potential toxicity concerns that may arise during degradation. In addition to direct flow injection mass spectrometry, a chromatographic separation step with a C18 column allowed for additional details including structural isomerism of the degradation products. And finally, tandem mass spectrometry (MS/MS) was critical for accurate structural determination of each degradation product. **The degradation products from each polymer system were characterized using TOF-MS to complement full characterization of the polymers, particularly during the degradation process. One of our main concerns was to address whether the polyesters would degrade into individual monomers, with the potential of increasing localized acidity. Fortunately, our results show that the degradation products were primarily esters, as dimers and beyond, rather than the starting acidic monomers. The results presented in this chapter should pave the way for the future development of biodegradable polymers intended for biomedical applications. Particularly**

since the methodology presented can be used when a device intended to be for medical use undergoes the ISO 10993 series Biological Evaluation of Medical Devices.

Chapter 5. The fifth chapter represents the work performed in an international collaborative effort to use a new chiral metal-organic framework (MOF) as a chiral stationary phase (CSP) for chiral resolution. A chiral MOF designed and synthesized by Prof. Galán-Mascarós' group was provided to the Reynolds group to investigate potential applications. The chiral-MOF (called TAMOF-1) was packed in-house into an empty HPLC column with the primary objective of achieving chiral resolution of chiral compounds. **The results presented in this chapter strongly suggest that chiral-MOFs can and should be used for chiral chromatograph since efficient chiral resolution was observed using solvent systems that range from normal to reversed phase.** The ability of TAMOF-1 to be used as a CSP is very promising since to this day, chiral resolution continues to be an expensive, time consuming and complex analytical challenge.

Summarizing remarks. This dissertation presents studies emphasizing the benefits of incorporating mass spectrometric analyses to a variety of biomedically oriented projects. While it is an expensive technique and not available to every research group/industry, appropriate mass spectrometric methods can answer questions difficult to explore otherwise. Difficulties in mass spectrometric analysis of polysaccharides were addressed by exploring derivatization of dextran to mimic protein-like ionization. Byproducts of catalytic reactions and potential interferences in cell viability assays were confirmed using mass spectrometric analyses. The degradation products from poly(phosphazene) and polyester based polymers intended for biomedical applications were identified, in aims to provide information necessary and of importance for biological evaluation of medical devices. Finally, an international collaborative effort presented the opportunity to investigate the potential of a chiral-MOF CSP intended to advance chiral chromatography.

Collectively, the projects and findings outlined in this dissertation advance the field of bioanalytical mass spectrometry and chiral chromatography.

CHAPTER 1 – REFERENCES

- (1) Harvey, D. J. Mass Spectrometry: Overview. In *Reference Module in Chemistry, Molecular Sciences and Chemical Engineering*; Elsevier, 2018; Vol. 6, 337–344.
- (2) Sparkman, O. D. Mass Spectrometry: Overview and History. In *Encyclopedia of Analytical Chemistry*; John Wiley & Sons, Ltd: Chichester, UK, 2000; 1–58.
- (3) Mellon, F. A. MASS SPECTROMETRY | Principles and Instrumentation. In *Encyclopedia of Food Sciences and Nutrition*; Elsevier, 2003; 3739–3749.
- (4) Urban, P. L. Quantitative Mass Spectrometry: An Overview. *Philos. Trans. R. Soc. A Math. Phys. Eng. Sci.* **2016**, 374 (2079), 20150382.
- (5) Harvey, D. J. MASS SPECTROMETRY | Ionization Methods Overview. In *Reference Module in Chemistry, Molecular Sciences and Chemical Engineering*; Elsevier, 2013; 350–359.
- (6) Traeger, J. C. The Development of Electron Ionization. In *The Encyclopedia of Mass Spectrometry*; Elsevier, 2016; 77–82.
- (7) Jagtap, R. N.; Ambre, A. H. Overview Literature on Matrix Assisted Laser Desorption Ionization Mass Spectroscopy (MALDI MS): Basics and Its Applications in Characterizing Polymeric Materials. *Bull. Mater. Sci.* **2005**, 28 (6), 515–528.
- (8) Niessen, W. M. A. Electrospray Ionization Mass Spectrometry. In *Encyclopedia of Analytical Science*; Elsevier, 2016; Vol. 6, 334–350.
- (9) Rebane, R.; Kruve, A.; Liigand, P.; Liigand, J.; Herodes, K.; Leito, I. Establishing Atmospheric Pressure Chemical Ionization Efficiency Scale. *Anal. Chem.* **2016**, 88 (7), 3435–3439.

- (10) Morelato, M.; Beavis, A.; Kirkbride, P.; Roux, C. Forensic Applications of Desorption Electrospray Ionisation Mass Spectrometry (DESI-MS). *Forensic Sci. Int.* **2013**, *226* (1–3), 10–21.
- (11) Mirsaleh-Kohan, N.; Robertson, W. D.; Compton, R. N. Electron Ionization Time-of-Flight Mass Spectrometry: Historical Review and Current Applications. *Mass Spectrom. Rev.* **2008**, *27* (3), 237–285.
- (12) Banerjee, S.; Mazumdar, S. Electrospray Ionization Mass Spectrometry: A Technique to Access the Information beyond the Molecular Weight of the Analyte. *Int. J. Anal. Chem* **2012**, *2012*, 1–40.
- (13) Ho, C. S.; Lam, C. W. K.; Chan, M. H. M.; Cheung, R. C. K.; Law, L. K.; Lit, L. C. W.; Ng, K. F.; Suen, M. W. M.; Tai, H. L. Electrospray Ionisation Mass Spectrometry: Principles and Clinical Applications. *Clin. Biochem. Rev.* **2003**, *24* (1), 3–12.
- (14) Greaves, J.; Roboz, J. *Mass Spectrometry for the Novice*; CRC Press Taylor and Francis Group: Boca Raton, FL, 2014.
- (15) Rizzarelli, P.; Carroccio, S. Modern Mass Spectrometry in the Characterization and Degradation of Biodegradable Polymers. *Anal. Chim. Acta* **2014**, *808*, 18–43.
- (16) Fenn, J. B.; Mann, M.; Meng, C. K.; Wong, S. F.; Whitehouse, C. M. Electrospray Ionization for Mass Spectrometry of Large Biomolecules. *Science* **1989**, *246* (6), 64–71.
- (17) Klampfl, C. W.; Himmelsbach, M. Direct Ionization Methods in Mass Spectrometry: An Overview. *Anal. Chim. Acta* **2015**, *890*, 44–59.
- (18) Demarque, D. P.; Crotti, A. E. M.; Vessecchi, R.; Lopes, J. L. C.; Lopes, N. P. Fragmentation Reactions Using Electrospray Ionization Mass Spectrometry: An Important Tool for the Structural Elucidation and Characterization of Synthetic and Natural Products.

- Nat. Prod. Rep.* **2016**, 33 (3), 432–455.
- (19) Kebarle, P.; Verkerk, U. H. On the Mechanism of Electrospray Ionization Mass Spectrometry (ESIMS). In *Electrospray and MALDI Mass Spectrometry*; Cole, R. B., Ed.; John Wiley & Sons, Inc.: Hoboken, NJ, USA, 2012; 1–48.
- (20) Henchman, M.; Steel, C. Understanding the Quadrupole Mass Filter through Computer Simulation. *J. Chem. Educ.* **1998**, 75 (8), 1049–1054.
- (21) March, R. E. An Introduction to Quadrupole Ion Trap Mass Spectrometry. *J. Mass Spectrom.* **1997**, 32 (4), 351–369.
- (22) Loo, J. A. The Tools of Proteomics. In *Advances in Protein Chemistry*; 2003; Vol. 65, 25–56.
- (23) Zubarev, R. A.; Makarov, A. Orbitrap Mass Spectrometry. *Anal. Chem.* **2013**, 85 (11), 5288–5296.
- (24) Chen, Y. .; Gonin, M.; Fuhrer, K.; Dodonov, A.; Su, C. .; Wollnik, H. Orthogonal Electron Impact Source for a Time-of-Flight Mass Spectrometer with High Mass Resolving Power. *Int. J. Mass Spectrom.* **1999**, 221–226.
- (25) Guilhaus, M.; Mlynski, V.; Selby, D. Perfect Timing: Time-of-flight Mass Spectrometry. *Rapid Commun. Mass Spectrom.* **1997**, 11 (9), 951–962.
- (26) Agilent. Time-of-Flight Mass Spectrometry - Technical Overview. **2011**, 1–16.
- (27) Zhang, J.; Gardner, B. D.; Enke, C. G. Simple Geometry Gridless Ion Mirror. *J. Am. Soc. Mass Spectrom.* **2000**, 11 (9), 765–769.
- (28) Zhang, J.; Enke, C. G. Simple Cylindrical Ion Mirror with Three Elements. *J. Am. Soc. Mass Spectrom.* **2000**, 11 (9), 759–764.
- (29) Niessen, W. M. . MS–MS and MS_n. In *Encyclopedia of Spectroscopy and Spectrometry*;

- Elsevier, 2017; 936–941.
- (30) Čmelík, R.; Štikarovská, M.; Chmelík, J. Different Behavior of Dextran in Positive-Ion and Negative-Ion Mass Spectrometry. *J. Mass Spectrom.* **2004**, *39* (12), 1467–1473.
- (31) Kailemia, M. J.; Ruhaak, L. R.; Lebrilla, C. B.; Amster, I. J. Oligosaccharide Analysis by Mass Spectrometry: A Review of Recent Developments. *Anal. Chem.* **2014**, *86* (1), 196–212.
- (32) Karas, M.; Hillenkamp, F. Laser Desorption Ionization of Proteins with Molecular Masses Exceeding 10,000 Daltons. *Anal. Chem.* **1988**, *60* (20), 2299–2301.
- (33) Harvey, D. J. Matrix-Assisted Laser Desorption/Ionization Mass Spectrometry of Carbohydrates. *Mass Spectrom. Rev.* **1999**, *18* (6), 349–450.
- (34) Winger, M.; Christen, M.; van Gunsteren, W. F. On the Conformational Properties of Amylose and Cellulose Oligomers in Solution. *Int. J. Carbohydr. Chem.* **2009**, *2009*, 1–8.
- (35) de Belder, a. N. Handbooks from Amersham Biosciences: Dextran. *Amersham Biosci.* **2003**, 13.
- (36) Ghiulai, R. M.; Sarbu, M.; Ilie, C.; Zamfir, A. D. A Straightforward Electrospray Ionization High Resolution Mass Spectrometry Method for Underivatized Long Chain Polysaccharides. *Open Chem.* **2015**, *13* (1), 32–41.
- (37) Feng, S.; Bagia, C.; Mpourmpakis, G. Determination of Proton Affinities and Acidity Constants of Sugars. *J. Phys. Chem. A* **2013**, *117* (24), 5211–5219.
- (38) Zaia, J. Mass Spectrometry of Oligosaccharides. *Mass Spectrom. Rev.* **2004**, *23* (3), 161–227.
- (39) Mock, K. K.; Davey, M.; Cottrell, J. S. The Analysis of Underivatized Oligosaccharides by Matrix-Assisted Laser Desorption Mass Spectrometry. *Biochem. Biophys. Res. Commun.*

- 1991**, *177* (2), 644–651.
- (40) Stahl, B.; Steup, M.; Karas, M.; Hillenkamp, F. Analysis of Neutral Oligosaccharides by Matrix-Assisted Laser Desorption/Ionization Mass Spectrometry. *Anal. Chem.* **1991**, *63* (14), 1463–1466.
- (41) Hsu, N.-Y.; Yang, W.-B.; Wong, C.-H.; Lee, Y.-C.; Lee, R. T.; Wang, Y.-S.; Chen, C.-H. Matrix-Assisted Laser Desorption/Ionization Mass Spectrometry of Polysaccharides with 2',4',6'-Trihydroxyacetophenone as Matrix. *Rapid Commun. Mass Spectrom.* **2007**, *21* (13), 2137–2146.
- (42) Bahr, U.; Karas, M.; Hillenkamp, F. Analysis of Biopolymers by Matrix-Assisted Laser Desorption/Ionization (MALDI) Mass Spectrometry. *Fresenius. J. Anal. Chem.* **1994**, *348* (12), 783–791.
- (43) Mann, M.; Meng, C. K.; Fenn, J. B. Interpreting Mass Spectra of Multiply Charged Ions. *Anal. Chem.* **1989**, *61* (15), 1702–1708.
- (44) Vasanthi, K. Biodegradable Polymers - A Review. *Polym. Sci.* **2017**, *3*, 1–7.
- (45) Doppalapudi, S.; Jain, A.; Khan, W.; Domb, A. J. Biodegradable Polymers-an Overview. *Polym. Adv. Technol.* **2014**, *25* (5), 427–435.
- (46) Sudesh, K.; Doi, Y. Molecular Design and Biosynthesis of Biodegradable Polyesters. *Polym. Adv. Technol.* **2000**, *11* (8–12), 865–872.
- (47) Luckachan, G. E.; Pillai, C. K. S. Biodegradable Polymers- A Review on Recent Trends and Emerging Perspectives. *J. Polym. Environ.* **2011**, *19* (3), 637–676.
- (48) Leja, K.; Lewandowicz, G. Polymer Biodegradation and Biodegradable Polymers - a Review. *Polish J. Environ. Stud.* **2010**, *19* (2), 255–266.
- (49) Nair, L. S.; Laurencin, C. T. Biodegradable Polymers as Biomaterials. *Prog. Polym. Sci.*

- 2007**, 32 (8–9), 762–798.
- (50) Mangeon, C.; Renard, E.; Thevenieau, F.; Langlois, V. Networks Based on Biodegradable Polyesters: An Overview of the Chemical Ways of Crosslinking. *Mater. Sci. Eng. C* **2017**, 80, 760–770.
- (51) Manavitehrani, I.; Fathi, A.; Badr, H.; Daly, S.; Negahi Shirazi, A.; Dehghani, F. Biomedical Applications of Biodegradable Polyesters. *Polymers (Basel)*. **2016**, 8 (1), 20.
- (52) Browning, M. B.; Cereceres, S. N.; Luong, P. T.; Cosgriff-Hernandez, E. M. Determination of the in Vivo Degradation Mechanism of PEGDA Hydrogels. *J. Biomed. Mater. Res. Part A* **2014**, 102 (12), 4244–4251.
- (53) Dempsey, D. K.; Carranza, C.; Chawla, C. P.; Gray, P.; Eoh, J. H.; Cereceres, S.; Cosgriff-Hernandez, E. M. Comparative Analysis of in Vitro Oxidative Degradation of Poly(Carbonate Urethanes) for Biostability Screening. *J. Biomed. Mater. Res. Part A* **2014**, 102 (10), 3649–3665.
- (54) Tortolano, L.; Hammami, S.; Manerlax, K.; Do, B.; Yagoubi, N. RP-HPLC Detection and Dosage Method for Acrylic Monomers and Degradation Products Released from Implanted Medical Devices. *J. Chromatogr. B* **2016**, 1038, 26–33.
- (55) Chen, F.; Qi, R.; Huyer, L. D.; Amsden, B. G. Degradation of Poly(5-Hydroxy-Trimethylene Carbonate) in Aqueous Environments. *Polym. Degrad. Stab.* **2018**, 158, 83–91.
- (56) Sikorska, W.; Adamus, G.; Dobrzynski, P.; Libera, M.; Rychter, P.; Krucinska, I.; Komisarczyk, A.; Cristea, M.; Kowalczyk, M. Forensic Engineering of Advanced Polymeric Materials – Part II: The Effect of the Solvent-Free Non-Woven Fabrics Formation Method on the Release Rate of Lactic and Glycolic Acids from the Tin-Free

- Poly(Lactide-Co-Glycolide) Nonwovens. *Polym. Degrad. Stab.* **2014**, *110*, 518–528.
- (57) Carter, S.; Kavros, A.; Rimmer, S. The Enzymatic Synthesis of Some Functional Oligomers Based on ϵ -Caprolactone or Vinyl Acetate Repeat Structures. *React. Funct. Polym.* **2001**, *48* (1–3), 97–105.
- (58) Kowalczyk, M.; Adamus, G. Mass Spectrometry for the Elucidation of the Subtle Molecular Structure of Biodegradable Polymers and Their Degradation Products. *Mass Spectrom. Rev.* **2016**, *35* (1), 188–198.
- (59) Zhou, H.-C.; Long, J. R.; Yaghi, O. M. Introduction to Metal–Organic Frameworks. *Chem. Rev.* **2012**, *112* (2), 673–674.
- (60) Keskin, S.; Kizilel, S. Biomedical Applications of Metal Organic Frameworks. *Ind. Eng. Chem. Res.* **2011**, *50* (4), 1799–1812.
- (61) Furukawa, H.; Cordova, K. E.; O’Keeffe, M.; Yaghi, O. M. The Chemistry and Applications of Metal-Organic Frameworks. *Science* **2013**, *341* (6149), 1230444–1230444.
- (62) Mason, J. A.; Oktawiec, J.; Taylor, M. K.; Hudson, M. R.; Rodriguez, J.; Bachman, J. E.; Gonzalez, M. I.; Cervellino, A.; Guagliardi, A.; Brown, C. M.; et al. Methane Storage in Flexible Metal-Organic Frameworks with Intrinsic Thermal Management. *Nature* **2015**, *527* (7578), 357–361.
- (63) Jagadeesh, R. V.; Murugesan, K.; Alshammari, A. S.; Neumann, H.; Pohl, M. M.; Radnik, J.; Beller, M. MOF-Derived Cobalt Nanoparticles Catalyze a General Synthesis of Amines. *Science* **2017**, *358* (6361), 326–332.
- (64) Horcajada, P.; Chalati, T.; Serre, C.; Gillet, B.; Sebrie, C.; Baati, T.; Eubank, J. F.; Heurtaux, D.; Clayette, P.; Kreuz, C.; et al. Porous Metal-Organic-Framework Nanoscale Carriers as a Potential Platform for Drug Delivery and Imaging. *Nat. Mater.* **2010**, *9* (2), 172–178.

- (65) Zhou, H.-C. “Joe”; Kitagawa, S. Metal–Organic Frameworks (MOFs). *Chem. Soc. Rev.* **2014**, *43* (16), 5415–5418.
- (66) Harding, J. L.; Reynolds, M. M. Metal Organic Frameworks as Nitric Oxide Catalysts. *J. Am. Chem. Soc.* **2012**, *134* (7), 3330–3333.
- (67) Neufeld, M. J.; Lutzke, A.; Tapia, J. B.; Reynolds, M. M. Metal–Organic Framework/Chitosan Hybrid Materials Promote Nitric Oxide Release from S - Nitrosoglutathione in Aqueous Solution. *ACS Appl. Mater. Interfaces* **2017**, *9* (6), 5139–5148.
- (68) Huxford, R. C.; Della Rocca, J.; Lin, W. Metal-Organic Frameworks as Potential Drug Carriers. *Curr. Opin. Chem. Biol.* **2010**, *14* (2), 262–268.
- (69) Cadiau, A.; Adil, K.; Bhatt, P. M.; Belmabkhout, Y.; Eddaoudi, M. A Metal-Organic Framework-Based Splitter for Separating Propylene from Propane. *Science* **2016**, *353* (6295), 137–140.
- (70) Duerinck, T.; Denayer, J. F. M. Metal-Organic Frameworks as Stationary Phases for Chiral Chromatographic and Membrane Separations. *Chem. Eng. Sci.* **2015**, *124*, 179–187.
- (71) Das, S.; Xu, S.; Ben, T.; Qiu, S. Chiral Recognition and Separation by Chirality-Enriched Metal–Organic Frameworks. *Angew. Chemie - Int. Ed.* **2018**, *57* (28), 8629–8633.
- (72) Navarro-Sánchez, J.; Argente-García, A. I.; Moliner-Martínez, Y.; Roca-Sanjuán, D.; Antypov, D.; Campíns-Falcó, P.; Rosseinsky, M. J.; Martí-Gastaldo, C. Peptide Metal-Organic Frameworks for Enantioselective Separation of Chiral Drugs. *J. Am. Chem. Soc.* **2017**, *139* (12), 4294–4297.
- (73) Peng, Y.; Gong, T.; Zhang, K.; Lin, X.; Liu, Y.; Jiang, J.; Cui, Y. Engineering Chiral Porous Metal-Organic Frameworks for Enantioselective Adsorption and Separation. *Nat. Commun.*

- 2014**, 5 (1), 4406.
- (74) Nguyen, L. A.; He, H.; Pham-Huy, C. Chiral Drugs: An Overview. *Int. J. Biomed. Sci.* **2006**, 2 (2), 85–100.
- (75) Ward, T. J.; Ward, K. D. Chiral Separations: A Review of Current Topics and Trends. *Anal. Chem.* **2012**, 84 (2), 626–635.
- (76) Sun, B.; Kim, Y.; Wang, Y.; Wang, H.; Kim, J.; Liu, X.; Lee, M. Homochiral Porous Nanosheets for Enantiomer Sieving. *Nat. Mater.* **2018**, 17 (7), 599–604.

CHAPTER 2

DERIVATIZATION OF DEXTRAN TO IMPROVE ELECTROSPRAY IONIZATION TIME-OF-FLIGHT MASS SPECTROMETRIC ANALYSIS OF POLYSACCHARIDES

2.1 Background

The use of NO-releasing materials for biomedical applications have been extensively studied in Prof. Melissa M. Reynolds group to combat bacterial infections and device biofouling. The incorporation of stable NO moieties onto polymer substrates such as dextran continues to be a critical part of NO materials development. The work described in this study was originally intended to design a mass spectrometric method to track the degradation of NO-releasing dextran (approx. molecular mass of 40 kDa) as a function of time in the presence of dextranase as NO was released. The hypothesis was that tracking the change in molecular weight could eventually be correlated to the decay of NO-releasing dextran after it is administered intravenously. Preliminary studies revealed that the dextran's molecular mass was too large for the instrument's measurement range, leading to severe changes of the initial hypothesis. The project became a more fundamental study regarding ionization of underivatized dextran and a derivatization study aimed at improving ionization and mass spectrometric measurement of dextran and its derivatives. The initial hypothesis evolved to shift focus to develop an appropriate derivatization procedure for dextran to improve ionization. For this purpose, the goal was to attempt mimicking protein-like ionization for mass spectrometric analysis. Due to the highly available terminal amines found in proteins (such as the basic amino acids arginine, histidine and lysine), proteins with very large molecular weights (up to megadalton range) are ionizable by supercharging them with multiple protonations. This supercharging phenomenon shifts the molecular weight of proteins toward a lower m/z range,

therefore making them measurable within the limits of typical mass spectrometers. Our approach was to find a way to attach the compound ethylenediamine ($\text{H}_2\text{NCH}_2\text{CH}_2\text{NH}_2$) to the dextran in a manner that would leave one of the terminal amine groups freely available. If successful, multiple ethylenediamine attachments would take place allowing for ionization of dextran by means of multiple protonations. The results were promising (as will be shown in this chapter) in that we found a one-pot derivatization technique that allowed ethylenediamine-derivatized dextran to ionize by means of multiple charges, similar to the behavior of proteins when analyzed by MS. This work was originally published in the Journal of The American Society of Mass Spectrometry (Tapia, J. B.; Hibbard, H. A. J.; Reynolds, M. M. Derivatization of Dextran for Multiply Charged Ion Formation and Electrospray Ionization Time-of-Flight Mass Spectrometric Analysis. *J. Am. Soc. Mass Spectrom.* **2017**, 28 (10), 2201–2208). The work has been reprinted with permission from the American Chemical Society (Copyright 2017). The synthetic procedure was designed by Hailey A. J. Hibbard. Characterization of the reactants and products using ATR-IR, H-NMR and MS was done by Jesus B. Tapia. Prof. Melissa M. Reynolds acted as the advisor on this project.

2.2 Introduction

Molecular weight and structural analysis of polysaccharides by mass spectrometry (MS) continues to be a challenging task. Compared to the rate of advances in method development for protein analysis, progress in the use of MS for polysaccharide analysis continues to evolve relatively slowly¹. The most widely used ionization methods for large biomolecules, including polysaccharides, are matrix-assisted laser desorption ionization (MALDI) and electrospray ionization (ESI) coupled with time-of-flight (TOF) mass analyzers^{2,3}. These ionization techniques are commonly used for the analysis of large proteins² and nucleic acids⁴, but both methods have had little success when applied to polysaccharides⁵. The limited success in mass spectrometric

analysis of polysaccharides can be primarily attributed to ionization limitations. Ionization efficiency is low for negative mode ESI because polysaccharides lack the acidic groups typically needed for efficient proton abstraction. Also, for positive mode, ionization efficiency is weak with ESI because polysaccharides have low proton affinity, leading to the more commonly observed metal cation adduct formation⁶⁻⁸.

Even though both MALDI and ESI have been used for ionization of polysaccharides, MALDI has been the preferred method⁹⁻¹². Unfortunately, MALDI is susceptible to lack of reproducibility due to limited control during the crystallization process, which leads to the formation of “sweet spots” (inhomogeneous distribution of analyte in the matrix, leading to localized high analyte signal intensities), as well as higher likelihood of in-source fragmentation¹³⁻¹⁵. Although ESI is typically considered poorly suited for analyzing polysaccharides because it is less effective for ionization of neutral molecules, and sensitivity decreases as the weight of the molecule increases, it does not suffer from the same drawbacks of using MALDI ionization^{7,14,16,17}.

To increase ionization efficiency, derivatization processes that may allow for polysaccharides to carry multiple charges can be used. This would allow for mass spectrometric measurements of multiply-charged polysaccharides. While multiple charges using ESI can be detrimental when complex mixtures are analyzed, this feature could allow high molecular weight polysaccharides to be observed in a low m/z region¹³. To date however, there is limited literature regarding the use of derivatization techniques to enhance ionization of polysaccharides with ESI by means of multiple charges.

2.2.1 Dextran

An early study of dextran was performed by Pasteur in which it was proven that dextran formation in wine was caused by microbial activity¹⁸. The term “dextran” was coined after

Scheibler¹⁹ determined that dextran was a carbohydrate of the empirical formula $(C_6H_{10}O_6)_n$ having a positive optical rotation. The dextran-forming bacterium *Leuconostoc mesenteroides* was identified by Van Tieghem²⁰ and further investigated by Beijerinck²¹ and Hehre²². Historically, scientific interest in dextran was stimulated by studies suggesting its use as a blood plasma volume expander (BPE)²³.

Dextran is defined as a homopolysaccharide of glucose that exhibits primarily consecutive α -1,6-glycosidic linkages in the major chain (Figure 2.1)^{15,24-27}. These α -D-glucan can also possess side chains stemming from α -1,2-, α -1,3-, or α -1,4- branch linkages. The exact structure, branching type and degree of branching depends on its specific microbial strain of origin. Dextran from the lactic acid bacteria strain *Leuconostoc mesenteroides* NRRL B-512F are the most widely used due to the presence of ~95% linear α -1,6-linkages^{15,28,29}.

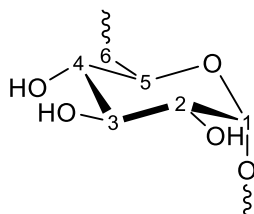


Figure 2.1 Structure of dextran. Dextran is a homopolysaccharide of glucose primarily composed of α -1,6-glycosidic linkages.

Dextran is biosynthesized by the enzyme dextransucrase which catalyzes the production of dextran from sucrose. The majority of dextrans in nature are secreted mainly by *Leuconostoc*, *Streptococcus* and *Lactobacillus* bacterial species. *Leuconostoc mesenteroides* NRRL B512F dextransucrase has received the most attention and it is utilized to produce dextran commercially due to its linearity. Dextransucrase is an extracellular glucosyltransferase (GTF), which catalyzes the transfer of D-glucose residues from sucrose to dextran, releasing fructose as a byproduct (Figure 2.2)²⁶.

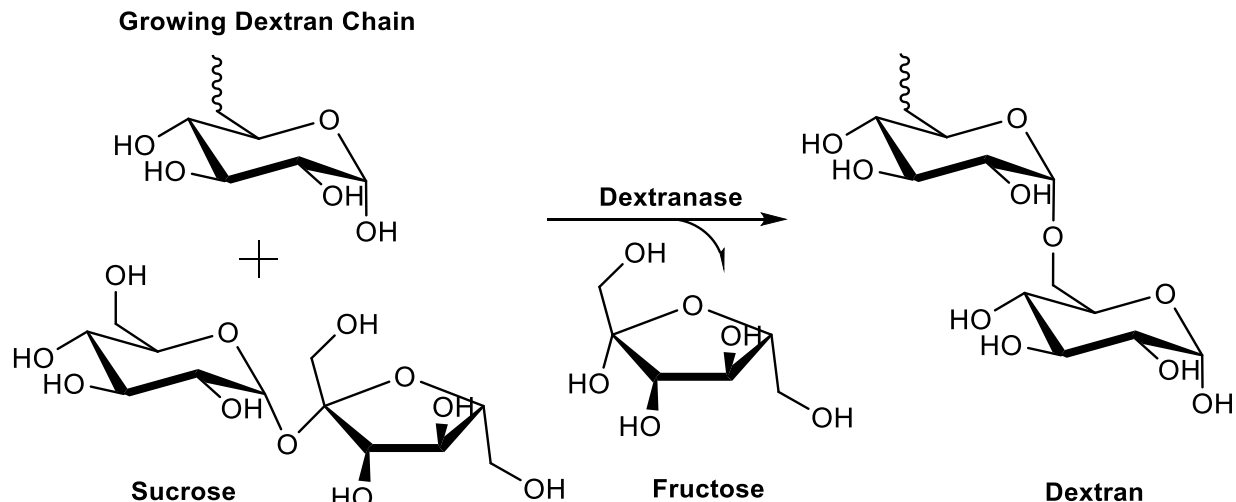


Figure 2.2 Synthesis of dextran. Dextranase adds glucose monomers to the growing dextran chain by attaching a new glucose unit to the reducing end and giving fructose as the byproduct.

2.2.2 Dextran Uses and Applications

As a naturally occurring polysaccharide, there has been interest in the development of useful applications for native dextran, partially degraded dextran, and its derivatives (summarized in Table 2.1). At the end of 1942, considerable effort was put at the time to the freeze-drying of blood plasma for military medicine. Within a few months, the idea of using a hydrolyzed dextran as a plasma substitute was discovered^{15,25,30}. After a series of studies, a Swedish pharmaceutical company adopted the project in 1943. The dextran used at the time was derived from *Leuconostoc mesenteroides* 7E, from which the use of a 6% dextran (fraction) solution was approved for clinical use in Sweden, and shortly thereafter, in the UK^{15,26}. Eventually, the dextran utilized was optimized and designated Dextran 70 (70 kDa). The production of clinical dextran has since grown throughout the world and Dextran 70 is generally marketed as a 6% solution in normal saline and continues to be the plasma volume expander of choice. This clinical dextran is recommended for the treatment of shock or impending shock due, for example, to hemorrhage, severe burns, surgery or trauma as well as reducing the risk for thrombosis^{15,25,30}.

Table 2.1 Applications of Dextran

Applications	Reference(s)
Bakery Improves freshness, mouthfeel, softness, crumb texture, loaf volume, and shelf life	31
Ice Cream, Frozen and Dried foods Cryoprotectant and protection from oxidation and chemical changes and preservation in texture and flavor	15,32
Cheese Making Improves water binding and increases moisture in nonfat cheese	33
Blood Plasma Expander Therapeutic agent in restoring blood plasma volume	15,24,32,34
Anemia Treatment Iron dextran derivative intravenously administered to alleviate iron deficiency anemia	35
Separations Purification/separation of proteins, nucleic acids and polysaccharides	15

2.2.3 Current Methods for Dextran Analysis

Size exclusion chromatography (SEC) has been and continues to be the major choice to obtain molecular mass information of polysaccharides¹⁴, along with other techniques including field-flow fractionation (FFF)³⁶. Dextran studies have been monitored by analyzing the polysaccharide primarily by coupling SEC with refractive index (RI) and/or light scattering detection (LS)^{14,36}. To obtain molecular mass measurements of dextran, a calibration curve is obtained by utilizing a set of dextran standards with known molecular masses that correlate molecular mass with retention time/volume³⁶. Unfortunately, the use of SEC with RI and or/LS detection generally provides results with poor resolution that only allow for an estimate of the molecular mass. This is an issue when we need to observe single monomer changes in molecular

weight due to degradation over time. Under typical SEC conditions, it is not easily possible to measure such small changes in molecular weight of polysaccharides/polymers. If the goal is to perform real time measurements, time sensitive measurements, or time-point degradation measurements, single monomer unit changes would not be observed. Therefore, MS detection would be able to detect subtle changes in MW from the starting polymer while simultaneously detecting increase(s) in abundance of the monomer units.

2.2.4 Derivatization Method for Dextran to Achieve Improved Ionization Efficiency

In this study, we investigated the use of a derivatization technique to impart charged functional moieties onto dextran to enhance its ability to ionize in a TOF MS. Dextran was chosen because it is a difficult polysaccharide to ionize due to the lack of acidic groups for proton abstraction and its low proton affinity for proton adduction. To encourage ionization of dextran by means of multiple proton adducts for ESI-TOF MS analysis, we used a one-pot derivatization procedure with ethylenediamine that has been previously utilized as the first step to produce water soluble Dextran-Taxol conjugates³⁷. We selected dextran-T1 (approximately 1 kDa) because its molecular weight allowed us to track the mass changes and determine the number of ethylenediamine attachments from underivatized to derivatized dextran T1 (EDA-dex-T1). With the attached groups, we took advantage of multiply charged ions typical of ESI to observe a shift of the molecular weight distribution toward the low m/z region in the form of ions with multiple charges, depending on the number of successful attachments. To the best of our knowledge, this is the first report of successful use of multiple charges via ESI to analyze the polysaccharide dextran in the form of multiple proton adducts.

2.3 Experimental

2.3.1 Chemicals

1,1'-Carbonyldiimidazole (CDI) was obtained from Sigma (St Louis, MO, USA). Dextran T1 (average $M_r \sim 1100$) was obtained from Pharmacosmos (Holbaek, Denmark). Spectra/Por dialysis membranes with a molecular weight cutoff of 100–500 Da were obtained from Spectrum Labs (Rancho Domingues, CA, USA). Ethylenediamine (Alfa Aesar), dimethyl sulfoxide (DMSO), liquid chromatography–MS grade methanol, liquid chromatography–MS grade water, herein referred to as methanol and water, were obtained from VWR (Denver, CO, USA). All chemicals were used as received without further purification.

2.3.2 Derivatization Procedure

The derivatization of dextran was performed on a half-gram scale, following an established procedure³⁷ (Figure 2.3) in which 0.5 g dextran was dissolved in 6 mL DMSO, to which a solution of 0.2 g 1,1'-carbonyldiimidazole dissolved in 2 mL DMSO was added, and the reaction was allowed to proceed for 15 min at 60 °C to activate the dextran. Following the activation step, 1 mL ethylenediamine was added and the resulting mixture was allowed to react for 18 h at 60 °C. After the reaction reached completion, the mixture was allowed to reach room temperature, and the EDA-dex-T1 was precipitated out of the DMSO with use of excess methanol. The precipitate was then filtered by vacuum filtration and washed with methanol to remove any DMSO still present and impurities soluble in methanol. The solid was then re-dissolved in Millipore water and dialyzed for 24 h in 0.5% w/v NaCl solution and then for an additional 24 h in 0.01% v/v acetic acid solution. The dialyzed product was then lyophilized for 4 days to recover the purified solid. The recovered solid was stored at -20 °C until analysis.

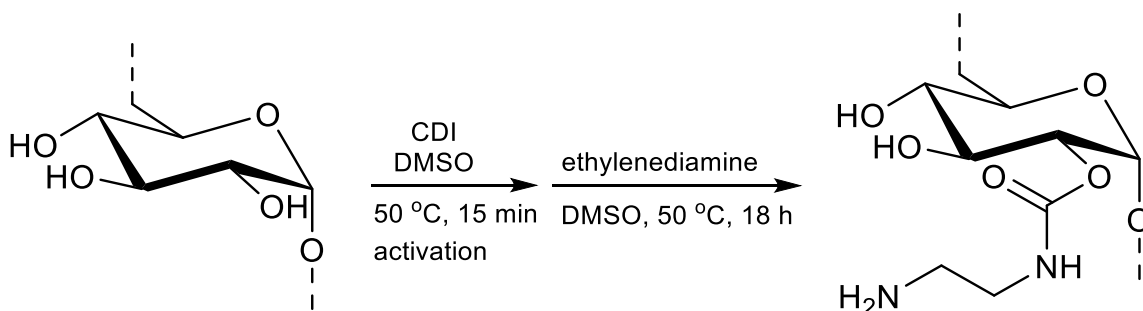


Figure 2.3 Derivatization of dextran. This one-pot derivatization produced EDA-dex with the purpose of giving dextran free terminal amine groups.

2.3.3 General Characterization Techniques

NMR spectra were obtained with a Varian Inova 400-MHz Fourier transform NMR spectrometer (Agilent Technologies Inc., Santa Clara, CA, USA). ^1H NMR spectra were referenced relative to the solvent (DMSO) and tetramethylsilane (TMS). Attenuated total reflectance (ATR) Fourier transform infrared (FT-IR) spectra were collected between 650 and 4000 cm^{-1} with a Nicolet 6700 FT-IR spectrometer (Thermo Electron Corp., Madison, WI, USA) fitted with a Smart iTR ATR sampling accessory and a ZnSe crystal plate.

2.3.4 Mass Spectrometry

ESI-TOF MS. All experiments were performed with a 6224 TOF mass spectrometer (Agilent, Palo Alto, CA, USA) equipped with a dual electrospray ion source operated in positive mode. EDA-dex-T1 solutions were prepared at a concentration of 1 mg/mL in 0.1% acetic acid solution. The solutions were directly injected into the ion source (without a pre-separation step) at a flow rate of 0.15 mL/min with use of the autosampler on a 1260 Infinity high-performance liquid chromatograph (Agilent, Palo Alto, CA, USA) with an isocratic mobile phase consisting of 90% water and 10% methanol, both with 0.1% acetic acid. The ion source conditions were as follows: 4.0-kV capillary voltage, 80-V fragmentor voltage, 75-V skimmer voltage, 650-V octopole voltage, 12.5 L/min gas flow (N_2), and 45-psi nebulizer pressure. The detection range was set at 100–3200 m/z .

ESI-MS/MS. All MS/MS experiments were performed with a Thermo Finnigan linear trap quadrupole (LTQ) equipped with an ESI probe operated in positive mode. Underivatized dextran T1 solutions were prepared at a concentration of 1 mg/mL in a methanol–water (40:60, v/v), and the EDA-dex-T1 solutions were prepared at a concentration of 1 mg/mL in 0.1% acetic acid solution. The solutions were directly injected into the ion source by syringe infusion at a flow rate of 15 μ L/min. The following instrument conditions were automatically optimized: electrospray voltage, heated capillary temperature (voltage), tube lens voltage, capillary voltage, sheath gas flow rate, auxiliary gas flow rate and sweep gas flow rate (N_2). The conditions were automatically adjusted with use of the automatic tune function optimizing on ion m/z 689 for dextran T1 (m/z of 689 corresponds to a four-glucose monomer dextran with a sodium adduct) and on ion m/z 753 for EDA-dex-T1 (m/z 753 corresponds to a four-glucose monomer dextran with one ethylenediamine attachment and a proton adduct). For the fragmentation studies, the collision-induced dissociation (CID) energy was set as 30 V.

2.3.5 Data Analysis

Data were reported from a minimum of triplicate measurements, unless otherwise noted, and all data were analyzed with Agilent MassHunter Qualitative Analysis B.07.00 (ESI-TOF data) and Thermo Xcalibur Qual Browser 2.2 SP1.48 (ESI-MS/MS data).

2.4 Results and Discussion

2.4.1 Initial derivatization techniques for dextran

2.4.1.1 Carboxymethylation of dextran

Carboxymethylation of dextran to produce carboxymethylated dextran (CM-dextran) was the first derivatization attempted to improve ionization of dextran (Figure 2.4). The purpose of this derivatization was to attach free terminal carboxylic acid groups with to improve ionization in

negative polarity. The derivatization procedure was performed as follows, following a previously established procedure³⁸: dextran-6 (6 kDa, 5 g) and sodium hydroxide (5 g) were mixed together in 125 mL 80% isopropanol (IPA) solution in Millipore water and stirred at 60 °C until a clear solution was obtained. A solution of chloroacetic acid (5.62 g) in 40 mL 80% IPA solution was prepared separately and slowly charged to the reaction using a pressure equilibrium addition funnel over a period of 30 min. The reaction was maintained at 60 °C for 5 h and after 5 h, the reaction was cooled to room temperature and the pH was adjusted to 5 by adding glacial acetic acid. The CM-dextran was precipitated into excess methanol and the crude product was isolated by filtration, washed with methanol and dried under vacuum. The CM-dextran was redissolved in 25 mL Millipore water and dialyzed against Millipore water using dialysis membranes for one week with multiple changes per day.

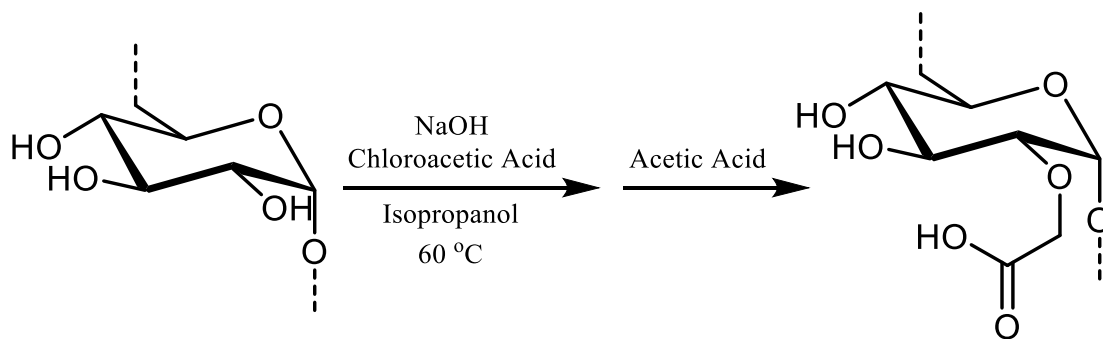


Figure 2.4 Carboxymethylation of dextran. This derivatization produced CM-dextran with the purpose of giving dextran terminal acidic groups.

The obtained CM-dextran was analyzed using ESI-TOF MS with the main purpose of multiply charging dextran in negative mode. The carboxylic acid moieties were excellent candidates for deprotonation that would lead to multiple negative charges, therefore moving the mass of CM-dextran to a lower m/z range. The production of CM-dextran however, did not improve ionization as originally intended and a new derivatization was performed. This was determined by not finding CM-dextran within the 100 – 3200 m/z range of the instrument.

Additionally, using dextran-6 did not give promising results prior to derivatization since the mass was outside the instrument limits.

2.4.1.2 Carbodiimide coupling of ethylenediamine to CM-dextran

While the synthesis of CM-dextran did not improve ionization, CM-dextran was previously shown to be further derivatized³⁸ by using carbodiimide coupling chemistry to form amide bonds between the terminal carboxylic acid and free amines (Figure 2.5).

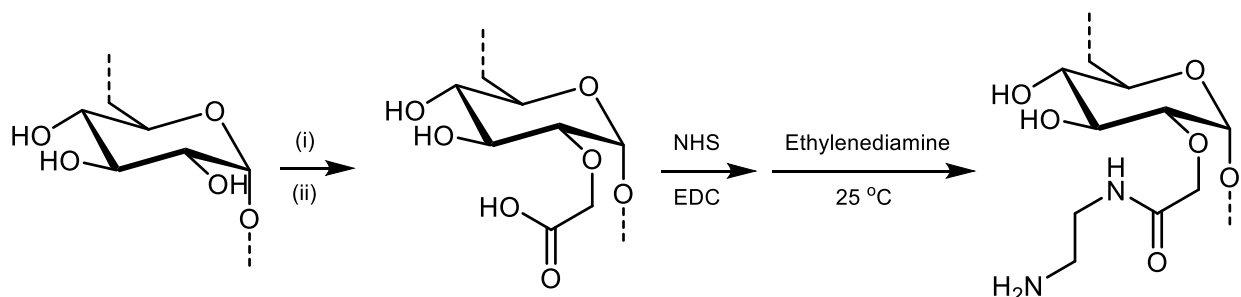


Figure 2.5 Carbodiimide coupling of ethylenediamine to CM-dextran. CM-dextran synthesis: (1) MCA, NaOH, 80% IPA; (ii) acetic acid (see section 2.4.1.1). CM-dextran was used to attach ethylenediamine and give dextran free terminal amine functional groups.

The dextran-ethylenediamine (CM-EDA-dextran) was prepared by first derivatizing dextran using the procedure in section 2.4.1.1 to produce CM-dextran. CM-dextran (1 g) was first pre-activated by reacting with *N*-hydroxysuccinimide (1.5 g) and *N*-(3-dimethylaminopropyl)-*N*'-ethylcarbodiimide hydrochloride (EDC·HCl, 2.5 g) in Millipore water. To this solution, 3.5 g of ethylenediamine were charged. The solution was stirred at 25 °C for 5 h. The produced CM-EDA-dextran was dialyzed against Millipore water using dialysis membranes for one week with multiple changes per day.

The obtained CM-EDA-dextran was analyzed using ESI-TOF MS with the main purpose of multiply charging dextran in positive mode. The free terminal amine moieties were excellent candidates for protonation that would lead to multiple positive charges, therefore moving the mass of CM-EDA-dextran to a lower *m/z* range. The production of CM-EDA-dextran however, did not

improve ionization as originally intended and a new derivatization was performed. The corrections that had to be made were: use dextran with a lower MW that is well within the limits of the instrument to confirm the presence of dextran, and to be able to track the mass changes observed when dextran is derivatized.

2.4.1.3 Final derivatization procedure to synthesize EDA-dextran

The final and successful derivatization procedure, as described in the experimental section (2.3.2 Derivatization Procedure) allowed for a direct attachment of ethylenediamine to dextran. Direct coupling of ethylenediamine to dextran was ideal because the use of harsh conditions to make CM-dextran were avoided, limiting potential degradation of dextran. For this specific reaction procedure, dextran-T1 (Technical grade, 1 kDa) was first characterized to confirm that it was measurable using our instrument (see following sections). Following characterization, dextran was derivatized and characterized using NMR, IR and the developed ESI-TOF MS methodology presented in sections 2.3.3 (General Characterization Techniques) and 2.3.4 (Mass Spectrometry) and explained in the following sections.

2.4.2 Characterization of dextran and EDA-dextran

Derivatization of dextran T1 with ethylenediamine resulted in the attachment of –(C=O)NH(CH₂)₂NH₂ moieties through the formation of carbamate linkages to the polysaccharide as depicted in Figure 2.3. We found the ¹H NMR spectrum of EDA-dex-T1 (Figure 2.6c) to be largely consistent with that of dextran T1 (Figure 2.6b) with broadened features appearing between 3.71 and 2.88 ppm corresponding to the C₂–C₆ protons. The major feature change between dextran T1 and EDA-dex-T1 was the appearance of two proton shifts at 3.01 and 1.87 ppm, corresponding to the methylene groups from –(C=O)NH(CH₂)₂NH₂ attachments. Compared with the spectrum for ethylenediamine (Figure 2.6a), we expected this peak to split into two

different peaks and shift downfield because of the carbamate linkage formation. Infrared spectroscopy (ATR FT-IR) was also performed on dextran T1 and EDA-dex-T1 (Figure 2.7), from which we observed the formation of the carbonyl stretch at 1705 cm^{-1} . This corresponds to the carbonyl on the carbamate linkage formed from derivatization of EDA-dex-T1, further confirming the desired product.

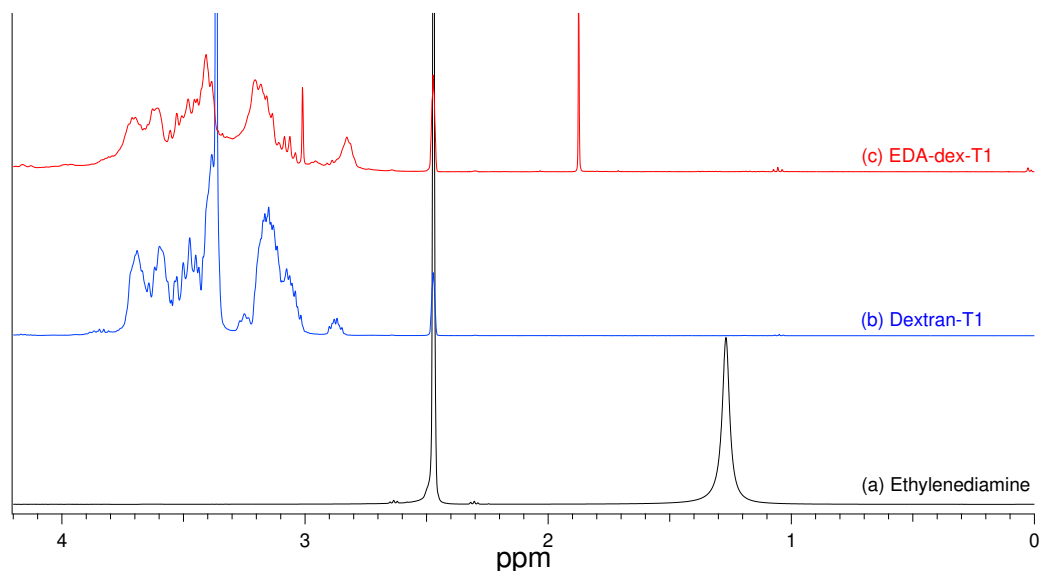


Figure 2.6 ^1H NMR (400 MHz, DMSO, solvent peak $\delta 2.50$ ppm) spectrum of (a) ethylenediamine, $\delta 1.28$ ppm, (b) dextran-T1, $\delta 3.71 - 2.88$ ppm $\text{C}_2 - \text{C}_6$ protons, and (c) $\delta 3.71 - 2.88$ ppm $\text{C}_2 - \text{C}_6$ protons, and $\delta 3.01$ and 1.87 ppm $-(\text{C}=\text{O})\text{NH}(\text{CH}_2)_2\text{NH}_2$ methylene protons.

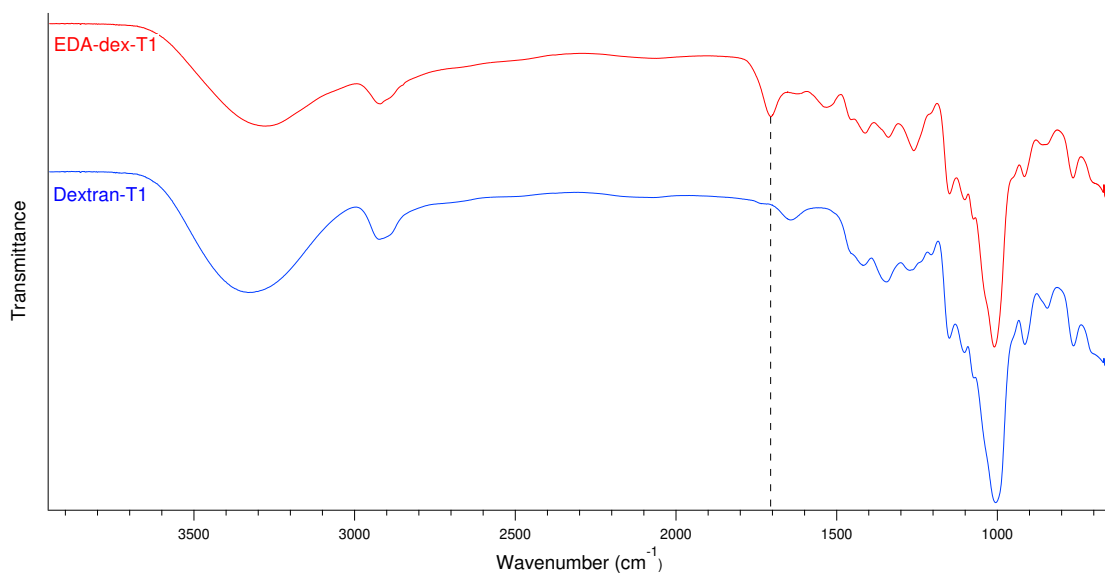


Figure 2.7 Top: ATR-IR spectrum of EDA-dex-T1. IR: Appearance of stretch at 1705 cm^{-1} after derivatization. Bottom: ATR-IR spectrum of dextran-T1.

2.4.3 ESI-TOF MS Analysis of dextran T1 and EDA-dex-T1

We quantified the efficiency of derivatization by counting the number of ethylenediamine attachments and comparing the starting mass spectrum of dextran T1 with the spectrum of EDA-dex-T1. In the ESI mass spectrum shown in Figure 2.8, we observed dextran T1 to range from two to nine repeating glucose residues, corresponding to neutral masses ranging from 342 to 1476 Da as either $[M + \text{NH}_4]^+$ ions or $[M + \text{Na}]^+$ ions, with peak differences of 162 Da that account for one repeating glucose residue. The collected mass spectrum is similar to previously observed distributions for dextran obtained with ESI in which the observed peaks are primarily a product of Na^+ ion adduct formation⁷.

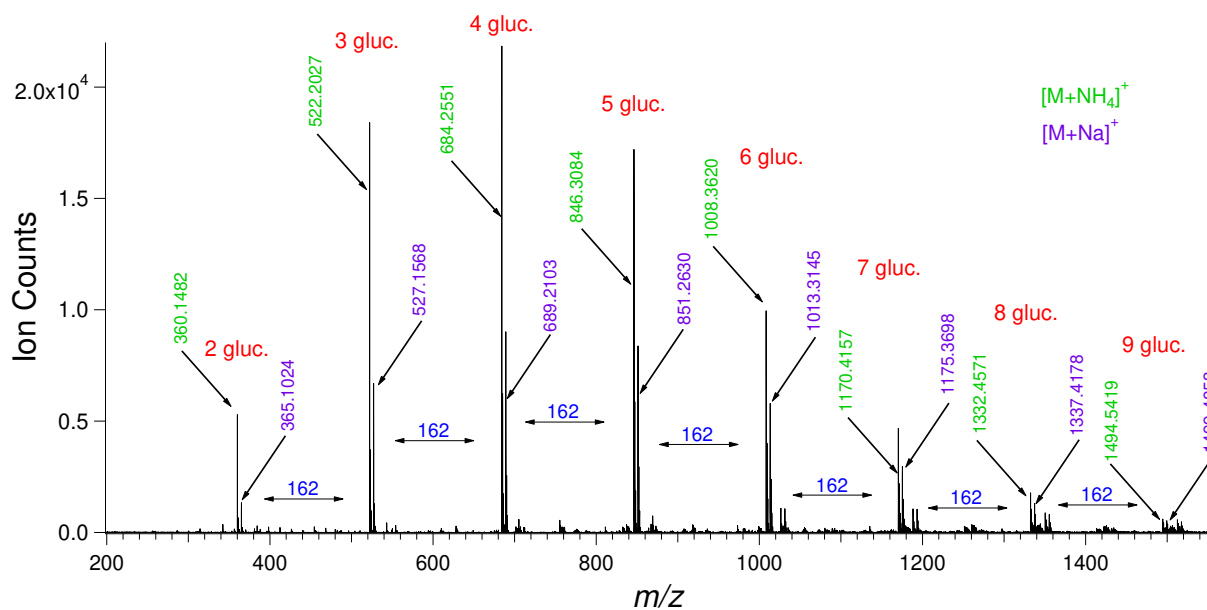


Figure 2.8 Electrospray ionization (ESI) mass spectrum of dextran T1. The observed mass distribution corresponds to two to nine repeating glucose residue chains with the m/z range 360 to 1494 as $[M + \text{NH}_4]^+$ ions and the m/z range from 365 to 1499 as $[M + \text{Na}]^+$ ions. *gluc.* glucose

The ESI mass spectrum generated from EDA-dex-T1 is shown in Figure 2.9. We found that the two to nine glucose unit distribution observed in dextran T1 had been offset by a mass

gain of 86 Da, indicating successful derivatization due to $-(\text{C}=\text{O})\text{NH}(\text{CH}_2)_2\text{NH}_2$ attachment. We observed ionization to have occurred through the formation of H^+ adducts rather than Na^+ or NH_4^+ adducts, one of the intended purposes of derivatizing dextran. The new observed distribution ranged from m/z 429 to m/z 1563 in the form of $[\text{M} + 86 + \text{H}]^+$, which corresponds to a single ethylenediamine attachment onto the dextran.

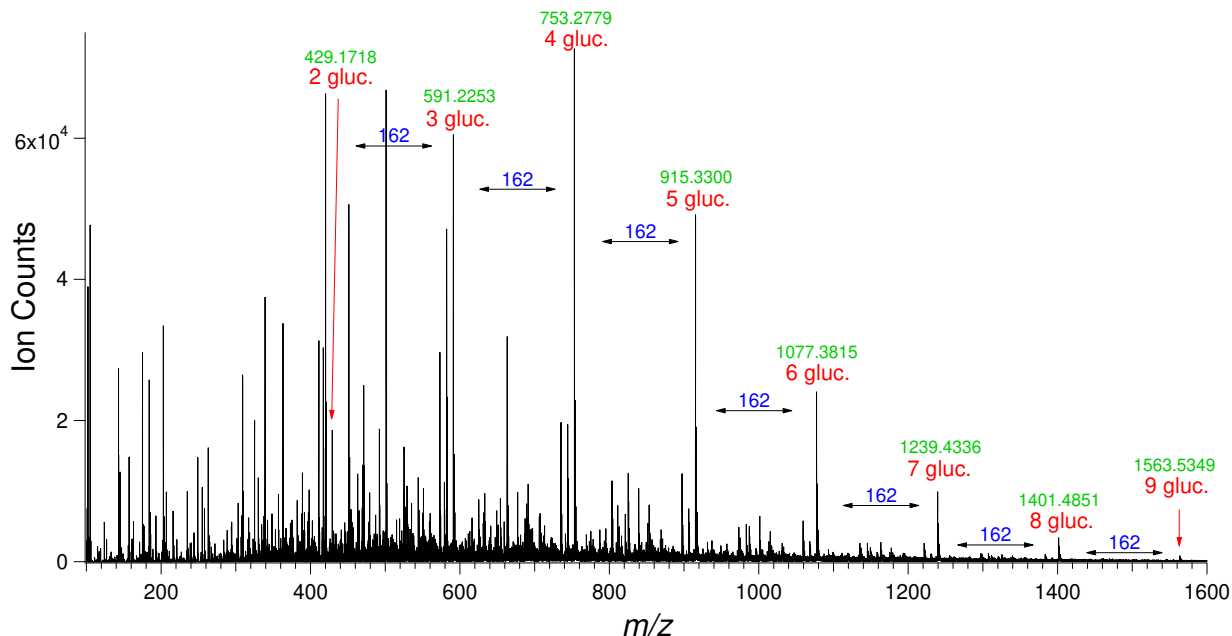


Figure 2.9 ESI mass spectrum for ethylenediamine-derivatized dextran T1 (EDA-dex-T1). The two to nine glucose residue distribution is shown with an m/z range from 429 to 1563 with a mass offset of 86 Da from the dextran T1 distribution. This 86-Da mass increase indicates attachment of a single ethylenediamine to each dextran chain. *gluc.* glucose

On further investigation of each ion, we found that some dextran chains had more than one ethylenediamine attachment. A second distribution that ranged from m/z 258 to m/z 825 corresponded to the same two to nine glucose residue chains, but with two ethylenediamine attachments and two charges (two H^+ adducts). The extracted mass distributions are shown in Figure 2.10, in which the same results for triple attachments/charges (255 to 579 Da) and quadruple attachments/charges (253 to 455 Da) for the two to nine glucose residue chains are observed. The multiply charged ion distributions for derivatized dextran were the first evidence

to show that a polysaccharide can be ionized by means of multiple H^+ adducts. This is remarkably important since we achieved multiple charges on a polysaccharide and shifted the mass distribution toward the lower m/z region, the first step toward reducing the problem of low ionization efficiency for polysaccharides.

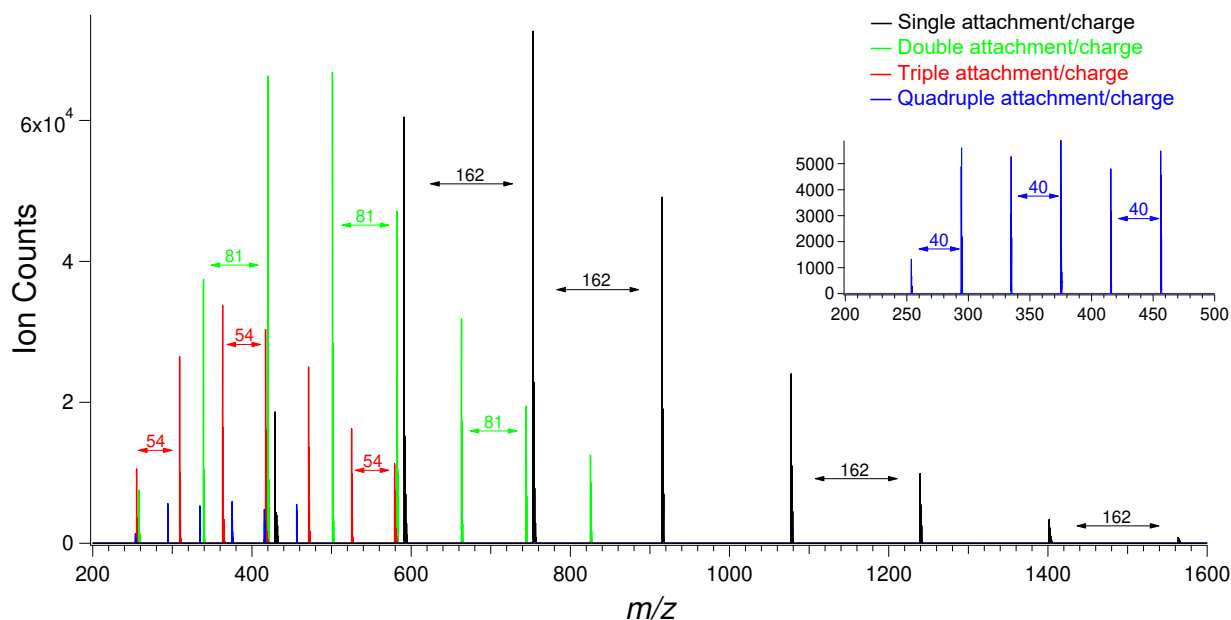


Figure 2.10 Extracted mass distributions showing single attachment/charge to quadruple attachments/charges. For single attachment/charge, we saw the 162 Da mass increments corresponding to a single repeating glucose residue. We observed similar distribution for double attachments/charges, triple attachments/charges, and quadruple attachments/charges with mass increments of 81, 54, and 40 Da respectively, each corresponding to the mass of a single glucose residue (162 Da) divided by the corresponding number of charges

After further investigation of the ion peaks, we found protein-like charge distributions for EDA-dex-T1. For example, in Figure 2.11 we show the charge distribution observed for a four-glucose-unit chain with four ethylenediamine attachments. The three ion peaks correspond to m/z 253, 337, and 506 as 4+, 3+, and 2+ ions respectively, all corresponding to the formula $C_{36}H_{66}N_8O_{25}$ with a deconvoluted mass of 1010 Da. We determined that these ions were multiply charged from the spectrum as indicated by the 0.25-Da interval for the quadruply charged ion, the 0.33-Da interval for the triply charged ion, and the 0.50-Da interval for the doubly charged

ion shown in the insets in Figure 2.11. The remainder of the combinations of ethylenediamine attachments, charges, and charge distributions are shown in Table 2.2.

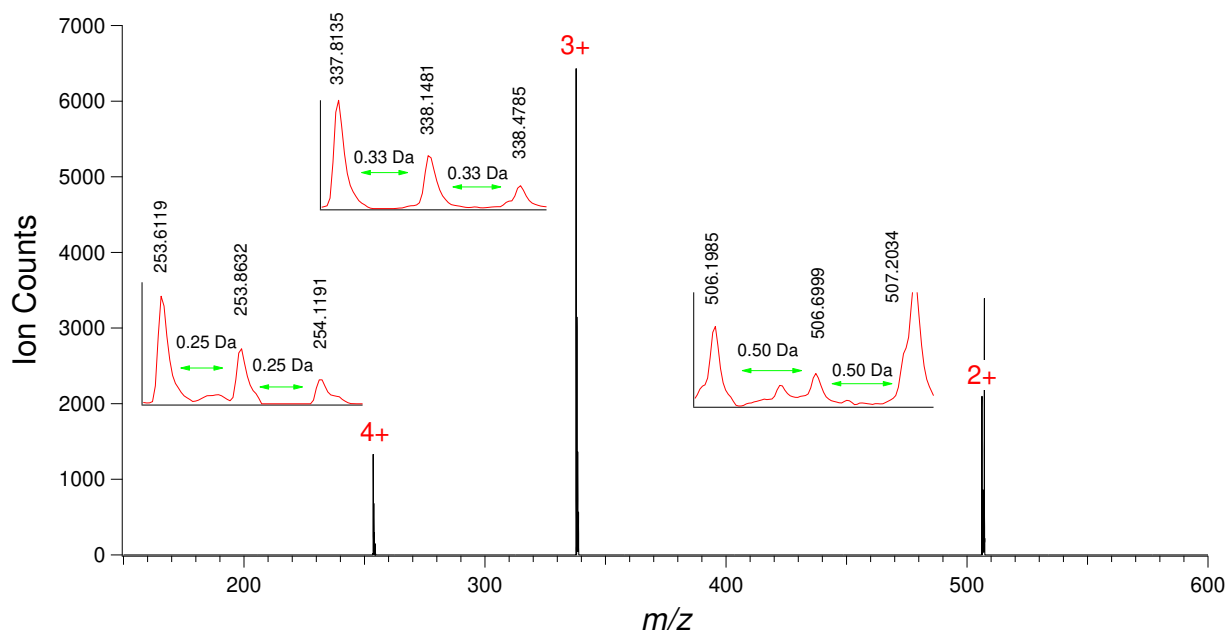


Figure 2.11 Extracted charge distribution showing the peaks 253, 337, and 506 as 4+, 3+, and 2+ respectively. The deconvoluted mass corresponds to $C_{36}H_{66}N_8O_{25}$, or the four-glucose chain with four ethylenediamine attachments with a mass of 1010 Da. The 0.25-, 0.33-, and 0.50-Da intervals for the quadruply, triply and doubly charged ions are shown in the *insets*. Note that the 507.2034 peak exhibited severe peak overlap

Also, we determined that there is also no evidence that EDA-dex-T1 degraded in the sample derivatization, preparation, or ionization as we did not find the m/z 162 or m/z 249 ion peaks that would correspond to a single repeating glucose residue or single-attachment glucose residue, respectively, indicative of glycosidic bond cleavage during our ESI-TOF analyses.

Table 2.2 Assignment of Several Representative Ions for EDA-dex-T1

<i>m/z</i>	Charge, adduct type	Deconvoluted <i>m/z</i>	Formula	# of glucose units	# of attachments
429.1730	+1, H ⁺	428.1652	C ₁₅ H ₂₈ N ₂ O ₁₂	2	1
258.1146	+2, H ⁺	514.2136	C ₁₈ H ₃₄ N ₄ O ₁₃	2	2
591.2256	+1, H ⁺	590.2178	C ₂₁ H ₃₈ N ₂ O ₁₇	3	1
339.1413	+2, H ⁺	676.2670	C ₂₄ H ₄₄ N ₄ O ₁₈	3	2
677.2693	+1, H ⁺	676.2615	C ₂₄ H ₄₄ N ₄ O ₁₈	3	2
255.1129	+3, H ⁺	762.3153	C ₂₇ H ₅₀ N ₆ O ₁₉	3	3
382.1639	+2, H ⁺	762.3122	C ₂₇ H ₅₀ N ₆ O ₁₉	3	3
753.2787	+1, H ⁺	752.2709	C ₂₇ H ₄₈ N ₂ O ₂₂	4	1
420.1676	+2, H ⁺	838.3196	C ₃₀ H ₅₄ N ₄ O ₂₃	4	2
839.3229	+1, H ⁺	838.3151	C ₃₀ H ₅₄ N ₄ O ₂₃	4	2
309.1313	+3, H ⁺	924.3705*	C ₃₃ H ₆₀ N ₆ O ₂₄	4	3
463.1909	+2, H ⁺	924.3662	C ₃₃ H ₆₀ N ₆ O ₂₄	4	3
253.6122	+4, H ⁺	1010.4176	C ₃₆ H ₆₆ N ₈ O ₂₅	4	4
337.8128	+3, H ⁺	1010.4150	C ₃₆ H ₆₆ N ₈ O ₂₅	4	4
506.2108	+2, H ⁺	1010.4060	C ₃₆ H ₆₆ N ₈ O ₂₅	4	4
915.3306	+1, H ⁺	914.3228	C ₃₃ H ₅₈ N ₂ O ₂₇	5	1
501.1942	+2, H ⁺	1000.3728	C ₃₆ H ₆₄ N ₄ O ₂₈	5	2
1001.3760	+1, H ⁺	1000.3682	C ₃₆ H ₆₄ N ₄ O ₂₈	5	2
363.1484	+3, H ⁺	1086.4218	C ₃₉ H ₇₀ N ₆ O ₂₉	5	3
544.2170	+2, H ⁺	1086.4184	C ₃₉ H ₇₀ N ₆ O ₂₉	5	3
1087.4209	+1, H ⁺	1086.4131*	C ₃₉ H ₇₀ N ₆ O ₂₉	5	3
294.1300**	+4, H ⁺	1172.4888*	C ₄₂ H ₇₆ N ₈ O ₃₀	5	4
391.8306	+3, H ⁺	1172.4684	C ₄₂ H ₇₆ N ₈ O ₃₀	5	4
1077.3825	+1, H ⁺	1076.3747	C ₃₉ H ₆₈ N ₂ O ₃₂	6	1
582.2204	+2, H ⁺	1162.4252	C ₄₂ H ₇₄ N ₄ O ₃₃	6	2
1163.4277	+1, H ⁺	1162.4199	C ₄₂ H ₇₄ N ₄ O ₃₃	6	2
417.1667	+3, H ⁺	1248.4767	C ₄₅ H ₈₀ N ₆ O ₃₄	6	3
625.2437	+2, H ⁺	1248.4718	C ₄₅ H ₈₀ N ₆ O ₃₄	6	3
334.6389	+4, H ⁺	1334.5244	C ₄₈ H ₈₆ N ₈ O ₃₅	6	4
445.8480	+3, H ⁺	1334.5206	C ₄₈ H ₈₆ N ₈ O ₃₅	6	4
668.2636	+2, H ⁺	1334.5116*	C ₄₈ H ₈₆ N ₈ O ₃₅	6	4
1239.4347	+1, H ⁺	1238.4269	C ₄₅ H ₇₈ N ₂ O ₃₇	7	1
663.2468	+2, H ⁺	1324.4780	C ₄₈ H ₈₄ N ₄ O ₃₈	7	2
1325.4801	+1, H ⁺	1324.4723	C ₄₈ H ₈₄ N ₄ O ₃₈	7	2
471.1899	+3, H ⁺	1410.5463	C ₅₁ H ₉₀ N ₆ O ₃₉	7	3
706.2701	+2, H ⁺	1410.5246	C ₅₁ H ₉₀ N ₆ O ₃₉	7	3
375.1567**	+4, H ⁺	1496.5956	C ₅₄ H ₉₆ N ₈ O ₄₀	7	4
499.8653**	+3, H ⁺	1496.5725	C ₅₄ H ₉₆ N ₈ O ₄₀	7	4
749.2900**	+2, H ⁺	1496.5644	C ₅₄ H ₉₆ N ₈ O ₄₀	7	4
1401.4879	+1, H ⁺	1400.4801	C ₅₁ H ₈₈ N ₂ O ₄₂	8	1
744.2731	+2, H ⁺	1486.5306	C ₅₄ H ₉₄ N ₄ O ₄₃	8	2
1487.5321	+1, H ⁺	1486.5243	C ₅₄ H ₉₄ N ₄ O ₄₃	8	2
525.2026	+3, H ⁺	1572.5844	C ₅₇ H ₁₀₀ N ₆ O ₄₄	8	3
787.2975	+2, H ⁺	1572.5794	C ₅₇ H ₁₀₀ N ₆ O ₄₄	8	3
415.6656	+4, H ⁺	1658.6312	C ₆₀ H ₁₀₆ N ₈ O ₄₅	8	4
1563.5349	+1, H ⁺	1562.5271	C ₅₇ H ₉₈ N ₂ O ₄₇	9	1
579.2191	+3, H ⁺	1734.6339	C ₆₃ H ₁₁₀ N ₆ O ₄₉	9	3
868.3222	+2, H ⁺	1734.6288	C ₆₃ H ₁₁₀ N ₆ O ₄₉	9	3
456.1802	+4, H ⁺	1820.6896	C ₆₆ H ₁₁₆ N ₈ O ₅₀	9	4

*mass error > 5 ppm

**peak overlap

2.4.4 ESI-MS/MS of dextran T1 and EDA-dex-T1 Trisaccharides

To further investigate the properties of our derivatized dextran, we collected MS/MS data to determine where the ethylenediamine attachments occurred. We collected fragmentation for a dextran T1 trisaccharide, and then compared this with that of an EDA-dex-T1 trisaccharide with single, double, and triple ethylenediamine attachments. The MS/MS spectrum for the dextran T1 trisaccharide is shown in Figure 2.12. We assigned the molecular ions and fragment ions using the nomenclature of Domon and Costello³⁹. We observed fragment ions that correspond to glycosidic bond cleavages, such as C_1 (m/z 203), B_2 (m/z 347), and C_2 (m/z 365), and cross-ring cleavage fragment ions, $^{0,2}A$, $^{0,3}A$, and $^{0,4}A$, which correspond to the second and third residues from the nonreducing end. All the ions we observed in Figure 2.12 we found to be largely consistent with the literature⁴⁰.

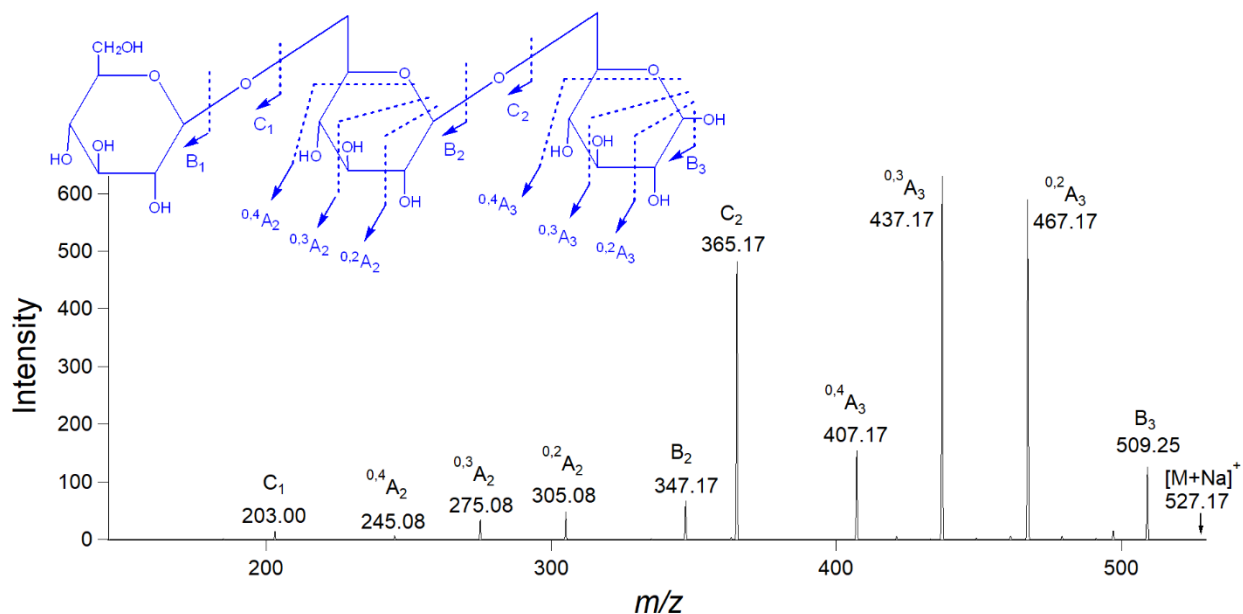


Figure 2.12 Tandem mass spectrometry (MS/MS) spectrum of dextran T1 trisaccharide

The MS/MS spectrum for the EDA-dex-T1 trisaccharide with a single ethylenediamine attachment is shown in Figure 2.13. We observed the fragment ions that correspond to glycosidic bond cleavages such as Z_1 (m/z 249), Y_1 (m/z 267), Z_2 (m/z 411), and Y_2 (m/z 429). We also

identified cross-ring cleavage fragment ions such as $^{0,2}X_1$ (m/z 309), $^{0,2}X_2$ (m/z 471), and $^{1,5}A_3$ (m/z 544), which suggested the location of attachment to be at the C-2 position of the reducing-end glucose monomer. Determination of the exact location of attachment further confirms that ethylenediamine was attached to the dextran trisaccharide and supports our finding that ionization occurred in the form of a proton adduct.

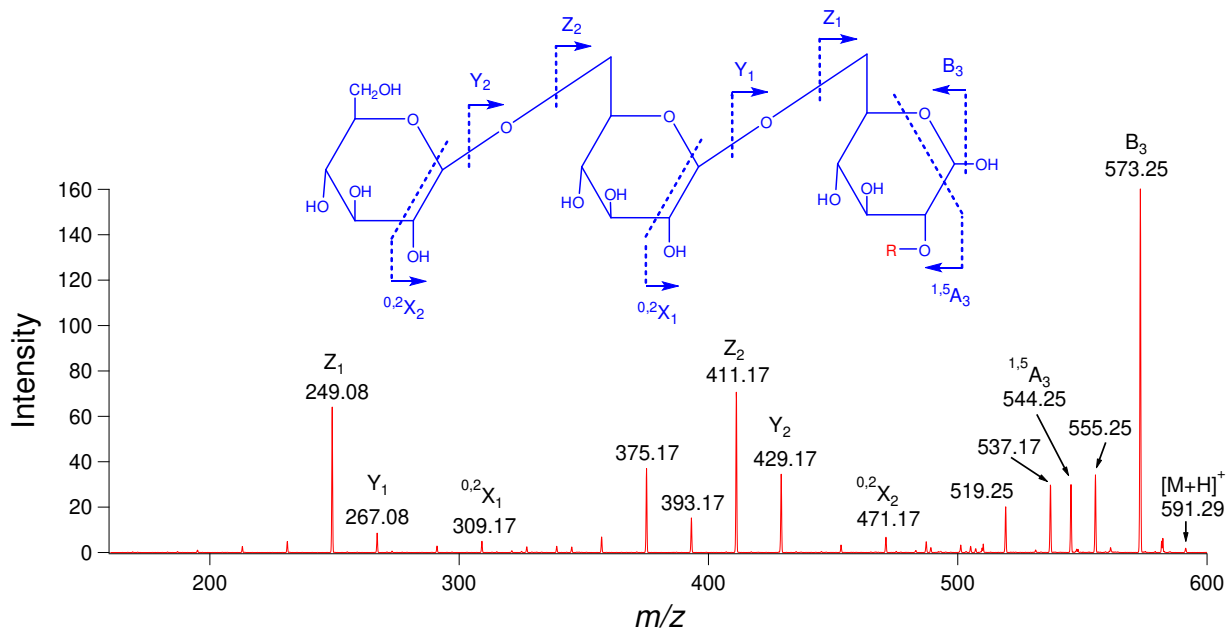


Figure 2.13 MS/MS spectrum of EDA-dex-T1 trisaccharide with a single attachment as indicated by m/z 591. *R* denotes the ethylenediamine attachment ($-(C=O)NH(CH_2)_2NH_2$), which our data suggest to be at the C-2 position of the reducing-end glucose monomer

The MS/MS spectra for the EDA-dex-T1 trisaccharide with double and triple ethylenediamine attachments are shown in Figure 2.14. For EDA-dex-T1 with two attachments (Figure 2.14a), we observed the fragment ions that correspond to glycosidic bond cleavages: C_1 (m/z 353) and C_2 (m/z 515). The ions m/z 353 and m/z 515 indicate that two attachments occurred on the glucose at the nonreducing end, as well as the ions Z_1 (m/z 249), Y_1 (m/z 411), and m/z 573, which suggests that one attachment occurred at the glucose on the reducing end and a second attachment occurred at the glucose on the nonreducing end. This was the first evidence that

suggests attachment to be a random occurrence when more than one ethylenediamine is attached to dextran.

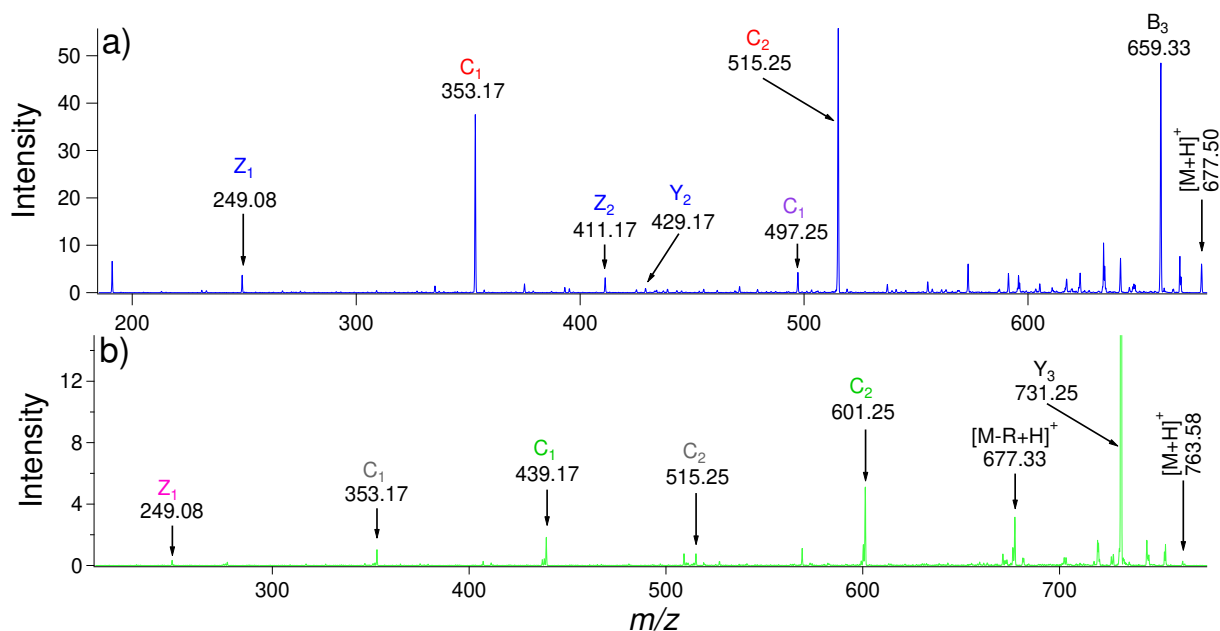


Figure 2.14 MS/MS spectra of EDA-dex-T1 trisaccharide with double and triple ethylenediamine attachments. **a** EDA-dex-T1 with double ethylenediamine attachments as indicated by m/z 677. The fragment ions Z₁, Z₂, and Y₂ in blue are indicative of one attachment at the reducing end and one at the nonreducing end. The fragment ions C₁ and C₂ in red are indicative of two attachments at the glucose at the nonreducing end and the fragment ion C₁ in purple is indicative of one attachment at the middle glucose and a second attachment at the reducing-end glucose. **b** EDA-dex-T1 with triple ethylenediamine attachments as indicated by m/z 763. The fragment ion Z₁ in pink is indicative of a single attachment at the reducing end and the fragment ions C₁ and C₂ in green are indicative of three attachments at the glucose at the nonreducing end. The fragment ions C₁ and C₂ in gray are indicative of two attachments at the glucose at the nonreducing end and the third attachment at the reducing-end glucose

For EDA-dex-T1 with three attachments (Figure 2.14b) we also observed fragment ions that correspond to glycosidic bond cleavages, such as C₁ (m/z 353 and 439) and C₂ (m/z 515 and 601). The C₁ (m/z 439) ion was further indicative of random ethylenediamine attachment since it corresponds to all three attachments occurring at the glucose at the nonreducing end. This further suggests that attachment of multiple ethylenediamine groups to dextran occurs at random available hydroxyl groups on the polysaccharide. Even though attachment of ethylenediamine to

dextran appears to be random, our goal of achieving multiple proton adducts was not diminished by this phenomenon as we show in Figures 2.9 and 2.10 and Table 2.2.

2.5 Conclusions

This is the first report of a simple, one-pot derivatization of a polysaccharide that allows for multiple charge ionization, typical of proteins and glycoproteins, but not previously shown for polysaccharides. ESI-MS is capable of detecting derivatized dextran by allowing for multiple charging and thus shifting detection of the polysaccharide toward lower m/z ratios. The one-pot derivatization reaction was ideal to attach ethylenediamine groups via carbamate bonds to the polysaccharide resulting in EDA-dex-T1. Evidence of single attachment/charge to quadruple attachment/charge was shown, as well as protein-like charge distributions with ionization taking place as proton adducts due to the terminal amine groups present in EDA-dex-T1, rather than the more common metal cation adducts seen with underivatized dextran. Our MS/MS studies indicate that multiple attachments to dextran after the derivatization step occur at random locations on the polysaccharide. This did not limit EDA-dex-T1's ability to carry multiple charges and differences in exact location of the attachments did not impair our primary goal of attaching ethylenediamine groups to encourage ionization to take place by proton adduct formation and achieve multiple charges on a polysaccharide. Collectively, the data obtained from this work show that EDA-dex-T1 is capable of ionizing with multiple proton adducts, thereby shifting the molecular weight distribution to the lower m/z ratio detection range. Based on our findings, the derivatization may be adaptable for use with larger molecular weight dextran. For example, with the assumption that only a maximum of four ethylenediamine attachments are possible, theoretically, we could detect dextran with a maximum molecular weight of upwards of 12 kDa resulting in a measured m/z of 3000 Da with four charges using our current derivatization method and instrument settings.

CHAPTER 2 – REFERENCES

- (1) Kailemia, M. J.; Ruhaak, L. R.; Lebrilla, C. B.; Amster, I. J. Oligosaccharide Analysis by Mass Spectrometry: A Review of Recent Developments. *Anal. Chem.* **2014**, *86* (1), 196–212.
- (2) Hillenkamp, F.; Karas, M.; Beavis, R. C.; Chait, B. T. Matrix-Assisted Laser Desorption/Ionization Mass Spectrometry of Biopolymers. *Anal. Chem.* **1991**, *63* (24), 1193-1203.
- (3) Fenn, J. B.; Mann, M.; Meng, C. K.; Wong, S. F.; Whitehouse, C. M. Electrospray Ionization for Mass Spectrometry of Large Biomolecules. *Science* **1989**, *246* (6), 64–71.
- (4) Berkenkamp, S.; Kirpekar, F.; Hillenkamp, F. Infrared MALDI Mass Spectrometry of Large Nucleic Acids. *Science* **1998**, *281* (5374), 260–262.
- (5) Hsu, N.-Y.; Yang, W.-B.; Wong, C.-H.; Lee, Y.-C.; Lee, R. T.; Wang, Y.-S.; Chen, C.-H. Matrix-Assisted Laser Desorption/Ionization Mass Spectrometry of Polysaccharides with 2',4',6'-Trihydroxyacetophenone as Matrix. *Rapid Commun. Mass Spectrom.* **2007**, *21* (13), 2137–2146.
- (6) Feng, S.; Bagia, C.; Mpourmpakis, G. Determination of Proton Affinities and Acidity Constants of Sugars. *J. Phys. Chem. A* **2013**, *117* (24), 5211–5219.
- (7) Čmelík, R.; Štikarovská, M.; Chmelík, J. Different Behavior of Dextran in Positive-Ion and Negative-Ion Mass Spectrometry. *J. Mass Spectrom.* **2004**, *39* (12), 1467–1473.
- (8) Ghiulai, R. M.; Sarbu, M.; Ilie, C.; Zamfir, A. D. A Straightforward Electrospray Ionization High Resolution Mass Spectrometry Method for Underivatized Long Chain Polysaccharides. *Open Chem.* **2015**, *13*, 32–41.

- (9) Karas, M.; Hillenkamp, F. Laser Desorption Ionization of Proteins with Molecular Masses Exceeding 10 000 Daltons. *Anal. Chem.* **1988**, *60* (20), 2299–2301.
- (10) Garrozzo, D.; Impallomeni, G.; Spina, E.; Sturiale, L.; Zanetti, F. Matrix-Assisted Laser Desorption/Ionization Mass Spectrometry of Polysaccharides. *Rapid Commun. Mass Spectrom.* **1995**, *9* (10), 937–941.
- (11) Harvey, D. J. Matrix-Assisted Laser Desorption/Ionization Mass Spectrometry of Carbohydrates. *Mass Spectrom. Rev.* **1999**, *18* (6), 349–450.
- (12) Chang, W. C.; Huang, L. C. L.; Wang, Y. S.; Peng, W. P.; Chang, H. C.; Hsu, N. Y.; Yang, W. Bin; Chen, C. H. Matrix-Assisted Laser Desorption/Ionization (MALDI) Mechanism Revisited. *Anal. Chim. Acta* **2007**, *582* (1), 1–9.
- (13) Ozdemir, A.; Lin, J. L.; Gillig, K. J.; Gulfen, M.; Chen, C. H. Analysis of Saccharides by the Addition of Amino Acids. *J. Am. Soc. Mass Spectrom.* **2016**, *27* (6), 1113–1121.
- (14) Chang, Y. L.; Lee, Y. C.; Yang, W. Bin; Chen, C. H. Ionic Liquid-Assisted Electrospray Ionization of Polysaccharides. *J. Mass Spectrom.* **2011**, *46* (4), 367–375.
- (15) Naessens, M.; Cerdobbel, A.; Soetaert, W.; Vandamme, E. J. Leuconostoc Dextranase and Dextran: Production, Properties and Applications. *J. Chem. Technol. Biotechnol.* **2005**, *80* (8), 845–860.
- (16) Dols, M.; Remaud-Simeon, M.; Monsan, P. F. Dextranase Production by *Leuconostoc Mesenteroides* NRRL B-1299. Comparison with *L. Mesenteroides* NRRL B-512F. *Enzyme Microb. Technol.* **1997**, *20* (7), 523–530.
- (17) Santos, M.; Teixeira, J.; Rodrigues, A. Production of Dextranase, Dextran and Fructose from Sucrose Using *Leuconostoc Mesenteroides* NRRL B512(F). *Biochem. Eng. J.* **2000**, *4* (3), 177–188.

- (18) Pasteur, L. On the Viscous Fermentation and the Butyrous Fermentation. *Bull. Soc. Chim. Fr.* **1861**, *11*, 30–31.
- (19) Scheibler, C. Investigation on the Nature of the Gelatinous Secretion (so-Called Frog's Spawn) Which Is Observed in Production of Beet-Sugar Juices. *Z. Ver. Dtsch. ZuckerInd.* **1874**, *24*, 309–335.
- (20) Van Tieghem, P. On Sugar-Mill Gum. *Ann. Sci. Nat. Bot. Biol. Veg* **1878**, *7*, 180–203.
- (21) Beijerinck, M. W. K. Mucilaginous Substances of the Well Wall Produced from Cane Sugar by Bacteria. *Folia Microbiol.* **1912**, *1*, 377.
- (22) Hehre, E. J. Production from Sucrose of A-Serologically Reactive Polysaccharide by a Sterile Bacterial Extract. *Science*. March 7, 1941, pp 237–238.
- (23) Grönwall, A.; Ingelman, B. Dextran as a Substitute for Plasma. *Nature* **1945**, 45.
- (24) Patel, S.; Majumder, A.; Goyal, A. Potentials of Exopolysaccharides from Lactic Acid Bacteria. *Indian J. Microbiol.* **2012**, *52* (1), 3–12.
- (25) Khalikova, E.; Susi, P.; Korpela, T. Microbial Dextran-Hydrolyzing Enzymes : Fundamentals and Applications. **2005**, *69* (2), 306–325.
- (26) de Belder, a. N. Handbooks from Amersham Biosciences: Dextran. *Amersham Biosci.* **2003**, 13.
- (27) Ahmed, R. Z.; Siddiqui, K.; Arman, M.; Ahmed, N. Characterization of High Molecular Weight Dextran Produced by *Weissella Cibaria* CMGDEX3. *Carbohydr. Polym.* **2012**, *90* (1), 441–446.
- (28) Jeanes, A.; Haynes, W. C.; Wilham, C. A.; Rankin, J. C.; Melvin, E. H.; Austin, M. J.; Cluskey, J. E.; Fisher, B. E.; Tsuchiya, H. M.; Rist, C. E. Characterization and Classification of Dextrans from Ninety-Six Strains of Bacteria 1b. *J. Am. Chem. Soc.* **1954**, *76* (20), 5041–

5052.

- (29) Lindberg, B.; Svensson, S.; Sjövall, J.; Zaidi, N. A. Structural Studies on Dextran from *Leuconostoc Mesenteroides* NRRL B-512. *Acta Chem. Scand.* **1968**, *22*, 1907–1912.
- (30) Kulicke, W. M.; Heinze, T. Improvements in Polysaccharides for Use as Blood Plasma Expanders. *Macromol. Symp.* **2006**, *231*, 47–59.
- (31) Katina, K.; Maina, N. H.; Juvonen, R.; Flander, L.; Johansson, L.; Virkki, L.; Tenkanen, M.; Laitila, A. In Situ Production and Analysis of *Weissella Confusa* Dextran in Wheat Sourdough. *Food Microbiol.* **2009**, *26* (7), 734–743.
- (32) Bhavani, A. L.; Nisha, J. Dextran - The Polysaccharide with Versatile Uses. *Int. J. Pharma Bio Sci.* **2010**, *1* (4), 569–573.
- (33) Awad, S.; Hassan, A. N.; Halaweish, F. Application of Exopolysaccharide-Producing Cultures in Reduced-Fat Cheddar Cheese: Composition and Proteolysis. *J. Dairy Sci.* **2005**, *88* (12), 4195–4203.
- (34) Patel, S.; Kasoju, N.; Bora, U.; Goyal, A. Structural Analysis and Biomedical Applications of Dextran Produced by a New Isolate *Pediococcus Pentosaceus* Screened from Biodiversity Hot Spot Assam. *Bioresour. Technol.* **2010**, *101* (17), 6852–6855.
- (35) Ahsan, N. Intravenous Infusion of Total Dose Iron Is Superior to Oral Iron in Treatment of Anemia in Peritoneal Dialysis Patients: A Single Center Comparative Study. *J. Am. Soc. Nephrol.* **1998**, *9* (4), 664–668.
- (36) Pitkänen, L.; Striegel, A. M. Polysaccharide Characterization by Hollow-Fiber Flow Field-Flow Fractionation with on-Line Multi-Angle Static Light Scattering and Differential Refractometry. *J. Chromatogr. A* **2015**, *1380*, 146–155.
- (37) Nakamura, J.; Nakajima, N.; Matsumura, K.; Hyon, S. H. Water-Soluble Taxol Conjugates

- with Dextran and Targets Tumor Cells by Folic Acid Immobilization. *Anticancer Res.* **2010**, *30* (3), 903–910.
- (38) Damodaran, V. B.; Place, L. W.; Kipper, M. J.; Reynolds, M. M. Enzymatically Degradable Nitric Oxide Releasing S-Nitrosated Dextran Thiomers for Biomedical Applications. *J. Mater. Chem.* **2012**, *22* (43), 23038.
- (39) Domon, B.; Costello, C. E. A Systematic Nomenclature for Carbohydrate Fragmentations in FAB-MS/MS Spectra of Glycoconjugates. *Glycoconj. J.* **1988**, *5* (4), 397–409.
- (40) Yi, L.; Sun, X.; Du, K.; Ouyang, Y.; Wu, C.; Xu, N.; Linhardt, R. J.; Zhang, Z. UP-HILIC-MS/MS to Determine the Action Pattern of Penicillium Sp. Dextranase. *J. Am. Soc. Mass Spectrom.* **2015**, *26* (7), 1174–1185.

CHAPTER 3

DEVELOPMENT OF MASS SPECTROMETRIC METHODS TO IDENTIFY UNKNOWN COMPOUNDS AND REACTION PRODUCTS IN COMPLEX SYSTEMS

3.1 Background

Accurate mass spectrometric measurements using high resolution mass spectrometers is a reasonable approach to characterize and identify known/unknown compounds of interest. This is particularly important during the discovery phase of research projects in which every possible outcome of a process/reaction and the potential for unwanted interferences have not been fully identified. One example is the application of metal–organic frameworks (MOFs) embedded into polymer substrates to induce catalytic release of nitric oxide (NO) from *S*-nitrosothiols (RSNOs). The MOF, Cu-BTtri, used in this project has been widely studied in the Reynolds group because of its water stability. Multiple reports have demonstrated the NO generation capabilities of the CuBTtri MOF alone as well as the MOF-polymer composites materials. While others have extensively studied NO release from these MOF materials, no studies have performed that to determine the other products/byproducts formed from the MOF-catalyzed decomposition of RSNOs to form NO. Originally, it had been hypothesized that the release of NO from *S*-nitrosoglutathione (GSNO) would lead to the formation of glutathione disulfide (GSSG) using our MOF-chitosan films, however, this had not been confirmed experimentally. Additionally, interest in identifying any potential hydrolytic degradation products of the MOF itself would add to full characterization of the system. To test the hypothesis that the decomposition of GSNO via Cu-BBTri would produce NO + GSSH as shown in equation (3.1), samples from the media collected after the NO-release experiments were analyzed using accurate mass MS.

A second example of the power of accurate mass MS is to identify potential chemical interferences in common cell assays. In particular, a MS study was employed to identify interfering compounds in the commonly used, commercially available CellTiter Blue and MTT assays. The purpose of these assays is to assess cell viability spectroscopically by measuring the number of metabolically active cells. Previous studies found that these spectroscopy assays produced false positives or negatives, depending on whether the therapeutic of interest interferes with the cell viability assay¹. For example, colleagues noted that the addition of non-nitrosated, reduced glutathione to a solution of the MTT starting reagent caused the solution to change from yellow to purple, suggesting a chemical transformation. This observation was a critical indicator that the assays typically used to test for viable cells may be susceptible to false positives or negatives in the absence of cells. The possibility for false positives or negatives led to an in-depth study of several small molecules effect on the CellTiter Blue and MTT assays using mass spectrometry. The main question addressed in these interference experiments was whether it would be possible to use accurate mass MS to track the transformation of resazurin to resorufin and MTT to MTT-formazan while in the absence of cells. To do so, the cell viability assays were performed in the presence of compounds suspected of interference while in the absence of cells.

Altogether, this chapter describes mass spectrometric methods were developed to perform the following analyses:

1. To confirm that after NO is released from GSNO in the presence of chitosan-CuBTTri films, the byproduct is oxidized glutathione (GSSG);
2. To probe for the presence of H₃BTTri during the reaction mentioned previously (1), which if present, would indicate MOF decomposition from within chitosan-MOF matrix;

3. To identify interferent species that would lead to false positives or false negative during the use of the cell viability assays CellTiter Blue and MTT *in vitro* cytotoxicity methods.

Alec Lutzke performed the synthesis of the MOF and fabricated the MOF-polymer films. Megan J. Neufeld performed the NO-release studies and provided the sample aliquots used for the MS studies. Jesus B. Tapia performed the MS studies to investigate the catalytic products and potential degradation products. The MS work regarding the MOF-polymer composites was published in *ACS Applied Materials and Interfaces* (Neufeld, M. J.; Lutzke, A.; Tapia, J. B.; Reynolds, M. M. Metal – Organic Framework/Chitosan Hybrid Materials Promote Nitric Oxide Release from *S*-nitrosoglutathione. *ACS Appl. Mater. Interfaces* **2017**, 9(6), 5139–5148). Alec Lutzke provided guidance and support for the *in vitro* cytotoxicity assays, including identifying the molecules to be tested. Bella H. Neufeld provided the *in vitro* assay samples used to perform the MS experiments. Jesus B. Tapia performed the MS studies to track the chemical transformation of the *in vitro* assays. The MS work regarding the investigation for *in vitro* assay interferences was published in *ACS Analytical Chemistry* (Neufeld, B. H.; Tapia, J. B.; Lutzke, A.; Reynolds, M. M. Small Molecule Interferences in Resazurin and MTT-Based Metabolic Assays in the Absence of Cells. *Anal. Chem.* **2018**, 90 (11), 6867–6876). The work has been reprinted for both manuscripts with permission from the American Chemical Society (Copyright 2017 and 2018).

3.2 Introduction

The usefulness of applying mass spectrometry to complex systems is shown in two different systems: a chitosan-MOF composite system (section 3.2.1) used to induce catalytic release of NO, and in two cell viability assays (section 3.2.2) that were suspected to be negatively affected by interferences. In the case of the chitosan-MOF composites, their main purpose of inducing catalytic release of nitric oxide (NO) from *S*-nitrosoglutathione (GSNO) was successfully

characterized, therefore making the composites great candidates for the purpose of catalyzing release of NO. However, as with many devices, their implementation is not only reliant on success of their primary purpose, but also knowledge of byproducts and potential degradation of the devices that may lead to toxicity concerns or product degradation. As will be shown in this chapter, mass spectrometry was used to address those potential concerns.

Specific to cell viability studies, well-established and widely used techniques for cytotoxicity studies have the potential for negative interfering effects from compounds to be used as therapeutics that may lead to false positives or false negatives. As described in this chapter, the uncertainties that may arise from interfering species in the UV-vis stereoscopic measurements used for CellTiter Blue/MTT cell viability assays were identified using mass spectrometry. With the use of mass spectrometry, it was possible to determine the identity of the interfering species and to assign whether the uncertainty regarding false positives, false negatives, or spectroscopic suppression was the reason for any inconclusive results from the assays.

3.2.1 Chitosan-MOF composites

Metal-organic frameworks (MOFs) are crystalline structures that consist of organic linkers bound to metal centers² characterized by ultrahigh porosity (up to 90% free volume) and ultrahigh surface areas, exceeding 6000 m²/g³. MOFs have been frequently used in gas storage and heterogeneous catalysis, among other applications⁴⁻⁷. It has been previously reported that copper-based MOFs may be capable of inducing decomposition of *S*-nitrosothiols (RSNOs)^{8,9}.

Nitric oxide (NO) is endogenously produced in the body to contribute to the immune response, neurotransmission and regulation of vascular tone¹⁰. Additionally, since NO has been determined to be essential to the wound-healing process, exogenous NO supplementation has been shown to promote accelerated wound healing^{11,12}. To take advantage of endogenously present

NO^{13,14}, the copper-based MOF CuBTri was investigated for its application to induce the release of NO from the physiologically present *S*-nitrosoglutathione (GSNO).

Incorporation of MOFs capable of inducing release of NO onto polymer support systems is highly desirable, particularly when designing extracorporeal systems that are blood-contacting devices. The MOF-polymer materials investigated were developed by incorporating CuBTri onto the polysaccharide chitosan. Chitosan is a naturally derived polysaccharide that consists of β -1,4-linked glucosamine and *N*-acetylglucosamine, generally regarded as nontoxic^{15,16}. Chitosan was the ideal candidate because it has been used as an antimicrobial material in the form of chitosan-based wound dressings that can significantly accelerate the wound healing process¹⁷⁻¹⁹.

The incorporation of CuBTri onto chitosan led to successful release of NO from GSNO and supported the potential use of the hybrid materials in extracorporeal systems. In addition to investigating the capability of NO release from GSNO using the hybrid materials, mass spectrometric methodology was developed to confirm the production of oxidized glutathione (GSSG) and to investigate the degradation of the polymer support system and to probe for the decomposition of the MOF. The compounds of interest from chitosan were glucosamine and *N*-acetylglucosamine, and to screen for MOF decomposition, the compound of interest was the H₃BTri ligand.

3.2.2 Cell viability studies

In vitro assays are very important for pharmaceutical and therapeutic agents due to their ability to rapidly and efficiently evaluate cytotoxicity of compounds without the need for *in vivo* testing^{20,21}. These assays are frequently used because they rely on the ability of metabolically active cells to transform the starting assay compound to a final compound²². The most common *in vitro* cytotoxicity assays are the resazurin \rightarrow resorufin dyes (commercially available as CellTiter

Blue and Alamar Blue)¹ and the MTT assay (3-(4,5-dimethylthiazol-2-yl)-2,5-siphenyl-tetrazolium bromide)²³. These assays work by cellular conversion of the starting dye (either resazurin or MTT) to the final compound (resorufin or MTT formazan). The transformations resazurin → resorufin and MTT → MTT formazan shown in Figure 3.1 are determined spectroscopically by monitoring the absorbance values associated with the formation of resorufin or MTT formazan over time^{1,23}.

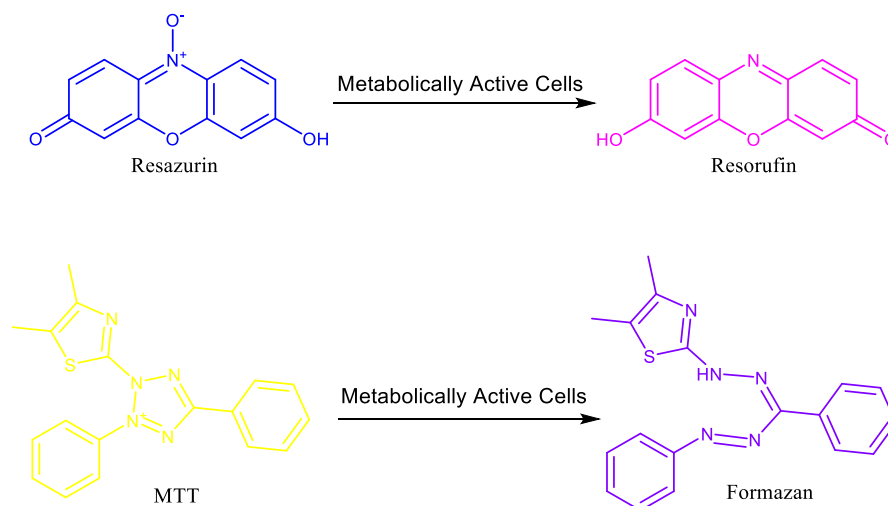


Figure 3.1 Commonly used *in vitro* cytotoxicity assays. Resazurin is converted to resorufin in the presence of metabolically active cells and MTT is converted to formazan in the presence of metabolically active cells.

These chemical transformations expected from metabolically active cells have been shown to also be induced by functional groups and moieties that may be present within a therapeutic agent of interest causing interferences^{1,22,24,25}. These interferences negatively lead to false positives or negatives that can inappropriately classify the use of therapeutics. A false positive occurs when for example (as will be demonstrated in this chapter) glutathione interacts with resazurin (CellTiter Blue assay), converting it to resorufin in the absence of metabolically active cells. Using the typical UV-vis spectroscopic detection for the assay, the presence of resorufin and the absence of resazurin would inaccurately indicate metabolically active cells. A false negative could occur for example (as will be demonstrated in this chapter), severe ion suppression from oxidized glutathione (GSSG)

indicates the absence of resorufin (CellTiter Blue assay), therefore inaccurately indicating the absence of metabolically active cells.

To study whether interferences would lead to false positives/negatives, mass spectrometry was an ideal addition to the spectroscopic studies performed by Bella H. Neufeld because mass spectrometric analyses were not affected by the interferences studied. Any studies that would produce inconclusive results using spectroscopic measurements were determined using mass spectrometry because the m/z 's of resazurin, resorufin, MTT and MTT-formazan were accurately identified regardless of the selected interference. To emphasize this, the exact masses of resazurin and resorufin are 229.0375 (230.0448 m/z as $[M-H]^-$) and 213.0426 (212.0353 m/z as $[M-H]^-$) respectively. If the assay suffers from severe signal suppression using the UV-vis spectroscopic detection (GSSG for example), complementing the studies with mass spectrometry would accurately indicate whether resazurin or resorufin are present or both. This is possible because the exact mass of GSSG is 612.1520 (611.1447 m/z as $[M-H]^-$) which does not interfere in the mass spectrometric method's ability to detect the presence of resazurin/resorufin and if GSSG has effectively converted any of the resazurin to resorufin over time. Therefore, the complementary use of mass spectrometry for the cell viability assays can help accurately determine, when not possible by UV-vis spectroscopic measurements, whether compounds of interest interfere with the assays.

3.2.3 Goals for this chapter

The experiments presented in this chapter show the successful use of mass spectrometry to determine/identify analytes of interest such as reaction byproducts, biodegradation products and interfering species in complex systems. Two research questions will be addressed:

- 1) Is GSSG the reaction byproduct MOF-catalyzed release of NO from GSNO in MOF-chitosan materials?
- 2) From the MOF-chitosan material, what are the degradation products resulting from the chitosan support system?
- 3) What are the identities of the interferences in the cell-titre blue assay? Do these interfering species give a false positive or false negative outcome?

3.3 Experimental

3.3.1 Materials and Methods

3.3.1.1 Chitosan-MOF membranes Materials

LC-MS grade acetonitrile, water and formic acid were purchased from VWR (Solon, OH, USA). Glutathione (98%) was purchased from AMRESCO (Solon, OH, USA). Deionized water (18.2 M Ω ·cm) was obtained from a Millipore Direct-Q water purification system (EMD Millipore, Billerica, MA, USA). Chitosan-CuBTTri membranes and GSNO were provided by Alec Lutzke and Megan Neufeld.

3.3.1.2 Chitosan-MOF membranes Methods

The products formed following exposure of CuBTTri membrane to GSNO were determined by suspension of approximately 20 mg of chitosan-CuBTTri membrane in a 1 mM solution of GSNO. The experiment was protected from light and maintained at 37 °C until the characteristic pink color of GSNO disappeared in solution. A control experiment was conducted in a similar manner using a chitosan membrane without the CuBTTri MOF intended to reflect the thermal decomposition of GSNO. A second control experiment was performed by exposing GSNO only to 365 nm UV light to encourage UV decomposition of GSNO.

The collected solutions were analyzed using an Agilent 6224 TOF LC/MS. The instrument was equipped with an Agilent multimode (MMI) ion source capable of electrospray ionization (ESI) and atmospheric pressure chemical ionization (APCI). For all the analyses, ESI in positive polarity was used. The sample solutions were introduced into the ion source by direct flow injection using an Agilent 1260 Infinity at a flow rate of 0.220 mL/min via the ESI nebulizer using a mobile phase consisting of 80/20/0.1 water/acetonitrile/formic acid. The mass spectrometer conditions were as follows: 3000 V capillary voltage, 200 V fragmentor voltage, 60 V skimmer voltage, 310 °C drying gas (N₂) temperature, 10 l/min drying gas flow rate, and 45 psi nebulizer pressure. All data were processed with Agilent MassHunter Qualitative Analysis B.07.00.

3.3.1.3 Cell viability studies Materials

Glutathione, MTT cell viability assay and LC-MS grade methanol were purchased from VWR (Solon, OH, USA). Dimethyl sulfoxide, oxidized glutathione, D-penicillamine, and *N*-acetyl-D-penicillamine were purchased from Sigma Aldrich (St. Louis, MO, USA). L-cysteine and mercaptosuccinic acid were purchased from Alfa Aesar (Ward Hill, MA, USA). CellTiter Blue (resazurin-resorufin) was purchased from Promega (Madison, WI, USA). Deionized water (18.2 MΩ·cm) was obtained from a Millipore Direct-Q water purification system (MilliporeSigma, Billerica, MA, USA).

3.3.1.4 Cell viability studies Methods

All MS analyses were performed on an Agilent 6224 TOF LC/MS. The instrument was equipped with an Agilent multimode ion (MMI) source capable of electrospray ionization (ESI) and atmospheric pressure chemical ionization (APCI). For the assays, mixed-mode ionization was used. The sample solutions were introduced to the ion source by direct flow injection using an Agilent 1260 Infinity at a flow rate of 0.220 mL/min via the ESI nebulizer with methanol as the

mobile phase. The mass spectrometer conditions were as follows: 2500 V capillary voltage, 120 V fragmentor voltage, 60 V skimmer voltage, 2000 V corona charging voltage, 310 °C drying gas (N₂) temperature, 10 l/min drying gas flow rate, and 45 psi nebulizer pressure. All data were processed with Agilent MassHunter Qualitative Analysis B.07.00.

The samples for the resazurin → resorufin assay were prepared by Bella H. Neufeld using Millipore water to minimize potential interfering ions and ion suppression in the mass spectrometer and the analyses were performed in negative polarity. The samples for the MTT → MTT formazan assay were prepared by Bella H. Neufeld using a solvent mixture containing PBS and DMSO that were diluted in ethanol (to 0.1%) to facilitate dissolution before injection into the mass spectrometer. All analyses were performed in positive polarity for the MTT → MTT-formazan assay.

3.4 Results

3.4.1 Chitosan-MOF membranes

The main purpose of the MS studies regarding the chitosan-CuBTTri membranes was to determine the reaction products as GSNO decomposed in the presence of Cu-BTTri to produce NO and other products (Figure 3.2). Additionally, since the CuBTTri was embedded into a chitosan support, it was important to track the degradation of chitosan as well as any potential degradation of the CuBTTri MOF. GSNO products other than NO were determined by probing for the presence of the H₃BTTri (Figure 3.2b) precursor ligand which would indicate CuBTTri degradation. Secondly, in the case of the chitosan support system, degradation was probed by searching for the presence of glucosamine and *N*-acetylglucosamine monomers.

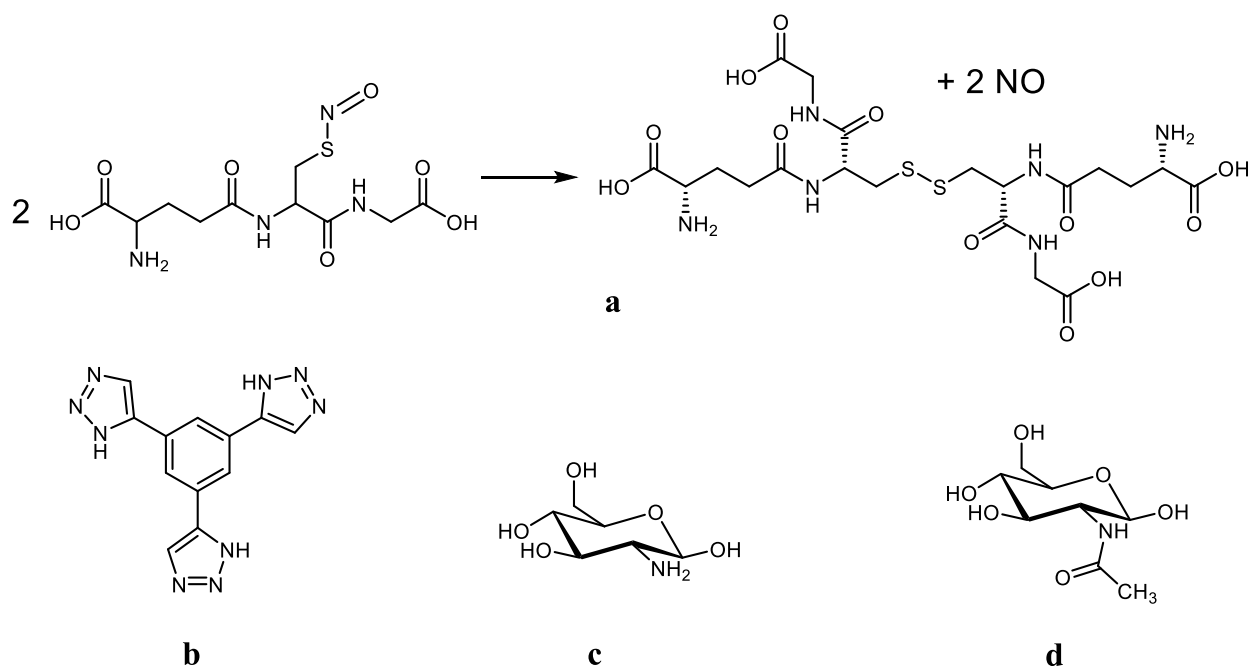


Figure 3.2 Compounds investigated using MS. (a) the production of GSSG from release of NO from GSNO. (b) H₃BTTri ligand, building block from the CuBTTri MOF. (c) glucosamine and (d) *N*-acetylglucosamine, building blocks (monomers) form chitosan.

3.4.1.1 Identification of GSNO decomposition products, chitosan degradation products and screening for H₃BTTri ligand

Upon exposure of GSNO to the chitosan-CuBTTri composite films, the GSNO was expected to be decomposed as NO was released as has been previously demonstrated⁸. As part of additional investigative studies, as shown in Figure 3.3, GSSG was accurately identified by ESI-TOF MS as the [M+H]⁺ ion at 613.1598 *m/z*. Additionally, dehydrated glucosamine, glucosamine and dehydrated *N*-acetyl glucosamine were found as the [M+H]⁺ ions at 162.0767, 180.0868, and 204.0875 *m/z*, respectively. These monomers should appear as hydrolytic degradation of the chitosan support system takes place over time. The last component of the investigative process was to probe for the potential decomposition of the CuBTTri MOF. To do so, in the mass spectrometric analyses, the ligand H₃BTTri (C₁₂H₉N₉) was searched for, which if present, would appear as the [M+H]⁺ ion at 280.1054 *m/z*. The absence of the H₃BTTri ligand suggests no decomposition of the MOF over time.

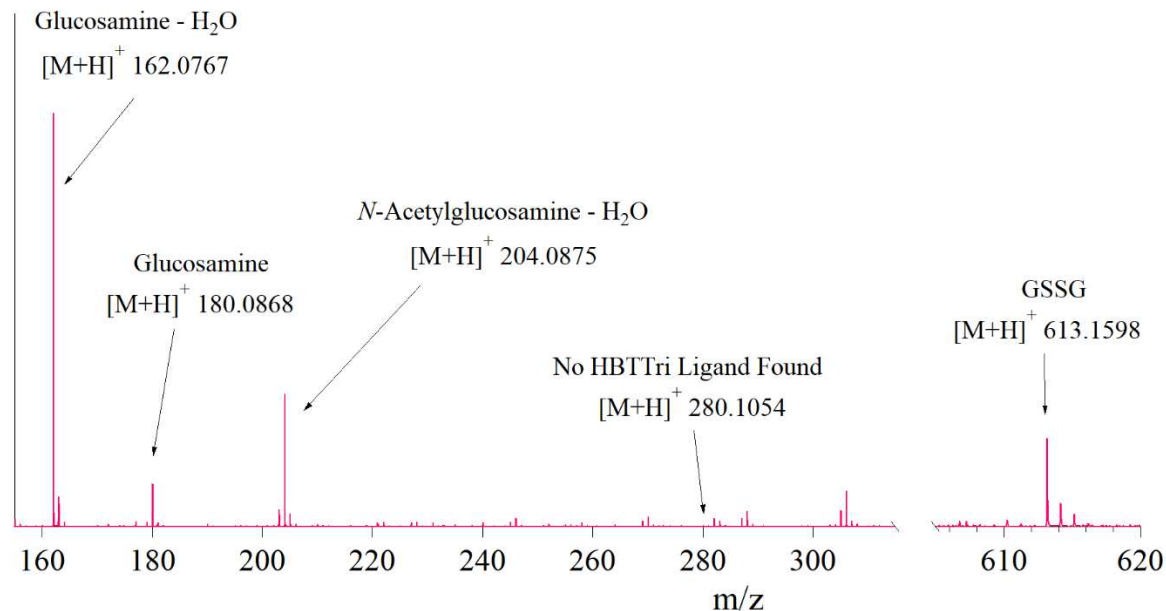


Figure 3.3 Mass spectrum of the investigative analysis of potential degradation of chitosan-CuBTTri hybrid materials. Glucosamine and *N*-acetylglucosamine are a product of hydrolytic degradation of chitosan and GSSG was confirmed to be the product of NO release from GSNO when exposed to the hybrid materials.

3.4.2 Cell viability studies

Both cell viability assays work by reduction of resazurin and MTT to their counterparts (resorufin and formazan) in the presence of metabolically active cells (Figure 3.1). Therefore, the relative conversion of resazurin and MTT to resorufin and formazan is directly correlated to the number of healthy cells^{1,23}. While the exact mechanistic pathways for both assays are not entirely understood, it is suggested that resazurin is reduced either in chemically reduced media produced by cellular growth or enzymatic reduction within the mitochondria, while MTT reduction is likely to occur exclusively intracellularly by mitochondrial enzymes^{1,22-25}.

After careful investigation, the resazurin assay was studied for potential interferences from glutathione, oxidized glutathione, D-penicillamine, and mercaptosuccinic acid (Figure 3.4). The selection included a primary thiol (glutathione), a secondary thiol (mercaptosuccinic acid), a tertiary thiol (D-penicillamine) and a disulfide (oxidized glutathione) that are also of biological relevance. In the case of the MTT assay, the potential interferences investigated were glutathione

(primary thiol), D-penicillamine (tertiary thiol), L-cysteine (primary thiol), mercaptosuccinic acid (secondary thiol) and *N*-acetyl-D-penicillamine (tertiary thiol).

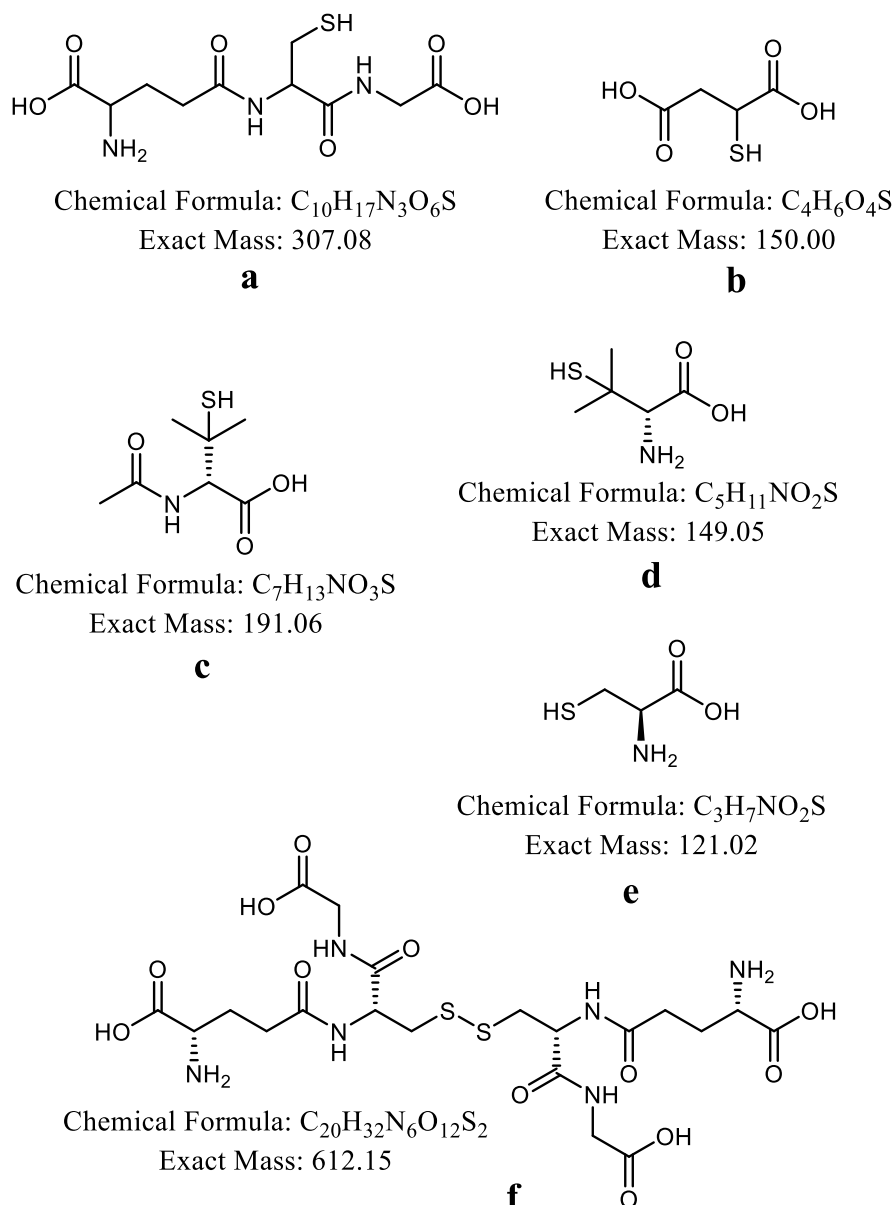


Figure 3.4 Selected compounds to probe for interference in the resazurin and MTT metabolic assays. (a) glutathione, (b) mercaptosuccinic acid, (c) *N*-acetyl-D-penicillamine, (d) D-penicillamine, (e) L-cysteine, (f) oxidized glutathione. Resazurin was investigated for potential interferences from (a), (b), (d) and (f). MTT was investigated for potential interferences from (a), (b), (c), (d) and (e).

A typical spectroscopic assay performed with resazurin looks like that shown in Figure 3.5 in which *E. coli* was incubated with resazurin. The trace in black corresponds to 0 h of cell

incubation where no reduction of resazurin to resorufin is expected as shown by the λ_{\max} at ~ 600 nm which corresponds to resazurin. After 1 hour of incubation, and until the 4 hour incubation mark (colored traces), the spectroscopic results indicate the effective conversion of resazurin to resorufin expected from metabolically active cells since the λ_{\max} at ~ 570 nm corresponds to resorufin.

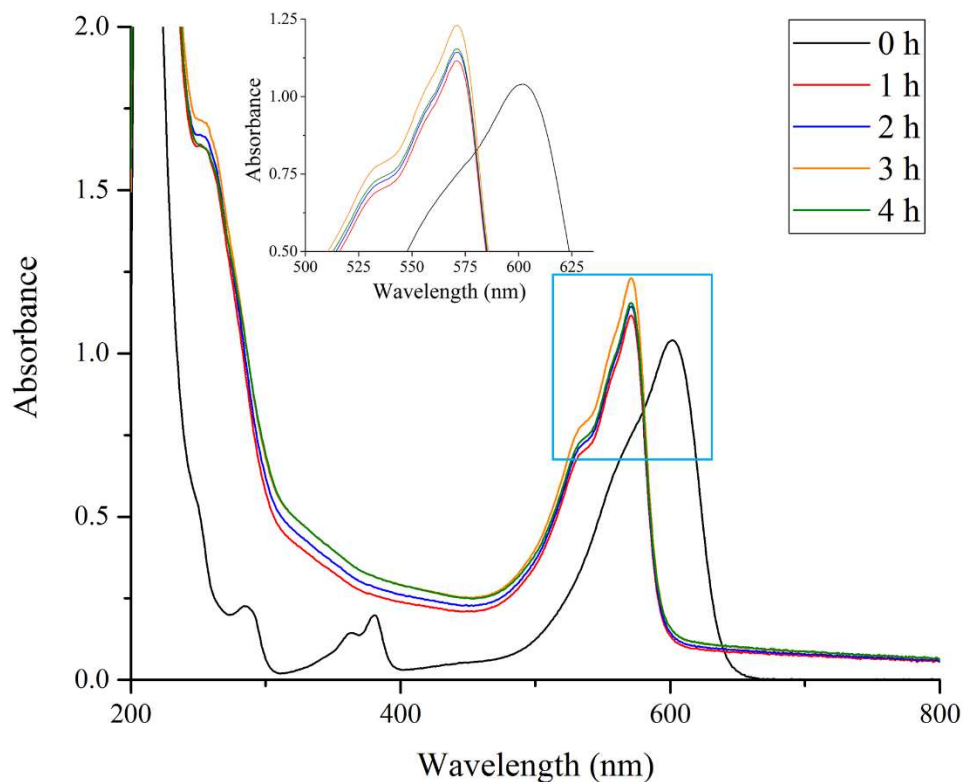


Figure 3.5 Typical spectroscopic traces from the resazurin assay performed on *E. coli* cells by Bella H. Neufeld. The transformation of resazurin to resorufin is visible by the transition from 600 nm (resazurin) to 570 nm (resorufin).

In Figure 3.6, a typical MTT assay in the presence of *E. coli* cells is shown. The trace in black corresponds to 0 h of the cell incubation process in the presence of MTT where no reduction of MTT to formazan was expected as shown by the λ_{\max} at ~ 380 nm which corresponds to MTT. After 1 hour of incubation, and until the 4-hour incubation mark (colored traces), the spectroscopic results indicate the effective conversion of MTT to formazan expected from metabolically active cells since the λ_{\max} at ~ 550 nm corresponds to formazan.

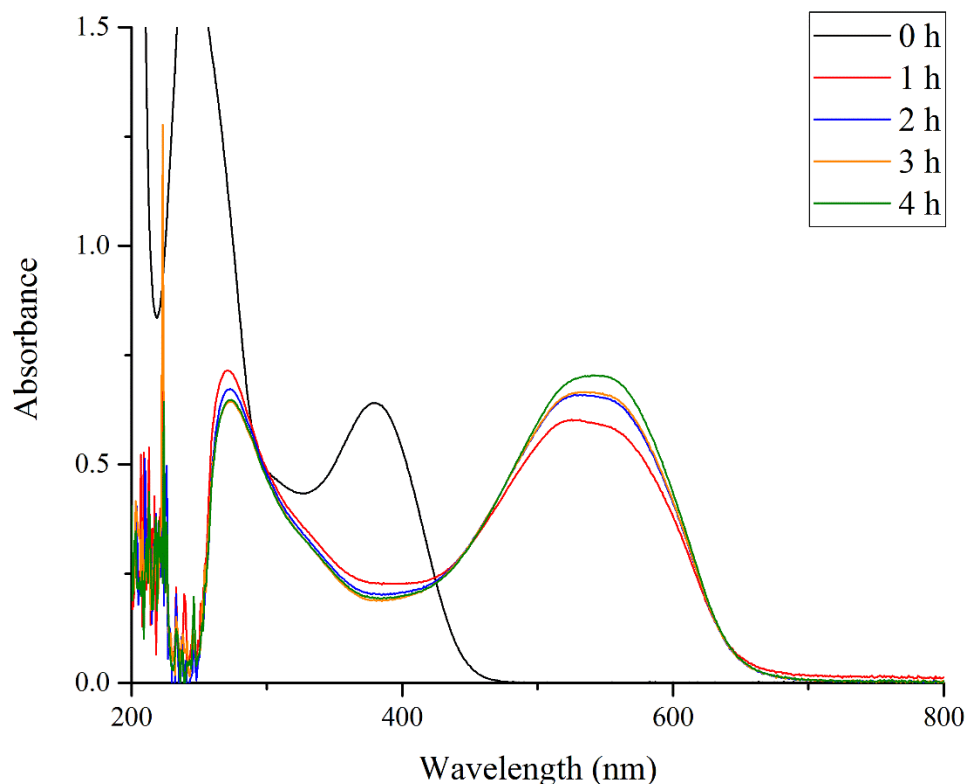


Figure 3.6 Typical spectroscopic results from the resazurin assay performed on *E. coli* cells by Bella H. Neufeld. The transformation of MTT to formazan is visible by the transition from 380 nm (MTT) to 550 nm (formazan).

To study the interference effects of glutathione, mercaptosuccinic acid, D-penicillamine and oxidized glutathione on the resazurin assay, each interference was incubated for 4-hours in the absence of cells. In the case of glutathione, the spectroscopic results collected by Bella H. Neufeld suggested full conversion of resazurin to resorufin over the incubation period as indicated by the disappearance of the ~600 nm absorption band and the appearance of the ~570 nm absorption bands. The conversion of resazurin to resorufin in the absence of cells would indicate a false positive when the assay is performed in the presence of glutathione. To confirm that indeed resazurin was converted to resorufin, MS analysis was performed. As shown in Figure 3.7, after only 1 hour of incubation, resazurin appears to be largely converted to resorufin and by the time the incubation is complete (4 h), the majority of resazurin has been converted to resorufin. The

mass spectra collected confirms the spectroscopic results that glutathione induces conversion in the absence of cells and therefore a false positive.

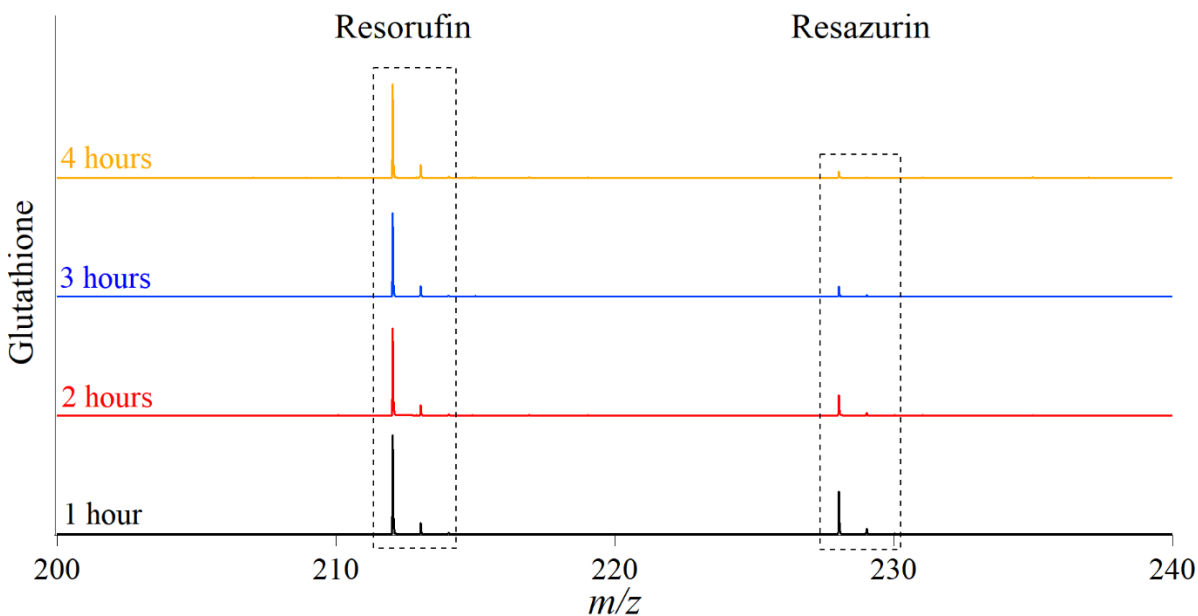


Figure 3.7 Mass spectra of the incubation of resazurin with glutathione in the absence of cells. As indicated by the black spectrum, conversion of resazurin began after 1 hour. By the 4-hour period, the resazurin appears to be mostly converted to resorufin.

The spectroscopic results collected by Bella H. Neufeld suggested that D-penicillamine also induces the conversion of resazurin to resorufin. Over the course of the incubation period, the ~600 nm absorption band for resazurin disappeared and the ~570 nm band for resorufin bands were more prominent. After performing MS analysis (Figure 3.8) during the incubation process, D-penicillamine was only shown to induce a small amount of conversion to resorufin. This indicates that a small amount of resorufin may lead to a substantial false positive since spectroscopic measurements suggest full conversion of resazurin after the 4-hour incubation period. The mass spectra collected confirms the spectroscopic findings that D-penicillamine are a false positive since a small conversion to resorufin appears to indicate fully metabolically active cells.

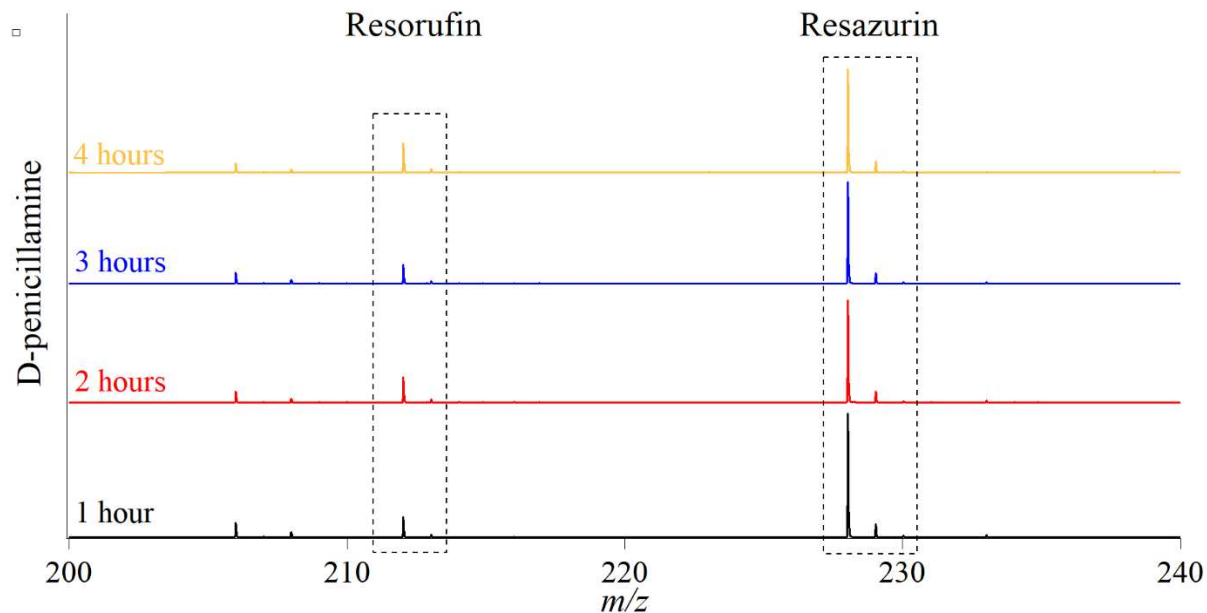


Figure 3.8 Mass spectra of the incubation of resazurin with D-penicillamine in the absence of cells. As indicated by all spectra, only a minor fraction of resazurin was converted to resorufin during the entire incubation process.

The third interference investigated was mercaptosuccinic acid. The collected spectroscopic data showed substantial suppression of both absorbances indicative of resazurin or resorufin. In this case it was difficult to label mercaptosuccinic acid as a false positive or negative since neither absorbance bands were present. However, the mass spectra collected (Figure 3.9) show that after the first hour of incubation the majority of resazurin had been converted to resorufin. The interference of mercaptosuccinic acid was not expected to be this severe since there was no absorbance band indicative of resorufin. In this case, if the assay is performed by only monitoring the presence of resorufin, it would lead to a false negative as shown by the MS results.

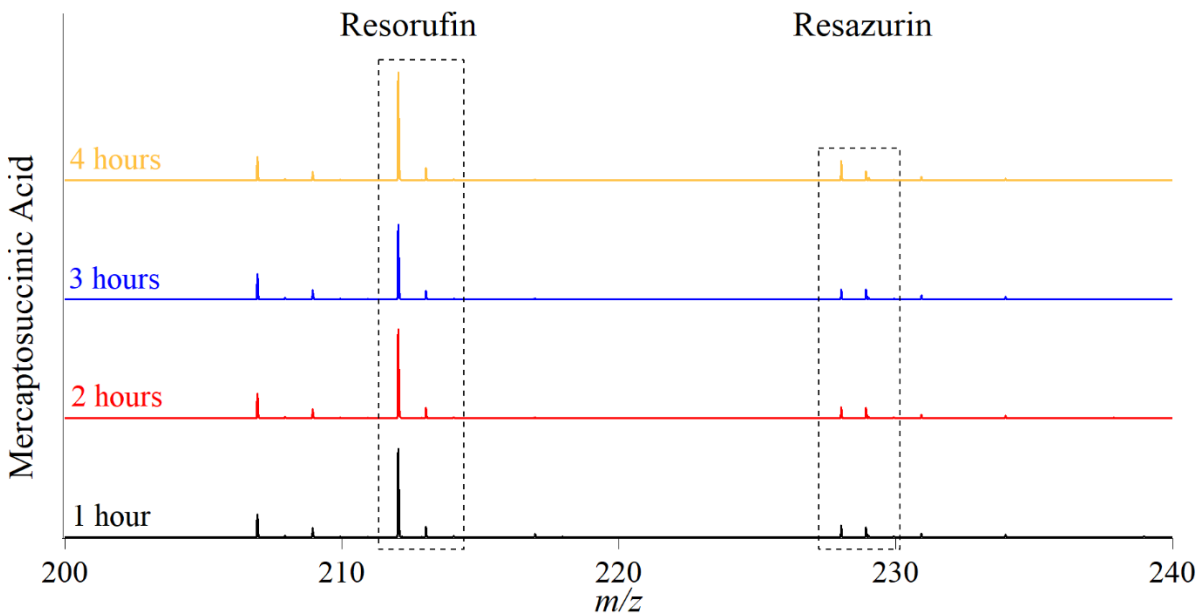


Figure 3.9 Mass spectra of the incubation of resazurin with mercaptosuccinic acid in the absence of cells. As indicated by the black spectrum, conversion of resazurin appears to be complete after 1 hour.

The fourth interference investigated for the resazurin assay was oxidized glutathione or GSSG. The spectroscopic data collected by Bella H. Neufeld labeled GSSG's interference as neither a false positive nor negative. GSSG produced inconclusive spectroscopic results because it appears to induce severe suppression from both resazurin and resorufin signals making it difficult to decide whether there are viable cells. This may not be considered an actual problem since the MS results (Figure 3.10) show that GSSG did not induce any conversion from resazurin to resorufin during the entirety of the study. However, when cells are being treated with, for example, *S*-nitrosated glutathione (GSNO), the byproduct of GSNO release is GSSG which may lead to inconclusive results due to severe signal suppression.

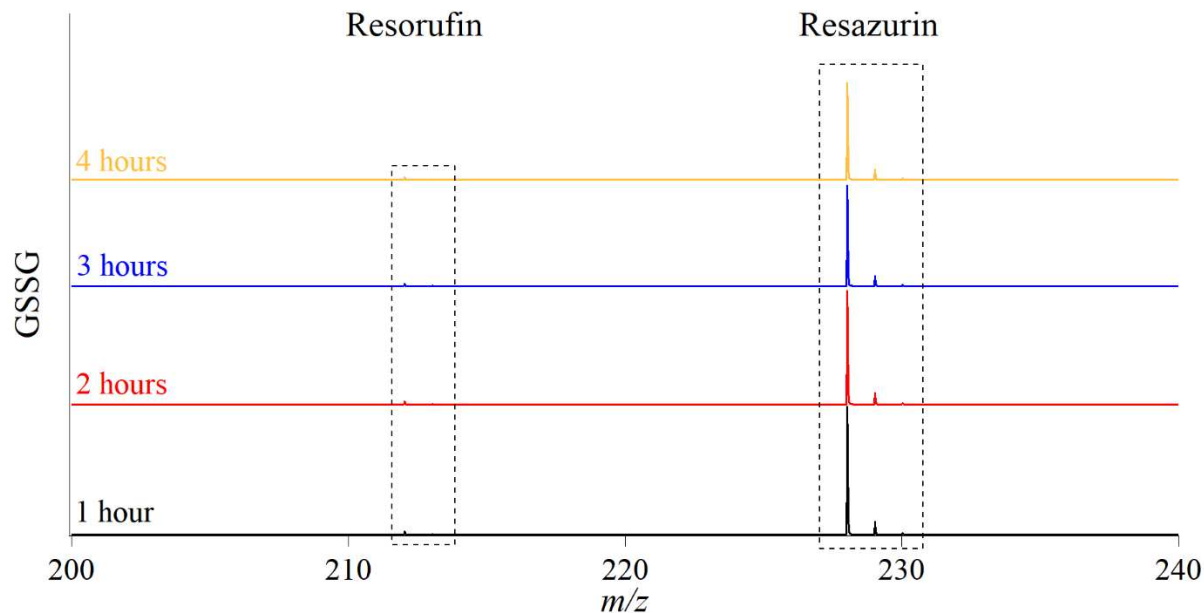


Figure 3.10 Mass spectra of the incubation of resazurin with GSSG in the absence of cells. As indicated by all spectra, no conversion of resazurin to resorufin was observed.

To study the interference effects of glutathione, D-penicillamine, L-cysteine, mercaptosuccinic acid and *N*-acetyl-D-penicillamine on the MTT assay, each interference was incubated for 4-hours in the absence of cells. In the case of glutathione, D-penicillamine and L-cysteine, the spectroscopic results collected by Bella H. Neufeld suggested that MTT had been converted to formazan since the absorption band at ~380 nm corresponding to MTT was no longer visible and the absorption band at ~550 nm corresponding to formazan was very prominent. It is possible that the features indicative of MTT were hidden under the absorbance features from formazan, and to test whether glutathione, D-penicillamine and L-cysteine were responsible for conversion of MTT to formazan, ESI-TOF MS was also performed. The MS results from interference studies by glutathione, D-penicillamine and L-cysteine are shown in Figures 3.11, 3.12 and 3.13. As shown in Figure 3.11, it appears that incubation of MTT with glutathione induces conversion of MTT to formazan starting at hour 1 of incubation. The conversion appears to be mostly steady until hour 4 in which there appears to be a slight excess of formazan, but overall, the results confirm conversion which indicates potential for a false positive.

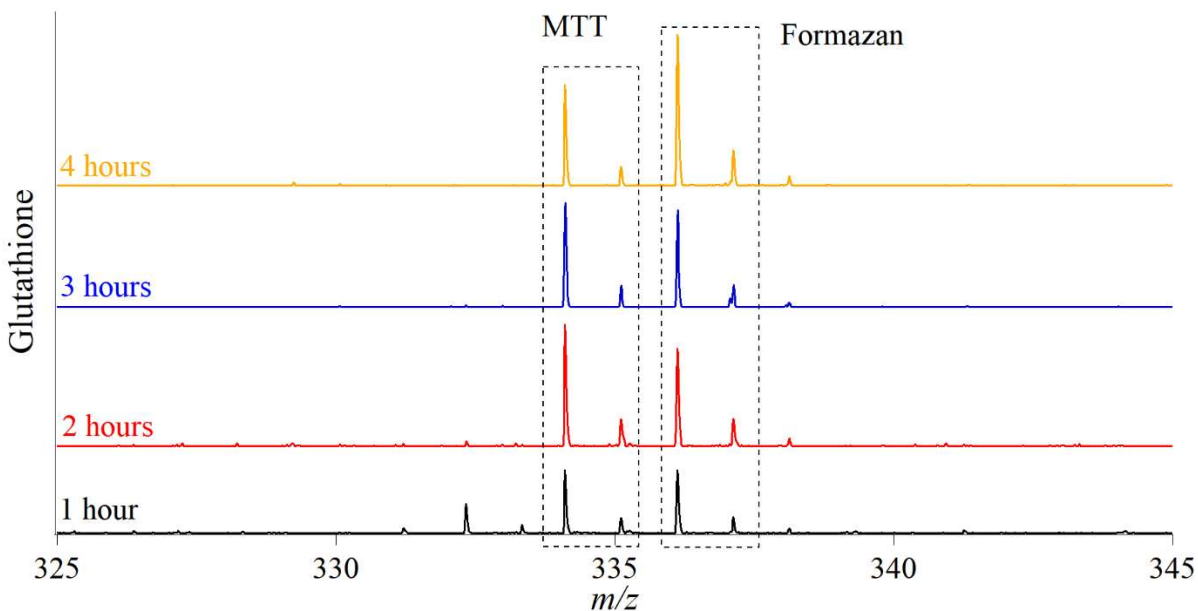


Figure 3.11 Mass spectra of the incubation of MTT with glutathione in the absence of cells. As indicated by the black spectrum, conversion of MTT begins after 1 hour.

As shown in Figure 3.12, MTT appears to be fully converted to formazan after the first hour of incubation with D-penicillamine. This results directly confirm the spectroscopic results obtained by Bella H. Neufeld that show full conversion and this results strongly indicate that D-penicillamine can be responsible for a false positive in the assay.

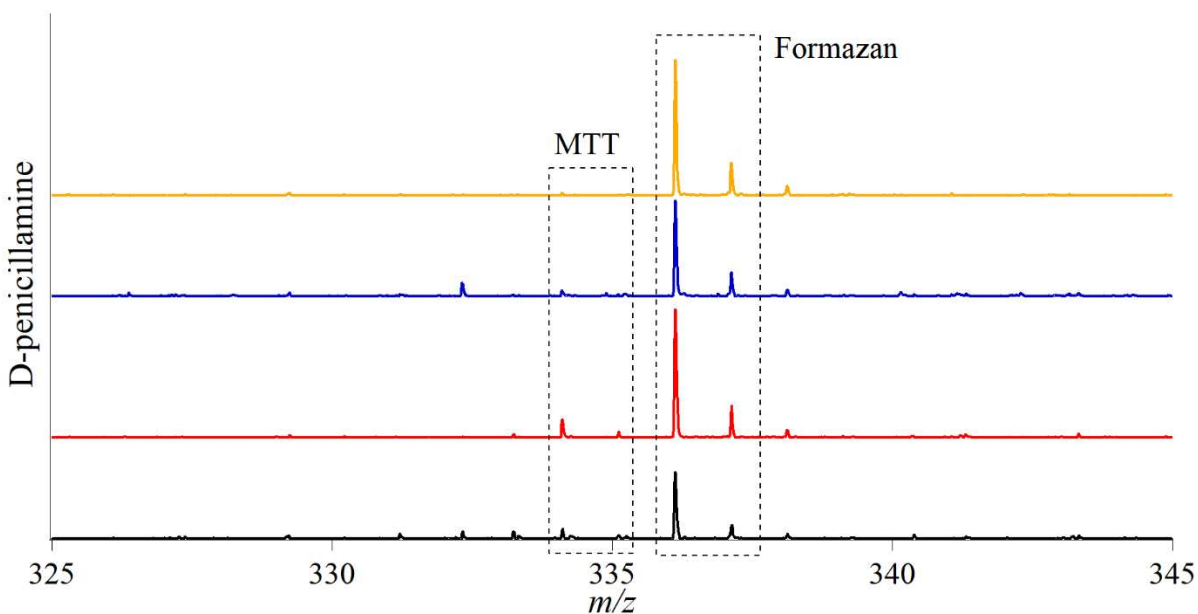


Figure 3.12 Mass spectra of the incubation of MTT with D-penicillamine in the absence of cells. As indicated by the black spectrum, full conversion of MTT to formazan is evident after 1 hour.

As shown in Figure 3.13, MTT appears to be fully converted to formazan after the first hour of incubation with L-cysteine. This MS results directly confirm the spectroscopic results obtained by Bella H. Neufeld that show full conversion of MTT to formazan and strongly indicates that L-cysteine can be responsible for a false positive in the assay.

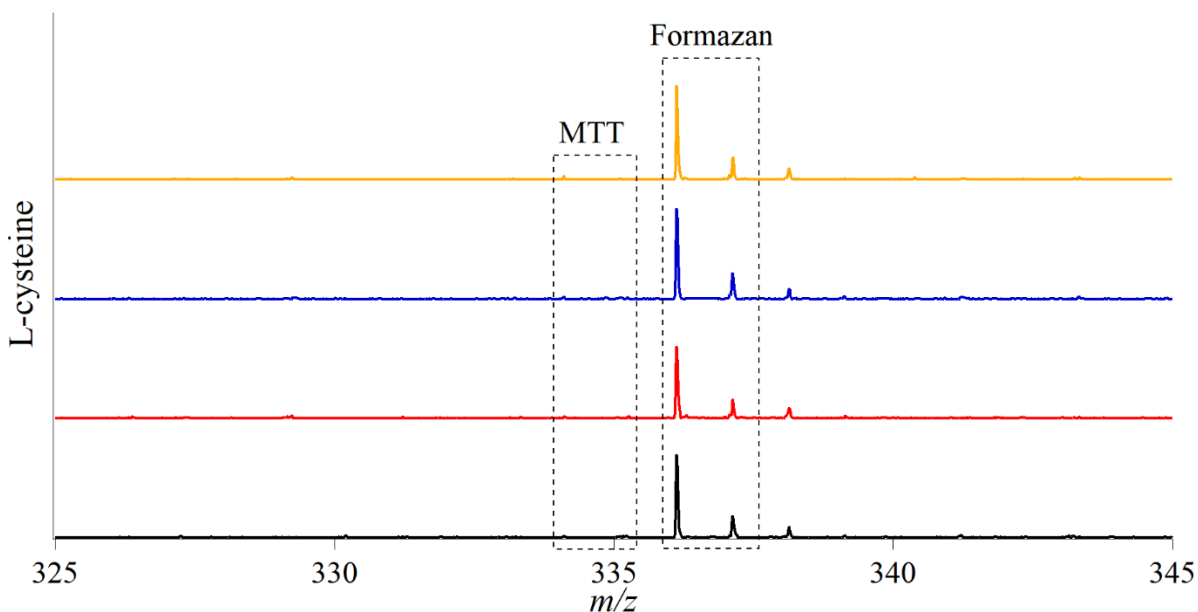


Figure 3.13 Mass spectra of the incubation of MTT with L-cysteine in the absence of cells. As indicated by the black spectrum, full conversion of MTT to formazan is evident after 1 hour.

In the case of mercaptosuccinic acid and *N*-acetyl-D-penicillamine, the spectroscopic results obtained by Bella H. Neufeld suggested no conversion of MTT to formazan during the incubation period. To confirm the findings on whether mercaptosuccinic acid and *N*-acetyl-D-penicillamine do not interfere and are not responsible for conversion of MTT to formazan, ESI-TOF MS was also performed. The MS results from interference studies by mercaptosuccinic acid and *N*-acetyl-D-penicillamine are shown in Figures 3.14 and 3.15. As shown in Figure 3.14, it appears that incubation of MTT with mercaptosuccinic acid does not induce significant conversion of MTT to formazan. In this case, both spectroscopic and mass spectrometric analyses suggest that mercaptosuccinic acid will not result in a false positive when performing the assay.

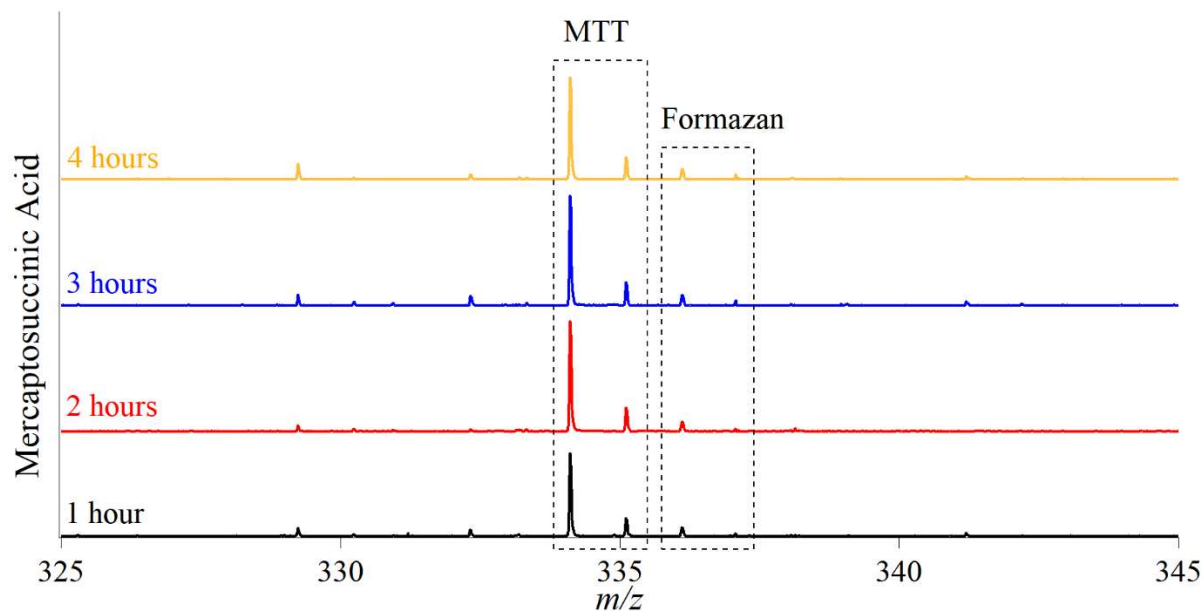


Figure 3.14 Mass spectra of the incubation of MTT with mercaptosuccinic acid in the absence of cells. Mercaptosuccinic acid does not induce significant conversion of MTT to formazan over the entire incubation period.

As shown in Figure 3.15, it also appears that the incubation of MTT with *N*-acetyl-D-penicillamine does not induce significant conversion of MTT to formazan. Also in this case, both spectroscopic and mass spectrometric analyses suggest that *N*-acetyl-D-penicillamine will result not in a false positive when performing the assay.

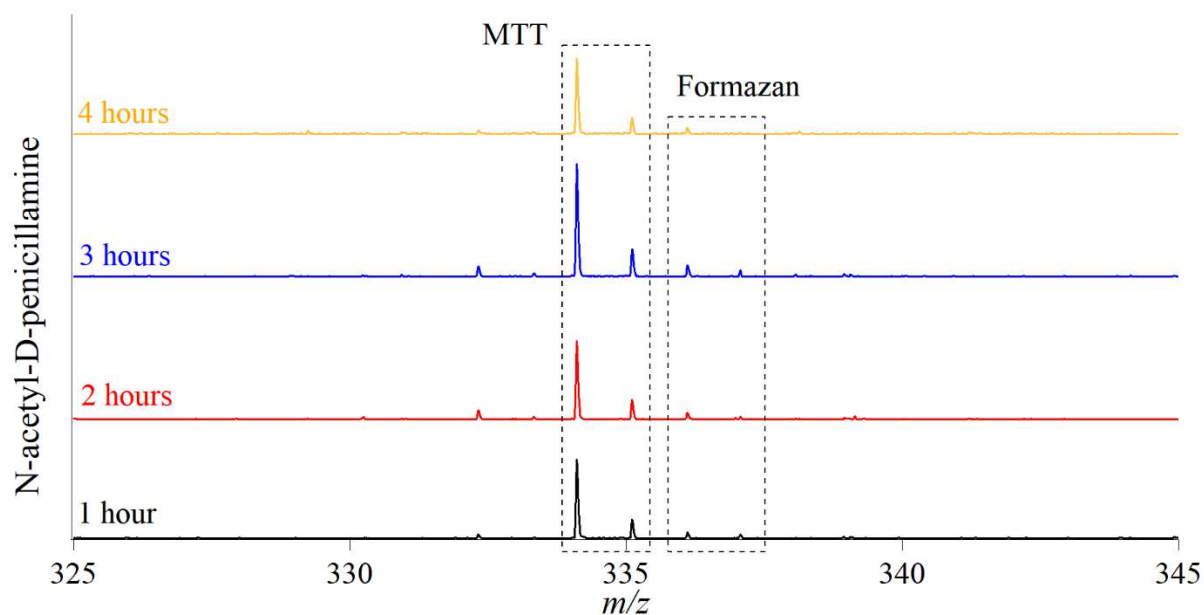


Figure 3.15 Mass spectra of incubation of MTT with *N*-acetyl-D-penicillamine in the absence of cells. *N*-acetyl-D-penicillamine does not induce significant conversion of MTT to formazan over the entire incubation period.

3.4 Conclusions

The collaborative efforts presented in this chapter show the importance and benefit of incorporating mass spectrometry to complex systems to identify reaction byproducts, potential degradation products and to further investigate inconclusive results provided by well-established analytical methods. In the case of the chitosan-MOF hybrid materials, the formation of GSSG from exposing GSNO to the hybrid materials was confirmed. Additionally, mass spectrometry was used to provide evidence that the MOF did not decompose over time during the use of the material and that any gravimetrically measured loss of material can primarily be attributed to degradation of the chitosan polymer support system.

Regarding the cell viability studies, the addition of mass spectrometric analyses strongly emphasized the importance of clearly identifying whether potentially selected therapeutics would lead to false positives/negatives in the absence of cells. This is of high importance because the resazurin and MTT assays are both widely used for *in vitro* studies aimed at making preliminary decisions regarding use of therapeutics. The results obtained suggest that without proper control studies, the data collected can lead to a significant number of false positives/negatives that minimize the reliability of the studies performed. Even when appropriate control studies are performed, the full UV-vis spectroscopic scans are not usually examined which may still lead to inconclusive results regarding potential interferences. This is particularly important for the cases in which the interference studied caused severe signal suppression that may lead to false negatives since the appearance of resorufin or formazan can't be observed.

CHAPTER 3 – REFERENCES

- (1) De Jong, D. W.; Woodlief, W. G. Fluorimetric Assay of Tobacco Leaf Dehydrogenases with Resazurin. *Biochim. Biophys. Acta - Enzymol.* **1977**, *484* (2), 249–259.
- (2) Furukawa, H.; Cordova, K. E.; O’Keeffe, M.; Yaghi, O. M. The Chemistry and Applications of Metal-Organic Frameworks. *Science* **2013**, *341* (6149), 1230444–1230444.
- (3) Zhou, H.-C.; Long, J. R.; Yaghi, O. M. Introduction to Metal–Organic Frameworks. *Chem. Rev.* **2012**, *112* (2), 673–674.
- (4) Mason, J. A.; Oktawiec, J.; Taylor, M. K.; Hudson, M. R.; Rodriguez, J.; Bachman, J. E.; Gonzalez, M. I.; Cervellino, A.; Guagliardi, A.; Brown, C. M.; et al. Methane Storage in Flexible Metal-Organic Frameworks with Intrinsic Thermal Management. *Nature* **2015**, *527* (7578), 357–361.
- (5) Jagadeesh, R. V.; Murugesan, K.; Alshammari, A. S.; Neumann, H.; Pohl, M. M.; Radnik, J.; Beller, M. MOF-Derived Cobalt Nanoparticles Catalyze a General Synthesis of Amines. *Science* **2017**, *358* (6361), 326–332.
- (6) Horcajada, P.; Chalati, T.; Serre, C.; Gillet, B.; Sebrie, C.; Baati, T.; Eubank, J. F.; Heurtaux, D.; Clayette, P.; Kreuz, C.; et al. Porous Metal-Organic-Framework Nanoscale Carriers as a Potential Platform for Drug Delivery and Imaging. *Nat. Mater.* **2010**, *9* (2), 172–178.
- (7) Corella-Ochoa, M. N.; Tapia, J. B.; Rubin, H. N.; Lillo, V.; González-Cobos, J.; Núñez-Rico, J. L.; Balestra, S. R. G.; Almora-Barrios, N.; Lledós, M.; Güell-Bara, A.; et al. Homochiral Metal–Organic Frameworks for Enantioselective Separations in Liquid Chromatography. *J. Am. Chem. Soc.* **2019**, *141* (36), 14306–14316.
- (8) Harding, J. L.; Reynolds, M. M. Metal Organic Frameworks as Nitric Oxide Catalysts. *J.*

- Am. Chem. Soc.* **2012**, *134* (7), 3330–3333.
- (9) Neufeld, M. J.; Lutzke, A.; Tapia, J. B.; Reynolds, M. M. Metal–Organic Framework/Chitosan Hybrid Materials Promote Nitric Oxide Release from S-Nitrosoglutathione in Aqueous Solution. *ACS Appl. Mater. Interfaces* **2017**, *9* (6), 5139–5148.
- (10) Ignarro, L. J.; Freeman, B. *Nitric Oxide: Biology and Pathobiology*, Third.; Elsevier: San Diego, CA, 2017.
- (11) Witte, M. B.; Barbul, A. Role of Nitric Oxide in Wound Repair. *Am. J. Surg.* **2002**, *183* (4), 406–412.
- (12) Lowe, A.; Bills, J.; Verma, R.; Lavery, L.; Davis, K.; Balkus, K. J. Electrospun Nitric Oxide Releasing Bandage with Enhanced Wound Healing. *Acta Biomater.* **2015**, *13*, 121–130.
- (13) Stamler, J. S. S -Nitrosothiols in the Blood. *Circ. Res.* **2004**, *94* (4), 414–417.
- (14) Giustarini, D.; Milzani, A.; Dalle-Donne, I.; Rossi, R. Detection of S-Nitrosothiols in Biological Fluids: A Comparison among the Most Widely Applied Methodologies. *J. Chromatogr. B* **2007**, *851* (1–2), 124–139.
- (15) Ravi Kumar, M. N. . A Review of Chitin and Chitosan Applications. *React. Funct. Polym.* **2000**, *46* (1), 1–27.
- (16) Rinaudo, M. Chitin and Chitosan: Properties and Applications. *Prog. Polym. Sci.* **2006**, *31* (7), 603–632.
- (17) Croisier, F.; Jérôme, C. Chitosan-Based Biomaterials for Tissue Engineering. *Eur. Polym. J.* **2013**, *49* (4), 780–792.
- (18) Dai, T.; Tanaka, M.; Huang, Y.-Y.; Hamblin, M. R. Chitosan Preparations for Wounds and Burns: Antimicrobial and Wound-Healing Effects. *Expert Rev. Anti. Infect. Ther.* **2011**, *9*

- (7), 857–879.
- (19) Azad, A. K.; Sermsintham, N.; Chandkrachang, S.; Stevens, W. F. Chitosan Membrane as a Wound-Healing Dressing: Characterization and Clinical Application. *J. Biomed. Mater. Res. - Part B Appl. Biomater.* **2004**, *69* (2), 216–222.
- (20) Goh, J.-Y.; Weaver, R. J.; Dixon, L.; Platt, N. J.; Roberts, R. A. Development and Use of in Vitro Alternatives to Animal Testing by the Pharmaceutical Industry 1980–2013. *Toxicol. Res. (Camb).* **2015**, *4* (5), 1297–1307.
- (21) In Vitro Basal Cytotoxicity Test Methods for Estimating Acute Oral Systemic Toxicity. Vol.1. *Natl. Toxicol. Progr. Interag. Cent. Eval. Altern. Toxicol. Methods* **2006**, *1*.
- (22) Riss, T. L.; Moravec, R. A.; Niles, A. L.; Duellman, S.; Benink, H. A.; Worzella, T. J.; Minor, L. Cell Viability Assays. *Assay Guid. Man.* **2013**, 1–25.
- (23) Mosmann, T. Rapid Colorimetric Assay for Cellular Growth and Survival: Application to Proliferation and Cytotoxicity Assays. *J. Immunol. Methods* **1983**, *65* (1–2), 55–63.
- (24) Goegan, P.; Johnson, G.; Vincent, R. Effects of Serum Protein and Colloid on the AlamarBlue Assay in Cell Cultures. *Toxicol. Vitro.* **1995**, *9* (3), 257–266.
- (25) Shoemaker, M.; Cohen, I.; Campbell, M. Reduction of MTT by Aqueous Herbal Extracts in the Absence of Cells. *J. Ethnopharmacol.* **2004**, *93* (2–3), 381–384.

CHAPTER 4

MASS SPECTROMETRIC METHODS FOR ANALYSIS OF DEGRADATION PRODUCTS FROM POLYPHOSPHAZENE AND POLYESTER BIODEGRADABLE POLYMERS

4.1 Background

The development of polymeric materials with the intended purpose of becoming biomedical devices is extensively studied in Prof. Melissa M. Reynolds research group. The bulk of the materials consist of a polymer that is biodegradable and is capable of release NO over time. Part of the characterization performed on said polymers is to assess their ability to release NO during extended periods of time, have the correct mechanical properties, and hold structural integrity over the life of the material. A crucial part of the characterization process is to determine what biodegradable polymers decompose into as they degrade. This is of high importance if the material developed can be used as a biomedical device because it must undergo biological evaluation, typically the International Standards ISO-10993 series. To identify the degradation products of biodegradable polymers, a tertiary *S*-nitrosothiol-based polyphosphazene and a series of polyester derived polymers were used. The underlying question was whether we could identify the degradation products of our polymer systems and specific to the polyester polymers, our main concern was to address whether the polymer systems would degrade into the individual monomers, with the potential of increasing localized acidity. Ideally, the smallest degradation products would be at least a dimer of the starting monomers, thereby reducing the risk of diacids lowering the local pH. With the use of MS, LC-MS and LC-MS/MS it was possible to identify the degradation products from each polymer, and for a selected set of polymers, structural identification was accomplished using LC-MS and LC-MS/MS. The MS work done for the polyphosphazene

polymer was originally published in ACS Applied Materials and Interfaces (Lutzke, A.; Tapia, J. B.; Neufeld, M. J.; Reynolds, M. M. Sustained Nitric Oxide Release from a Tertiary S-Nitrosothiol-based Polyphosphazene Coating. *ACS Appl. Mater. Interfaces* **2017**, 9(3), 2104–2113) and has been reprinted with permission from the American Chemical Society (Copyright 2017). Alec Lutzke synthesized the polyphosphazene polymers. Jesus B. Tapia performed all MS studies. The MS work done for the polyester polymers was published in the Journal of Materials Chemistry B (Yapor, J. P.; Neufeld, B. H.; Tapia, J. B.; Reynolds, M. M. Biodegradable crosslinked polyesters derived from thiomalic acid and S-nitrosothiol analogues for nitric oxide release. *J. Mater. Chem. B* **2018**, 6 (24), 4071–4081) and has been adapted with permission from the Royal Society of Chemistry. Janet P. Yapor synthesized the polyester polymers and performed the initial polymer degradation studies. Jesus B. Tapia performed all MS studies. The MS, LC-MS and LC-MS/MS work performed on two selected polyester polymers was published in the Journal of Polymer Degradation and Stability (Tapia, J. B.; Haines, J.; Yapor, J. P.; Reynolds, M. M. Identification of the degradation products of a crosslinked polyester using LC-MS. *Polym. Degrad. Stabil.* **2019**, 168, 108948) and has been adapted with permission from Elsevier. Janet P. Yapor provided the polymers for the subsequent degradation studies. Jason Haines performed the LC-MS/MS studies. Jesus B. Tapia performed all MS and LC-MS studies. Prof. Melissa M. Reynolds acted as the advisor on this project.

4.2 Introduction

The importance of the use of nitric oxide (NO) as a biotherapeutic agent is can be emphasized by its incorporation onto NO-releasing materials¹⁻³. NO is a naturally-occurring molecule with physiological functions in the cardiovascular and immune systems⁴. Endogenously produced NO by endothelial cells regulates vascular tone and inhibits platelet adhesion and

aggregation⁵. NO is used by phagocytes as an antimicrobial agent during immune response⁶. Additionally, NO's ability to exert antithrombic, wound healing, and broad-spectrum antimicrobial effects has led to the incorporation of NO onto polymeric substrates for biointerfacial applications⁷. The purpose of incorporating NO onto polymeric devices is primarily to have the device slowly release NO over time. This is important for devices that are meant to be thromboresistant, blood-contacting medical devices such as stents and catheters⁸. Biodegradable polymeric devices can also offer the benefits of NO-release in addition to their many application that include drug delivery, tissue engineering and wound dressings. These materials have been extensively studied for their hydrolytic degradation and potential to match application-oriented moduli^{2,9-12}. After matching the desired moduli for the intended application of a device, the device must undergo biological evaluation before it is cleared for use. The most widely accepted standard for device evaluation is the ISO 10993 series (Biological Evaluation of Medical Devices). Part of the biological evaluation includes determination of the biodegradation products of the device, which falls under ISO 10993-9, "biological evaluation of medical devices – part 9: framework for identification and quantification of potential degradation products." Identification of the degradation products can help determine potential side effects that could render a device as toxic either during or after its intended use. Addressing potential toxicity concerns falls under ISO 10993-1, "biological evaluation of medical devices – part 1: evaluation and testing within a risk management process."

Current techniques used to determine the biodegradation of a device over time are gravimetric analysis, Fourier transform infrared spectroscopy (FT-IR), nuclear magnetic resonance spectroscopy (NMR), scanning electron microscopy (SEM), high-performance liquid chromatography (HPLC) and mass spectrometry (MS). For example, the degradation mechanism

of acrylate-derivatized poly(ethylene glycol) (PEGDA) hydrogels was determined by tracking the cleavage of networked groups that result in a reduced crosslink density over time. The changes in crosslink density were monitored by measuring the swelling ratio and/or modulus of the hydrogel¹³. Another example follows the oxidative degradation of poly(carbonate urethanes) (PCU) that was tracked using FT-IR by monitoring selected functional groups over time. Additionally, SEM was used to track surface damage of the PCUs over time¹⁴. A different study developed an HPLC method to track the degradation of implanted medical devices by determining acrylic monomers and degradation products¹⁵. The degradation of poly(5-hydroxy-trimethylene carbonate) in aqueous environment was monitored using ¹H-NMR and the main degradation products were identified with electrospray ionization mass spectrometry (ESI-MS)¹⁶. The combination of these techniques facilitates exceptionally accurate determination of the biodegradation mechanism of polymeric devices, and as we show from the work performed, the combination of LC-MS and LC-MS/MS provide additional structural information regarding the complexity of the degradation process.

To develop mass spectrometric methods to identify the degradation products of polymer devices intended for biomedical applications, four polymer systems and their nitrosated analogues were used (Figure 4.1). The polyphosphazene (POP) polymer POP-Gly-MMB, which contained a tertiary free thiol, was subsequently nitrosated to produce the *S*-nitrosated analogue POP-Gly-MMB-NO. Additionally, the polyester polymers designed for implantable meshes composed of combinations of 1,8-octanediol, maleic acid, citric acid and thiomalic acid (Poly(thiomalic-*co*-maleic acid-*co*-1,8-octanediol) or PTMO, poly(thiomalic-*co*-citric acid-*co*-1,8-octanediol) or PTCO and poly(thiomalic acid-*co*-1,8-octanediol or PTO), as well as the *S*-nitrosated analogues (PTMO-NO, PTCO-NO and PTO-NO) were used to investigate the degradation products as the

polymers are hydrolytically degraded. POP-Gly-MMB-NO was developed to evaluate its ability to release NO as a tertiary RSNO and the purpose of developing the polyester polymer systems was to mitigate limitations regarding mismatch of mechanical properties and adverse reactions that typically limit polymeric devices' use as biomaterials.

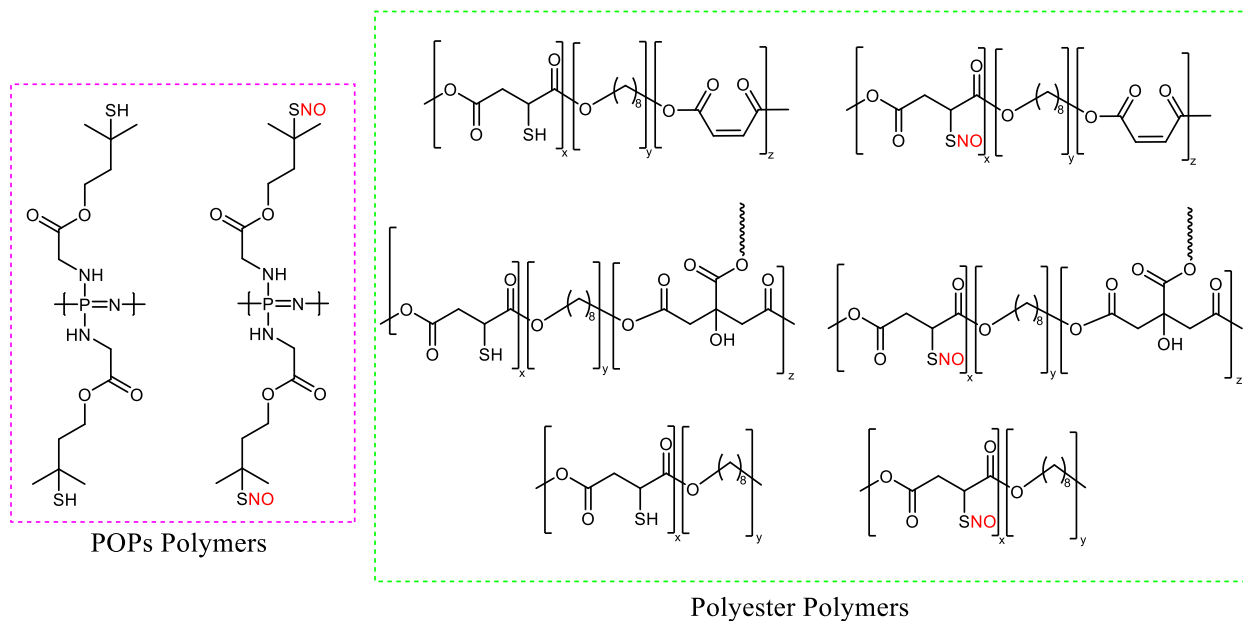


Figure 4.1 Polymer systems used to develop mass spectrometric methods to identify hydrolytic degradation products.

Herein we report mass spectrometric and liquid chromatography mass spectrometric methodology to separate and identify each component of the degradation of biodegradable POPs, polyesters and their nitrosated analogues, potential candidates for use in biomedical devices. This study sought to provide structural elucidation of each component found during the degradation of these polymers, which will aid in the deduction of the degradation mechanisms and for elucidation of potential toxicity concerns of a biomedical device. The goals for each polymer system were as follows:

- POPs polymer system: determine the products formed due to hydrolytic degradation

- Polyester polymer systems: determine the products formed due to hydrolytic degradation for each system (PTO, PTCO, PTMO and their *S*-nitrosated analogues)
- PTMO and PTMO-NO: expand upon the determination of products of hydrolytic degradation by developing LC-MS and LC-MS/MS methodology for structural elucidation

4.3 Experimental

4.3.1 Polyphosphazene Degradation

4.3.1.1 Materials

LC-MS grade methanol and water were purchased from VWR (Solon, OH, USA). Media from POP-Gly-MMB and POP-Gly-MMB-NO were provided by Alec Lutzke. A Millipore Direct-Q water purification system was used to produce 18.2 M Ω water for the polymer degradation studies (MilliporeSigma). All degradation experiments were performed in Millipore water instead of using the PBS buffer system due to phosphate buffers detrimental effects on mass spectrometric detectors, leading to severe ion suppression and unreliable analyses.

4.3.1.2 Mass Spectrometry Methods

Degradation of POP-Gly-MMB and POP-Gly-MMB-NO

To identify the potential hydrolytic degradation products from POP-Gly-MMB and POP-Gly-MMB-NO, samples from each polymer were hydrolyzed in Millipore water at 37 °C under ambient atmosphere for 2 weeks. The media were subsequently analyzed by time-of-flight (TOF) mass spectrometry (TOF-MS). All mass spectrometric analyses were performed on an Agilent 6224 TOF LC/MS. The instrument was equipped with an Agilent multimode ionization (MMI) source capable of electrospray ionization (ESI) and atmospheric pressure chemical ionization (APCI). For all experiments, mixed-mode ionization in both positive and negative polarity was employed with the mass range set to 70–3200 *m/z*. The sample solutions were introduced by flow

injection at a flow rate of 0.200 mL/min *via* the ESI nebulizer using methanol as the mobile phase. The MS conditions were as follows: capillary voltage, 2500 V; fragmentor voltage, 120 V; skimmer voltage, 60 V; charging voltage, 2000 V; drying gas (N₂) flow rate, 10 l/min; drying gas temperature 310 °C; and nebulizer pressure, 45 psi. All data were processed using Agilent MassHunter Qualitative Analysis B.07.00.

4.3.2 Biodegradable Polyester Degradation

4.3.2.1 Materials

LC-MS grade methanol and water were purchased from VWR (Solon, OH, USA). The polymer films PTO, PTMO, PTCO and their nitrosated analogues PTO-NO, PTMO-NO and PTCO-NO were provided by Janet P. Yapor². Ammonium acetate ($\geq 98\%$) was obtained from MilliporeSigma (St. Louis, MO, USA). A Millipore Direct-Q water purification system was used to produce 18.2 M Ω water for the polymer degradation studies (MilliporeSigma). All degradation experiments were performed in Millipore water instead of using the PBS buffer system due to phosphate buffers detrimental effects on mass spectrometric detectors, leading to severe ion suppression and unreliable analyses.

4.3.2.2 Methods

Degradation of PTO, PTMO, PTCO and their S-nitrosated analogues

The hydrolytic degradation potential of the polymers was assessed by immersing samples ($n=3$) of PTO, PTO-NO, PTCO, PTCO-NO, PTMO, and PTMO-NO in Millipore water at 37 °C in the absence of light for up to 6 weeks. Samples were collected every 7 days ($n=3$), washed with Millipore water, and lyophilized for 24 h. Since the samples were incubated longer than 1 week, the water was replaced at the end of each week.

Degradation of PTMO and PTMO-NO for LC-MS and LC-MS/MS

Three 100-mg samples from each polymer were incubated in 10-mL Millipore water at 37 °C for up to 10 weeks. Samples were collected during weeks 1, 3, 6 and 10 (100 µL, $n = 3$) and immediately analyzed using direct flow injection mass spectrometry to complete a 10-week study. After direct flow injection MS analysis, the samples were stored at -20 °C for LC-MS and LC-MS/MS analysis.

Chromatographic and Mass Spectrometric Methods

The products from the polymer degradation studies were identified using an Agilent 6224 TOF LC/MS. The instrument was equipped with a dual electrospray ion (dual ESI) source. For the experiments, ionization was performed in negative polarity. The sample solutions were introduced to the ion source by direct flow injection using an Agilent 1260 Infinity at a flow rate of 0.200 mL/min via the ESI nebulizer with methanol as the mobile phase. The mass spectrometer conditions were as follows: 4000 V capillary voltage, 120 V fragmentor voltage, 60 V skimmer voltage, 310 °C drying gas (N₂) temperature, 10 l/min drying gas flow rate, and 25 psi nebulizer pressure. All data were processed with Agilent MassHunter Qualitative Analysis B.07.00.

The LC-MS analyses were performed on the Agilent 6224 TOF LC/MS with use of the Agilent 1260 Infinity chromatograph for chromatographic separations. A Zorbax SB-C18, (150 × 4.6, 3.5 µm, Agilent) rapid resolution column, kept at 40 °C was used for all chromatographic separations. The mobile phase was composed of water with 10 mM ammonium acetate designated as solvent A, and methanol with 10 mM ammonium acetate designated as solvent B. A linear gradient was used from 15% to 100% B from 0 to 30 min, kept isocratic at 100% B from 30 to 40 min, and returned to 15% B using a linear gradient from 40 to 50 min at 0.250 mL/min. Since a gradient was utilized, to re-equilibrate the column to the starting conditions, approximately 10 column volumes were used at the end of each run.

The LC-MS/MS analyses were performed on a Bruker maXis UHT-QTOF MS (Bellirica, MA, USA) coupled with a Waters ACQUITY-H UPLC (Milford, MA, USA). The instrument was equipped with an electrospray ion source. For the LC-MS/MS experiments, the mass spectrometer settings were as follows: 2400 V capillary voltage, 500 V end plate offset, 300 °C drying gas (N₂) temperature, 10 l/min drying gas flow rate, and 3.0 bar nebulizer pressure. All fragmentations were performed with a collision energy of 35 eV.

Data analysis for MS only and LC-MS analyses were reported from a minimum of triplicate measurements, unless otherwise noted, and all data were analyzed with Agilent MassHunter Qualitative Analysis B.07.00. Data for LC-MS/MS analyses were reported from a single run for a PTMO sample and a single run for PTMO-NO sample. All data were analyzed with Bruker Compass DataAnalysis 4.4.

4.4 Results

4.4.1 Mass Spectrometric Identification of Degradation Products

4.4.1.1 Method to Identify the Degradation Products of the POPs Polymers:

The first step for the development the MS method for analysis of POPs degradation products was to look at the synthetic procedure followed to synthesize the polymers. From the synthetic procedure, the identified building blocks for the polymer were a poly(phosphazene) backbone, glycine, and 3-mercapto-3-methylbutanol. Glycine (Figure 4.4) can be ionized in either positive mode (-NH₂ moiety) or negative mode (-COOH), with positive mode as the preferred polarity for ionization. 3-mercapto-3-methylbutanol (Figure 4.4) is more likely to be ionized in negative mode due to the potential to deprotonate the thiol group. Knowledge of the synthetic building blocks and their potential polarity of ionization led to analyzing the samples twice: first in positive mode and then in negative mode as will be shown in the next sections. The parameters

presented in section 4.2.1 were determined using recommendations from CSU's central instrument facility and recommendations when methanol is the mobile phase¹⁷.

4.4.1.2 Degradation and Direct Injection MS analysis of POPs polymers.

The general synthetic procedures for the POP-Gly-MMB-NO polymer have been reported previously³ and are shown in Figure 4.2.

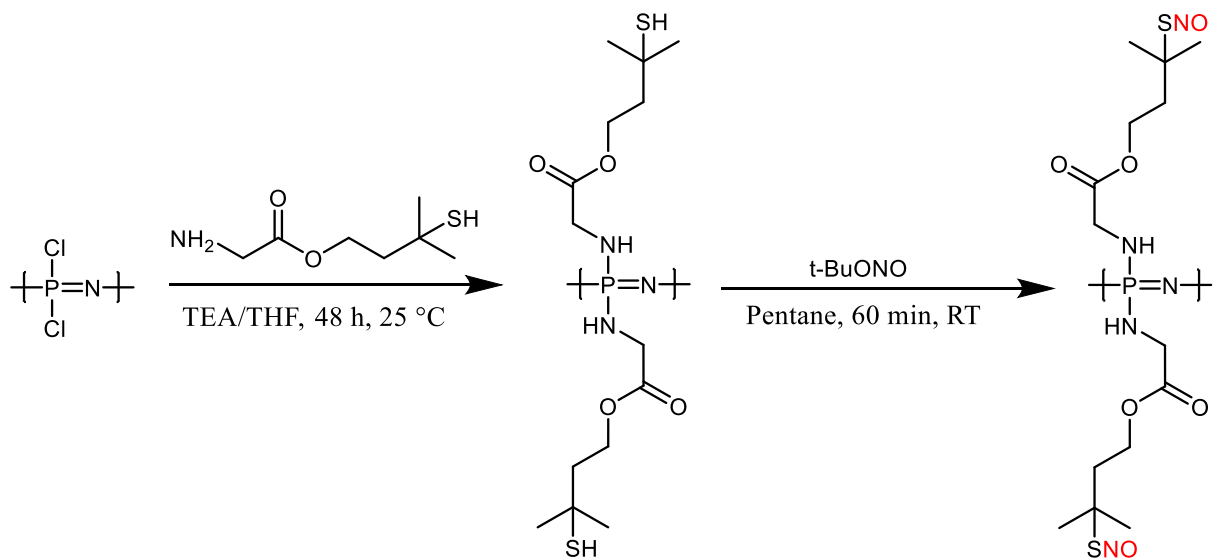


Figure 4.2 Synthesis of POP-Gly-MMB-NO

Based on the connectivity between glycine, 3-mercapto-3-methylbutanol, and the poly(phosphazene) backbone, we suspected to find glycine (Gly), 3-mercapto-3-methylbutanol (MMB), the combination of the two (Gly-MMB) and during the NO-release from the S-nitrosated polymer, potentially disulfide bridges (Figure 4.3, Figure 4.4).

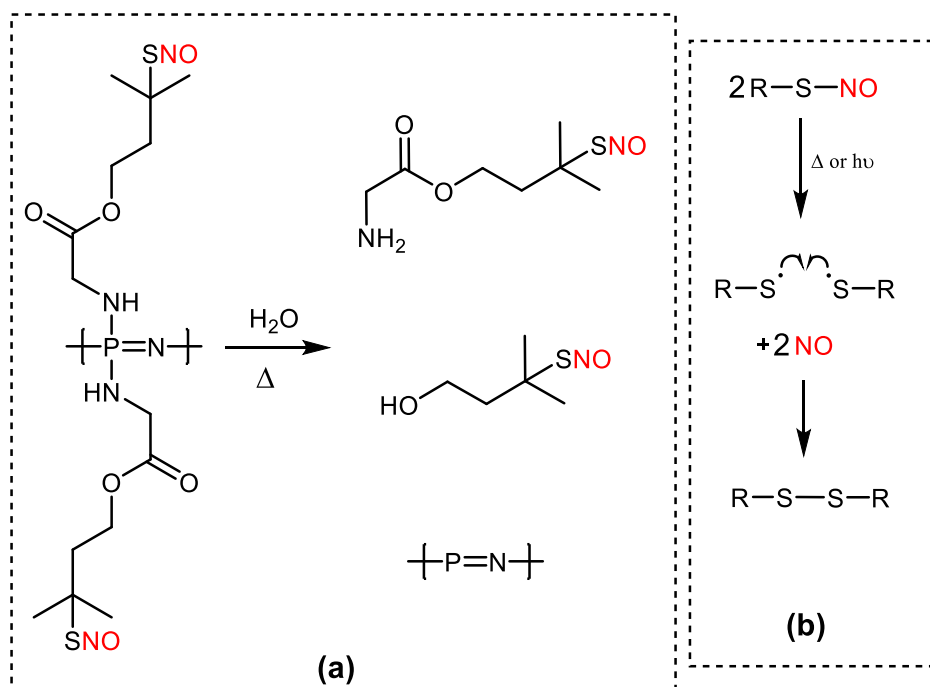


Figure 4.3 Hydrolytic degradation and disulfide bond formation. (a) possible degradation products of hydrolytic degradation. (b) disulfide bond formation after release of NO.

Based on the predicted degradation products, glycine, Gly-MMB and Gly-MMB disulfide were more likely to be successfully ionized in positive mode, while MMB and MMB disulfide were more likely to be ionized successfully in negative mode. Therefore, the solutions provided by Alec were ran twice, in positive and negative mode.

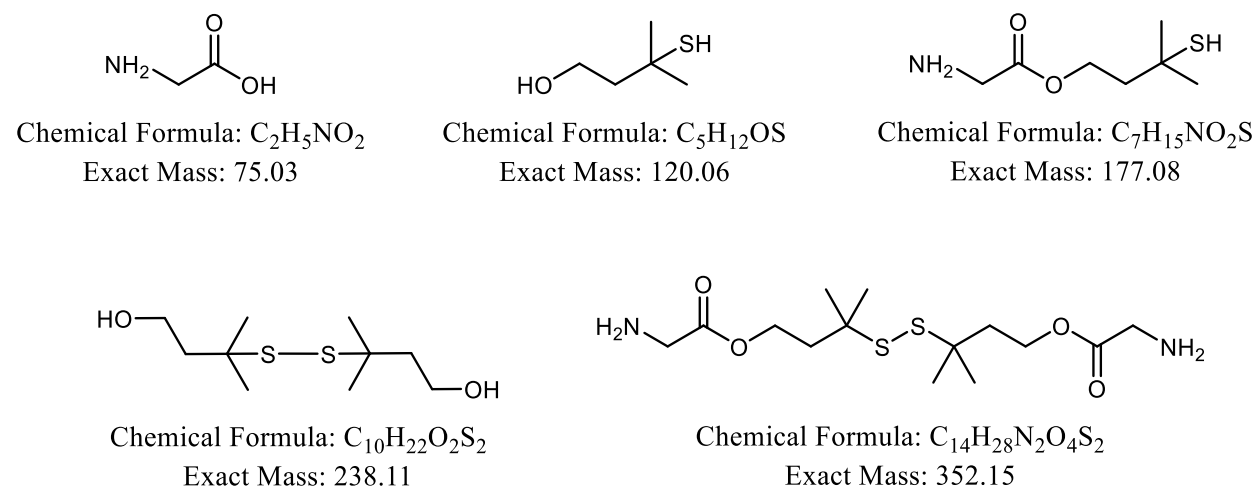


Figure 4.4 Potential degradation products from POP-Gly-MMB and POP-Gly-MMB-NO

The primary identifiable degradation products common to both POP-Gly-MMB and POP-Gly-MMB-NO were glycine, MMB and the Gly-MMB dimer. This is consistent with the anticipated degradation of the amine-substituted POPs polymer backbone. In Figure 4.5, glycine is shown at m/z 76.0398 and Gly-MMB is shown at m/z 178.0889. Both ions are consistent with the masses of glycine and Gly-MMB forming as $[M+H]^+$ ions. To find MMB, ionization was performed in negative mode as shown in Figure 4.6. Based on the structure of MMB, ionization in positive mode was unlikely due to the lack of basic sites. However, both the free thiol and alcohol would allow for removal of a proton leading to the ion at m/z 119.0543 which corresponds to MMB as $[M-H]^-$ ion.

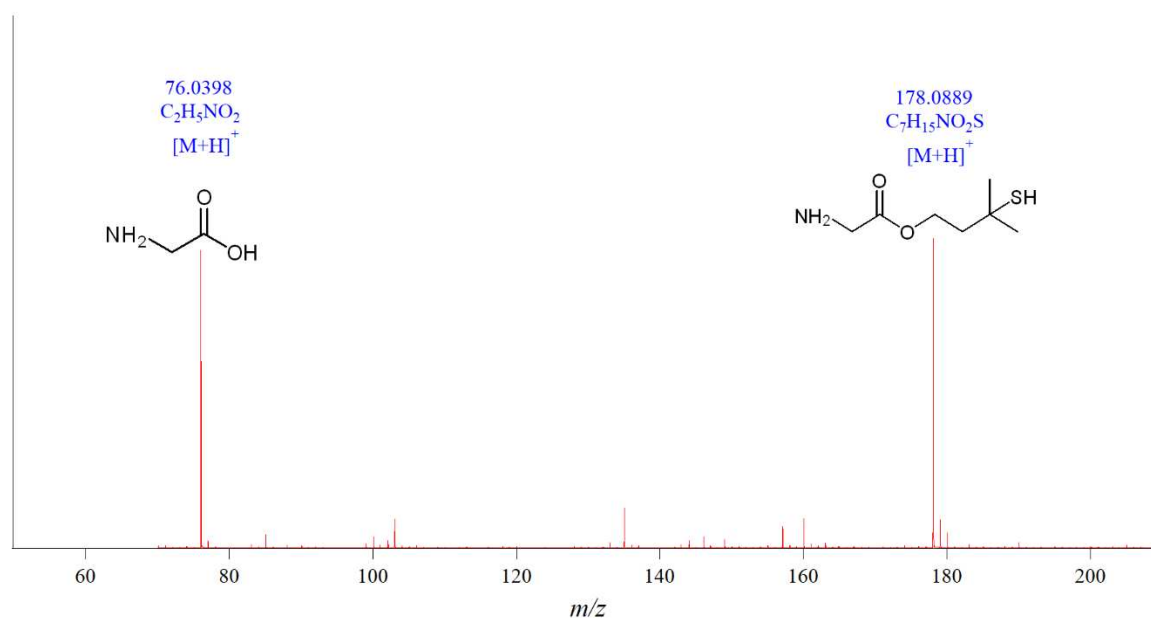


Figure 4.5 Positive ionization of degradation products from POP-Gly-MMB. Glycine and Gly-MMB were found at m/z 76 and 178 respectively.

In the case of the *S*-nitrosated POP-Gly-MMB-NO, the ions corresponding to glycine, MMB and gly-MMB were found, with the addition of the ions that correspond to 3-[(4-hydroxy-2-methylbutan-2-yl)disulfanyl]-3-methylbut-1-yl glycinate (C₁₂H₂₅NO₃S₂) and 3-[(4-glycyloxy-2-methylbutan-2-yl)disulfanyl]-3-methylbut-1-yl 2-hydroxyacetate (C₁₄H₂₇NO₅S₂). Both

molecules are likely to represent disulfide-bond degradation products that formed during the decomposition of the POP-Gly-MMB-NO *S*-nitrosothiol (Figure 4.7).

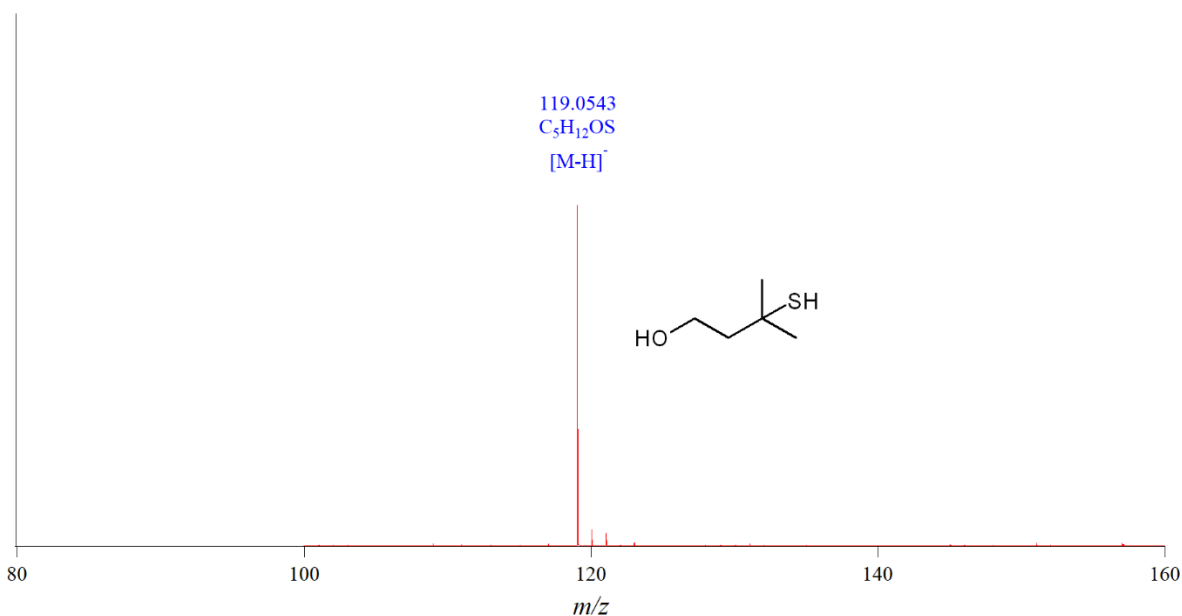


Figure 4.6 Negative ionization of degradation products from POP-Gly-MMB. 3-mercapto-3-methylbutanol was found at *m/z* 119.

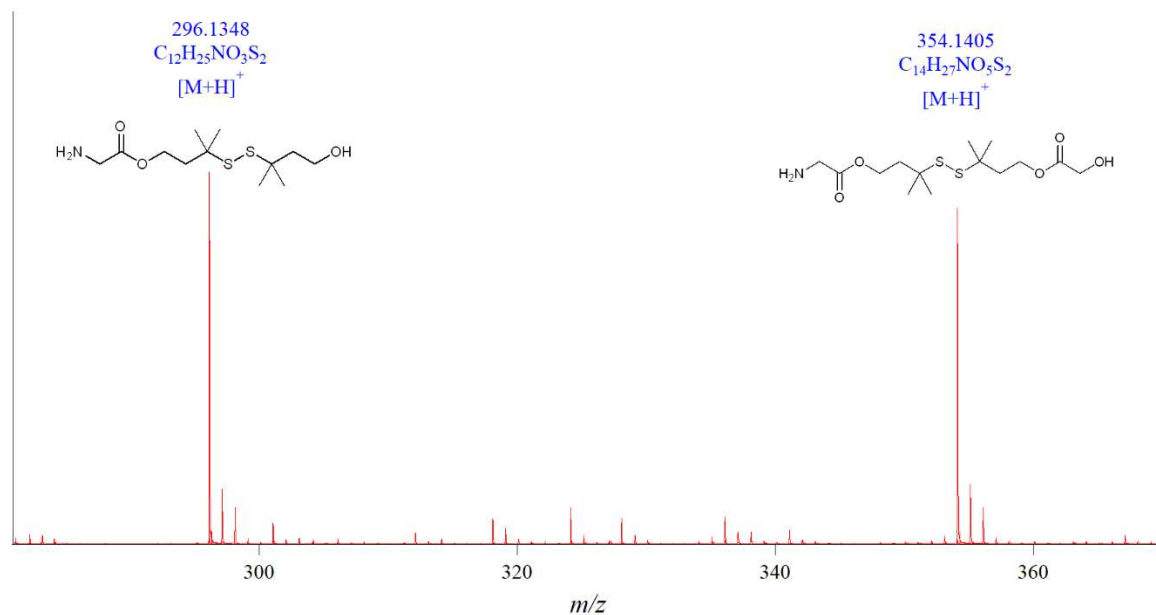


Figure 4.7 Positive ionization of degradation products from POP-Gly-MMN-NO. The ions found at *m/z* 296 and 354 were found only as products from the *S*-nitrosated polymer.

Mass spectrometric analysis of the degradation products from POP-Gly-MMB and POP-Gly-MMB-NO allowed for the development of a preliminary analytical model that aids in the

appropriate screening of biodegradable polymer degradation products. This analytical model paved the way to develop mass spectrometric methods to identify the degradation products from PTO, PTCO, PTMO and their *S*-nitrosated analogues.

4.4.1.3 Method to Measure the Degradation Products of Polyesters

Similar to the development of mass spectrometric methods for analysis of degradation products of the POPs polymers, the first step was to examine the synthetic procedure for each of the polyesters to be studied. The building blocks for the polymers were a combination of thiomalic acid, maleic acid, citric acid and 1,8-octanediol. For all cases, it was determined that ionization in negative mode would be most appropriate due to the -COOH moieties present in thiomalic, maleic and citric acid and the -OH moieties in 1,8-octanediol. As will be shown for each polymer system, ionization in negative polarity was appropriate to identify each degradation product.

4.4.1.4 Degradation and Direct Injection MS Analysis of Polyester Polymers

The synthesis of poly(thiomalic acid-*co*-1,8-octanediol) or PTO and the *S*-nitrosated analogue is shown in Figure 4.8. Based on the polycondensation reaction and *S*-nitrosation, the monomers were initially predicted to be found during the degradation process (Figure 4.8).

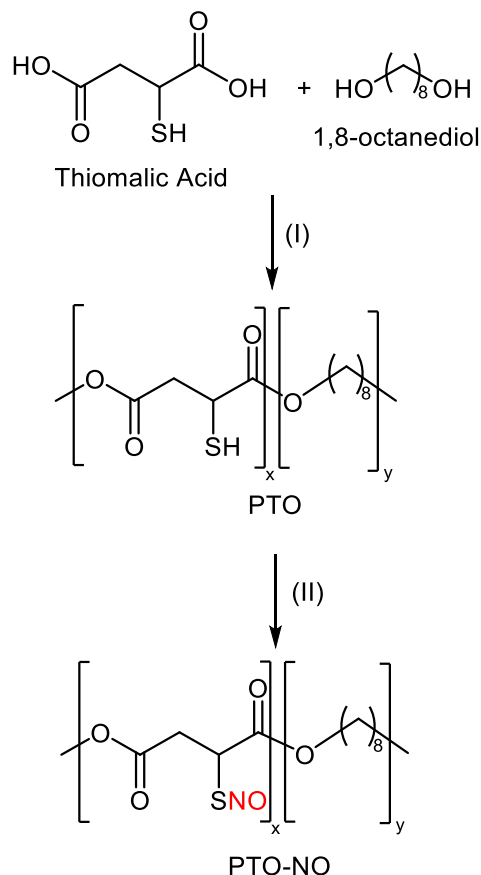


Figure 4.8 Synthesis of PTO and PTO-NO. (I) Polycondensation to synthesize PTO. (II) S-nitrosation of PTO.

As shown in Figure 4.8, PTO was prepared *via* melt-phase polycondensation using thiomalic acid and 1,8-octanediol. The polycondensation took place at 140 °C for 17 h under nitrogen to obtain a viscous polymer. To reduce the amount of disulfide bonds formed during the polycondensation reaction, the crude polymer was dissolved in ethyl ether anhydrous and treated with DL-dithiothreitol (DTT) and triethyl amine (TEA). S-nitrosation was subsequently performed by stirring PTO in ethanol with *tert*-butyl nitrite (*t*-BuONO) to make PTO-NO. The degradation product from PTO is shown in Figure 4.9 in which the major product identified is a dimer of thiomalic acid and 1,8-octanediol.

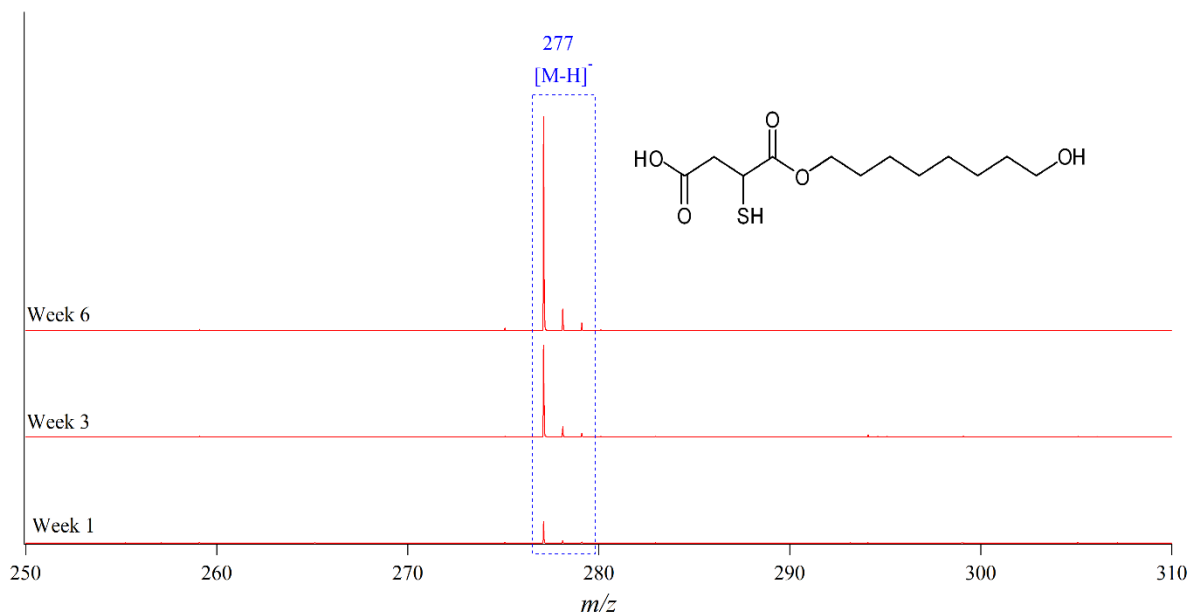


Figure 4.9 Degradation product from PTO. The dimer corresponds to the combination of the starting monomers thiomalic acid and 1,8-octanediol.

The degradation products from PTO-NO are shown in Figure 4.10. The same dimer shown in Figure 4.9 was found as well as the ions m/z 393 and 521 also shown in Figure 4.10. The structures shown in Figure 4.10 were products only found from degradation of the nitrosated PTO polymer.

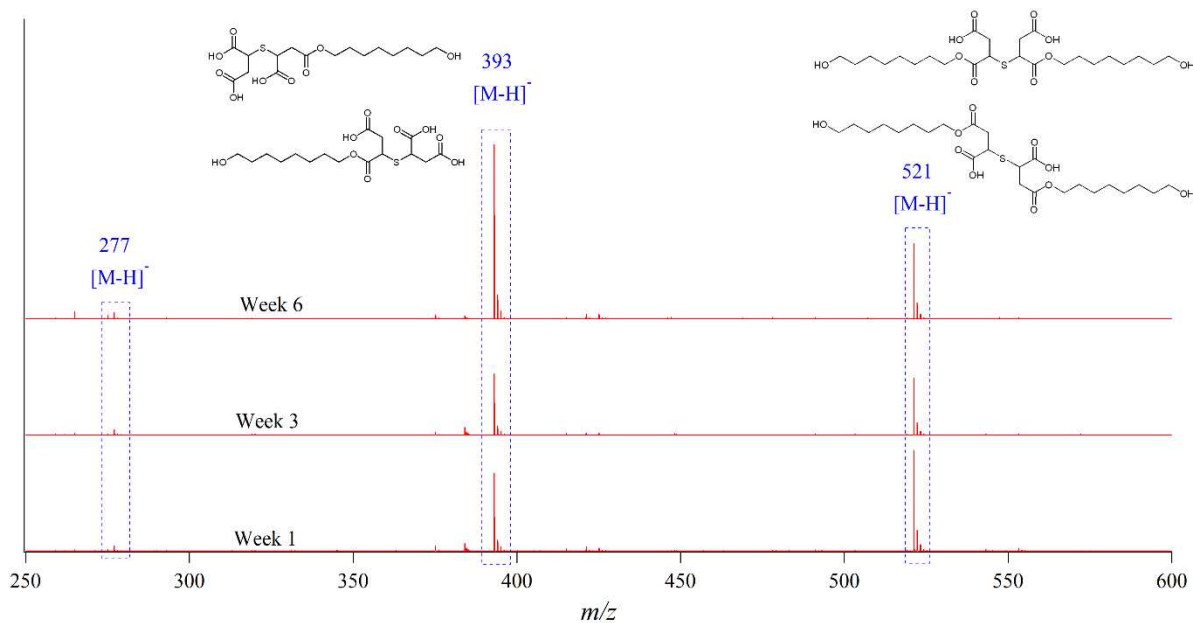


Figure 4.10 Degradation products from PTO-NO.

The synthesis of poly(thiomalic-*co*-citric acid-*co*-1,8-octanediol) or PTCO and the *S*-nitrosated analogue is shown in Figure 4.11. Based on the polycondensation reaction and *S*-nitrosation, the monomers were initially predicted to be found during the degradation process (Figure 4.11).

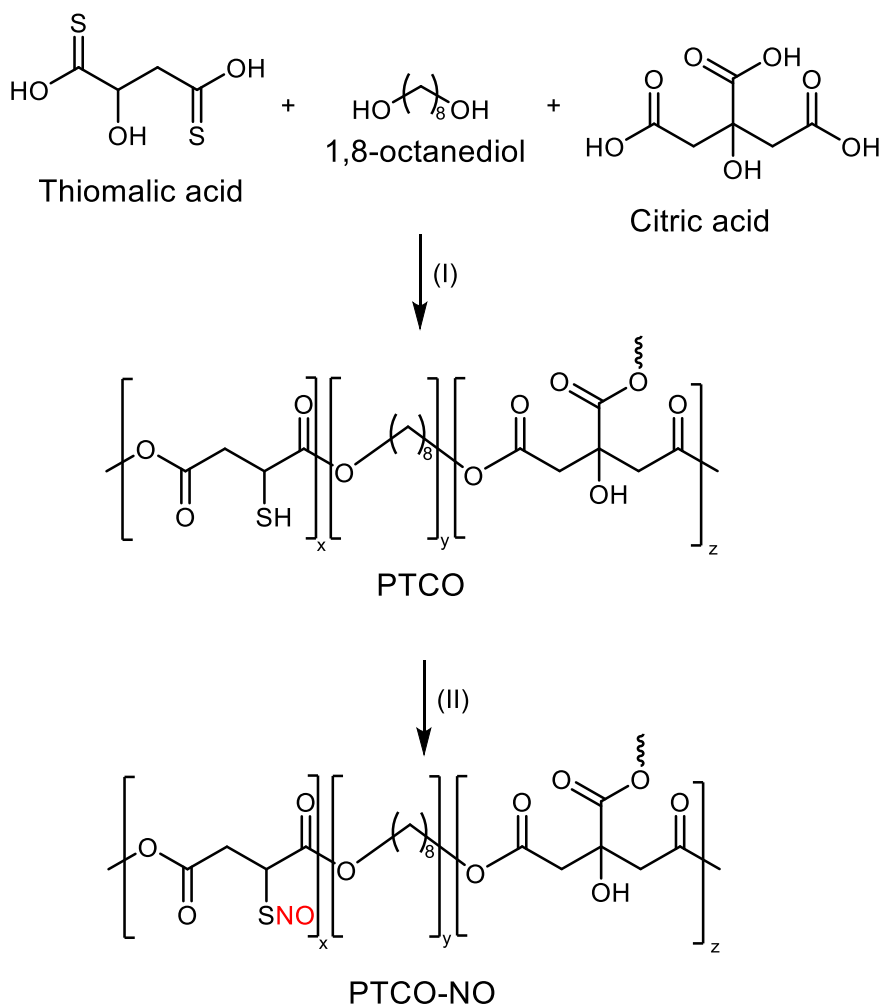


Figure 4.11 Synthesis of PTCO and PTCO-NO. (I) Polycondensation to synthesize PTCO. (II) *S*-nitrosation of PTCO.

As shown in Figure 4.11, PTCO also was prepared *via* melt-phase polycondensation using thiomalic acid, citric acid, and 1,8-octanediol. The polycondensation took place at 140 °C for 1 h under nitrogen to obtain a viscous polymer. To reduce the amount of disulfide bonds formed during the polycondensation reaction, the crude polymer was dissolved in absolute ethanol and treated

with DTT and TEA. *S*-nitrosation was subsequently performed by stirring PTCO in ethanol with *t*-BuONO to make PTCO-NO. The resulting mass spectrum for PTCO is shown in Figure 4.12 and the structural candidates are shown in Figure 4.13.

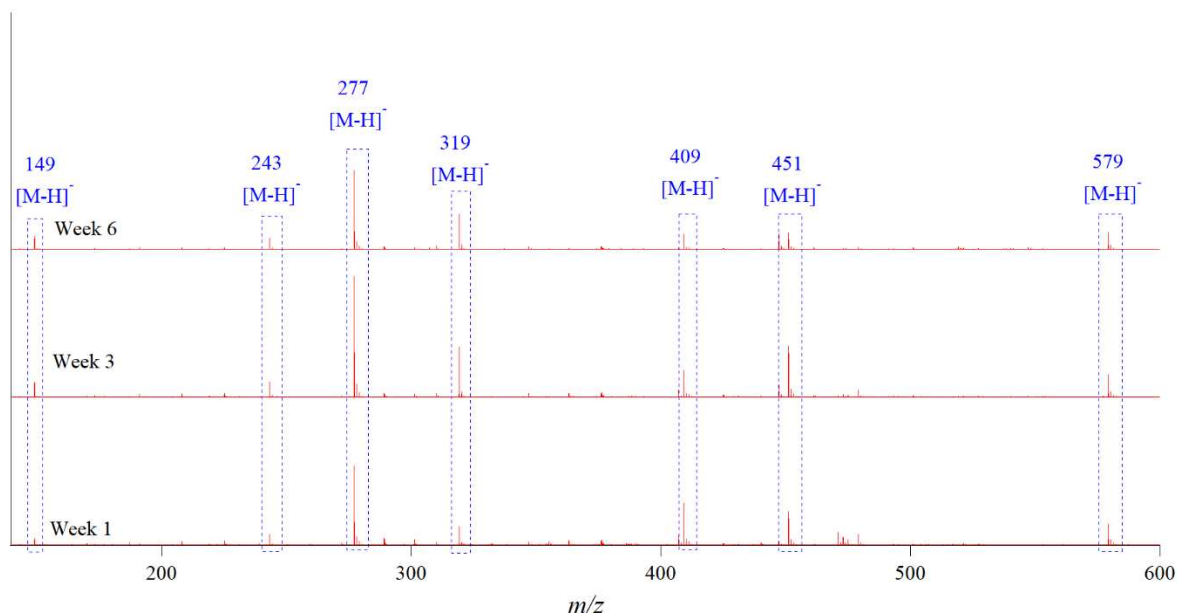
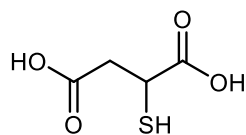
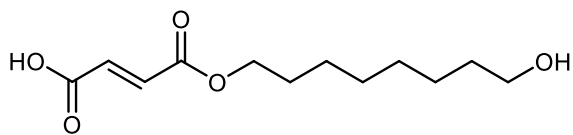


Figure 4.12 Mass spectrum from the degradation of PTCO.

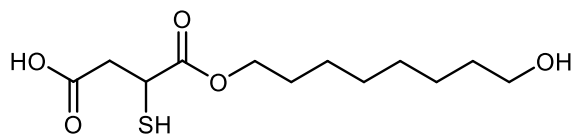
As shown in Figure 4.12, more ions were found from PTCO than from PTO and PTO-NO. This can be attributed to the addition of citric acid to the starting maleic acid and 1,8-octanediol monomers for the polycondensation reaction. All the potential degradation products are shown in Figure 4.13 where thiomalic acid was the only monomer found and the majority of the remaining products are a combination of the starting monomers as dimers and beyond.



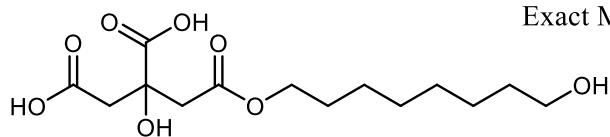
Chemical
Formula: $C_4H_6O_4S$
Exact Mass: 150.00



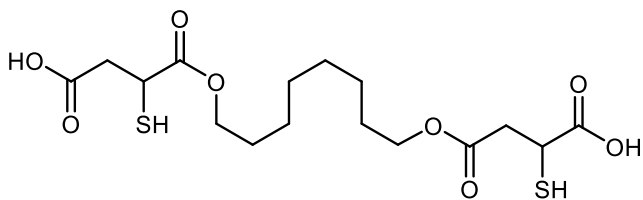
Chemical Formula: $C_{12}H_{20}O_5$
Exact Mass: 244.13



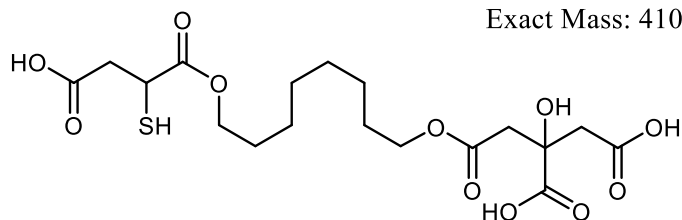
Chemical Formula: $C_{12}H_{22}O_5S$
Exact Mass: 278.12



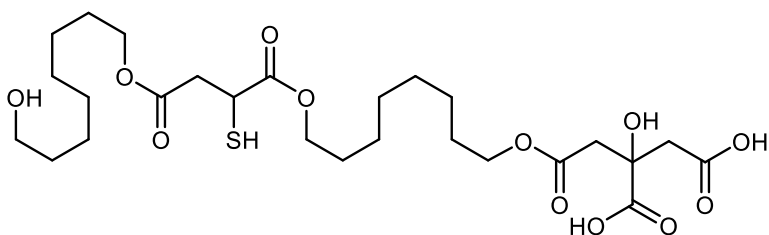
Chemical Formula: $C_{14}H_{24}O_8$
Exact Mass: 320.15



Chemical Formula: $C_{16}H_{26}O_8S_2$
Exact Mass: 410.11



Chemical Formula: $C_{18}H_{28}O_{11}S$
Exact Mass: 452.14



Chemical Formula: $C_{26}H_{44}O_{12}S$
Exact Mass: 580.26

Figure 4.13 Potential structures for the ions found during the degradation of PTCO.

The resulting mass spectrum for PTCO-NO is shown in Figure 4.14 and the structural candidates are the same as m/z 149, 243, 277 and 319.

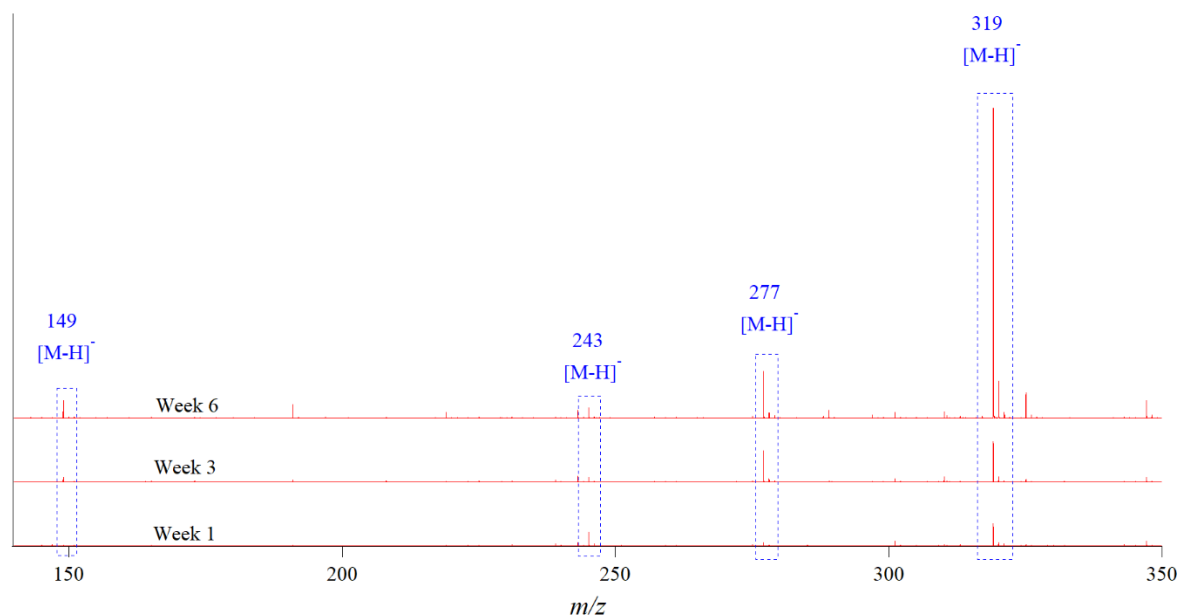


Figure 4.14 Mass spectrum of the degradation products from PTCO-NO.

The synthesis of poly(thiomalic-*co*-maleic acid-*co*-1,8-octanediol) or PTMO and the *S*-nitrosated analogue is shown in Figure 4.15. Based on the polycondensation reaction and *S*-nitrosation, the monomers were initially predicted to be found during the degradation process (Figure 4.15).

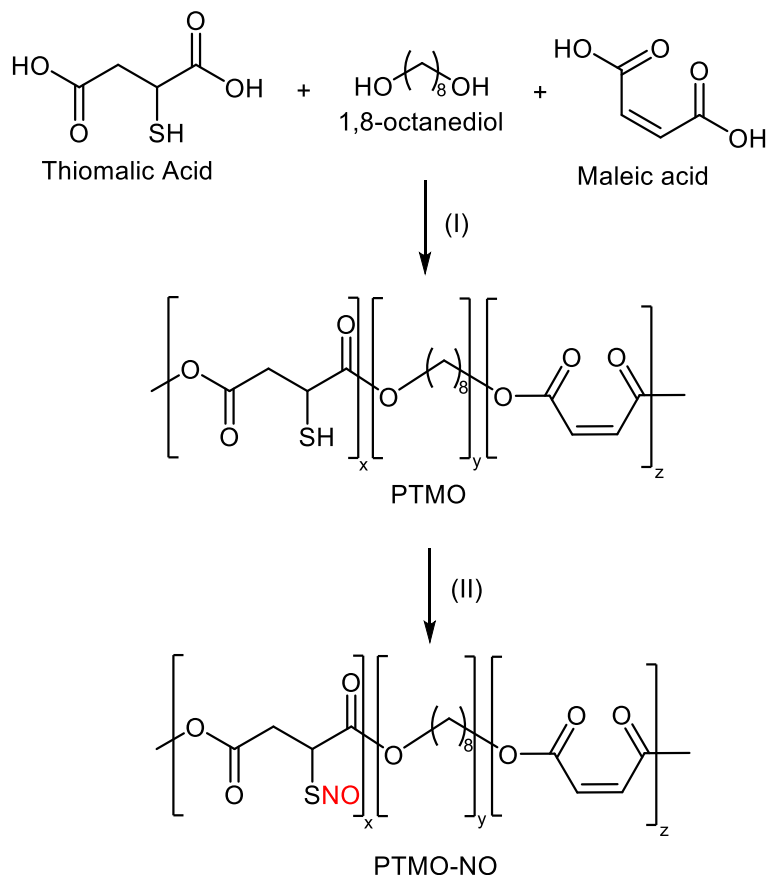


Figure 4.15 Synthesis of PTMO and PTMO-NO. (I) Polycondensation to synthesize PTMO. (II) S-nitrosation of PTMO.

As shown in Figure 4.15, PTMO also was prepared *via* melt-phase polycondensation using thiomalic acid, maleic acid, and 1,8-octanediol. The polycondensation took place at 140 °C for 38 min under nitrogen to obtain a viscous polymer. To reduce the amount of disulfide bonds formed during the polycondensation reaction, the crude polymer was dissolved in absolute ethanol and treated with DTT and TEA. S-nitrosation was subsequently performed by stirring PTMO in ethanol with *t*-BuONO to make PTMO-NO. The collected mass spectrum from the degradation products is shown in Figure 4.16.

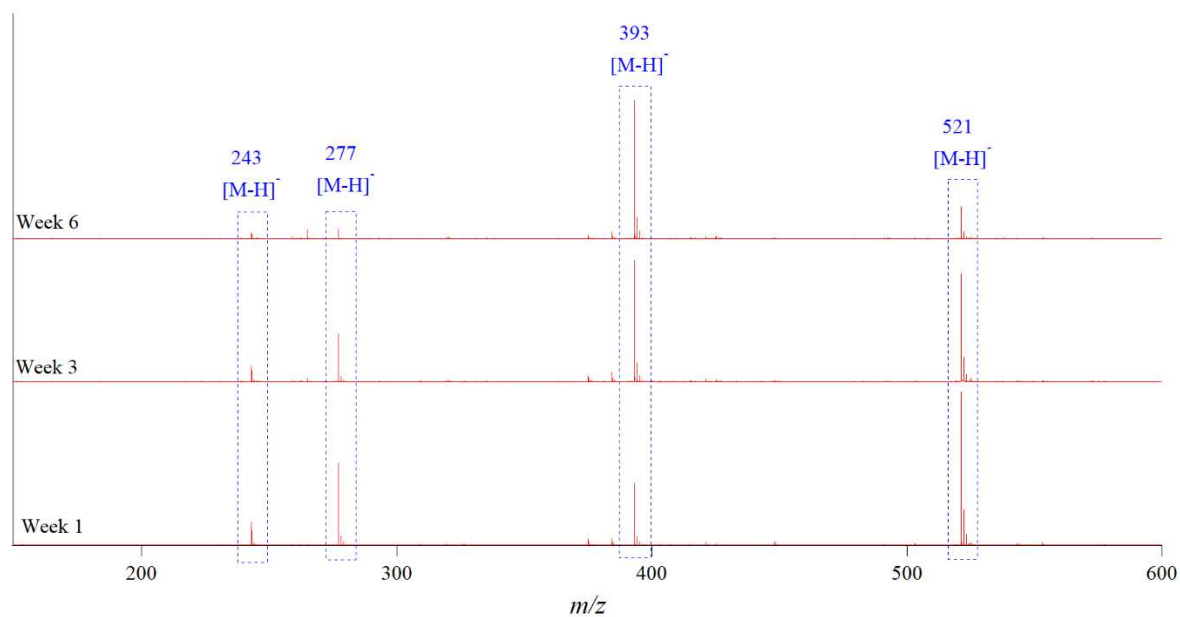
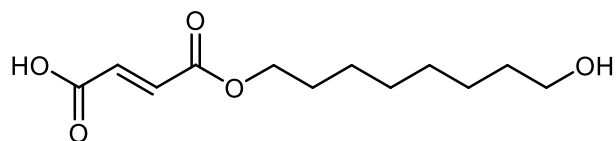


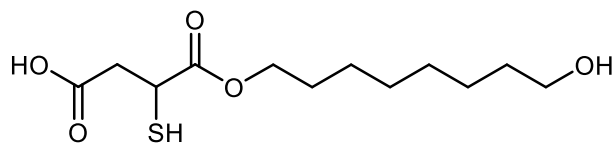
Figure 4.16 Mass spectrum of the degradation products from PTMO.

The candidate structures of the degradation products from PTMO are shown in Figure 4.17. The ions m/z 243 and 277 are the dimers composed of maleic acid – 1,8-octanediol and thiomalic acid – 1,8-octanediol. The ions m/z 393 and 521 were later identified as the four major structures shown in Figure 4.17 as well.



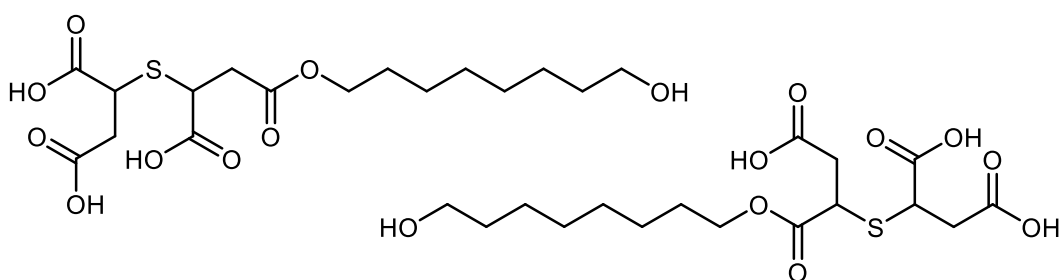
Chemical Formula: $C_{12}H_{20}O_5$

Exact Mass: 244.13



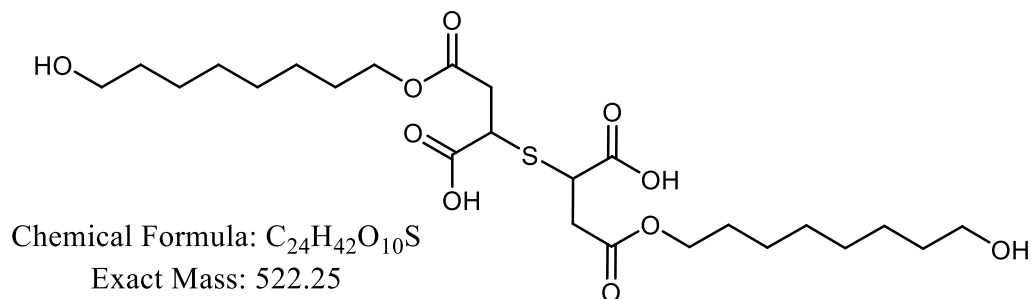
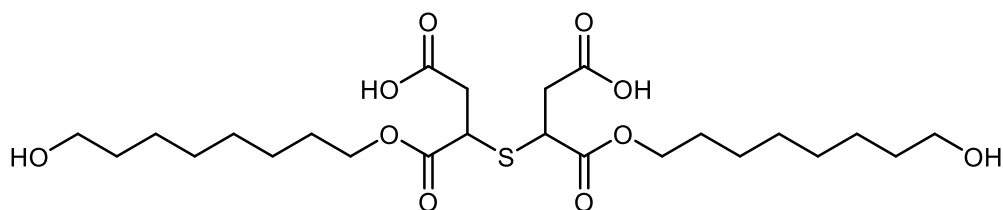
Chemical Formula: $C_{12}H_{22}O_5S$

Exact Mass: 278.12



Chemical Formula: $C_{16}H_{26}O_9S$

Exact Mass: 394.13



Chemical Formula: $C_{24}H_{42}O_{10}S$

Exact Mass: 522.25

Figure 4.17 Potential structures of the degradation products from PTMO.

The degradation products from PTMO-NO are shown in the mass spectrum in Figure 4.18. As shown in the mass spectrum, the same ions found from PTMO were also found in PTMO-NO with the exception of m/z 277.

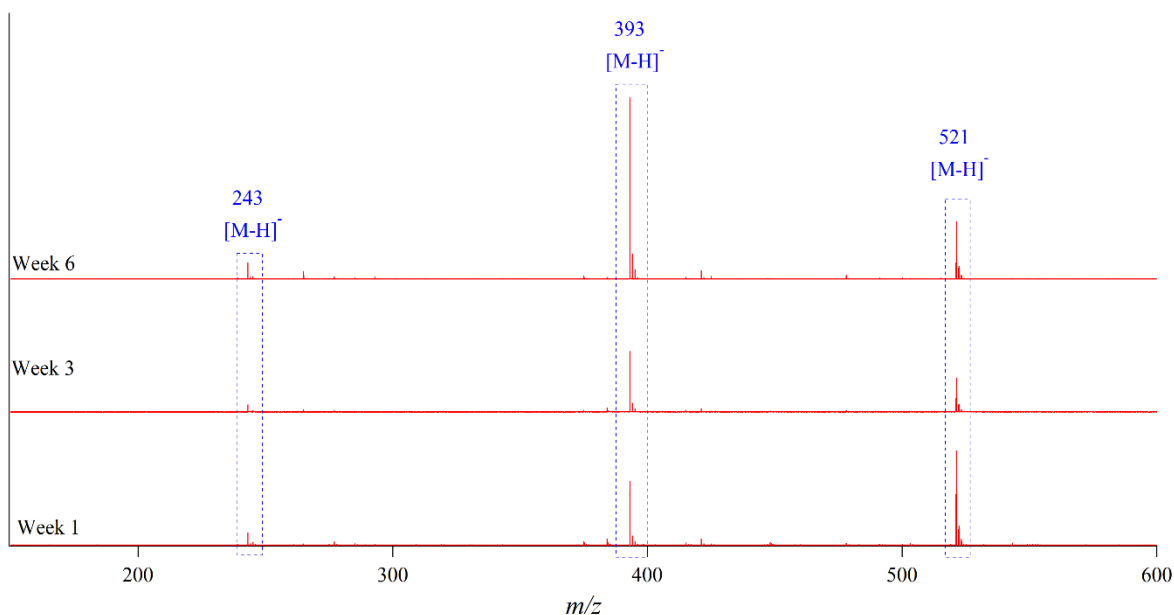


Figure 4.18 Mass spectrum of the degradation products from PTMO-NO.

The degradation products were expected due to the connectivity between the monomers used for each polycondensation reaction. Based on the ions shown in each Figure showing the degradation products, the m/z ions remained questionable. After J. Pamela Yapor determined PTMO and PTMO-NO to be the best candidate for use as a biodegradable polymer with the desirable properties for potential biological applications, the next step was to include a chromatographic separation to further isolate the components from degradation and perform fragmentation studies (LC-MS and LC-MS/MS) to obtain accurate structural information.

4.4.2 Liquid Chromatography-Mass Spectrometric Analysis

Following the recommendation from J. Pamela Yapor, PTMO and PTMO-NO were selected for further studies. PTMO and PTMO-NO demonstrated the most efficient hydrolytic degradation of the three sets of polymers which may be of interest for development of

biodegradable devices. A new set of PTMO and PTMO-NO were provided by J. Pamela Yapor to perform a 10-week study of the hydrolytic degradation products. As shown in Figure 4.19 and Figure 4.20, both PTMO and PTMO-NO degraded into the same three ions (m/z 243, 393, 521) during the 10-week period. As described previously (Figure 4.17), only the maleic acid-1,8-octanediol dimer was successfully identified. However, it was still hypothesized that the unidentified ions were a combination of the starting monomers from the synthetic procedure.

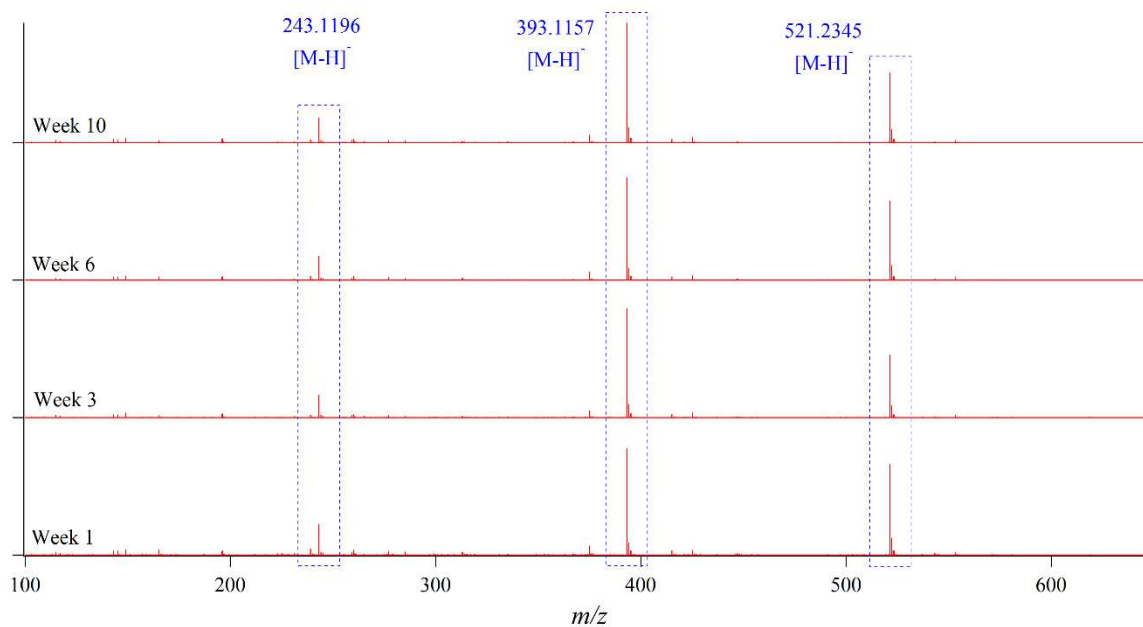


Figure 4.19 Mass spectrum of PTMO products during the degradation process. All three ions continued to be present during the 10-week period.

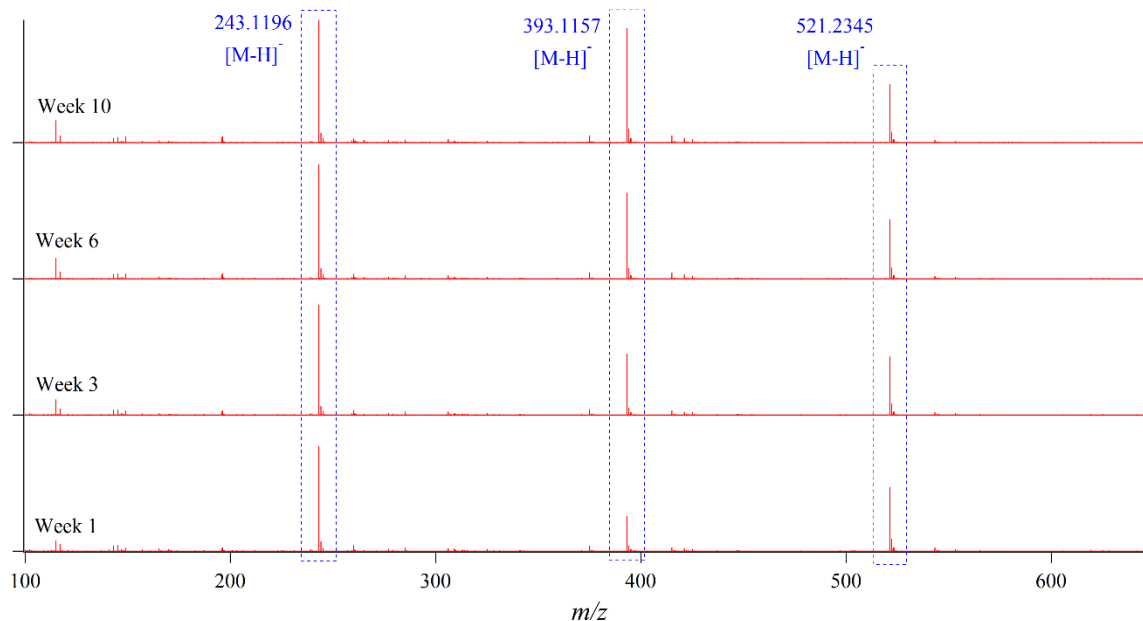


Figure 4.20 Mass spectrum of PTMO-NO products during the degradation process. All three ions continued to be present during the 10-week period.

The initial target was to isolate the three major ions found during the degradation process. To do so, a series of chromatographic separations were performed using a Zorbax SB-C18, 4.6×150 mm, 3.5-micron rapid resolution column using the collected media from PTMO and PTMO-NO degradation that eventually led to the method established in section 4.2. The main challenge that had to be addressed was not having a complete knowledge of each individual degradation product's structure. This led to multiple sample injections keeping the chromatography isocratic at different solvent compositions that ranged from 90:10 aqueous/organic to 0:100 aqueous/organic with 10% changes in solvent composition. Contrary to the initially expected three major ions (Figures 4.19 and 4.20), the 10 chromatographic analyses at each solvent composition revealed the presence of components not previously detected by flow injection MS only, and the presence of structural isomers (Figure 4.21). With these series of isocratic chromatographic separations, the final gradient method described in section 4.2.2.2 was selected.

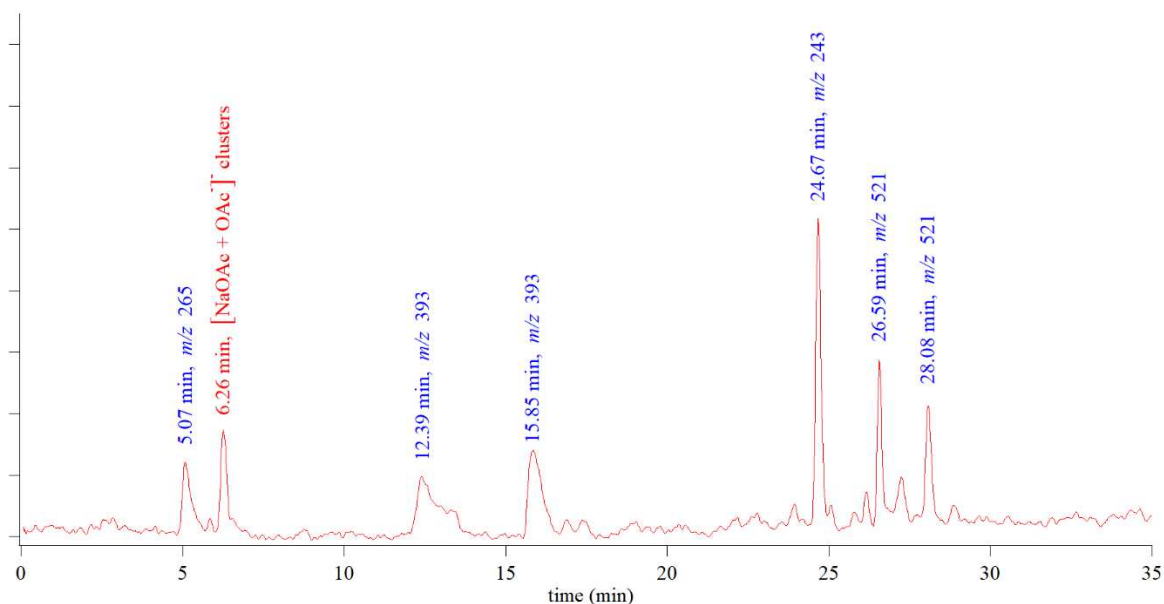


Figure 4.21 Representative chromatogram from PTMO-NO degradation products.

After the initial MS screenings (Figures 4.19, 4.20), the optimized LC-MS method described in the methodology section allowed for separation (Figure 4.21) and identification of 7 major chromatographic peaks. From each chromatogram, the mass spectrometric data was extracted to identify the ions found under each peak. The peak at 5.07 min corresponds to the ion m/z 265, the broad peak at 12.39 min and the peak at 15.85 min correspond to identical ions m/z 393, the peak at 24.67 min corresponds to the ion m/z 243 and the peaks at 26.59 and 28.08 min correspond to identical ions m/z 521. Triplicates for weeks 1, 3, 6 and 10 for PTMO-NO are found in Appendix A1.

4.4.3 LC-MS/MS Structural Elucidation of Degradation Products

Following the chromatographic separation of each peak, fragmentation data was obtained using the LC-MS/MS method described in the methodology section, in combination with the use of the program CFM-ID¹⁸ to determine the structure of each identified peak (Figure 4.21). Based on the starting monomers and polymerization reaction (Figure 4.15), the ion found at 5.07 min (m/z 265) corresponds to the structure shown in Figure 4.22a, matching the formula $C_8H_{10}O_8S$ as

[M-H]⁻. The structure is feasible based on the expected connectivity of the monomers after the polymerization reaction and is confirmed by LC-MS/MS (Figure A1.5). The peak at 6.26 min corresponds to the sodium acetate + acetate ions clusters that arise from the ammonium acetate mobile phase (Figure A1.6) used during the LC-MS analyses.

The ions found at 12.39 and 15.85 min (m/z 393) correspond to the structures shown in Figure 4.22b-c, matching the formula C₁₆H₂₆O₉S as [M-H]⁻. These ions were of interest due to suspected structural isomerism from the MS only data and the presence of two peaks with the same m/z during the LC-MS analyses. The structure of each isomer was identified by LC-MS/MS as shown in Figures A1.7 and A1.8. The ion found at 24.67 min corresponds to the structure shown in Figure 4.22d and Figure A1.9 matching the formula C₁₂H₂₀O₅ as [M-H]⁻. The formula and structure of this ion was previously identified to be the combination of 1,8-octanediol and maleic acid².

Lastly, the ions found at 26.59 and 28.08 min correspond to the structures shown in Figure 4.22e-f, matching the formula C₂₄H₄₂O₁₀S as [M-H]⁻. These ions were also of high interest due to the suspected structural isomerism from the MS only data and the presence of two peaks with the same m/z during the LC-MS analyses. The structure of each isomer was identified by LC-MS/MS as shown in Figures A1.10 and A1.11.

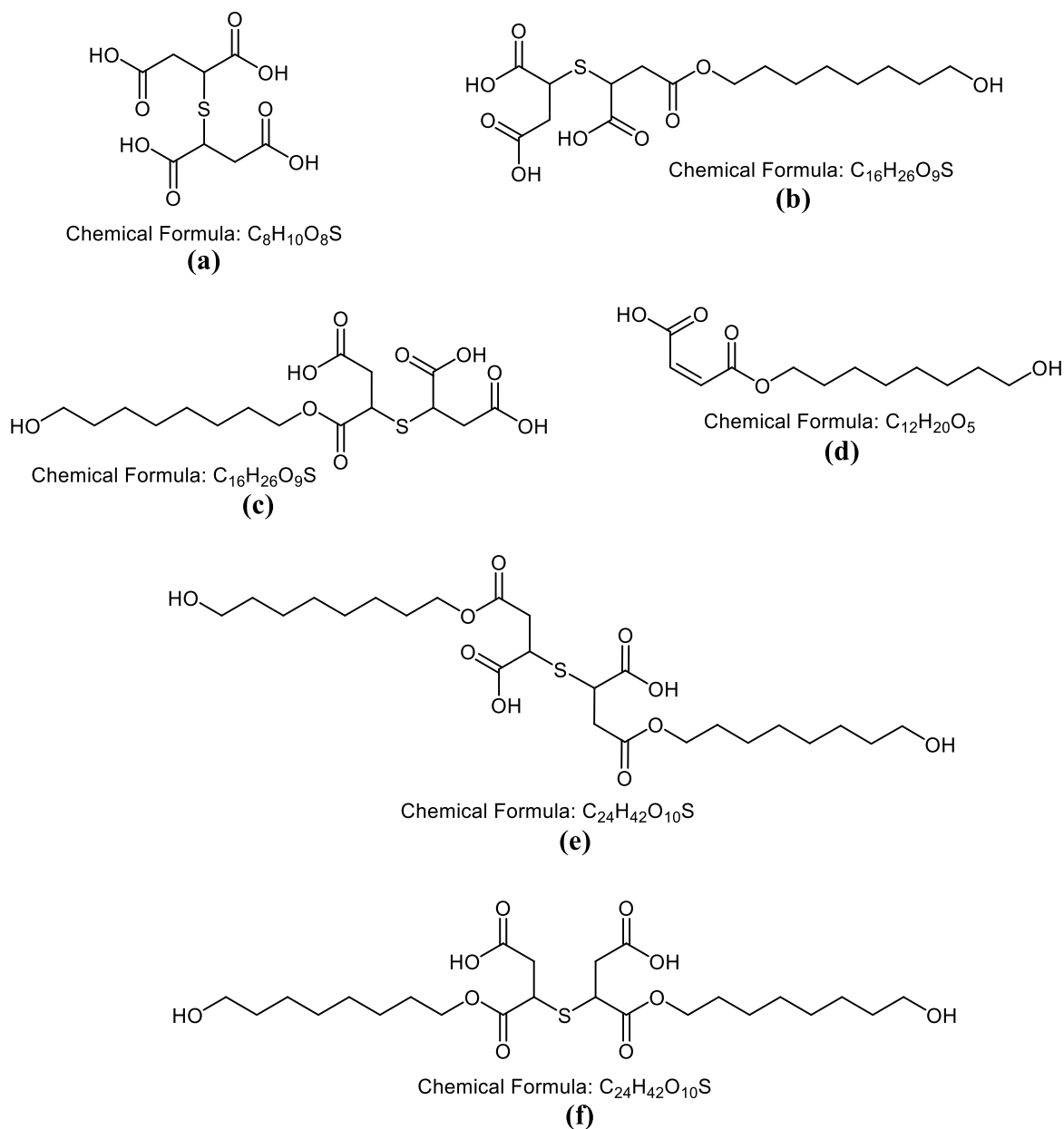


Figure 4.22 Structures of each component found during the degradation process.

Previous studies utilizing matrix-assisted laser desorption ionization (MALDI-MS) and ESI-MS have illustrated that PLGA polymer degradation occurs *via* hydrolytic degradation, providing additional support for our structural assignments^{19–22}. The compound that corresponds to the ion m/z 243 (Figure 4.22d) was a compound specifically expected to be released during degradation due to the melt-phase polycondensation using thiomalic acid, 1,8-octanediol and maleic acid. The polycondensation took place at 140 °C for 38 min under nitrogen to obtain a

viscous polymer allowing for disulfide bond formation. To reduce the amount of disulfide bond formation, the polymer was dissolved in absolute ethanol by sonication and treated with DL-dithiothreitol and triethylamine². Interestingly, the degradation process showed sulfide bridges that resemble thioethers (Figure 4.17 a-c, e-f). The thioether bonds are likely due to a thermally induced thiol-ene click reaction between the thiomalic acid and maleic acid units during the polycondensation that would not be removed by treating with DL-dithiothreitol²³. A second source of thioether bond formation is likely to occur during the release of the nitric oxide moiety in the nitrosated PTMO. It has been previously reported that NO-release from *S*-nitrosothiols (RSNOs) such as *S*-nitrosated glutathione (GSNO) can lead to the formation of glutathione disulfide (GSSG)²⁴. Additionally, the degradation of a tertiary *S*-nitrosothiol-based polyphosphazene polymer released disulfide degradation products during the hydrolytic degradation³. Specific to our PTMO-NO, nitrosation of the polymer takes place on the free thiol from the thiomalic acid monomer unit (Figure 4.15). As PTMO-NO is degraded thermally over time, the NO is released leaving behind a sulfur radical (RS[•]) that undergoes a thiol-ene click reaction between the RS[•] group and the double bond on the maleic acid units to form the thioether bonds rather than disulfide bridges²⁵.

4.5 Conclusions

The work presented here shows the importance of incorporating LC-MS and LC-MS/MS to aid in the identification of the degradation products from a device to be used for biomedical applications. Initially, we found direct injection MS helpful for preliminary identification of degradation products. The identification of the degradation products from the POPs polymers was done successfully and they matched some of the predicted results. Regarding the polyester polymers, our results both confirm the expected hydrolytic degradation¹⁹⁻²² and also illustrate

thioether bridge formation in lieu of commonly-seen disulfide bonds that result when NO is released from RSNOs. Additionally, the use of both LC-MS and LC-MS/MS facilitate the characterization of structural isomers and their corresponding structures. The identification of all the degradation products as esters (dimers and beyond) rather than the starting monomers was encouraging. The absence of the diacid monomers citric acid, maleic acid and thiomalic acid suggests a small impact in the localized acidity as the biopolymers degrade and further encourages the use of these polyesters for biomedical applications.

Our LC-MS methodology should serve as an example for elucidating the components of a device intended for biomedical applications. With our method, it is possible to track the degradation products of the device as it degrades over the entirety of the biodegradation study. With appropriate internal standards, as part of a future study, this methodology can be used to quantify each degradation product.

While there is currently no indication that the molecules identified are toxic, this work highlights the use of LC-MS and LC-MS/MS for degradation analysis to separate, elucidate and potentially quantify the degradation products of biomedically relevant polymers that can be used as devices. This opens the door for future studies regarding the toxicity of these compounds, complementing the implementation of the standards ISO 10993-1 and ISO 10993-9 when performing biological evaluation of medical devices as they will continue to be developed for the betterment of patients.

CHAPTER 4 - REFERENCES

- (1) Yapor, J. P.; Lutzke, A.; Pegalajar-Jurado, A.; Neufeld, B. H.; Damodaran, V. B.; Reynolds, M. M. Biodegradable Citrate-Based Polyesters with S-Nitrosothiol Functional Groups for Nitric Oxide Release. *J. Mater. Chem. B* **2015**, *3* (48), 9233–9241.
- (2) Yapor, J. P.; Neufeld, B. H.; Tapia, J. B.; Reynolds, M. M. Biodegradable Crosslinked Polyesters Derived from Thiomalic Acid and S-Nitrosothiol Analogues for Nitric Oxide Release. *J. Mater. Chem. B* **2018**, *6* (24), 4071–4081.
- (3) Lutzke, A.; Tapia, J. B.; Neufeld, M. J.; Reynolds, M. M. Sustained Nitric Oxide Release from a Tertiary S-Nitrosothiol-Based Polyphosphazene Coating. *ACS Appl. Mater. Interfaces* **2017**, *9* (3), 2104–2113.
- (4) Bogdan, C. Nitric Oxide and the Immune Response. *Nat. Immunol.* **2001**, *2* (10), 907–916.
- (5) Moncada, S.; Higgs, E. A. The Discovery of Nitric Oxide and Its Role in Vascular Biology. *Br. J. Pharmacol.* **2009**, *147* (S1), S193–S201.
- (6) Weinberg, J. B. Nitric Oxide Production and Nitric Oxide Synthase Type 2 Expression by Human Mononuclear Phagocytes: A Review. *Mol. Med.* **1998**, *4* (9), 557–591.
- (7) Carpenter, A. W.; Schoenfisch, M. H. Nitric Oxide Release: Part II. Therapeutic Applications. *Chem. Soc. Rev.* **2012**, *41* (10), 3742.
- (8) Reynolds, M. M.; Frost, M. C.; Meyerhoff, M. E. Nitric Oxide-Releasing Hydrophobic Polymers: Preparation, Characterization, and Potential Biomedical Applications. *Free Radic. Biol. Med.* **2004**, *37* (7), 926–936.
- (9) Hubbell, J. A. Biomaterials in Tissue Engineering. *Nat. Biotechnol.* **1995**, *13* (6), 565–576.
- (10) Li, S. Hydrolytic Degradation Characteristics of Aliphatic Polyesters Derived from Lactic

- and Glycolic Acids. *J. Biomed. Mater. Res.* **1999**, *48* (3), 342–353.
- (11) Bettinger, C. J. Synthetic Biodegradable Elastomers for Drug Delivery and Tissue Engineering. *Pure Appl. Chem.* **2010**, *83* (1), 9–24.
- (12) Nair, L. S.; Laurencin, C. T. Biodegradable Polymers as Biomaterials. *Prog. Polym. Sci.* **2007**, *32* (8–9), 762–798.
- (13) Browning, M. B.; Cereceres, S. N.; Luong, P. T.; Cosgriff-Hernandez, E. M. Determination of the in Vivo Degradation Mechanism of PEGDA Hydrogels. *J. Biomed. Mater. Res. Part A* **2014**, *102* (12), 4244–4251.
- (14) Dempsey, D. K.; Carranza, C.; Chawla, C. P.; Gray, P.; Eoh, J. H.; Cereceres, S.; Cosgriff-Hernandez, E. M. Comparative Analysis of in Vitro Oxidative Degradation of Poly(Carbonate Urethanes) for Biostability Screening. *J. Biomed. Mater. Res. Part A* **2014**, *102* (10), 3649–3665.
- (15) Tortolano, L.; Hammami, S.; Manerlax, K.; Do, B.; Yagoubi, N. RP-HPLC Detection and Dosage Method for Acrylic Monomers and Degradation Products Released from Implanted Medical Devices. *J. Chromatogr. B* **2016**, *1038*, 26–33.
- (16) Chen, F.; Qi, R.; Huyer, L. D.; Amsden, B. G. Degradation of Poly(5-Hydroxy-Trimethylene Carbonate) in Aqueous Environments. *Polym. Degrad. Stab.* **2018**, *158*, 83–91.
- (17) Kebarle, P.; Verkerk, U. H. On the Mechanism of Electrospray Ionization Mass Spectrometry (ESIMS). In *Electrospray and MALDI Mass Spectrometry*; Cole, R. B., Ed.; John Wiley & Sons, Inc.: Hoboken, NJ, USA, 2012; pp 1–48.
- (18) Competitive Fragmentation Modeling for Metabolite Identification <http://cfmid.wishartlab.com/> (accessed May 5, 2019).

- (19) Rizzarelli, P.; Carroccio, S. Modern Mass Spectrometry in the Characterization and Degradation of Biodegradable Polymers. *Anal. Chim. Acta* **2014**, *808*, 18–43.
- (20) Sikorska, W.; Adamus, G.; Dobrzynski, P.; Libera, M.; Rychter, P.; Krucinska, I.; Komisarczyk, A.; Cristea, M.; Kowalczyk, M. Forensic Engineering of Advanced Polymeric Materials – Part II: The Effect of the Solvent-Free Non-Woven Fabrics Formation Method on the Release Rate of Lactic and Glycolic Acids from the Tin-Free Poly(Lactide-Co-Glycolide) Nonwovens. *Polym. Degrad. Stab.* **2014**, *110*, 518–528.
- (21) Carter, S.; Kavros, A.; Rimmer, S. The Enzymatic Synthesis of Some Functional Oligomers Based on ϵ -Caprolactone or Vinyl Acetate Repeat Structures. *React. Funct. Polym.* **2001**, *48* (1–3), 97–105.
- (22) Kowalczyk, M.; Adamus, G. Mass Spectrometry for the Elucidation of the Subtle Molecular Structure of Biodegradable Polymers and Their Degradation Products. *Mass Spectrom. Rev.* **2016**, *35* (1), 188–198.
- (23) Campos, L. M.; Killops, K. L.; Sakai, R.; Paulusse, J. M. J.; Damiron, D.; Drockenmuller, E.; Messmore, B. W.; Hawker, C. J. Development of Thermal and Photochemical Strategies for Thiol–Ene Click Polymer Functionalization. *Macromolecules* **2008**, *41* (19), 7063–7070.
- (24) Neufeld, M. J.; Lutzke, A.; Tapia, J. B.; Reynolds, M. M. Metal–Organic Framework/Chitosan Hybrid Materials Promote Nitric Oxide Release from S-Nitrosoglutathione in Aqueous Solution. *ACS Appl. Mater. Interfaces* **2017**, *9* (6), 5139–5148.
- (25) Williams, D. L. H. The Chemistry of S-Nitrosothiols. *Acc. Chem. Res.* **1999**, *32* (10), 869–876.

CHAPTER 5

METAL-ORGANIC FRAMEWORK AS A STATIONARY PHASE FOR CHIRAL LIQUID CHROMATOGRAPHIC SEPARATIONS

5.1 Background

Practical applications of MOFs continue to expand as new MOFs are developed with desired properties. While most of the literature focused on the gas sorption and catalytic properties of MOFs, new interest has emerged as for their use as stationary phases in chromatographic separations. The resulting properties of a particular MOF is partially reliant on the type of ligands and metals used to construct the secondary building unit (SBU). In particular, chiral ligands can be synthesized resulting in MOFs with chiral behavior. In an international collaborative effort, a copper based, chiral MOF was used to pack an empty HPLC column and perform chiral chromatography. The goal of this project was to develop a system that performs similarly and/or exceeds the chromatographic efficiency of current commercial chiral columns. The primary objective was to efficiently pack an empty HPLC column with a MOF as a chiral stationary phase and test for chiral resolution capabilities. Exploring a chiral stationary phase based on a MOF system was a viable route since the pharmaceutical field has yet to find a way to fully and efficiently resolve the separation of enantiomeric drugs. In this process, the research question asked was: Could a water-stable MOF be employed as a stationary phase for the separation of enantiomeric compounds? This project involved developing a process for packing columns using MOFs as a stationary phase material and developing the mobile phase gradients to achieve baseline resolved separation of chiral mixtures. The majority of the work involved our efforts to match or improve upon chiral resolution from commercially available chiral columns (as we present in this

chapter). Prof. Jose Ramon Galán-Mascarós' group developed, synthesized and provided the chiral MOF. Heather N. Rubin performed the initial packing of the HPLC column. Jesus B. Tapia developed the methodology used and collected all chromatographic data and performed all the additional packings necessary for acceptable column performance. The work presented in this chapter was originally published in the Journal of the American Chemical Society (Corella-Ochoa, M. N.; Tapia, J. B.; Rubin, H. N.; Lillo, V.; Gonzalez-Cobos, J.; Núñez Rico, J. L.; Balestra, S. R. G.; Almora-Barrios, N.; Lledos, M.; Guell-Bara, A.; Cabezas-Giménez, J.; Escudero-Adán, E. C.; Vidal-Ferran, A.; Calero, S.; Reynolds, M. M.; Marti-Gastaldo, C.; Galan-Mascaros, J. R. Homochiral metal-organic frameworks for enantioselective separations in liquid chromatography. *JACS*. **2019**, *141* (36), 14306–14316). The work was adapted with permission from the American Chemical Society (Copyright 2019). Prof. Melissa Reynolds acted as the advisor on this project.

5.2 Introduction

Perhaps the most remarkable example of the need of efficient chiral resolution is the drug thalidomide. As Allen states, “no other drug has a name that evokes such emotions as that of thalidomide”, because its infamous and unexpected teratogenicity is the main reason for the current stringent regulations concerning drug development and use¹. Thalidomide, first synthesized in 1954 by the CIBA pharmaceutical company, and prescribed as a sedative, tranquilizer and antiemetic for morning sickness, quickly became popular due to its effectiveness and lack of acute toxicity^{1,2}. Several years after the negative effects of thalidomide were determined, Blaschke and colleagues³ reported that only the *S*-enantiomer of the drug is teratogenic. The discovery of enantiomer-specific toxicity emphasizes the importance of chiral chromatography to quickly, efficiently and reproducibly isolate enantiomers during drug synthesis processes. Despite the high importance and need of chiral separations for the pharmaceutical industry, chiral resolution

remains an expensive, time consuming and complex scientific challenge. To address the current challenges in chiral chromatographic resolution, metal-organic frameworks are becoming compounds of interest for chiral chromatography.

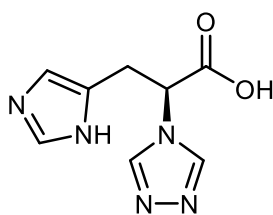
Metal-organic frameworks (MOFs) are defined by IUPAC as “coordination networks with organic ligands containing potential voids”⁴. MOFs are crystalline materials prepared by the combination of metal ions with customizable ligands to construct porous structures. The multitude of metal ions and organic linkers that can be used to prepare MOFs offers high flexibility to synthesize tailor-made MOFs. Due to their high customizability, MOFs have been presented as excellent candidates for gas storage⁵, catalysis⁶ and drug delivery⁷.

The ability to design MOFs with customizable metal ions and ligands allows for the development of MOFs with highly specific and unique pore size, shape and chemical functions. This has led to the design of MOFs for efficient and selective separation of gases, hydrocarbons or aromatic compounds⁸. Additionally, their potential as gas storage, led to their application as potential carriers of therapeutic gases such as NO^{9,10}. Additionally, copper-based MOFs have been studied for their use as catalysts for the release of NO from RSNOs in physiological conditions¹¹.

The ability to design MOFs with specific properties, allowed for the development of MOFs containing chiral linkers. The use of MOFs with highly specialized properties for the separation of gases and hydrocarbons led to studies in which MOFs were developed with enantiopure linkers. The design of chiral MOFs is gaining high interest for the development of new chiral stationary phases (CSPs) capable of separating chiral compounds¹². Examples of chiral MOFs from enantiopure organic linkers such as camphoric acid, tartaric acid, amino acids, or oligopeptides have been previously reported for their use for chiral separation^{13,14}. Unfortunately, small molecules such as camphoric acid and tartaric acid can limit the porosity of the resulting

frameworks, which can restrict the size and concentration of analyte concentrations¹³. Oligopeptides may be better designs for enantiomeric recognition since they can offer higher surface areas and tunable enantiomeric recognition by appropriate choice of the peptide sequence^{15,16}. Oligopeptides based chiral MOFs however, suffer from difficulties in large scale, affordable production of enantiopure MOFs, and decreased stability with multiple solvent systems and increase pressure required for chromatography¹⁷.

To address the challenges of using MOFs as CSPs, Prof. Galán-Mascarós' group synthetically modified amino acids rather than oligopeptides. Oligopeptides are more expensive to synthesize and display low chemical stability and poor robustness that can result in loss of structural integrity, usually uncontrolled collapse of the structure upon solvent removal¹⁷. Their approach was to use inexpensive, readily accessible, tunable amino acids that can be modified at the *C/N*-positions. Based on previously reported strategies¹⁸, the *N*-term was transformed into a 4*H*-1,2,4-triazole motif. The transformation led to the synthesis of the ligand (*S*)-3-(1*H*-imidazol-5-yl)-2-(4*H*-1,2,4-triazol-4-yl)propanoic acid (*S*-HTA) derived from L-histidine (Figure 5.1).



(*S*)-3-(1*H*-imidazol-5-yl)-2-(4*H*-1,2,4-triazol-4-yl)propanoic acid

Chemical Formula: C₈H₉N₅O₂

Figure 5.1 Structure of the *S*-HTA ligand.

The *S*-HTA ligand was reacted with a copper salt in water to produce the crystalline framework TAMOF-1 (triazole acid metal-organic framework). TAMOF-1 was sent to Prof. Reynolds' group as an enantiopure MOF with permanent porosity, ca. 1200 m² g⁻¹, with good stability in water and organic solvents to test for its chiral resolution capabilities. To do so,

TAMOF-1 was successfully packed into HPLC columns to test chiral resolution of multiple chiral compounds. The versatility of the columns was shown by the successful resolution of *trans*-2,3-diphenyloxirane (or *trans*-stilbene oxide), a compound used for calibration of commercial chiral HPLC columns, in multiple solvent systems.

5.3 Experimental

5.3.1 Materials

All reagents were of commercial grade and used without further purification. HPLC-grade methanol, ethanol, isopropanol, hexanes and acetonitrile were obtained from VWR (Solon, OH, USA). *trans*-2,3-diphenyloxirane (98%), furoin ($\geq 98\%$), benzoin (98%), 1-phenylethan-1-ol (98%) were obtained from Sigma-Aldrich (St. Louis, MO, USA). A stainless-steel empty HPLC column (100 \times 4.6 mm) was obtained from Restek (Bellefonte, PA, USA). TAMOF-1 was obtained from Prof. Jose Ramon Galán-Mascarós at the Institute of Chemical Research of Catalonia (ICIQ), The Barcelona Institute of Science and Technology (BIST).

5.3.2 Methods

5.3.2.1 Column Packing

To pack the empty HPLC column (100 mm \times 4.6 mm I.D.) with TAMOF-1, 737 mg were initially added via dry packing and the column was pressurized using 100% acetonitrile at a high flow rate (approx. 10 mL/min, approx. 1450 psi). After 10 h pressurization with acetonitrile, the column was opened and an additional amount of TAMOF-1 had to be added (due to packing of the material) and the eluent changed to 100% isopropanol (higher viscosity). This process of adding TAMOF-1 and packing was repeated until a total of 1550 mg were added to the column (fully packed). After the column was fully packed, it was pressurized with 100% isopropanol at a high moderate flow rate (2 mL/min, approx. 5000 psi) for 12 h to further ensure TAMOF-1 was indeed

fully packed and the column did not require any additional MOF. Before any data collection, the column was conditioned with the appropriate solvent system at a flow rate of 0.15 mL/min for 3 h before chromatographic experiments (approximately 15 column volumes).

5.3.2.2 Calculation of the chromatographic parameters

The selected parameters to assess separation efficiency of the selected enantiomers were the retention factor (k), separation factor (α), and resolution (R_S). These parameters were calculated using the following equations:

$$k = \frac{t_{R1} - t_M}{t_M} \quad (\text{eq. 1})$$

$$\alpha = \frac{t_{R2} - t_M}{t_{R1} - t_M} \quad (\text{eq. 2})$$

$$R_S = \frac{2(t_{R2} - t_{R1})}{w_1 + w_2} \quad (\text{eq. 3})$$

where t_M is the column void volume, t_{R1} and t_{R2} are the retention times for peaks 1 and 2 and w_1 and w_2 are the peak widths of each peak.

5.3.2.3 HPLC system

The HPLC system used to perform all chiral chromatographic separations consisted of a Varian 9002 HPLC pump and a Varian 9050 UV/Vis detector equipped with a Rheodyne 7725i 20- μ L manual injector and an Eldex CH-150 column oven kept at 35 °C. To compare the efficiency of our TAMOF-1 column to commercial columns, CHIRALPAK AD, CHIRALCEL OJ and CHIRALCEL OD (250 \times 4.6 mm) columns were used.

5.4 Results

5.4.1 Initial column packing

After the initial 737 mg MOF packing of the column, a series of baselines was collected as a first check for backpressure and to determine if more MOF needed to potentially be added. Over time, it was determined that tracking the baseline was not a good indicator of whether more MOF

needed to be added. Instead, the focus was placed on adding MOF, pressurizing it with solvent for 12h and reopening the column to perform a visual inspection. This proved to be a more effective method of packing the column until a total of 1550 mg of TAMOF-1 were added to the column.

The fully packed column was then conditioned with the appropriate solvent to be used for the chiral separations using at least 15 column volumes. To assess the potential of the TAMOF-1 column, racemic *trans*-2,3-diphenyloxirane (also called *trans*-stilbene oxide, a mixture of (2*S*,3*S*)-2,3-diphenyloxirane and (2*R*,3*R*)-2,3-diphenyloxirane) was selected. *trans*-2,3-diphenyloxirane is commonly used to determine the commercial chiral HPLC column's system suitability.

5.4.2 Chromatographic resolution of *trans*-2,3-diphenyloxirane

To test the versatility of the TAMOF-1 HPLC column, resolution of the racemic *trans*-2,3-diphenyloxirane was tested using multiple solvent systems. The solvents tested were 95:5 hexanes/isopropanol, commonly used with commercial chiral HPLC columns, 100% isopropanol, 100% methanol and 100% acetonitrile. The results shown in Figure 5.2 show that the racemic *trans*-2,3-diphenyloxirane can be baseline resolved using three out of the four solvents tested.

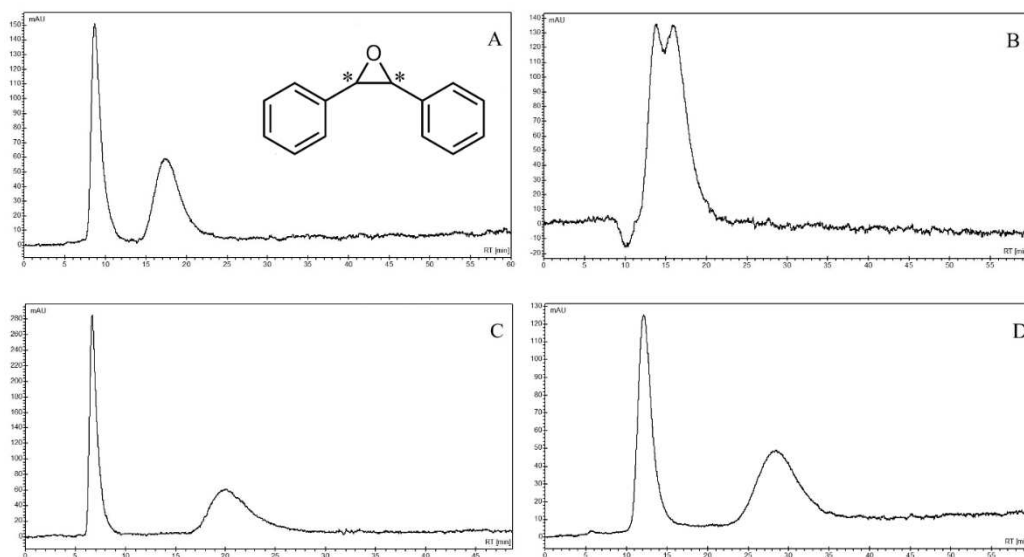


Figure 5.2 Resolution of *trans*-2,3-diphenyloxirane using the 100 mm \times 4.6 mm I.D. TAMOF-1 packed column. (A) 100% isopropanol, (B) 100% methanol, (C) 95:5 hexanes/isopropanol and (D) 100% acetonitrile each at a flow rate of 0.15 mL/min.

The chromatographic efficiency to resolve *trans*-2,3-diphenyloxirane using the TAMOF-1 column in each solvent system was calculated and is shown in Table 5.1.

Table 5.1 Chromatographic efficiency of the resolution of *trans*-2,3-diphenyloxirane using the TAMOF-1 column in different solvent systems^a

Mobile phase	R_s	α	t_{R1} (min)	t_{R2} (min)
Isopropanol	1.73	2.92	8.71	17.38
Methanol	— ^b	1.21	13.74	15.82
Acetonitrile	2.55	6.38	6.70	20.12
95:5 hexanes/ isopropanol	1.37	3.06	12.12	28.47

^aFlow rate = 0.15 mL/min, detection wavelength set to 254 nm. ^bNo baseline resolution achieved

To compare the results obtained from the TAMOF-1 column, *trans*-2,3-diphenyloxirane was also resolved using the commercial columns CHIRALPAK-AD, CHIRALCEL OD, AND CHIRALCEL-OJ as shown in Figure 5.3.

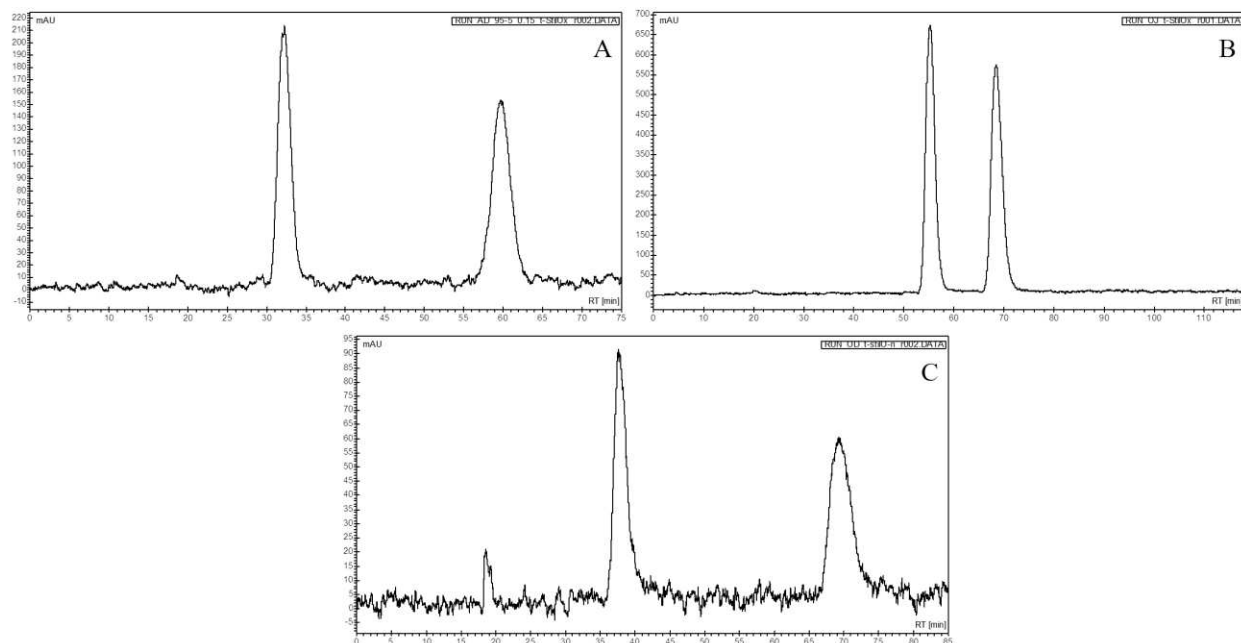


Figure 5.3 Resolution of *trans*-2,3-diphenyloxirane with the commercial columns (A) CHIRALPAK-AD, (B) CHIRALCEL-OJ, and CHIRALCEL-OD. The mobile phase and flow rate were selected to be the same as the analysis using the TAMOF-1 column (95:5 hexanes/isopropanol at 0.15 mL/min).

The optimal chromatographic conditions, separation times and resolutions of *trans*-2,3-diphenyloxirane with the TAMOF-1 column and each of the commercial chiral columns are shown in Table 5.2. While each column is capable of resolving *trans*-2,3-diphenyloxirane, the limitation of these columns is their ability to only be operational using normal phase conditions, such as 95:5 hexanes/isopropanol in this case. The TAMOF-1 column yields competitive resolution using the same parameters (Figure 5.2c and Table 5.2).

Table 5.2 Comparison of the resolution of *trans*-2,3-diphenyloxirane by the TAMOF-1 column versus CHIRALPAK AD, CHIRALCEL OD, and CHIRALCEL OJ commercial columns^a

	TAMOF-1	AD ^b	OD ^c	OJ ^d
Dimensions (mm)	100 × 4.6	250 × 4.6	250 × 4.6	250 × 4.6
(<i>S,S</i>) time (min)	12.1	32.3	37.6	55.3
(<i>R,R</i>) time (min)	28.5	59.6	69.2	68.4
Resolution (<i>R_s</i>)	1.37	4.98	5.75	2.63
% area (<i>S,S</i>)	50.4	49.5	50.8	49.8
% area (<i>R,R</i>)	49.6	50.5	49.2	50.2
Total time (min)	40	75	80	80

^aMobile phase 95:5 hexanes/isopropanol (v/v) at 0.15 mL/min, detection wavelength set to 254 nm. ^bCHIRALPAK AD. ^cCHIRALCEL OD. ^dCHIRALCEL OD.

The data suggests that the TAMOF-1 packed HPLC column yields highly efficient chiral resolutions that may exceed commercial column performance using similar conditions and particularly due to elution system versatility. The broader peaks obtained with TAMOF-1 could be attributed to in-house packing of the HPLC column as well as heterogeneous particle size between 0.2 and 10 μm as reported by Prof. Galán-Mascarós DLS data.

5.4.3 Application of TAMOF-1 column to other chiral compounds

Additional chiral compounds were selected to further study the potential of the TAMOF-1 column. The compounds 1-phenylethanol, benzoin and furoin were selected since they had been resolved previously by different chiral MOF columns¹⁹. With the TAMOF-1 column, some resolution was only achieved using mobile phase compositions consisting of hexanes and ethanol (Figures 5.4 – 5.7). In Figure 5.4 it is shown that using 100% ethanol does not resolve *trans*-2,3-diphenyloxirane, but some resolution of 1-phenylethanol, benzoin and furoin was observed, suggesting the potential for resolution by modification of the solvent composition.

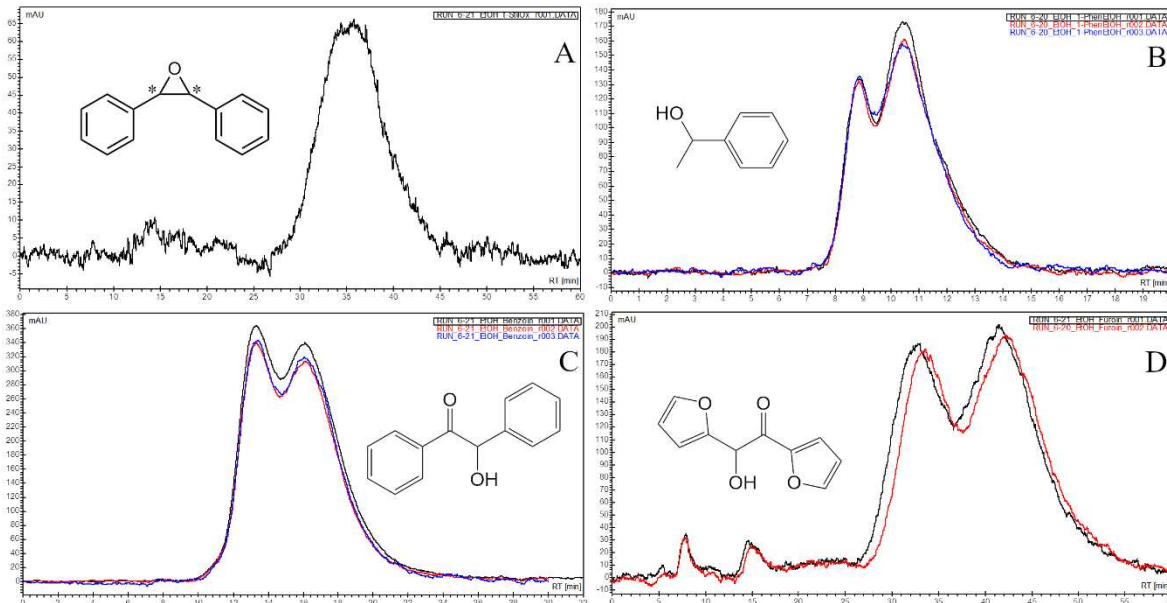


Figure 5.4 Chiral chromatography of (A) *trans*-2,3-diphenyloxirane, (B) 1-phenylethanol, (c) benzoin and (d) furoin using the TAMOF-1 column with 100% ethanol at 0.15 mL/min. *trans*-2,3-diphenyloxirane was retained as a single peak while 1-phenylethanol, benzoin and furoin showed some resolution but were not successfully baseline resolved.

Mobile phase compositions of 99:1 ethanol/hexanes, 95:5 ethanol/hexanes and 50:50 ethanol/hexanes were subsequently studied (Figures 5.5 – 5.7) in attempts to improve resolution of each analyte. Solvent compositions of 99:1 ethanol/hexanes (Figure 5.5) and 95:5

ethanol/hexanes (Figure 5.6) did not show improvements in resolution compared to each other and 100% ethanol (Figure 5.4). In the case of 50:50 ethanol/hexanes (Figure 5.7), 1-phenylethanol and benzoin appear to have worsened resolution, however, furoin appears to be baseline resolved (calculations shown in Table 5.3).

Table 5.3 Chromatographic efficiency of the resolution of furoin using the TAMOF-1 column^a

Mobile phase	R_s	α	t_{R1} (min)	t_{R2} (min)
50:50 ethanol/ hexanes	1.12	1.57	67.29	103.36

^aFlow rate = 0.15 mL/min, detection wavelength set to 254 nm.

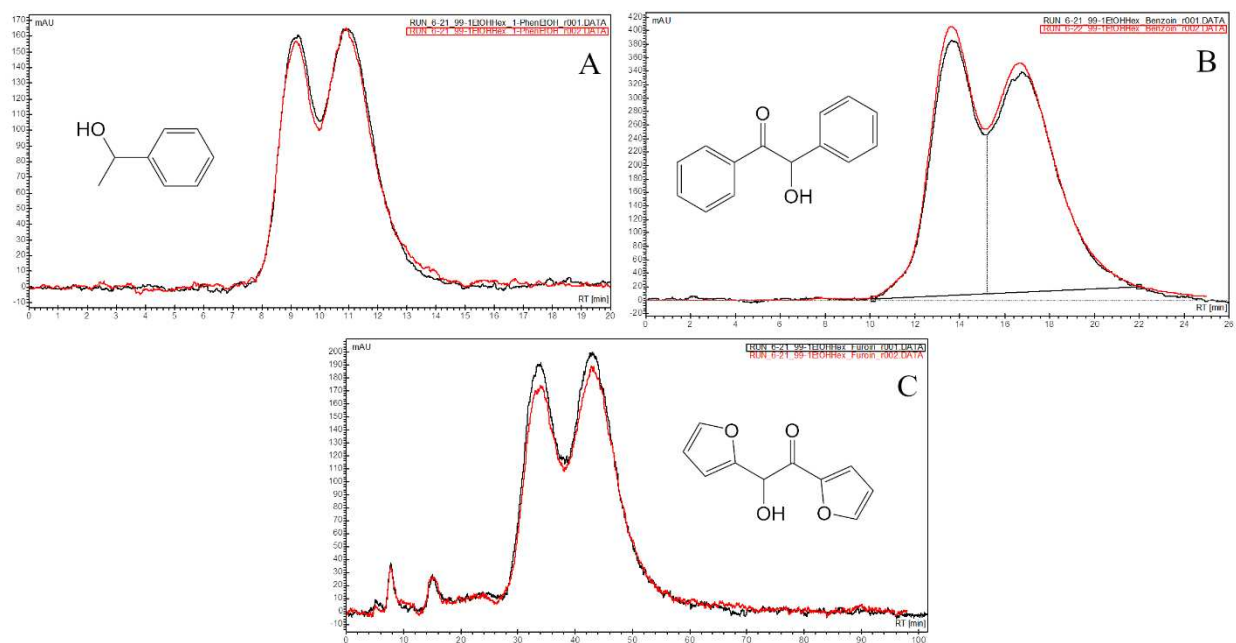


Figure 5.5 Chiral chromatography of (A) 1-phenylethanol, (B) benzoin and (C) furoin using the TAMOF-1 column with 99:1 ethanol/hexanes at 0.15 mL/min. All analytes showed some resolution but were not successfully baseline resolved.

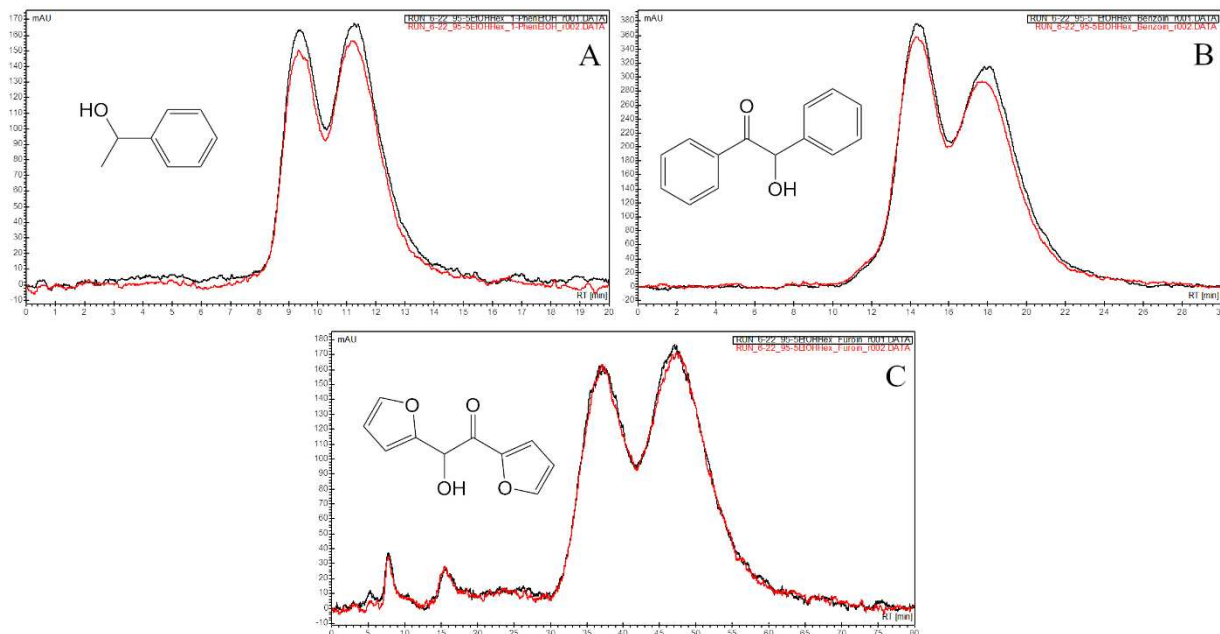


Figure 5.6 Chiral chromatography of (A) 1-phenylethanol, (B) benzoin and (C) furoin using the TAMOF-1 column with 95:5 ethanol/hexanes at 0.15 mL/min. All analytes showed some resolution but were not successfully baseline resolved.

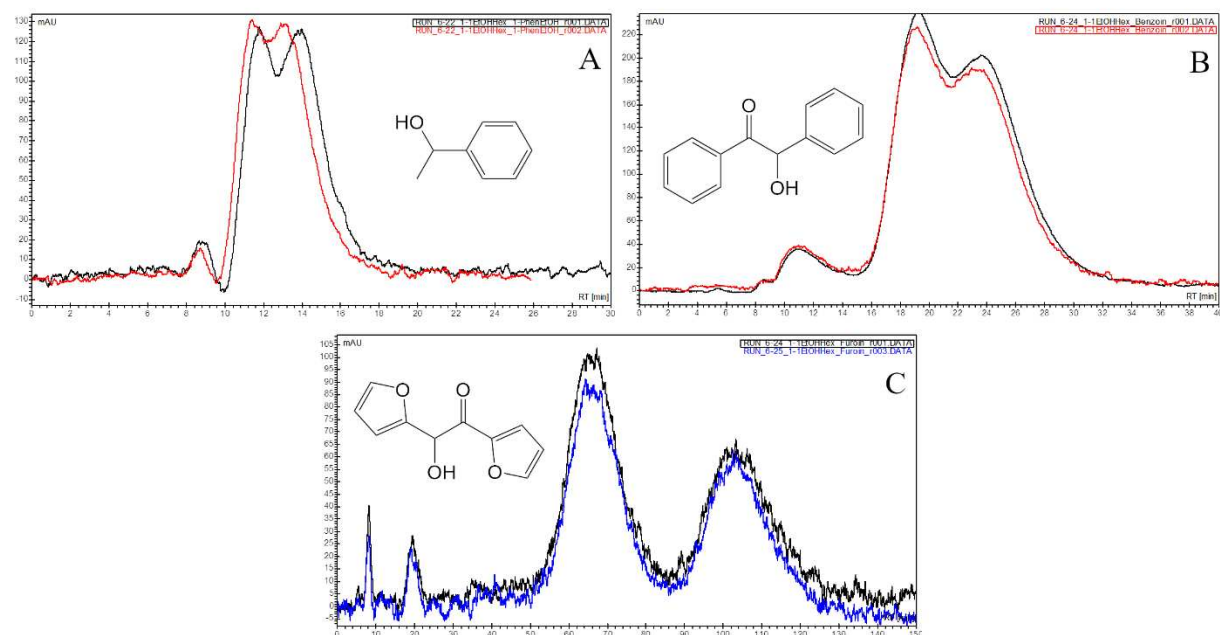


Figure 5.7 Chiral chromatography of (A) 1-phenylethanol, (B) benzoin and (C) furoin using the TAMOF-1 column with 50:50 ethanol/hexanes at 0.15 mL/min. 1-phenylethanol and benzoin appear to have worsened resolution, however, furoin appears to be baseline resolved.

5.5 Conclusions

Functionalization of the amino acid L-histidine with a 4*H*-1,2,4-triazole moiety, by transforming its -NH₂ group, yielded the enantiopure ligand *S*-HTA that assembled with copper in water to build a porous homochiral metal-organic framework, TAMOF-1. Upon packing of TAMOF-1 into an HPLC column, the chiral MOF was shown to work as a highly versatile chiral stationary phase (CSP) capable of enantiomeric resolution of chiral molecules using either polar (acetonitrile, alcohols) or nonpolar (hexanes) solvent conditions. This strongly suggests that TAMOF-1 packed columns can operate under both normal and reversed conditions for chiral resolution. The competitive resolution of *trans*-2,3-diphenyloxirane with TAMOF-1, along with its compatibility with multiple solvent systems, makes it highly desirable as a CSP for industrial size applications. In addition to the TAMOF-1's capability of resolution in either polar or nonpolar solvent conditions, our 100-mm column performed better than commercially available columns when resolving identical compounds. Success in applicability of TAMOF-1 as a CSP should pave the way for reliable, more efficient and cost-effective chiral resolution of enantiomeric pharmaceuticals.

CHAPTER 5 – REFERENCES

- (1) Allen, B. R. Thalidomide. *Br. J. Dermatol.* **2001**, *144* (2), 227–228.
- (2) Franks, M. E.; Macpherson, G. R.; Figg, W. D. Thalidomide. *Lancet*. May 2004, 1802–1811.
- (3) Tokunaga, E.; Yamamoto, T.; Ito, E.; Shibata, N. Understanding the Thalidomide Chirality in Biological Processes by the Self-Disproportionation of Enantiomers. *Sci. Rep.* **2018**, *8* (1), 17131.
- (4) Batten, S. R.; Champness, N. R.; Chen, X.; Garcia-Martinez, J.; Kitagawa, S.; Öhrström, L.; O’Keeffe, M.; Paik Suh, M.; Reedijk, J. Terminology of Metal–Organic Frameworks and Coordination Polymers (IUPAC Recommendations 2013). *Pure Appl. Chem.* **2013**, *85* (8), 1715–1724.
- (5) Mason, J. A.; Oktawiec, J.; Taylor, M. K.; Hudson, M. R.; Rodriguez, J.; Bachman, J. E.; Gonzalez, M. I.; Cervellino, A.; Guagliardi, A.; Brown, C. M.; et al. Methane Storage in Flexible Metal-Organic Frameworks with Intrinsic Thermal Management. *Nature* **2015**, *527* (7578), 357–361.
- (6) Jagadeesh, R. V.; Murugesan, K.; Alshammari, A. S.; Neumann, H.; Pohl, M. M.; Radnik, J.; Beller, M. MOF-Derived Cobalt Nanoparticles Catalyze a General Synthesis of Amines. *Science* **2017**, *358* (6361), 326–332.
- (7) Horcajada, P.; Chalati, T.; Serre, C.; Gillet, B.; Sebrie, C.; Baati, T.; Eubank, J. F.; Heurtaux, D.; Clayette, P.; Kreuz, C.; et al. Porous Metal-Organic-Framework Nanoscale Carriers as a Potential Platform for Drug Delivery and Imaging. *Nat. Mater.* **2010**, *9* (2), 172–178.
- (8) Cadiau, A.; Adil, K.; Bhatt, P. M.; Belmabkhout, Y.; Eddaoudi, M. A Metal-Organic

- Framework-Based Splitter for Separating Propylene from Propane. *Science* **2016**, 353 (6295), 137–140.
- (9) Keskin, S.; Kizilel, S. Biomedical Applications of Metal Organic Frameworks. *Ind. Eng. Chem. Res.* **2011**, 50 (4), 1799–1812.
- (10) Huxford, R. C.; Della Rocca, J.; Lin, W. Metal-Organic Frameworks as Potential Drug Carriers. *Curr. Opin. Chem. Biol.* **2010**, 14 (2), 262–268.
- (11) Neufeld, M. J.; Lutzke, A.; Tapia, J. B.; Reynolds, M. M. Metal–Organic Framework/Chitosan Hybrid Materials Promote Nitric Oxide Release from S-Nitrosoglutathione in Aqueous Solution. *ACS Appl. Mater. Interfaces* **2017**, 9 (6), 5139–5148.
- (12) Bhattacharjee, S.; Khan, M. I.; Li, X.; Zhu, Q. L.; Wu, X. T. Recent Progress in Asymmetric Catalysis and Chromatographic Separation by Chiral Metal–Organic Frameworks. *Catalysts* **2018**, 8, 120.
- (13) Duerinck, T.; Denayer, J. F. M. Metal-Organic Frameworks as Stationary Phases for Chiral Chromatographic and Membrane Separations. *Chem. Eng. Sci.* **2015**, 124, 179–187.
- (14) Das, S.; Xu, S.; Ben, T.; Qiu, S. Chiral Recognition and Separation by Chirality-Enriched Metal–Organic Frameworks. *Angew. Chemie - Int. Ed.* **2018**, 57 (28), 8629–8633.
- (15) Rabone, J.; Yue, Y.-F.; Chong, S. Y.; Stylianou, K. C.; Bacsa, J.; Bradshaw, D.; Darling, G. R.; Berry, N. G.; Khimyak, Y. Z.; Ganin, A. Y.; et al. An Adaptable Peptide-Based Porous Material. *Science* **2010**, 329 (5995), 1053–1057.
- (16) Navarro-Sánchez, J.; Argente-García, A. I.; Moliner-Martínez, Y.; Roca-Sanjuán, D.; Antypov, D.; Campíns-Falcó, P.; Rosseinsky, M. J.; Martí-Gastaldo, C. Peptide Metal-Organic Frameworks for Enantioselective Separation of Chiral Drugs. *J. Am. Chem. Soc.*

- 2017**, *139* (12), 4294–4297.
- (17) Martí-Gastaldo, C.; Antypov, D.; Warren, J. E.; Briggs, M. E.; Chater, P. A.; Wiper, P. V.; Miller, G. J.; Khimyak, Y. Z.; Darling, G. R.; Berry, N. G.; et al. Side-Chain Control of Porosity Closure in Single-and Multiple-Peptide-Based Porous Materials by Cooperative Folding. *Nat. Chem.* **2014**, *6* (4), 343–351.
- (18) Gómez, V.; Lillo, V.; Escudero-Adán, E. C.; Martín, E.; Galán-Mascarós, J. R. Aqueous Synthesis of Sulfonate-Functionalized 1,2,4-Triazole Ligands and Their 2D Cd²⁺ Coordination Networks: Crystal Structure and Photoluminescent Properties. *Dalt. Trans.* **2013**, *42* (18), 6374–6380.
- (19) Zhang, J.-H.; Nong, R.-Y.; Xie, S.-M.; Wang, B.-J.; Ai, P.; Yuan, L.-M. Homochiral Metal-Organic Frameworks Based on Amino Acid Ligands for HPLC Separation of Enantiomers. *Electrophoresis* **2017**, *38* (19), 2513–2520.

CHAPTER 6

CONCLUSIONS AND FUTURE DIRECTIONS

6.1 Conclusions

This dissertation has made significant contributions by the application of mass spectrometry to a variety of biomedical application driven discoveries. The fundamental studies regarding improvements in ionization of polysaccharides sets a foundation for future research to continue finding means to ionize and successfully characterize polysaccharides using mass spectrometry. The experiments described showed, for the first time, protein like ionization of derivatized dextran (EDA-dextran) of low molecular weight. The experiments suggest that under the right derivatization conditions, the potential for ionization by means of multiple charges can be successfully achieved and in theory applied to polysaccharides of up to 40 kDa.

Additionally, using the in-house developed methodology, the formation of oxidized glutathione (GSSG) was confirmed as a reaction byproduct from the catalytic release of NO from *S*-nitrosoglutathione using chitosan-MOF composites. The same methodology used to confirm the formation of GSSG, was also used simultaneously to determine whether the chitosan support system degraded over time as well as any potential decomposition of the MOF. This led the way to the development of yet another set of mass spectrometric methodology to successfully determine the degradation products from two polymeric systems intended for biomedical applications as part of our in-house pre-validated risk assessments.

The studies regarding potential cell viability interferences are a very important collaborative project completed within my graduate career. The findings strongly advise all fields that rely on commercial cell viability studies to perform their due diligence to account for potential

interferences within their experiments to minimize false positives/negatives that could lead to catastrophic consequences.

Finally, in an international collaborative effort, a chiral MOF (TAMOF-1) was used to perform chiral chromatographic separations in a variety of solvent systems that include both normal and reversed phase conditions. The work performed with the TAMOF-1 HPLC column should pave the way for the affordable, industrial use of a MOF-based chiral stationary phase for chiral chromatography needs in this still very expensive field.

6.2 Future Directions

6.2.1 Improvements for ionization of dextran and applications to larger polysaccharides

With the growing interest in polymeric materials from natural origin, particularly regarding biomedical applications, it is important to tackle the challenge of accurate analysis using analytical techniques such as mass spectrometry. While it continues to be difficult to ionize neutral polysaccharides and successfully analyze them, Chapter 2 described a derivatization that successfully attached free terminal amines. The attachment of free terminal amines allowed for ionization of EDA-dextran similar to protein ionization as was shown in Figure 2.11, reproduced here as Figure 6.1.

Future work should focus on increasing the number of ethylenediamine attachments to dextran, and any other polysaccharides of interest. Ideally, at least 1 successful attachment per glucose is recommended. With this goal in mind, as an example, a dextran polymer composed of 500 glucose residues would have a mass of approximately 81 kDa. If there is one ethylenediamine attachment per glucose, the mass increase would be to 124 kDa. However, if this hypothetical derivatized dextran only attains 10% charging (50 protonations), the m/z will effectively move the mass of this dextran to approximately 2488 Da. This m/z would make the measurement of an 81

kDa starting polysaccharide possible with the instrument used for the dextran work since the high-resolution mass ranges from 0 – 3200 m/z .

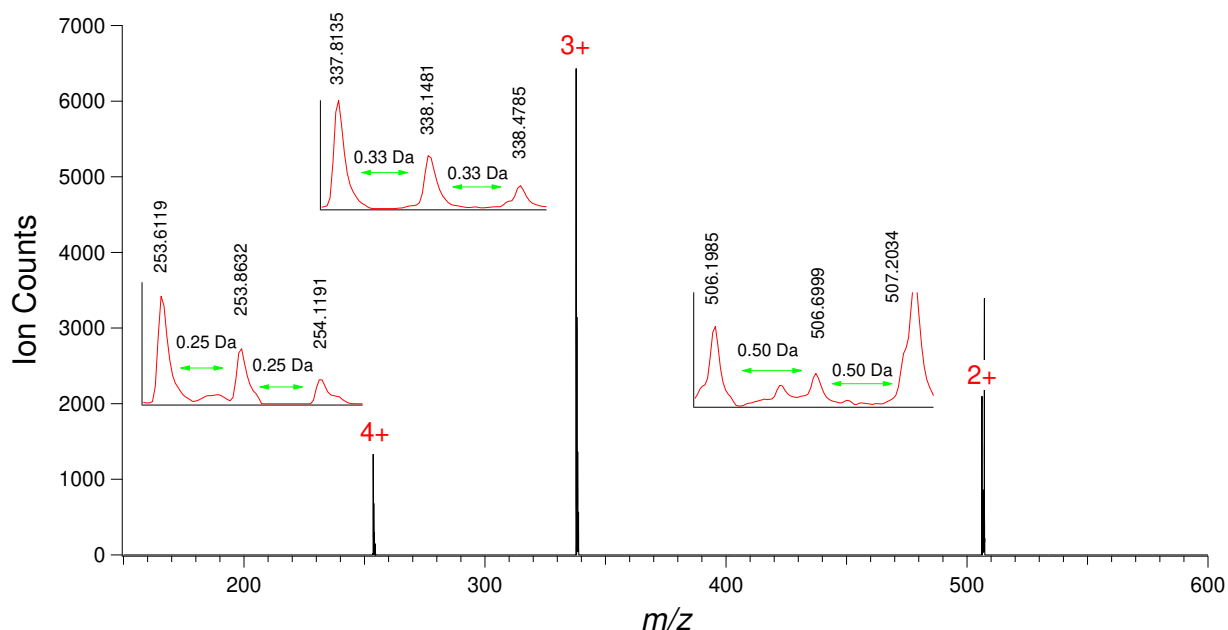


Figure 6.1 Reproduced figure from chapter 2 (Figure 2.11) showing the protein-like ionization of EDA-dextran. The same four glucose EDA-dextran chain was ionized by 2, 3 and 4 protonations.

6.2.2 Mass spectrometry application for degradation profiling of polymeric devices

Polymeric devices for biomedical applications continue to be developed to match required moduli for tissue engineering, wound healing meshes and extracorporeal systems. It was demonstrated that current mass spectrometry instrumentation is capable of accurate LC-MS and LC-MS/MS separation and elucidation of biodegradation products as discussed in Chapter 3 regarding chitosan-MOF composites and in Chapter 4 during the investigation of poly(phosphazene) and polyester polymers. It is recommended to actively screen commercially obtained and newly developed polymers for their degradation products and potentially unwanted leachates. Follow-up work for the degradation of chitosan composites, poly(phosphazene) and polyester based polymers should include the quantification of each degradation product, especially as the devices move closer to biological evaluation for medical devices.

6.2.3 Continuous use of mass spectrometry for analysis of reaction products

The continuous development of new methodology to test for reaction byproducts is of utmost importance to confirm the intended purpose of newly developed materials/devices. In a similar manner, the discoveries made in Chapter 3 regarding potential interferences affecting cell viability studies, it is strongly recommended to keep track of the effects of the therapeutics of interest on the selected assay. Perhaps an internal library of interfering compounds can be started within the lab, focused on therapeutics specific to the Reynolds group. Eventually, any potential false positives/negatives can be confirmed/rejected using the methods described in Chapter 3 that showed the successful use of mass spectrometry for this purpose. Once a robust library is obtained, when enough information is collected, it would be worthy of publication and potentially included as a point of reference when cell viability assays are purchased.

6.2.4 Chiral chromatography using chiral metal-organic frameworks

With the essentially unlimited designs of MOFs possible, chiral MOFs will certainly continue to be designed and synthesized for their use as CSPs. As shown in the work presented in Chapter 5 (*JACS*, **2019**, *141* (36), 14306–14316), taking advantage of enantiopure, naturally occurring building blocks such as amino acids for MOF ligand synthesis led to the highly specialized chiral MOF TAMOF-1. It is worth highlighting that TAMOF-1 was operational using a variety of solvents that ranged from normal to reversed phase leading to efficient resolution of *trans*-2,3-diphenyloxirane, greatly increasing the versatility of TAMOF-1 as a CSP. The limited resolution of additional chiral compounds of interest such as 1-phenylethanol, benzoin and furoin showed the potential of the TAMOF-1 CSP to resolve different chiral compounds, however, there is room for improvement. As stated in Chapter 5, heterogeneous particle size may be responsible for broad peaks and may also influence the poor resolution of the additional tested chiral

compounds. The work presented regarding chiral resolution using TAMOF-1 should pave the way for further studies regarding homogeneous particle size, different column dimensions, and other mixtures of solvents. The Varian HPLC system used for all the work in Chapter 5 did not allow for gradient elution, thereby limiting any improved resolution by implementation of gradients. Initial work regarding different column dimensions is shown in Figure 6.2 in which a longer column was packed (250×4.6 mm ID) with 3.79-g of TAMOF-1. The preliminary tests of the column were performed by separating *trans*-2,3-diphenyloxirane using a mobile phase of 100% acetonitrile at 1.0 mL/min. Additionally, TAMOF-1 should be tested using typical HPLC additives such as formic acid, ammonium formate, acetic acid, ammonium acetate and trifluoroacetic acid for stability under those conditions. Once stability is established, check for resolution of all the compounds already resolved with the new mobile phase conditions. A suggested series of steps is shown in table 6.1.

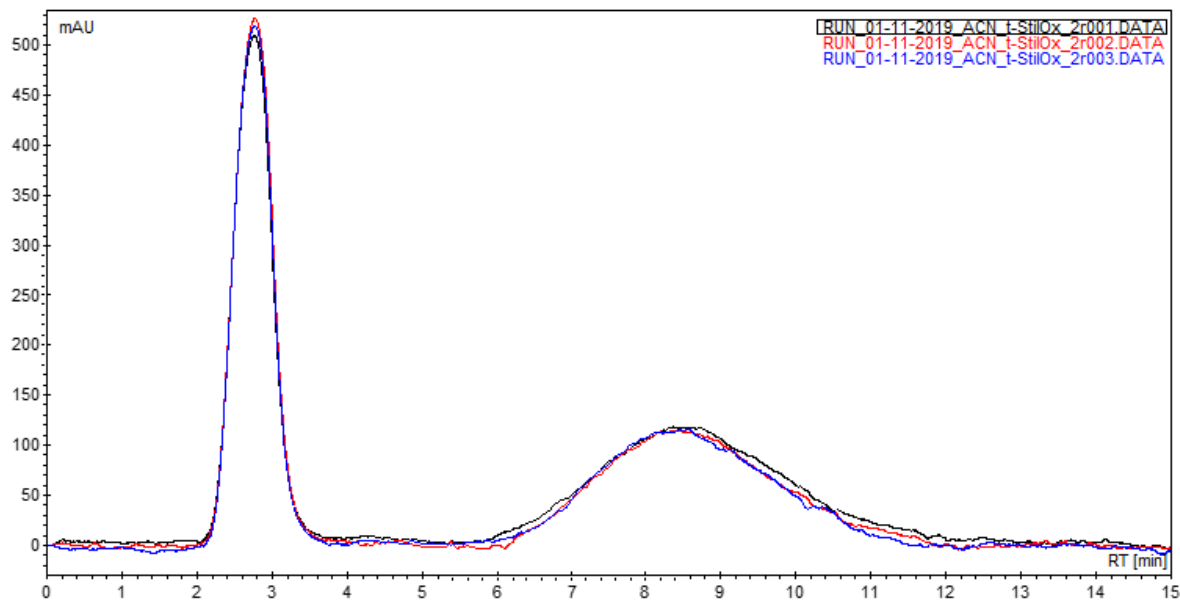


Figure 6.2 250×4.6 mm ID column packed with TAMOF-1. *trans*-2,3-diphenyloxirane was resolved using 100% acetonitrile at 1.0 mL/min.

Table 6.1 Suggested starting additive compatibility testing with TAMOF-1

Mobile phase additive	Solvent compatibility	Suggested addition
Formic acid/acetic acid	Acetonitrile	0.01% - 0.1% (v/v)
Formic acid/acetic acid	Methanol	0.01% - 0.1% (v/v)
Formic acid/acetic acid	Isopropanol	0.01% - 0.1% (v/v)
Ammonium formate/ Ammonium acetate	Acetonitrile	1mM - 10 mM
Ammonium formate/ Ammonium acetate	Methanol	1mM - 10 mM
Ammonium formate/ Ammonium acetate	Isopropanol	1mM - 10 mM
Trifluoroacetic acid	Hexanes/isopropanol	0.01% - 0.1% (v/v)
Trifluoroacetic acid	Hexanes/ethanol	0.01% - 0.1% (v/v)

APPENDIX A

Supporting Information for Chapter 4

A1. Additional Figures

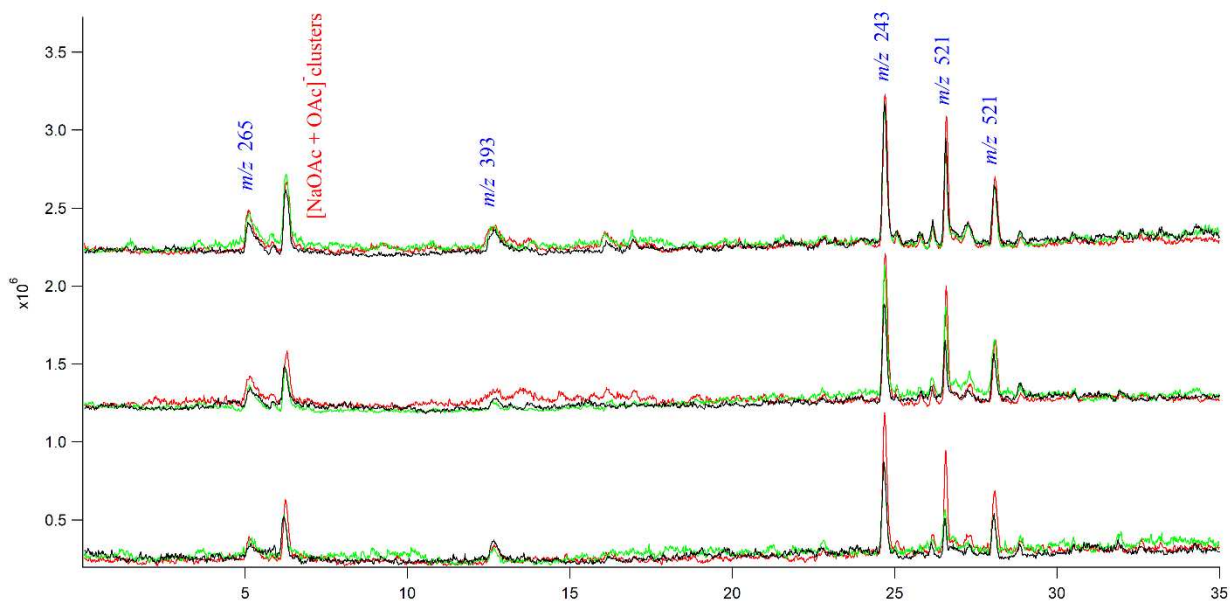


Figure A1.1 LC-MS triplicate runs of PTMO-NO degradation after 1 week.

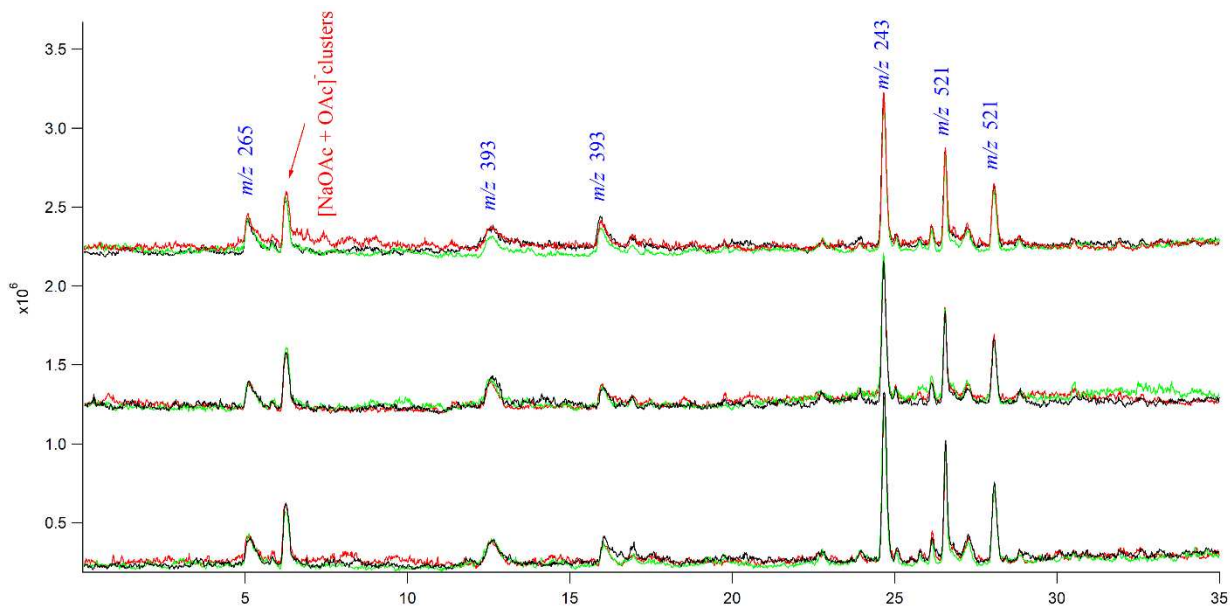


Figure A1.2 LC-MS triplicate runs of PTMO-NO degradation after 3 weeks.

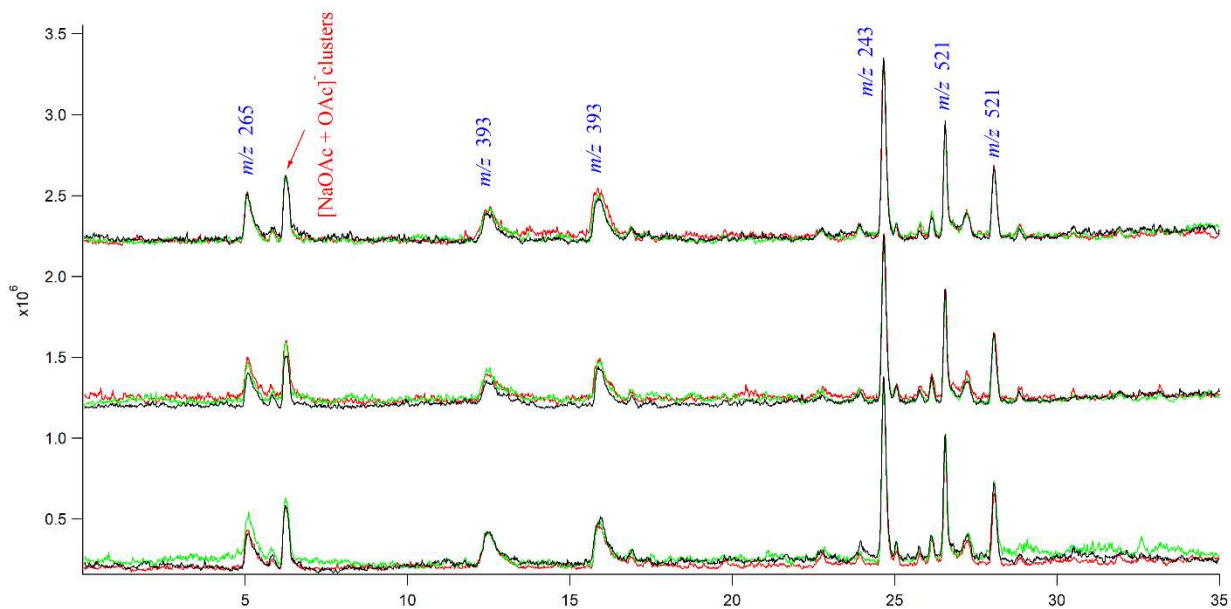


Figure A1.3 LC-MS triplicate runs of PTMO-NO degradation after 6 weeks.

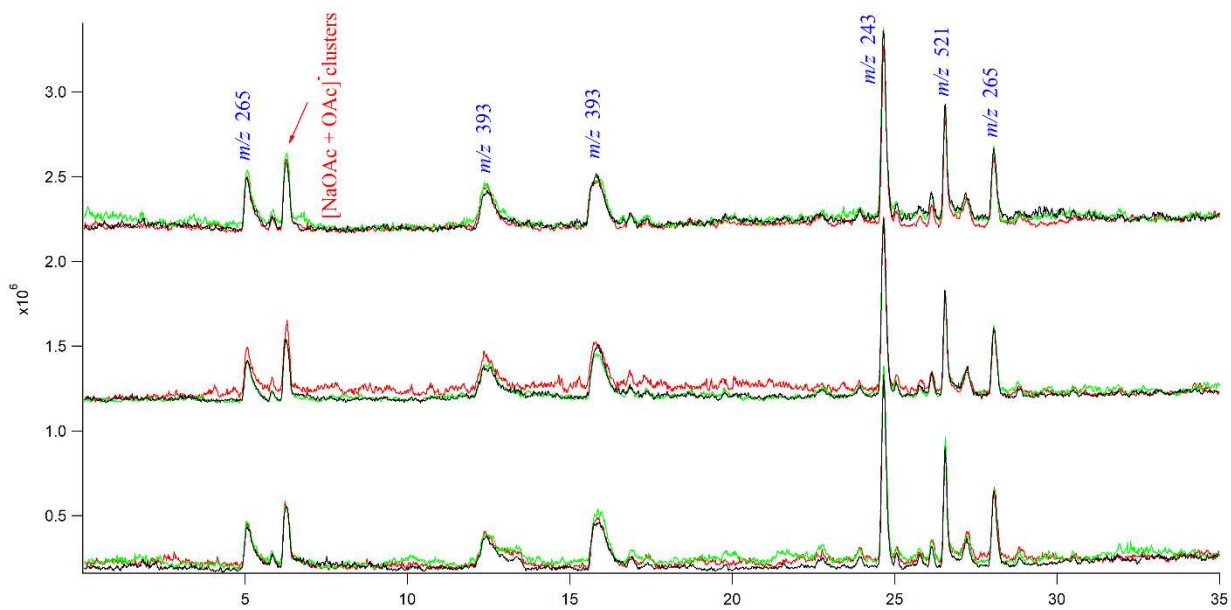
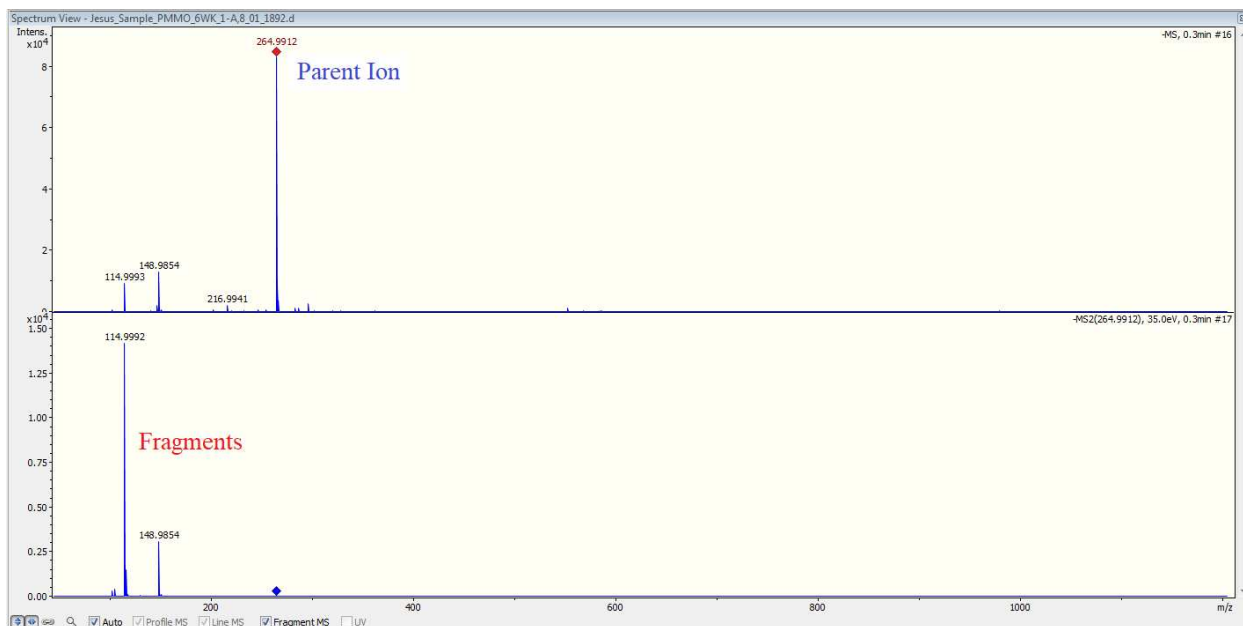
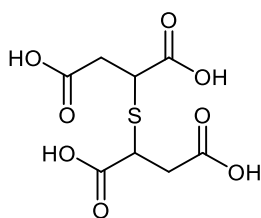


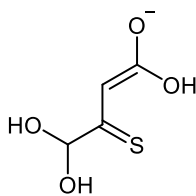
Figure A1.4 LC-MS triplicate runs of PTMO-NO degradation after 10 weeks.



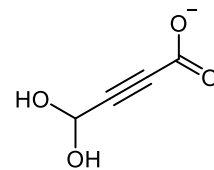
(a)



(b)



Chemical Formula: $C_4H_5O_4S^-$
Exact Mass: 148.99



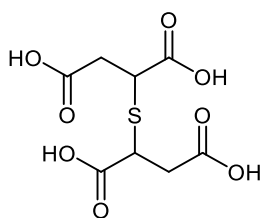
Chemical Formula: $C_4H_3O_4^-$
Exact Mass: 115.00

(c)

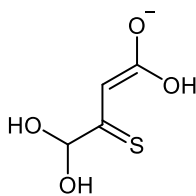
Figure A1.5 Fragmentation pattern of ion m/z 265. (a) MS/MS spectrum; (b) m/z 265 parent ion; (c) fragment ions from parent ion. Fragment ions confirmed using the CFM-ID fragmentation modeling software¹.



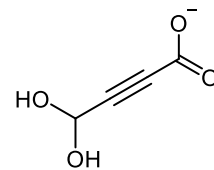
(a)



(b)



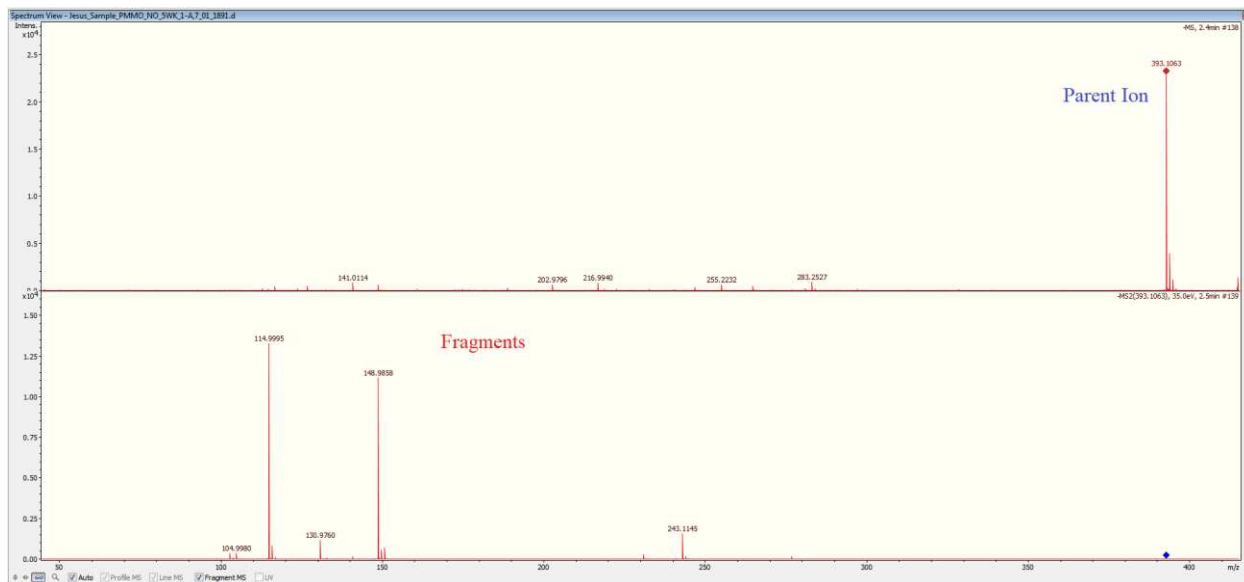
Chemical Formula: $C_4H_5O_4S^-$
Exact Mass: 148.99



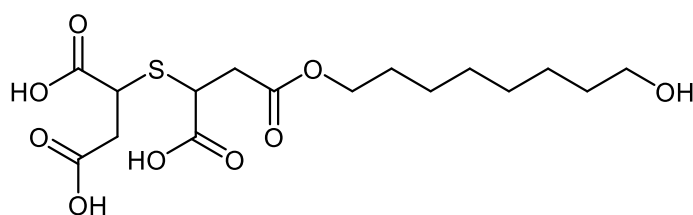
Chemical Formula: $C_4H_3O_4^-$
Exact Mass: 115.00

(c)

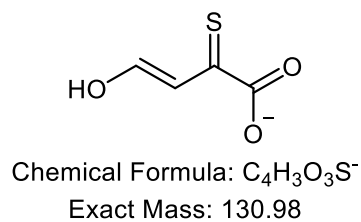
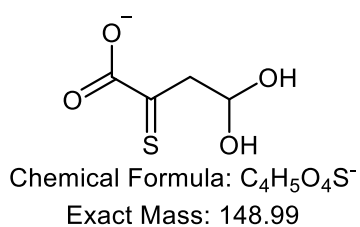
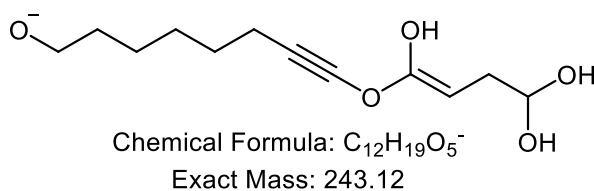
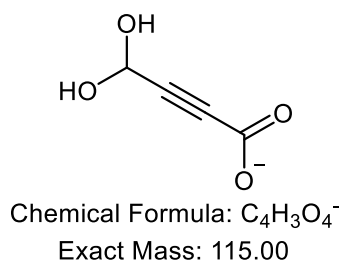
Figure A1.6 Fragmentation pattern of ion m/z 265. (a) MS/MS spectrum; (b) m/z 265 parent ion; (c) fragment ions from parent ion. Fragment ions confirmed using the CFM-ID fragmentation modeling software¹.



(a)

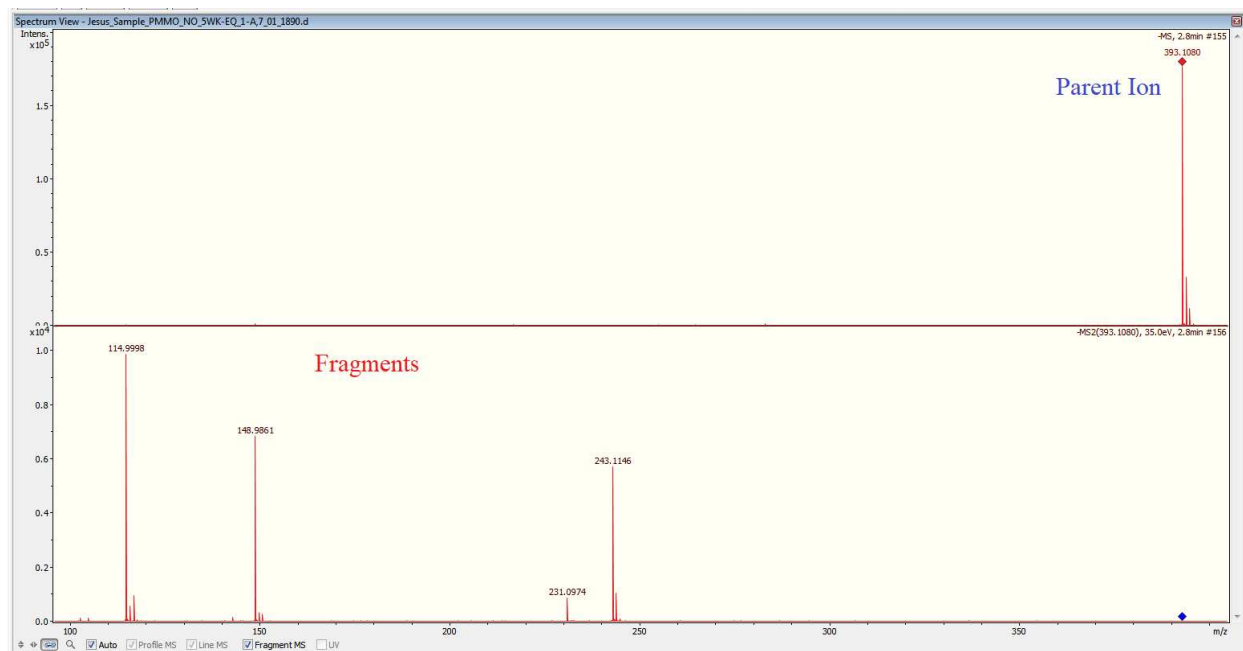


(b)

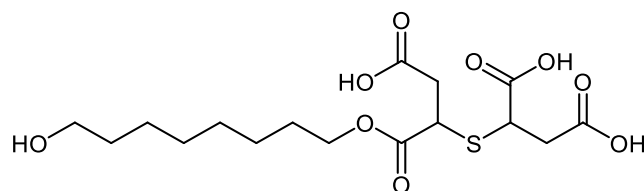


(c)

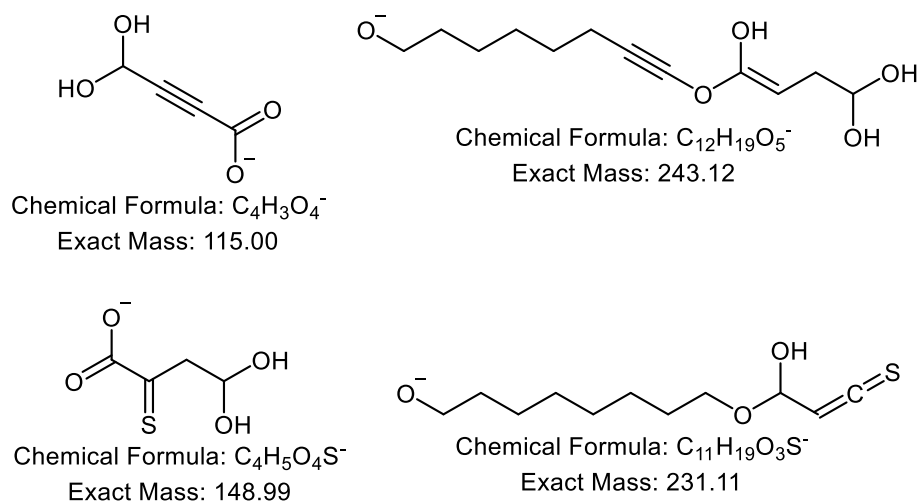
Figure A1.7 Fragmentation pattern for the first m/z 393 ion. (a) MS/MS spectrum; (b) m/z 393 parent ion; (c) fragment ions from parent ion. Fragment ions confirmed using the CFM-ID fragmentation modeling software¹.



(a)

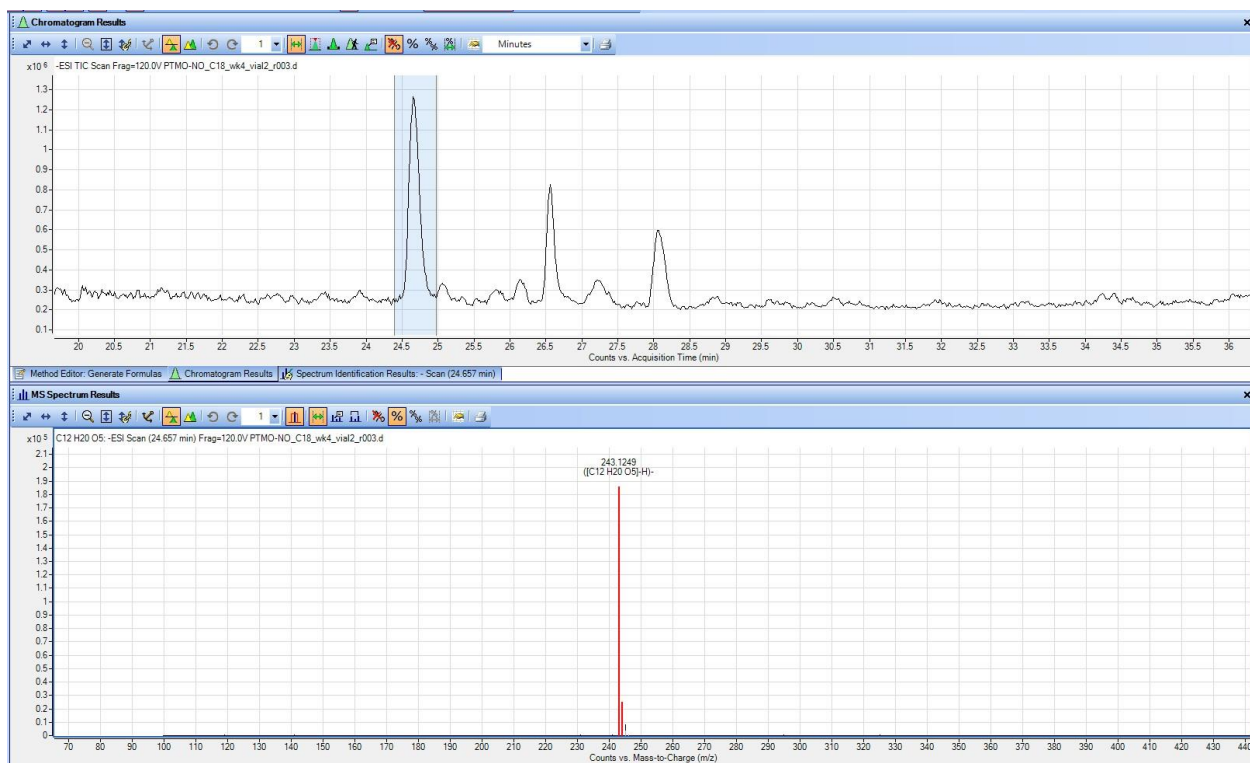


(b)

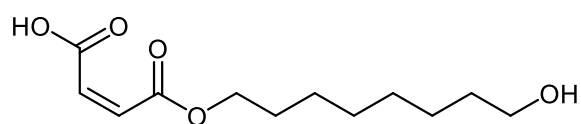


(c)

Figure A1.8 Fragmentation pattern for the second m/z 393 ion. (a) MS/MS spectrum; (b) m/z 393 parent ion; (c) fragment ions from parent ion. Fragment ions confirmed using the CFM-ID fragmentation modeling software¹.



(a)

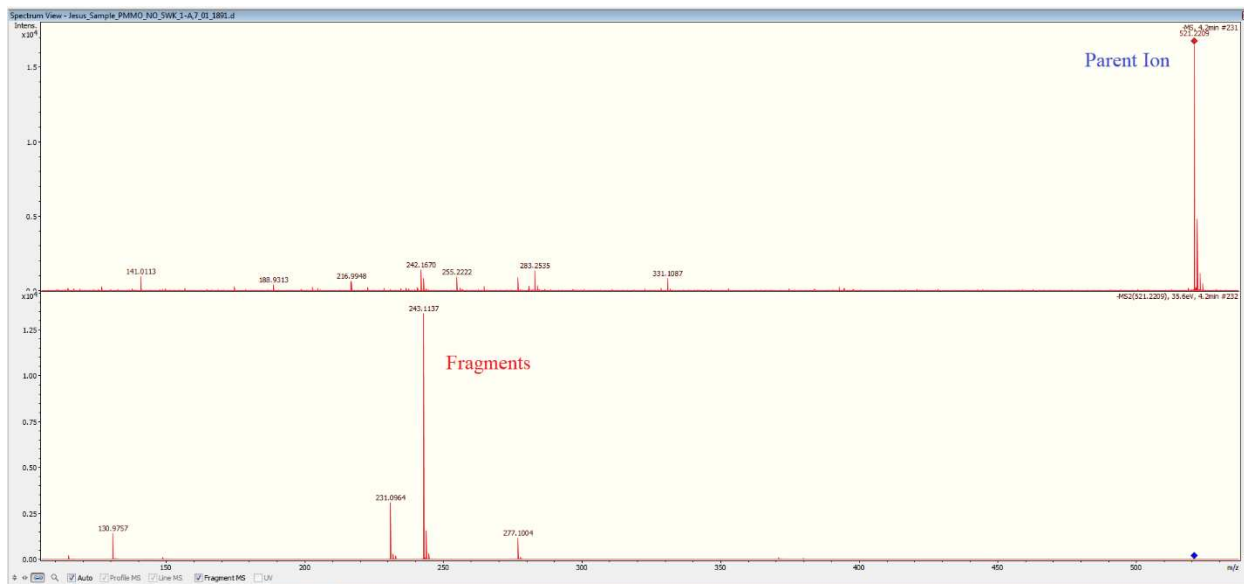


Chemical Formula: C₁₂H₂₀O₅

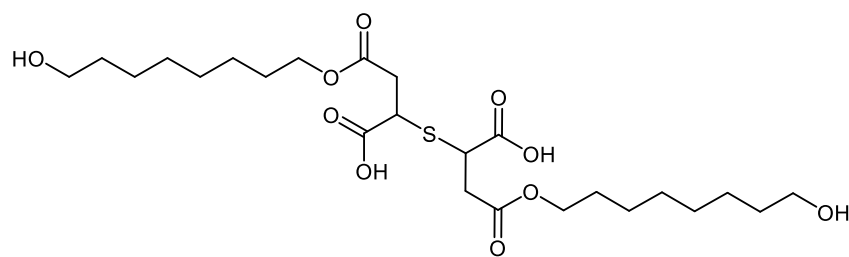
Exact Mass: 244.13

(b)

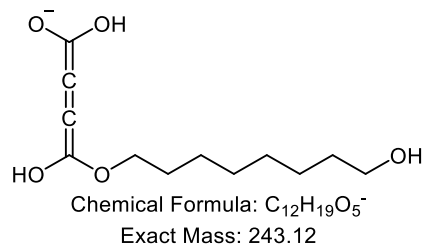
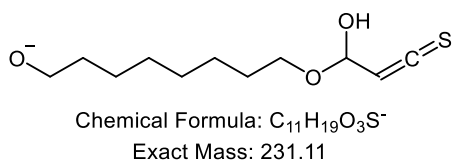
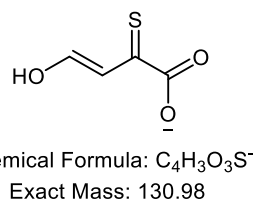
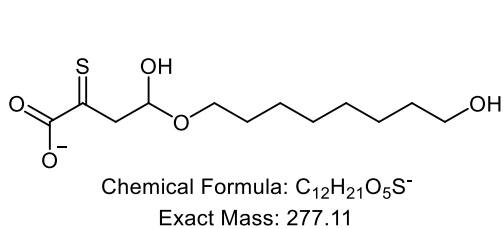
Figure A1.9 Identity of the m/z 243 ion. Previously identified². (a) MS spectrum. (b) Structure of m/z 243 ion.



(a)

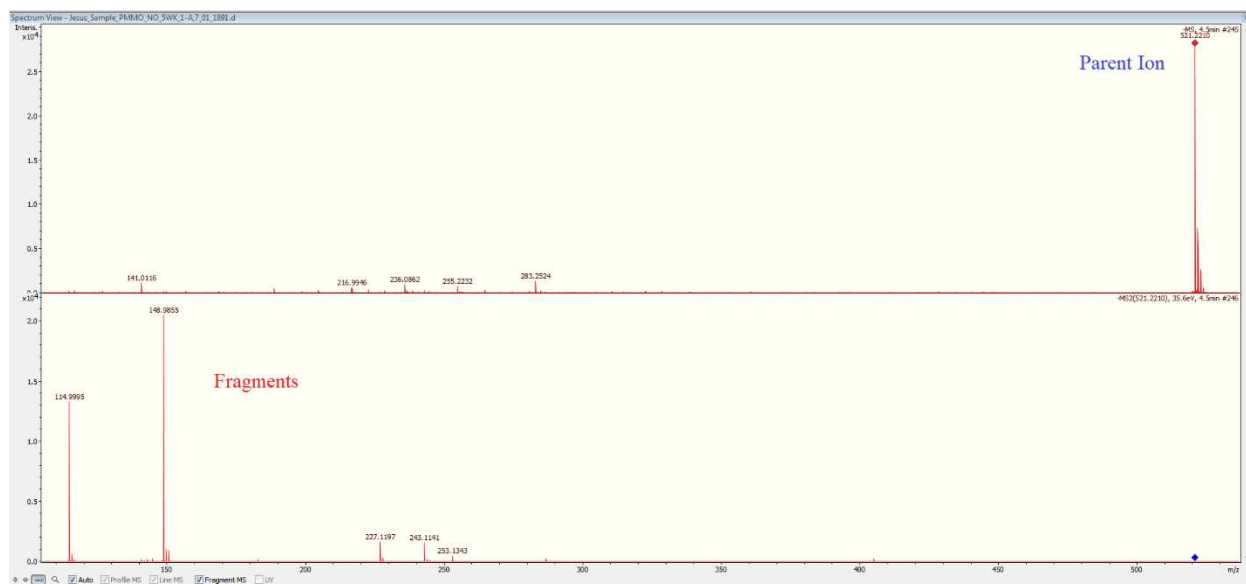


(b)

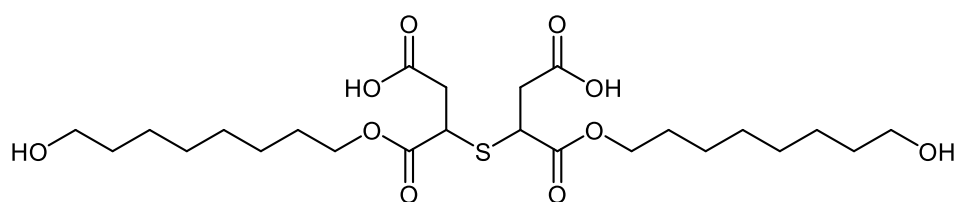


(c)

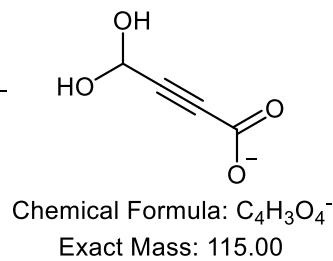
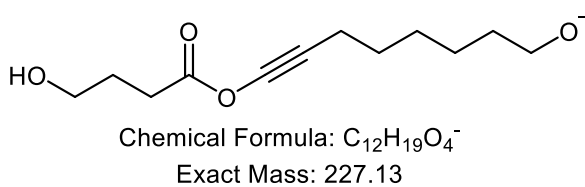
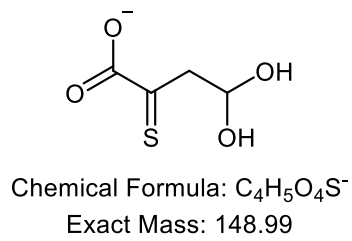
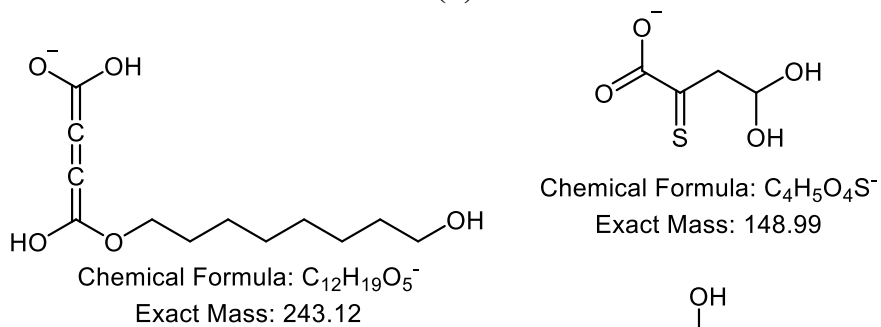
Figure A1.10 Fragmentation pattern for the first m/z 521 ion. A) MS/MS spectrum; (b) m/z 521 parent ion; (c) fragment ions from parent ion. Fragment ions confirmed using the CFM-ID fragmentation modeling software¹.



(a)



(b)



(b)

Figure A1.11 Fragmentation pattern for the second m/z 521 ion. A) MS/MS spectrum; (b) m/z 521 parent ion; (c) fragment ions from parent ion. Fragment ions confirmed using the CFM-ID fragmentation modeling software¹.

APPENDIX A – REFERENCES

- (1) Competitive Fragmentation Modeling for Metabolite Identification <http://cfmid.wishartlab.com/> (accessed May 5, 2019).
- (2) Yapor, J. P.; Neufeld, B. H.; Tapia, J. B.; Reynolds, M. M. Biodegradable Crosslinked Polyesters Derived from Thiomalic Acid and S-Nitrosothiol Analogues for Nitric Oxide Release. *J. Mater. Chem. B* **2018**, *6* (24), 4071–4081.

APPENDIX B

Derivatized Dextran Mass Spectrometric Analysis SOP (Chapter 2)¹

B1. Purpose

A direct flow injection with an LC-MS system is used for the molecular weight analysis of derivatized dextran.

B2. Scope

This test method provides instructions for the preparation and analysis of derivatized dextran.

B3. Responsibility

To be performed by personnel who are technically qualified and trained in the use of the LC-MS and associated techniques.

B4. Safety

The samples and reagents used in this procedure should be handled using good laboratory practices. Wear gloves and work in a fume hood. Read the Safety Data Sheets for all chemicals used in this procedure.

B5. Abbreviations

CAS	Chemical Abstracts Service
CDI	1,1'-Carbonyldiimidazole
Da	Dalton
DMSO	Dimethyl Sulfoxide
EDA	Ethylenediamine
ESI	Electrospray Ionization
LC-MS	Liquid Chromatography-Mass Spectrometry
MeOH	Methanol
MP	Mobile Phase
MW	Molecular Weight
NA	Not Applicable
NaCl	Sodium Chloride
RT	Room Temperature
TOF	Time-of-Flight

B6. Materials and Equipment

- B6.1 Agilent 1260 Infinity HPLC System
- B6.2 Agilent 6224 TOF Mass Spectrometer
- B6.3 Agilent dual ESI ion source
- B6.4 Analytical Column: NA
- B6.5 Guard Cartridge: NA
- B6.6 Analytical Balance: Ohaus Discovery DV215CD
- B6.7 1-mL Syringes
- B6.8 Agilent Captiva Econofilter 0.2- μ m PTFE Syringe Filters
- B6.9 Millipore Direct-Q Water Purification System
- B6.10 20-mL Amber Vials
- B6.11 2-mL Agilent LC-MS Amber Vials
- B6.12 Spectra/Por dialysis membranes (MW cutoff 100-500 Da)
- B6.13 -20 °C freezer
- B6.14 5-mL round bottom flask

B7. Reagents

- B7.1 Methanol, LC-MS grade, CAS# 67-18-6
- B7.2 Water, LC-MS grade, CAS# 7732-18-5
- B7.3 Derivatized dextran, obtain from interested parties, or Dextran T1, CAS# 9004-54-0
- B7.4 Water, Millipore Direct-Q grade
- B7.5 1,1'-Carbonyldiimidazole, CAS# 530-62-1
- B7.6 Dimethyl Sulfoxide, CAS# 67-68-5
- B7.7 Sodium Chloride, CAS# 7647-14-5
- B7.8 Acetic Acid, CAS# 64-19-7

1. Procedure

B8.1 Preparation of Mobile Phase

Note: The mobile phase solutions are stable for up to the expiration date of the reagent when no aqueous mobile phase is prepared when stored in glass bottles at room temperature. For aqueous mobile phases, 1% methanol is added to extend stability for 30 days.

B8.1.1 Mobile Phase A: 0.1% acetic acid in water

B8.1.1.1 Dilute 1.0-mL of acetic acid to 1-L with LC-MS water and mix thoroughly

B8.1.2 Mobile Phase B: 0.1% acetic acid in methanol

B8.1.2.1 Dilute 1.0-mL of acetic acid to 1-L with LC-MS methanol and mix thoroughly

B8.1.3 Transfer the desired volume of each mobile phase to the appropriate LC-MS solvent reservoir(s). Appropriately update solvent volumes on the instrument if necessary.

B8.2 Preparation of Derivatized Dextran Samples (following previously established procedures^{1,2})

B8.2.1 Derivatization of Dextran

B8.2.1.1 Prepare CDI solution by dissolving 0.2-g of CDI in 2-mL DMSO

B8.2.1.2 Weigh out 0.5-g of dextran and transfer into 25-mL round bottom flask

B8.2.1.3 Add 6-mL DMSO to round bottom flask with dextran and dissolve dextran

B8.2.1.4 Place the 25-mL round bottom flask containing dextran in DMSO in an oil bath at 60 °C allowing for dextran to completely dissolve and reach 60 °C

B8.2.1.5 Once at 60 °C, add the CDI solution from B8.2.1.1 to the dextran solution and still at 60 °C for 15 min

B8.2.1.6 After 15 min, add 1-mL ethylenediamine to the dextran-CDI mixture and allow to react for 18 h at 60 °C

B8.2.2 Dextran Derivatization Cleanup

B8.2.2.1 After the reaction is complete (B8.2.1.6), allow mixture to reach RT

B8.2.2.2 Precipitate derivatized dextran from solution by adding excess methanol. Approximately 100-mL will initiate precipitation

B8.2.2.3 Filter the precipitate by vacuum filtration and wash with methanol to remove leftover DMSO and any other impurities soluble in methanol

B8.2.2.4 Once the precipitate is dry, re-dissolve in Millipore water for dialysis. Try to keep the volume under 20-mL to maximize the dilution/cleanup by dialysis

B8.2.3 Dialysis (Use in-house dialysis apparatus to speed-up dialysis)

B8.2.3.1 Prepare a 0.5% w/v NaCl solution by dissolving 5-g NaCl for every 1-L of solution prepared

B8.2.3.2 Prepare 0.01% v/v acetic acid solution by diluting 100- μ L acetic acid for every 1-L of solution prepared

B8.2.3.3 Transfer the re-dissolved derivatized dextran (from B8.2.2.4) to a dialysis bag and seal the bag

B8.2.3.4 Dialyze the derivatized dextran (from B8.2.3.3) in approximately 10-L of 0.5% NaCl solution prepared as stated in B8.2.3.1 at RT for 24 hr

B8.2.3.5 Dialyze the derivatized dextran (from B8.2.3.3) in approximately 20-L of 0.01% acetic acid solution prepared as stated in B8.2.3.2 at RT for 24 hr

B8.2.4 Freeze dry product

B8.2.4.1 Transfer the dialyzed derivatized dextran from B8.2.3.5 to a freeze-dry compatible vessel

B8.2.4.2 If time allows, allow product to freeze overnight in the -20 °C freezer, OR:

B8.2.4.3 Freeze sample carefully using liquid nitrogen

B8.2.4.4 Freeze dry sample using the Labcono Freeze Dryer until all the water has been removed

Note: This may take as little as 24 hr or as long as 7 days depending on the volume of water that needs to be removed. Lower volume is always recommended; however, this is highly dependent on the dialysis steps (section 8.2.3)

B8.2.4.5 Transfer dried sample from 8.2.4.4 to an appropriate storage vial/bottle and store at -20 °C until LC-MS analysis

B8.2.5 Derivatized dextran sample preparation

B8.2.5.1 Prepare derivatized dextran samples at a concentration of 1-mg/mL in 0.1% acetic acid in water solution

B8.2.5.2 Transfer at least 1-mL of B8.2.5.1 into a 1-mL Agilent LC-MS vial using a 1-mL syringe and filtering through an Agilent Captiva Econofilter 0.2-µm PTFE Syringe Filter

B8.3 Analysis Method

Follow Table B.1 for instrument method conditions. **See appendix H for appropriate instrument setup and use.**

B8.3.1 Inject reagent blank in positive polarity

B8.3.2 Inject each sample in triplicate with instrument in positive polarity

B8.3.3 Load next sample sequence if needed repeating B8.3.1 – B8.3.2 or:

B8.3.4 Repeat B8.3.1

B8.3.5 Put instrument on Stand-by

Table B.1 LC-MS Method Parameters

HPLC Settings				
Column Type		NA		
Guard Column		NA		
Column Temperature		35 °C		
Sample Tray Temperature		RT		
Injection Volume		0.1 µL		
Needle Wash		Methanol in Rinse Vial, Position 1		
Flow Rate		0.15 mL/min		
Stop Time		2 min		
Post Time		NA		
Method Type		Isocratic Direct Injection		
MP A		0.1 % acetic acid in water		
MP B		0.1 % acetic acid in methanol		
Isocratic Injection			MS Settings	
Time, min	MPA, %	MPB, %	Ion Source	Dual ESI
0	90	10	Ionization Polarity	Positive
2	90	10	Capillary Voltage	4000 V
End Analysis			Fragmentor Voltage	80 V
			Skimmer Voltage	75 V
			Drying Gas Flow Rate	12.5 l/min (N ₂)
			Drying Gas Temperature	250 °C (N ₂)
			Nebulizer Pressure	45 psi

B9. Data Analysis

B9.1 Perform the necessary MW calculations for the potential derivatized dextran chains

B9.1.1 Use the MW of each expected dextran oligo or polysaccharide and design it as “M”

B9.1.2 To account for the number of ethylenediamine attachments use the formula $[M + 86x]$ where x is the number of ethylenediamine attachments

B9.1.3 To account for the number of protonations use the formula $[M + 86y + yH]^+$ where y is the number of protonations

B9.2 Analyze data using MassHunter Qualitative Analysis B.07.00

B9.2.1 Extract “Mass Spectrum” from data collected (data file looks similar to an unretained chromatographic peak)

B9.2.2 Extract “Background Spectrum” from data collected (extract from the baseline, not the unretained chromatographic peak)

B9.2.3 Subtract “background spectrum” from “extracted mass spectrum”

B9.2.4 Search for the predicted masses (found following the steps in section B9.1)

B9.2.5 Use the Agilent isotope distribution calculator to aid in the positive identification of the derivatized dextran chains

B9.2.6 In the processed data files (sections B9.2.1 – B9.2.3), visually inspect for multiple charging events by searching for isotopic distributions that are less than ~1 Da apart¹. A difference of ~0.5 Da denotes two charges, a difference of ~0.33 Da denotes three charges, a difference of ~0.25 Da denotes 4 charges and so on

B9.2.7 To deconvolute the multiply charged ions use the following series of equations:

B9.2.7.1 Using two adjacent peaks suspected of multiple charging use:

$$z = \frac{(m/z)_1 - x}{(m/z)_2 - (m/z)_1} \quad \text{Eq. B.1}$$

Where m/z_1 and m/z_2 are two adjacent ion peaks, x is the mass of the adduct (usually 1.0073 for proton adducts) and z is the calculated charge of m/z_2

B9.2.7.2 Once the charge is calculated, calculate the deconvoluted mass:

$$M = z((m/z)_2 - x) \quad \text{Eq. B.2}$$

Where M is the deconvoluted mass, z is the number of charges (calculated in 9.2.7.1) and x is the mass of the adduct (usually 1.0073 for proton adducts)

B10. Data Reporting

B10.1 Export data as csv file

B10.2 Use Origin or Igor to plot data files

B10.3 Appropriately label peaks of interest

B10.4 Submit data to interested parties/publications

APPENDIX B – REFERENCES

- (1) Tapia, J. B.; Hibbard, H. A. J.; Reynolds, M. M. Derivatization of Dextran for Multiply Charged Ion Formation and Electrospray Ionization Time-of-Flight Mass Spectrometric Analysis. *J. Am. Soc. Mass Spectrom.* **2017**, 28 (10), 2201–2208.
- (2) Nakamura, J.; Nakajima, N.; Matsumura, K.; Hyon, S. H. Water-Soluble Taxol Conjugates with Dextran and Targets Tumor Cells by Folic Acid Immobilization. *Anticancer Res.* **2010**, 30 (3), 903–910.

APPENDIX C

Chitosan-MOF Composites Catalysis/Degradation Mass Spectrometric Analysis SOP (Chapter 3)¹

C1. Purpose

A direct flow injection with an LC-MS system is used for the identification of the products from nitric oxide (NO) release from *S*-nitrosoglutathione (GSNO), screening for hydrolytic degradation of the chitosan support system, and screening for the presence of the MOF's building block H₃BTTri ligand.

C2. Scope

This test method provides instructions for the preparation and analysis of the collected media after GSNO is subjected to chitosan-MOF composites. The goals are to (1) clearly identify the byproduct from GSNO releasing NO; (2) screen for the degradation of the chitosan support system as it is exposed to GSNO in solution; (3) screen for the potential of the copper MOF degrading while exposed to GSNO solution by searching for the ligand used to make the MOF (H₃BTTri).

C3. Responsibility

To be performed by personnel who are technically qualified and trained in the use of the LC-MS and associated techniques.

C4. Safety

The samples and reagents used in this procedure should be handled using good laboratory practices. Wear gloves and work in a fume hood. Read the Safety Data Sheets for all chemicals used in this procedure.

C5. Abbreviations

ACN	Acetonitrile
APCI	Atmospheric Pressure Chemical Ionization
CAS	Chemical Abstracts Service
Cu-BTTri	H ₃ [(Cu ₄ Cl) ₃ -(BTTri) ₈]
ESI	Electrospray Ionization
GSNO	<i>S</i> -nitrosoglutathione
GSSG	Glutathione disulfide
H ₃ BTTri	1,3,5-tris(1 <i>H</i> -1,2,3-triazol-5-yl)benzene

LC-MS	Liquid Chromatography-Mass Spectrometry
MeOH	Methanol
MMI	Mixed-Mode Ionization
MOF	Metal-organic framework
MP	Mobile Phase
MW	Molecular Weight
NA	Not Applicable
NO	Nitric Oxide
RT	Room Temperature
TOF	Time-of-Flight

C6. Materials and Equipment

- C6.1 Agilent 1260 Infinity HPLC System
- C6.2 Agilent 6224 TOF Mass Spectrometer
- C6.3 Agilent MMI ion source
- C6.4 Analytical Column: NA
- C6.5 Guard Cartridge: NA
- C6.6 Analytical Balance: Ohaus Discovery DV15CD
- C6.7 1-mL Syringes
- C6.8 Agilent Captiva Econofilter 0.2- μ m PTFE Syringe Filters
- C6.9 Millipore Direct-Q Water Purification System
- C6.10 Aluminum Foil
- C6.11 20-mL Amber Vials
- C6.12 2-mL Agilent LC-MS Amber Vials
- C6.13 Incubator: Barnstead Lab-Line Max^Q 7000

C7. Reagents

- C7.1 Acetonitrile, LC-MS grade, CAS# 75-05-8
- C7.2 Water, LC-MS grade, CAS# 7732-18-5
- C7.3 Chitosan-MOF composites, obtain from interested parties
- C7.4 Water, Millipore Direct-Q grade
- C7.5 In-house synthesized GSNO, CAS# 57564-91-7 (if purchased)

C8. Procedure

C8.1 Preparation of Mobile Phase

Note: The mobile phase solutions are stable for up to the expiration date of the reagent when no aqueous mobile phase is prepared when stored in glass bottles at room temperature. For aqueous mobile phases, 1% methanol is added to extend stability for 30 days.

C8.1.1 Mobile Phase A: 0.1% formic acid in water

C8.1.1.1 Dilute 1.0-mL of formic acid to 1-L with LC-MS water and mix thoroughly

C8.1.2 Mobile Phase B: 0.1% formic acid in acetonitrile

C8.1.2.1 Dilute 1.0-mL of formic acid to 1-L with LC-MS acetonitrile

C8.1.3 Transfer the desired volume of mobile phase to the appropriate LC-MS solvent reservoir. Appropriately update solvent volumes on the instrument if necessary

C8.2 Preparation of chitosan-MOF + GSNO experiments (per Megan J. Neufeld's method¹)

C8.2.1 Incubation Process

C8.2.1.1 Weigh out 20 mg of provided or synthesized chitosan-Cu-BTTri composite and place in 20-mL amber vial

C8.2.1.2 Add the desired volume of a 1 mM solution of GSNO (at least 5-mL) and seal the vial

C8.2.1.3 Cover vial with aluminum foil to minimize exposure to light

C8.2.1.4 Incubate samples (minimum of three samples, repeat steps C8.2.1.1 – C8.2.1.3 as needed) at 37 °C for the desired length of time

Note: The disappearance of the characteristic red/pink color of GSNO in solution is usually a good indicator of when to stop the incubation process

C8.2.2 Sampling

C8.2.2.1 Remove vials from incubator

C8.2.2.2 Allow vials to reach RT

C8.2.2.3 Obtain a 1-mL sample aliquot using a 1-mL syringe

C8.2.2.4 Filter sample through an Agilent 0.2- μ m filter into an Agilent 2-mL LC-MS vial and seal the vial

C8.2.2.5 Appropriately dispose of the remaining incubation media

C8.3 Analysis Method

Follow Table C.1 for instrument method conditions. **See appendix H for appropriate instrument setup and use.**

C8.3.1 Inject reagent blank

C8.3.2 Inject each sample in triplicate

C8.3.3 Load next sample sequence if needed repeating C8.3.1 – C8.3.2 or:

C8.3.4 Repeat C8.3.1

C8.3.5 Put instrument on Stand-by

Table C.1 LC-MS Method Parameters

HPLC Settings				
Column Type		NA		
Guard Column		NA		
Column Temperature		35 °C		
Sample Tray Temperature		RT		
Injection Volume		0.1 µL		
Needle Wash		Acetonitrile in Rinse Vial, Position 1		
Flow Rate		0.22 mL/min		
Stop Time		2 min		
Post Time		NA		
Method Type		Isocratic Direct Injection		
MP A		0.1% formic acid in water		
MP B		0.1% formic acid in acetonitrile		
Isocratic Injection			MS Settings	
Time, min	MPA, %	MPB, %	Ion Source	MMI
0	80	20	Ionization Mode	ESI
2	80	20	Ion Polarity	Positive
End Analysis			Capillary Voltage	3000 V
			Fragmentor Voltage	200 V
			Skimmer Voltage	60 V
			Charging Voltage	NA
			Drying Gas Flow Rate	10 l/min (N ₂)
			Drying Gas Temperature	310 °C (N ₂)
			Nebulizer Pressure	45 psi

C9. Data Analysis

C9.1 Perform the necessary MW calculations for the analytes of interest

C9.1.1 GSNO: C₁₀H₁₆N₄O₇S; exact mass: 336.0740; *m/z* as [M+H]⁺: 337.0812

C9.1.2 GSSG: C₂₀H₃₂N₆O₁₂S₂; exact mass: 612.1520; *m/z* as [M+H]⁺: 613.1592; *m/z* as [M+2H]²⁺: 307.0833

Note: GSNO and doubly charged GSSG have near identical mass. Make sure to check for the mass difference in the isotopic distribution. For an explanation on this see ²

C9.1.3 Glucosamine: C₆H₁₃NO₅; exact mass: 179.0794; *m/z* as [M+H]⁺: 180.0866; *m/z* as [M - H₂O + H]⁺: 162.0761

C9.1.4 *N*-acetylglucosamine: C₈H₁₅NO₆; exact mass: 221.0899; *m/z* as [M+H]⁺: 222.0972

C9.1.5 H₃BTTri: C₁₂H₉N₉; exact mass: 279.0981; *m/z* as [M+H]⁺: 280.1054; *m/z* as [M+2H]²⁺: 140.5563

C9.2 Analyze data using MassHunter Qualitative Analysis B.07.00

C9.2.1 Extract “Mass Spectrum” from data collected (data file looks similar to an unretained chromatographic peak)

C9.2.2 Extract “Background Spectrum” from data collected (extract from the baseline, not the unretained chromatographic peak)

C9.2.3 Subtract “background spectrum” from “extracted mass spectrum”

C9.2.4 Search for the ions of interest (section C9.1)

C9.3 Data interpretation

C9.3.1 Upon completion of the reaction (section C8.2.1), search for the ions in section C9.1. The compounds in sections C9.1.1 – C9.1.4 are all possible, specially GSSG, glucosamine and *N*-acetylglucosamine

C9.3.1 If the compound in C9.1.5 is found, report to interested parties immediately!
The presence of H₃BTTri suggests Cu-BTTri MOF decomposition and the chitosan-MOF batch should not be used until it is further investigated for MOF decomposition and copper leaching

C10. Data Reporting

C10.1 Export data as csv file

C10.2 Use Origin or Igor to plot data files

C10.3 Appropriately label peaks of interest

C10.4 Submit data to interested parties/publications

APPENDIX C – REFERENCES

- (1) Neufeld, M. J.; Lutzke, A.; Tapia, J. B.; Reynolds, M. M. Metal–Organic Framework/Chitosan Hybrid Materials Promote Nitric Oxide Release from S - Nitrosoglutathione in Aqueous Solution. *ACS Appl. Mater. Interfaces* **2017**, 9 (6), 5139–5148.
- (2) Tapia, J. B.; Hibbard, H. A. J.; Reynolds, M. M. Derivatization of Dextran for Multiply Charged Ion Formation and Electrospray Ionization Time-of-Flight Mass Spectrometric Analysis. *J. Am. Soc. Mass Spectrom.* **2017**, 28 (10), 2201–2208.

APPENDIX D

CellTiter Blue Assay Interferences Mass Spectrometric Analysis SOP (Chapter 3)¹

D1. Purpose

A direct flow injection with an LC-MS system is used to track the conversion of resazurin to resorufin in the absence of cells.

D2. Scope

This test method provides instructions for the preparation and analysis of the cell viability assay CellTiter Blue (resazurin-resorufin) when subjected to potential interfering species in the absence of cells.

D3. Responsibility

To be performed by personnel who are technically qualified and trained in the use of the LC-MS and associated techniques.

D4. Safety

The samples and reagents used in this procedure should be handled using good laboratory practices. Wear gloves and work in a fume hood. Read the Safety Data Sheets for all chemicals used in this procedure.

D5. Abbreviations

APCI	Atmospheric Pressure Chemical Ionization
CAS	Chemical Abstracts Service
ESI	Electrospray Ionization
LC-MS	Liquid Chromatography-Mass Spectrometry
MeOH	Methanol
MMI	Mixed-Mode Ionization
MP	Mobile Phase
MW	Molecular Weight
NA	Not Applicable
POPs	Poly(phosphazenes)
RT	Room Temperature
TOF	Time-of-Flight

D6. Materials and Equipment

- D6.1 Agilent 1260 Infinity HPLC System
- D6.2 Agilent 6224 TOF Mass Spectrometer
- D6.3 Agilent MMI ion source
- D6.4 Analytical Column: NA
- D6.5 Guard Cartridge: NA
- D6.6 Analytical Balance: Ohaus Discovery DV215CD
- D6.7 1-mL Syringes
- D6.8 Agilent Captiva Econofilter 0.2- μ m PTFE Syringe Filters
- D6.9 Millipore Direct-Q Water Purification System
- D6.10 Aluminum Foil
- D6.11 20-mL Amber Vials
- D6.12 2-mL Agilent LC-MS Amber Vials
- D6.13 Incubator: Barnstead Lab-Line Max^Q 7000

D7. Reagents

- D7.1 Methanol, LC-MS grade, CAS# 67-18-6
- D7.2 Water, Millipore Direct-Q grade
- D7.3 CellTiter Blue interference samples, obtain from interested parties

D8. Procedure

D8.1 Preparation of Mobile Phase

Note: The mobile phase solutions are stable for up to the expiration date of the reagent when no aqueous mobile phase is prepared when stored in glass bottles at room temperature. For aqueous mobile phases, 1% methanol is added to extend stability for 30 days.

D8.1.1 Mobile Phase A: NA

D8.1.2 Mobile Phase B: 100% Methanol

D8.1.3 Transfer the desired volume of MeOH to the appropriate LC-MS solvent reservoir. Appropriately update solvent volumes on the instrument if necessary

D8.2 Preparation of Incubation Samples

D8.2.1 Incubation Process

D8.2.1.1 Prepare interference species to be tested at a concentration of 50 mM in Millipore water

D8.2.1.2 Combine the interference species with the CellTiter Blue dye in a 5:1 (interference/CellTiter Blue dye) fashion in a 20-mL amber vial to obtain a 10 mM final concentration of interference species

D8.2.1.3 Cover vial with aluminum foil to protect samples from exposure to light

D8.2.1.4 Incubate a total of four samples, one for each time period (hours 1 through 4), at 37 °C

D8.2.2 Hourly Sampling

D8.2.2.1 Remove sample vial from incubator

D8.2.2.2 Obtain a 1-mL sample aliquot using a 1-mL syringe

D8.2.2.3 Filter sample through an Agilent 0.2- μ m filter into an Agilent 2-mL LC-MS amber vial and seal the vial

D8.2.2.4 Appropriately dispose of the remaining incubation media

D8.2.2.5 Immediately analyze sample using the MS analysis method in section 8.3

D8.2.2.6 Repeat steps D8.2.2.1 – D8.2.2.5 for each subsequent sample

D8.3 Analysis Method

Follow Table D.1 for instrument method conditions. **See appendix H for appropriate instrument setup and use.**

D8.3.1 Inject reagent blank in negative polarity

D8.3.2 Inject each sample in triplicate with instrument in negative polarity

D8.3.3 Load next sample triplicate repeating D8.3.1 – D8.3.2 or:

D8.3.4 Repeat D8.3.1

D8.3.5 Put instrument on Stand-by

Table D.1 LC-MS Method Parameters

HPLC Settings			
Column Type		NA	
Guard Column		NA	
Column Temperature		35 °C	
Sample Tray Temperature		RT	
Injection Volume		0.1 µL	
Needle Wash		Methanol in Rinse Vial, Position 1	
Flow Rate		0.22 mL/min	
Stop Time		2 min	
Post Time		NA	
Method Type		Isocratic Direct Injection	
MP A		NA	
MP B		Methanol	
Isocratic Injection			MS Settings
Time, min	MPA, %	MPB, %	Ion Source MMI
0	0	100	Ion Polarity Negative
2	0	100	Capillary Voltage 2500 V
End Analysis			Fragmentor Voltage 120 V
			Skimmer Voltage 60 V
			Charging Voltage 2000 V
			Drying Gas Flow Rate 10 l/min (N ₂)
			Drying Gas Temperature 310 °C (N ₂)
			Nebulizer Pressure 45 psi

D9. Data AnalysisD9.1 CellTiter Blue molecular formula, exact mass and expected m/z

D9.1.1 Resazurin: C₁₂H₇NO₄, exact mass 229.0375 (calculated using Agilent Isotope Distribution Calculator), expected m/z 228.0302 as [M-H]⁻ (calculated using Agilent Isotope Distribution Calculator)

D9.1.2 Resorufin: C₁₂H₇NO₃, exact mass 213.0426 (calculated using Agilent Isotope Distribution Calculator), expected m/z 212.0353 as [M-H]⁻ (calculated using Agilent Isotope Distribution Calculator)

D9.1.3 Instrument default mass range set to 100 – 3200 m/z . If the MS detection of resazurin and resorufin are the only two of interest, set mass range to 205 – 235 m/z .

D9.2 Analyze data using MassHunter Qualitative Analysis B.07.00

D9.2.1 Extract “Mass Spectrum” from data collected (data file looks similar to an unretained chromatographic peak)

D9.2.2 Extract “Background Spectrum” from data collected (extract from the baseline, not the unretained chromatographic peak)

D9.2.3 Subtract “background spectrum” from “extracted mass spectrum”

D9.2.4 Examine for the presence of resazurin or resorufin or both (found using the parameters in section D9.1)

D9.2.5 Use the Agilent isotope distribution calculator to aid in the positive identification of resazurin or resorufin or both

D10. Data Reporting

D10.1 Export data as csv file

D10.2 Use Origin or Igor to plot data files

D10.3 Appropriately label peaks of interest

D10.4 Submit data to interested parties/publications

APPENDIX D – REFERENCES

- (1) Neufeld, B. H.; Tapia, J. B.; Lutzke, A.; Reynolds, M. M. Small Molecule Interferences in Resazurin and MTT-Based Metabolic Assays in the Absence of Cells. *Anal. Chem.* **2018**, *90* (11), 6867–6876.

APPENDIX E

MTT Assay Interferences Mass Spectrometric Analysis SOP (Chapter 3)¹

E1. Purpose

A direct flow injection with an LC-MS system is used to track the conversion of MTT to formazan in the absence of cells.

E2. Scope

This test method provides instructions for the preparation and analysis of the MTT cell viability assay (MTT-formazan) when subjected to potential interfering species in the absence of cells.

E3. Responsibility

To be performed by personnel who are technically qualified and trained in the use of the LC-MS and associated techniques.

E4. Safety

The samples and reagents used in this procedure should be handled using good laboratory practices. Wear gloves and work in a fume hood. Read the Safety Data Sheets for all chemicals used in this procedure.

E5. Abbreviations

APCI	Atmospheric Pressure Chemical Ionization
CAS	Chemical Abstracts Service
ESI	Electrospray Ionization
LC-MS	Liquid Chromatography-Mass Spectrometry
MeOH	Methanol
MMI	Mixed-Mode Ionization
MP	Mobile Phase
MW	Molecular Weight
NA	Not Applicable
POPs	Poly(phosphazenes)
RT	Room Temperature
TOF	Time-of-Flight

E6. Materials and Equipment

- E6.1 Agilent 1260 Infinity HPLC System
- E6.2 Agilent 6224 TOF Mass Spectrometer
- E6.3 Agilent MMI ion source
- E6.4 Analytical Column: NA
- E6.5 Guard Cartridge: NA
- E6.6 Analytical Balance: Ohaus Discovery DV215CD
- E6.7 1-mL Syringes
- E6.8 Agilent Captiva Econofilter 0.2- μ m PTFE Syringe Filters
- E6.9 Millipore Direct-Q Water Purification System
- E6.10 Aluminum Foil
- E6.11 20-mL Amber Vials
- E6.12 2-mL Agilent LC-MS Amber Vials
- E6.13 Incubator: Barnstead Lab-Line Max^Q 7000

E7.1 Reagents

- E7.1 Methanol, LC-MS grade, CAS# 67-18-6
- E7.2 Water, Millipore Direct-Q grade
- E7.3 MTT assay interference samples, obtain from interested parties

E8. Procedure

E8.1 Preparation of Mobile Phase

Note: The mobile phase solutions are stable for up to the expiration date of the reagent when no aqueous mobile phase is prepared when stored in glass bottles at room temperature. For aqueous mobile phases, 1% methanol is added to extend stability for 30 days.

E8.1.1 Mobile Phase A: NA

E8.1.2 Mobile Phase B: 100% Methanol

E8.1.3 Transfer the desired volume of MeOH to the appropriate LC-MS solvent reservoir. Appropriately update solvent volumes on the instrument if necessary.

E8.2 Preparation of Incubation Samples

E8.2.1 Incubation Process

E8.2.1.1 Prepare interference species to be tested at a concentration of 50 mM in Millipore water

E8.2.1.2 Per Bella H. Neufeld's MTT assay protocol¹, MTT was made in PBS with a final concentration of 12 mM

E8.2.1.3 Combine the interference species with the MTT dye (from E8.2.1.2) in a 5:1 (interference/MTT dye) fashion in a 20-mL amber vial to obtain a 10 mM final concentration of interference species

E8.2.1.4 Cover vial with aluminum foil to protect samples from exposure to light

E8.2.1.5 Incubate a total of four samples, one for each time period (hours 1 through 4), at 37 °C

E8.2.2 Hourly Sampling

E8.2.2.1 Remove sample vial from incubator

E8.2.2.2 To minimize ion suppression due to PBS on the mass spectrometer (sample incubation per section E8.2.1), the incubated mixture from E8.2.1.3 was diluted in ethanol to 0.1% before injection into the instrument¹

E8.2.2.3 Obtain a 1-mL sample aliquot using a 1-mL syringe

E8.2.2.4 Filter sample through an Agilent 0.2- μ m filter into an Agilent 2-mL LC-MS amber vial and seal the vial

E8.2.2.5 Appropriately dispose of the remaining incubation media

E8.2.2.6 Immediately analyze sample using the MS analysis method in section 8.3

E8.2.2.7 Repeat steps E8.2.2.1 – E8.2.2.6 for each subsequent sample

E8.3 Analysis Method

Follow Table E.1 for instrument method conditions. **See appendix H for appropriate instrument setup and use.**

E8.3.1 Inject reagent blank in negative polarity

E8.3.2 Inject each sample in triplicate with instrument in negative polarity

E8.3.3 Inject water blank to remove any potentially precipitated PBS in LC lines

E8.3.4 Load next sample triplicate repeating E8.3.1 – E8.3.3 or:

E8.3.5 Extensively rinse instrument with a mobile phase of 95:5 LC-MS water/LC-MS methanol to dissolve any PBS left in the lines

E8.3.6 Put instrument on Stand-by

E8.3.7 Perform an ion source cleaning

E8.3.7.1 Clean spray shield, backplate and ion source surfaces with LC-MS water using a lint-free cloth

E8.3.7.2 Clean spray shield, backplate and ion source surfaces with 1:1 LC-MS isopropanol/LC-MS water using a lint-free cloth

E8.3.7.3 Sonicate nebulizer in 1:1 LC-MS isopropanol/LC-MS water to remove any precipitated impurities

Table E.1 LC-MS Method Parameters

HPLC Settings				
Column Type		NA		
Guard Column		NA		
Column Temperature		35 °C		
Sample Tray Temperature		RT		
Injection Volume		0.1 µL		
Needle Wash		Methanol in Rinse Vial, Position 1		
Flow Rate		0.22 mL/min		
Stop Time		2 min		
Post Time		NA		
Method Type		Isocratic Direct Injection		
MP A		NA		
MP B		Methanol		
Isocratic Injection			MS Settings	
Time, min	MPA, %	MPB, %	Ion Source	MMI
0	0	100	Ion Polarity	Negative
2	0	100	Capillary Voltage	2500 V
End Analysis			Fragmentor Voltage	120 V
			Skimmer Voltage	60 V
			Charging Voltage	2000 V
			Drying Gas Flow Rate	10 l/min (N ₂)
			Drying Gas Temperature	310 °C (N ₂)
			Nebulizer Pressure	45 psi

E9. Data Analysis

E9.1 MTT molecular formula, exact mass and expected m/z

E9.1.1 MTT: $C_{18}H_{16}N_5S$, exact mass 334.1126 (calculated using Agilent Isotope Distribution Calculator), expected m/z 334.1121 as $[M]^+$ (calculated using Agilent Isotope Distribution Calculator)

E9.1.2 Formazan: $C_{18}H_{17}N_5S$, exact mass 335.1205 (calculated using Agilent Isotope Distribution Calculator), expected m/z 336.1277 as $[M+H]^+$ (calculated using Agilent Isotope Distribution Calculator)

E9.1.3 Instrument default mass range set to 100 – 3200 m/z . If the MS detection of resazurin and resorufin are the only two of interest, set mass range to 330 – 340 m/z

E9.2 Analyze data using MassHunter Qualitative Analysis B.07.00

E9.2.1 Extract “Mass Spectrum” from data collected (data file looks similar to an unretained chromatographic peak)

E9.2.2 Extract “Background Spectrum” from data collected (extract from the baseline, not the unretained chromatographic peak)

E9.2.3 Subtract “background spectrum” from “extracted mass spectrum”

E9.2.4 Examine for the presence of MTT or formazan or both (found using the parameters in section 9.1)

E9.2.5 Use the Agilent isotope distribution calculator to aid in the positive identification of MTT or formazan or both

E10. Data Reporting

E10.1 Export data as csv file

E10.2 Use Origin or Igor to plot data files

E10.3 Appropriately label peaks of interest

E10.4 Submit data to interested parties/publications

APPENDIX E – REFERENCES

- (1) Neufeld, B. H.; Tapia, J. B.; Lutzke, A.; Reynolds, M. M. Small Molecule Interferences in Resazurin and MTT-Based Metabolic Assays in the Absence of Cells. *Anal. Chem.* **2018**, *90* (11), 6867–6876.

APPENDIX F

POPs Mass Spectrometric Analysis SOP (Chapter 4)¹

F1. Purpose

A direct flow injection with an LC-MS system is used for the identification of products from hydrolytic degradation of POPs polymers.

F2. Scope

This test method provides instructions for the preparation and analysis of degradation products from the incubation of POPs polymers.

F3. Responsibility

To be performed by personnel who are technically qualified and trained in the use of the LC-MS and associated techniques.

F4. Safety

The samples and reagents used in this procedure should be handled using good laboratory practices. Wear gloves and work in a fume hood. Read the Safety Data Sheets for all chemicals used in this procedure.

F5. Abbreviations

APCI	Atmospheric Pressure Chemical Ionization
CAS	Chemical Abstracts Service
ESI	Electrospray Ionization
LC-MS	Liquid Chromatography-Mass Spectrometry
MeOH	Methanol
MMI	Mixed-Mode Ionization
MP	Mobile Phase
MW	Molecular Weight
NA	Not Applicable
POPs	Poly(phosphazenes)
RT	Room Temperature
TOF	Time-of-Flight

F6. Materials and Equipment

- F6.1 Agilent 1260 Infinity HPLC System
- F6.2 Agilent 6224 TOF Mass Spectrometer
- F6.3 Agilent MMI ion source
- F6.4 Analytical Column: NA
- F6.5 Guard Cartridge: NA
- F6.6 Analytical Balance: Ohaus Discovery DV215CD
- F6.7 1-mL Syringes
- F6.8 Agilent Captiva Econofilter 0.2- μ m PTFE Syringe Filters
- F6.9 Millipore Direct-Q Water Purification System
- F6.10 Aluminum Foil
- F6.11 20-mL Amber Vials
- F6.12 2-mL Agilent LC-MS Amber Vials
- F6.13 Incubator: Barnstead Lab-Line Max^Q 7000

F7.1 Reagents

- F7.1 Methanol, LC-MS grade, CAS# 67-18-6
- F7.2 Water, LC-MS grade, CAS# 7732-18-5
- F7.3 POPs Polymer Samples, obtain from interested parties
- F7.4 Water, Millipore Direct-Q grade

F8. Procedure

F8.1 Preparation of Mobile Phase

Note: The mobile phase solutions are stable for up to the expiration date of the reagent when no aqueous mobile phase is prepared when stored in glass bottles at room temperature. For aqueous mobile phases, 1% methanol is added to extend stability for 30 days.

F8.1.1 Mobile Phase A: NA

F8.1.2 Mobile Phase B: 100% Methanol

F8.1.3 Transfer the desired volume of mobile phase to the appropriate LC-MS solvent reservoir. Appropriately update solvent volumes on the instrument if necessary

F8.2 Preparation of Incubation Samples

F8.2.1 Incubation Process

F8.2.1.1 Weigh out 20 mg of provided or synthesized POPs polymer and transfer into a 20-mL amber vial

F8.2.1.2 Add 5-mL of Millipore water and seal the vial

F8.2.1.3 Cover vial with aluminum foil to protect samples from exposure to light

F8.2.1.4 Incubate samples (minimum of three samples, repeat steps F8.2.1.1 – F8.2.1.3 as needed) at 37 °C for the desired length of time

F8.2.2 Weekly Sampling

F8.2.2.1 Remove vials from incubator

F8.2.2.2 Allow vials to reach RT

F8.2.2.3 Obtain a 1-mL sample aliquot using a 1-mL syringe

F8.2.2.4 Filter sample through an Agilent 0.2- μ m filter into an Agilent 2-mL LC-MS vial and seal the vial

F8.2.2.5 Appropriately dispose of the remaining incubation media

F8.2.2.6 Rinse POPs polymer sample with Millipore water

F8.2.2.7 Add the rinsed POPs sample to a clean 20-mL amber vial and repeat steps F8.2.1.2 – F8.2.1.4

F8.2.3 Single Sampling (1-week or up to 10-week single sampling)

Follow steps F8.2.2.1 – F8.2.2.5

F8.3 Analysis Method

Follow Table F.1 for instrument method conditions. **See appendix H for appropriate instrument setup and use.**

F8.3.1 Inject reagent blank in selected polarity (positive or negative)

F8.3.2 Inject each sample in triplicate with instrument in selected polarity (positive or negative)

F8.3.3 Load next sample sequence if needed repeating F8.3.1 – F8.3.2 or:

F8.3.4 Repeat F8.3.1

F8.3.5 Put instrument on Stand-by

Table F.1 LC-MS Method Parameters

HPLC Settings				
Column Type		NA		
Guard Column		NA		
Column Temperature		35 °C		
Sample Tray Temperature		RT		
Injection Volume		0.1 µL		
Needle Wash		Methanol in Rinse Vial, Position 1		
Flow Rate		0.20 mL/min		
Stop Time		2 min		
Post Time		NA		
Method Type		Isocratic Direct Injection		
MP A		NA		
MP B		Methanol		
Isocratic Injection			MS Settings	
Time, min	MPA, %	MPB, %	Ion Source	MMI
0	0	100	Ion Polarity	Positive
2	0	100		Negative
End Analysis			Capillary Voltage	2500 V
			Fragmentor Voltage	120 V
			Skimmer Voltage	60 V
			Charging Voltage	2000 V
			Drying Gas Flow Rate	10 l/min (N ₂)
			Drying Gas Temperature	310 °C (N ₂)
			Nebulizer Pressure	45 psi

F9. Data Analysis

F9.1 Perform the necessary MW calculations for the predicted degradation products

F9.1.1 Use ChemDraw to draw the predicted structures based on the mode of degradation (hydrolytic degradation in this case)

F9.1.2 In ChemDraw, obtain the formula of the structure by selecting the structure of interest, right clicking on it, clicking analysis, and clicking “chemical formula”

F9.1.3 In ChemDraw, obtain the exact mass of the structure by selecting the structure of interest, right clicking on it, clicking analysis, and clicking “exact mass”

F9.2 Analyze data using MassHunter Qualitative Analysis B.07.00

F9.2.1 Extract “Mass Spectrum” from data collected (data file looks similar to an unretained chromatographic peak)

F9.2.2 Extract “Background Spectrum” from data collected (extract from the baseline, not the unretained chromatographic peak)

F9.2.3 Subtract “background spectrum” from “extracted mass spectrum”

F9.2.4 Search for the predicted masses (found following the steps in section 9.1)

F9.2.5 Use the Agilent isotope distribution calculator to aid in the positive identification of the degradation products. The isotope distribution calculator allows for calculations that include negative and positive charging of the ion of interest. Additionally, different types of adducts, including H^+ , Li^+ , Na^+ , K^+ , NH_4^+ , Cl^- , Br^- , $HCOO^-$ and CH_3COO^- can be accounted for in the calculations

F10. Data Reporting

F10.1 Export data as csv file

F10.2 Use Origin or Igor to plot data files

F10.3 Appropriately label peaks of interest

F10.4 Submit data to interested parties/publications

APPENDIX F – REFERENCES

- (1) Lutzke, A.; Tapia, J. B.; Neufeld, M. J.; Reynolds, M. M. Sustained Nitric Oxide Release from a Tertiary S-Nitrosothiol-Based Polyphosphazene Coating. *ACS Appl. Mater. Interfaces* **2017**, 9 (3), 2104–2113.

APPENDIX G

Polyesters MS and LC-MS Analysis SOP (Chapter 4)^{1,2}

G1. Purpose

A direct flow injection and a LC-MS chromatographic separation with an LC-MS system is used for the identification of products from hydrolytic degradation of polyester polymers.

G2. Scope

This test method provides instructions for the preparation and analysis of degradation products from the incubation of polyester polymers.

G3. Responsibility

To be performed by personnel who are technically qualified and trained in the use of the LC-MS and associated techniques.

G4. Safety

The samples and reagents used in this procedure should be handled using good laboratory practices. Wear gloves and work in a fume hood. Read the Safety Data Sheets for all chemicals used in this procedure.

G5. Abbreviations

CAS	Chemical Abstracts Service
ESI	Electrospray Ionization
LC-MS	Liquid Chromatography-Mass Spectrometry
MeOH	Methanol
MP	Mobile Phase
MW	Molecular Weight
NA	Not Applicable
POPs	Poly(phosphazenes)
RT	Room Temperature
TOF	Time-of-Flight

G6. Materials and Equipment

- G6.1 Agilent 1260 Infinity HPLC System
- G6.2 Agilent 6224 TOF Mass Spectrometer
- G6.3 Agilent dual ESI ion source
- G6.4 Analytical Column: Agilent Zorbax SB-C18, 150 × 4.6 mm, 3.5 μm, PN 863953-902
- G6.5 Guard Column Kit: Agilent Guard Column Hardware Kit, PN 820999-901
- G6.6 Guard Cartridge: Agilent Zorbax SB-C18, 12.5 × 4.6 mm, 5 μm, PN 820950-920
- G6.7 Analytical Balance: Ohaus Discovery DV215CD
- G6.8 1-mL Syringes
- G6.9 Agilent Captiva Econofilter PTFE 13-mm, 0.2-μm Syringe Filters, PN 5190-5265
- G6.10 Millipore Direct-Q Water Purification System
- G6.11 Aluminum Foil
- G6.12 20-mL Amber Vials
- G6.13 2-mL Agilent LC-MS Amber Vials
- G6.14 Incubator: Barnstead Lab-Line Max^Q 7000
- G6.15 100-mL volumetric flask
- G6.16 100-mL glass bottle
- G6.17 1000-mL volumetric flask
- G6.18 20-mL volumetric pipette
- G6.19 -20 °C freezer

G7. Reagents

- G7.1 Methanol, LC-MS grade, CAS# 67-18-6
- G7.2 Water, LC-MS grade, CAS# 7732-18-5
- G7.3 Polyester Polymer Samples, obtain from interested parties
- G7.4 Water, Millipore Direct-Q grade
- G7.5 Ammonium Acetate, CAS# 631-61-8

G8. Procedure

G8.1 Preparation of Mobile Phase

Note: The mobile phase solutions are stable for up to the expiration date of the reagent when no aqueous mobile phase is prepared when stored in glass bottles at room temperature. For aqueous mobile phases, 1% methanol is added to extend stability for 30 days.

G8.1.1 500 mM ammonium acetate stock (in 95:5 water/methanol)

G8.1.1.1 Weigh out 3.854 g ammonium acetate and quantitatively transfer to 100 mL volumetric flask

G8.1.1.2 Add approximately 50-mL of LC-MS water and dissolve the ammonium acetate

G8.1.1.3 Add 5-mL LC-MS methanol

G8.1.1.4 Dilute to 100-mL using LC-MS water and mix thoroughly

G8.1.1.5 Transfer to 100-mL glass bottle and store at 4 °C

G8.1.2 Mobile Phase A: 10 mM ammonium acetate in water

G8.1.2.1 Transfer 20-mL of ammonium acetate stock (500 mM, section 8.1.1) using a 20-mL volumetric pipette into a 1000-mL volumetric flask

G8.1.2.2 Transfer 10-mL of LC-MS methanol to the 1000-mL volumetric flask

G8.1.2.3 Dilute to 1000-mL using LC-MS water and mix thoroughly

G8.1.3 Mobile Phase B: 10 mM ammonium acetate in methanol

G8.1.3.1 Transfer 20-mL of ammonium acetate stock (500 mM, section G8.1.1) using a 20-mL volumetric pipette into a 1000-mL volumetric flask

G8.1.3.1 Dilute to 1000-mL using LC-MS methanol and mix thoroughly

G8.1.4 Transfer the desired volume of mobile phase to the appropriate LC-MS solvent reservoir(s). Appropriately update solvent volumes on the instrument if necessary

G8.2 Preparation of Incubation Samples

G8.2.1 Incubation Process

G8.2.1.1 Weigh out 100 mg of provided or synthesized POPs polymer and transfer into a 20-mL amber vial

G8.2.1.2 Add 20-mL of Millipore water and seal the vial

G8.2.1.3 Cover vial with aluminum foil to protect samples from exposure to light

G8.2.1.4 Incubate samples (minimum of three samples, repeat steps G8.2.1.1 – G8.2.1.3 as needed) at 37 °C for the desired length of time

G8.2.2 Weekly Sampling

G8.2.2.1 Remove vials from incubator

G8.2.2.2 Allow vials to reach RT

G8.2.2.3 Obtain a 1-mL sample aliquot using a 1-mL syringe

G8.2.2.4 Filter sample through an Agilent 0.2- μ m filter into an Agilent 2-mL LC-MS vial and seal the vial

G8.2.2.5 Appropriately dispose of the remaining incubation media

G8.2.2.6 Rinse polyester polymer sample with Millipore water

G8.2.2.7 Add the rinsed polyester sample to a clean 20-mL amber vial and repeat steps G8.2.1.2 – G8.2.1.4

G8.2.2.8 Samples to be analyzed by LC-MS at a later timeframe should be stored in the 20-mL vials amber vials or 2-mL LC-MS amber vials at -20 °C

G8.2.3 Single Sampling (1-week or up to 10-week single sampling)

Follow steps G8.2.2.1 – G8.2.2.5

G8.3 Analysis Method

Follow Table G.1 for instrument method conditions. **See appendix H for appropriate instrument setup and use.**

G8.3.1 Direct flow injection MS analysis

G8.3.1.1 For direct flow injection MS analysis, make sure to bypass the HPLC column

G8.3.1.2 Inject reagent blank

G8.3.1.3 Inject each sample in triplicate

G8.3.1.4 Load next sample sequence if needed or:

G8.3.1.5 Repeat G8.3.1

G8.3.1.6 Put instrument on Stand-by

G8.3.2 LC-MS analysis

G8.3.2.1 For LC-MS analysis, make sure the flow is set to go through the column

G8.3.2.2 Follow steps in sections G8.3.1.2 – G8.3.1.5 as needed

G8.3.2.3 To remove any leftover mobile phase additives, flush column at end of worklist/sequence by switching mobile phase to water and methanol only (no ammonium formate).

G8.3.2.4 Flush column with a high water percentage. Up to 95% water is acceptable depending on column specifications. For long term storage, at least 30 column volumes is recommended.

G8.3.2.5 In a linear gradient with an increase in methanol concentration, slowly (less than 5%/min increase) get the column to 100% methanol. For long term storage, at least 30 column volumes is recommended.

Table G.1 LC-MS Method Parameters

HPLC Settings				
Column Type		Zorbax SB-C18, 150 × 4.6 mm, 3.5 μm		
Guard Column		Zorbax SB-C18, 13 × 4.6 mm, 5 μm		
Column Temperature		40 °C		
Sample Tray Temperature		RT		
Injection Volume		0.1 μL (direct MS injection)		
		20 μL (LC-MS injection)		
Needle Wash		Methanol in Rinse Vial, Position 1		
Flow Rate		0.20 mL/min (direct MS injection)		
		0.25 mL/min (LC-MS injection)		
Stop Time		2 min (direct MS injection)		
		35 min (LC-MS injection, data collection ends)		
Post Time		15 min (LC-MS injection, data not collected)		
Method Type		Isocratic Direct Injection		
		Gradient LC-MS Injection		
MP B		Methanol (Isocratic, direct MS injection)		
MP A		10 mM ammonium acetate in water (Gradient)		
MP B		10 mM ammonium acetate in methanol (Gradient)		
Isocratic Injection			MS Settings	
Time, min	MPA, %	MPB, %	Ion Source	Dual ESI
0	0	100	Capillary Voltage	4000 V
2	0	100	Fragmentor Voltage	120 V
End Analysis			Skimmer Voltage	60 V
Gradient Injection			Drying Gas Flow Rate	10 l/min (N ₂)
Time, min	MPA, %	MPB, %	Drying Gas Temperature	310 °C (N ₂)
0	85	15	Nebulizer Pressure	25 psi
30	0	100		
40	0	100		
50	85	15		
Column Re-equilibration				

G9. Data Analysis

G9.1 Perform the necessary MW calculations for the predicted degradation products

G9.1.1 Use ChemDraw to draw the predicted structures based on the mode of degradation (hydrolytic degradation in this case)

G9.1.2 In ChemDraw, obtain the formula of the structure by selecting the structure of interest, right clicking on it, clicking analysis, and clicking “chemical formula”

G9.1.3 In ChemDraw, obtain the exact mass of the structure by selecting the structure of interest, right clicking on it, clicking analysis, and clicking “exact mass”

G9.2 Analyze data using MassHunter Qualitative Analysis B.07.00

G9.2.1 Analysis of direct injection MS data files

G9.2.1.1 Extract “Mass Spectrum” from data collected (data file looks similar to an unretained chromatographic peak)

G9.2.1.2 Extract “Background Spectrum” from data collected (extract from the baseline, not the unretained chromatographic peak)

G9.2.1.3 Subtract “background spectrum” from “extracted mass spectrum”

G9.2.1.4 Search for the predicted masses (found following the steps in section 9.1)

G9.2.1.5 Use the Agilent isotope distribution calculator to aid in the positive identification of the degradation products. The isotope distribution calculator allows for calculations that include negative and positive charging of the ion of interest. Additionally, different types of adducts, including H^+ , Li^+ , Na^+ , K^+ , NH_4^+ , Cl^- , Br^- , $HCOO^-$ and CH_3COO^- can be accounted for in the calculations

G9.2.2 Analysis of LC-MS data files

G9.2.2.1 Subtract blank chromatogram from sample chromatogram

G9.2.2.2 Extract “Mass Spectrum” from each chromatographic peak of interest

G9.2.2.3 Follow steps G9.2.1.4 – G9.2.1.5 to make peak assignments

G10. Data Reporting

G10.1 Export data as csv file

G10.2 Use Origin or Igor to plot data files

G10.3 Appropriately label peaks of interest

G10.4 Submit data to interested parties/publications

APPENDIX G – REFERENCES

- (1) Yapor, J. P.; Neufeld, B. H.; Tapia, J. B.; Reynolds, M. M. Biodegradable Crosslinked Polyesters Derived from Thiomalic Acid and S-Nitrosothiol Analogues for Nitric Oxide Release. *J. Mater. Chem. B* **2018**, *6* (24), 4071–4081.
- (2) Tapia, J. B.; Haines, J.; Yapor, J. P.; Reynolds, M. M. Identification of the Degradation Products of a Crosslinked Polyester Using LC-MS. *Polym. Degrad. Stab.* **2019**, *168*, 108948.

APPENDIX H

M-TOF Standard Operating Procedure for FLOW INJECTIONS ONLY¹

Username: Obtain from TMBR group after training

Password: Obtain from TMBR group after training

Part 1: Sample Preparation

1. Try to dissolve your analyte in methanol, ethanol, n-propanol, iso-propanol, acetonitrile, water or a mixture of this solvents that dissolves your sample (for example: 1:1 methanol/water; 1:1 acetonitrile/water; etc.).
2. It is acceptable to dissolve your analyte in mixtures that contain very small amounts of chlorinated solvents (<10% DCM, CHCl₃) and <10% DMSO. **Do not use normal phase solvents** such as hexanes, cyclohexanes, heptanes, THF, DMF, etc.
3. After your sample is prepared, filter through a 0.2- μ m filter before you perform your analysis.
4. **Sample concentration should not exceed 1.0 mg/mL!!**

Part 2: System Checks

1. Check solvent reservoirs to make sure the system will not run dry. The main solvent is usually 100% LC-MS methanol in line/bottle B1.
2. Check the rinse vial solvent level. Vial 1 should be filled up if needed with LC-MS methanol/water (~1:1). This may be changed to any solvent that will more appropriately dissolve your analyte and any potential residues (acetonitrile, acetonitrile/water, isopropanol, isopropanol/water, etc).
3. Agilent MassHunter Workstation Data Acquisition must be open after you log in (Figures H.1 & H.2). If it's not, get the mass spectrometry expert from the Reynolds group to check for any potential problems and/or an unwanted computer restart, log out or accidental shutdown.
4. **Make sure that the Tuning Mix bottle (bottle B on the TOF, door on bottom left corner) has enough tuning solution. Otherwise the instrument will not calibrate properly!**



Figure H.1 Data acquisition icon. Should always be open, if it's not please do not proceed!

¹ This SOP is not (designed) to help you run LC-MS analyses. Use only for direct flow injection MS analyses!

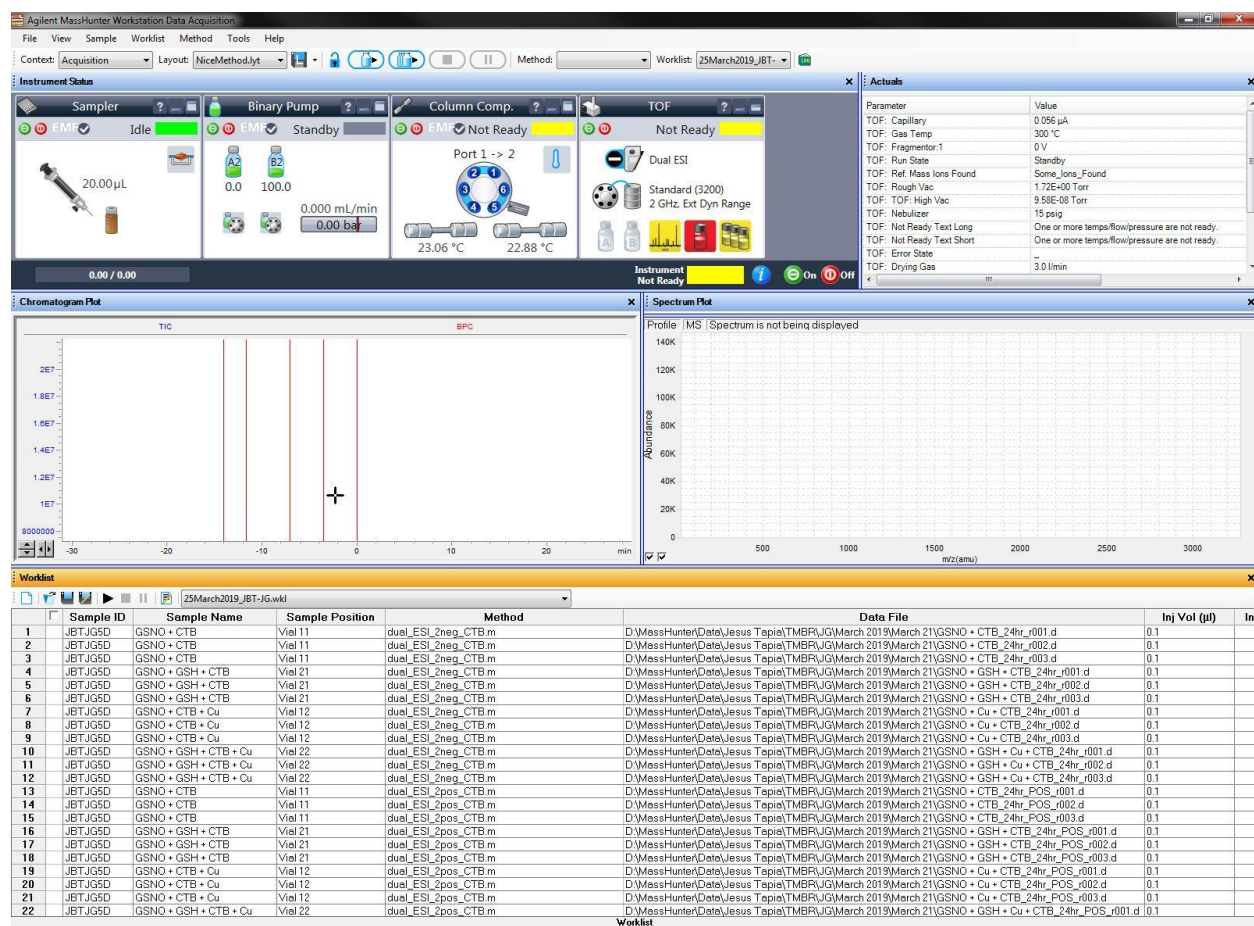


Figure H.2 Data Acquisition software. Again, this software window must already be open before you proceed!

- On the Data Acquisition software, check current vacuum readings (Figure H.3). The normal readings for Rough Vac are $1.xx \times 10^0$ Torr, this can fluctuate due to room temperature and depending on the last Rough Vac check. The normal readings for High Vac should be between $8.xx \times 10^{-8}$ and $2.xx \times 10^{-7}$ Torr. If the High Vac is reading higher than $9.xx \times 10^{-7}$ please let the mass spectrometry expert from the Reynolds group know because some major issues regarding the vacuum systems may be taking place.
- On the Data Acquisition software, once you have checked and/or filled your solvent levels (step 1 from Part 2: System Checks) change to the current levels so that the system does not stop your analyses (Figure H.4). Do this by right clicking on the solvent bottles and selecting Bottle Fillings... This will open the Bottle Fillings screen when you will be able to change the values as needed. Once any changes are made simply click Ok to close the window.

Parameter	Value
TOF: Capillary	0.056 μ A
TOF: Gas Temp	300 $^{\circ}$ C
TOF: Fragmentor:1	0 V
TOF: Run State	Standby
TOF: Ref. Mass Ions Found	Some Ions Found
TOF: Rough Vac	1.72E+00 Torr
TOF: TOF: High Vac	9.13E-08 Torr
TOF: Nebulizer	15 psig
TOF: Not Ready Text Long	One or more temps/flow/pressure are not ready.
TOF: Not Ready Text Short	One or more temps/flow/pressure are not ready.
TOF: Error State	-
TOF: Drying Gas	3.0 l/min

Figure H.3 Vacuum readings. Make sure the Rough Vac reads 1.xxE+00 Torr and the High Vac reads anywhere between 8.xxE-08 and 2.xxE-07 Torr.

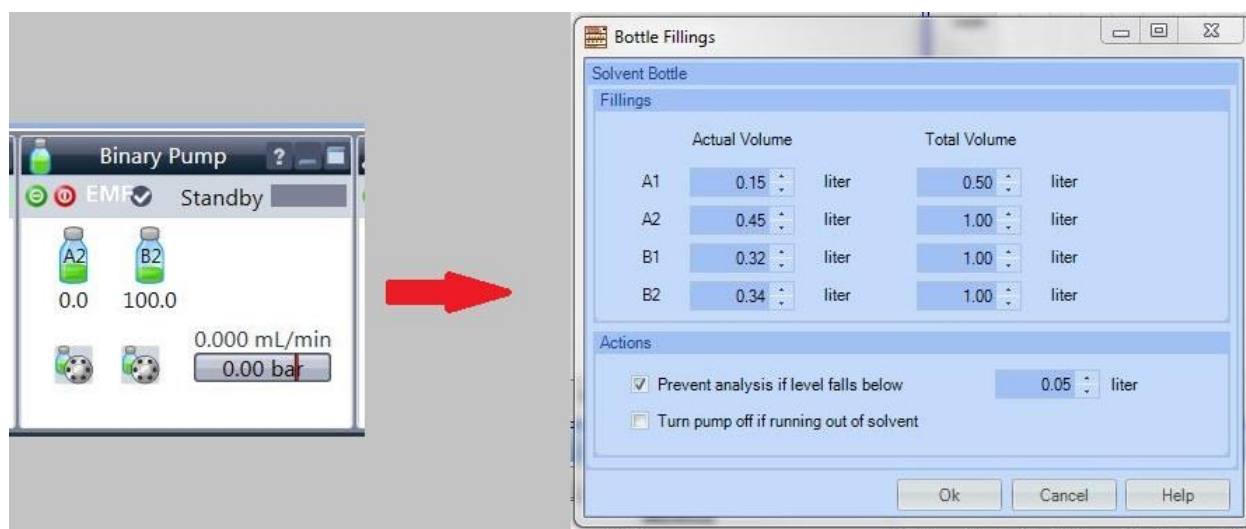


Figure H.4 Solvent levels window and changes.

- At this point, if all the system checks pass, you are ready to start the instrument to set up your runs.

Part 3: System Setup

A. System Startup and Calibration

1. Turn the system on by clicking the main power switch on the Data Acquisition software (Figure H.5). This power switch will turn on or off all the instrument components and set them ready to the last loaded/used acquisition method.



Figure H.5 Main power buttons. This power buttons will start or turn off all the instrument components and get them ready to the last loaded method (Sampler, Binary Pump, Column Comp. and the TOF).

2. Once the system is turned on, the Chromatogram Plot and Spectrum Plot windows will begin showing “data” as shown in Figure H.6. **If either window does not show any real time data, the software has glitched out and must be restarted.** Ask the mass spectrometry expert from the Reynolds group to perform a software restart because it is a multi-step process that requires a full software shutdown and startup.

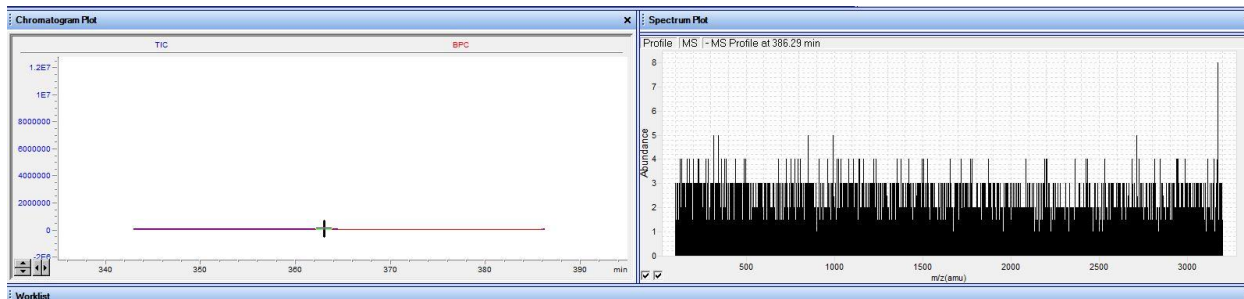


Figure H.6 Real time data. Make sure both windows have data being shown in real time. If either window stays blank, do not proceed, a full software restart is required.

3. Once the instrument is turned on, and data is being shown in real time, find the Context menu (Figure H.7). **It should read Context: Acquisition.** Click on the drop down menu

and select Tune. After changing to Tune, a new window will show up to Tune the instrument (Figure H.8).

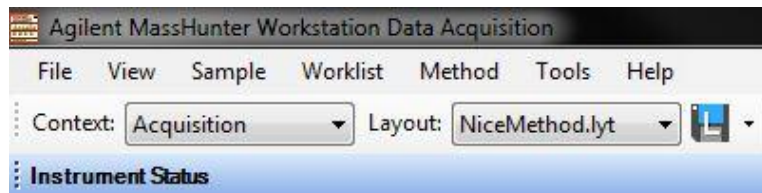


Figure H.7 Context menu.

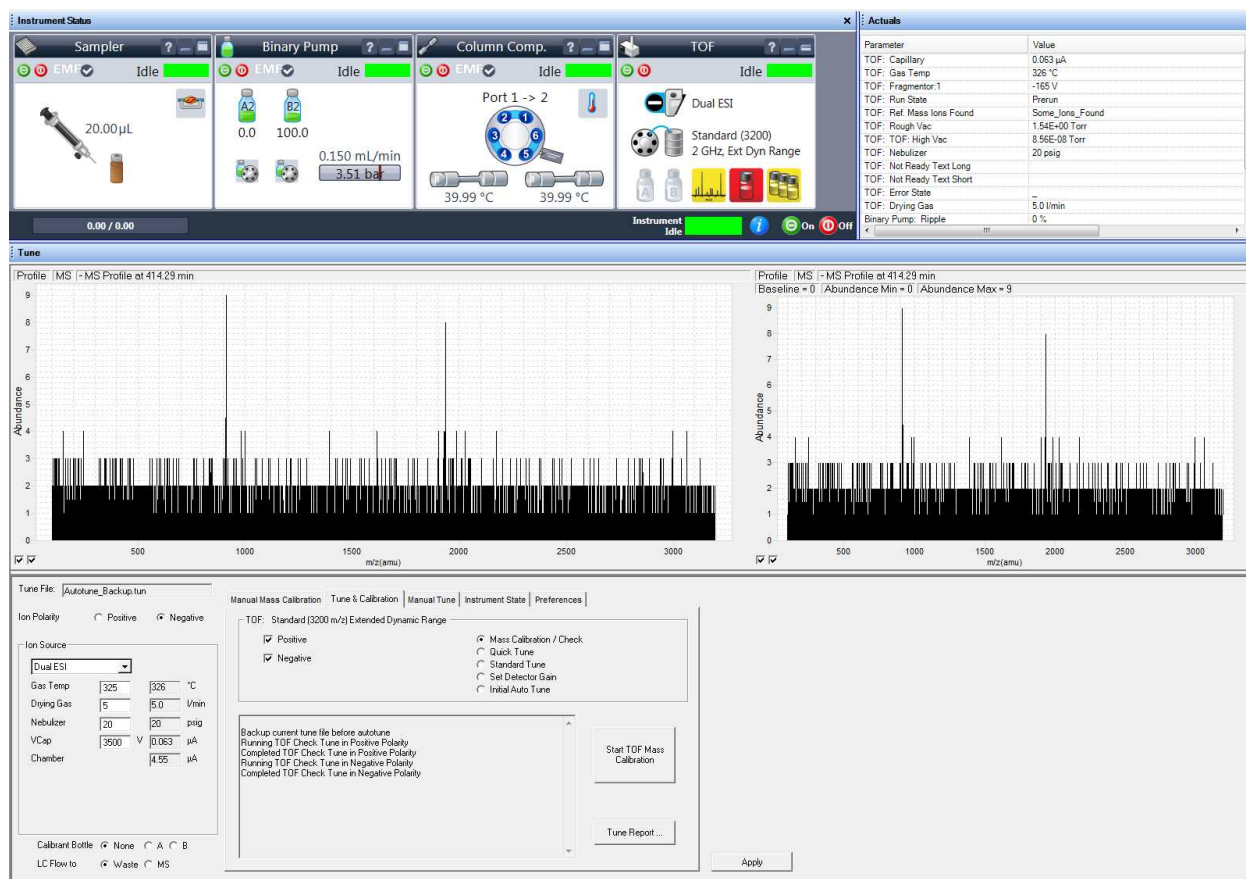


Figure H.8 Window that shows the Tune/Calibration contexts.

4. In the Tune context, under the tab labeled **Tune & Calibration** select both negative and positive with Mass Calibration/Check selected. Once all three are selected, click the Start TOF Mass Calibration button (Figure H.9).
5. Once “Start TOF Mass Calibration” is clicked, you will be asked if you are sure you want to tune the instrument (Figure H.10). Click yes to proceed. After you click yes, the instrument will proceed to be calibrated. A series of ions will show up that encompass the entire range of the mass spectrometer. Calibration will first take place in positive mode and then in negative mode. The process will take approximately 5 minutes.

6. Once calibration is complete, two PDF documents will show up with the details of the calibration.
7. Now that calibration is done, change the context back to Acquisition (top left corner, Figure H.7). **Two questions will pop up (Figure H.10). The first one will ask if you'd like to Proceed to Acquisition Context. Click Yes. The second one will ask if you'd like to save changes to your Tune file. Click No.** This will send you back to the original Data Acquisition windows. Now ready to collect data!

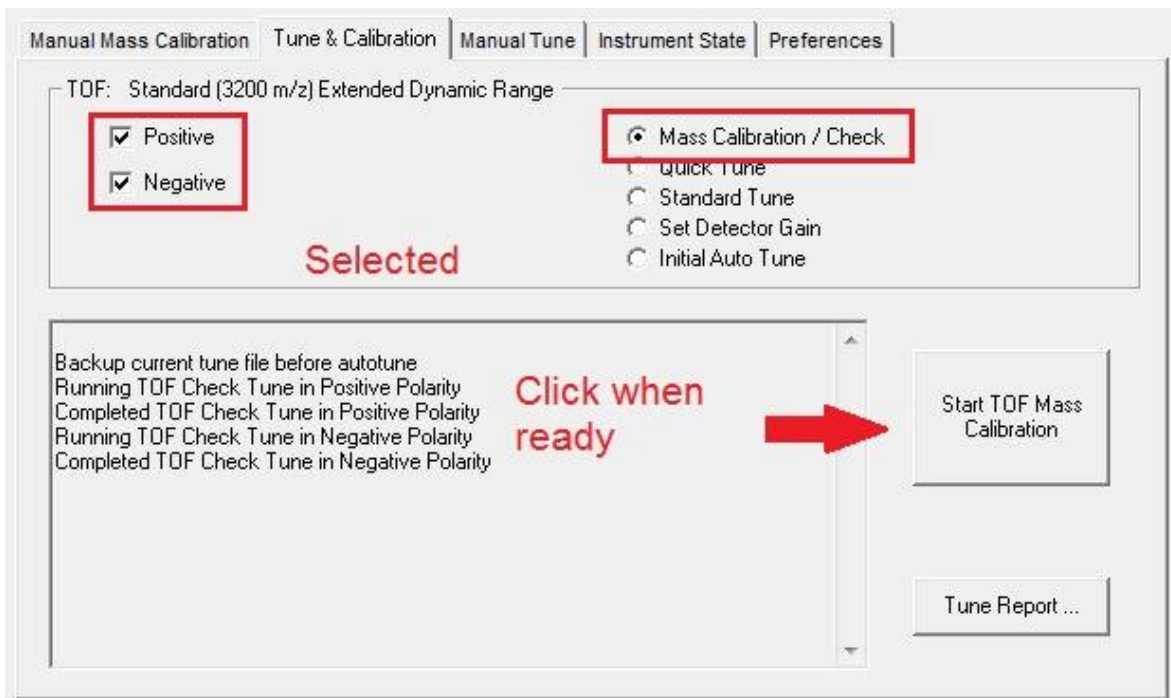


Figure H.9 Select Positive and Negative, and Mass Calibration/Check. Then click “Start TOF Mass Calibration” to begin the calibration process.

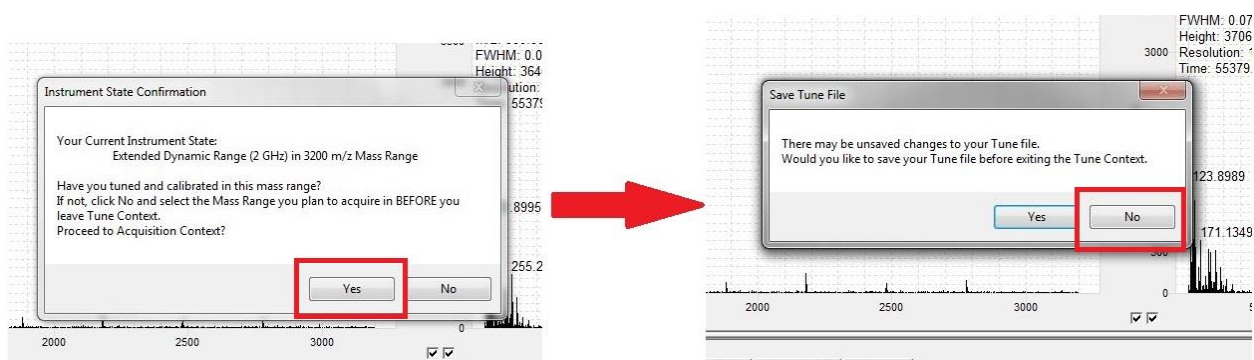


Figure H.10 Tune context exit. Once the calibration process is done and the two PDF reports are shown, exit the Tune context by going back to Acquisition. You will be asked if you want to **proceed to Acquisition Context? click Yes.** Then you will be asked if you want to **save changes to Tune file? click No.**

B. Worklist Setup

1. To set up a worklist, make sure the worklist tab is selected in the bottom left menu (Figure H.11). This will open a spreadsheet where you will be able to write a worklist to run your samples.

First fill out Sample ID, this can be your initials, your eID, etc.

Then fill out Sample Name, this is the name of your sample.

Then select the position of your sample vial, it can be anywhere from vial 2 to vial 100. **Do not use position 1 since it is the needle rinse vial. Make sure your samples are in the correctly labeled vial positions, otherwise the instrument will give you an error!**

Then select a method, this method should be developed for your sample needs with the help from the mass spectrometry expert from the Reynolds group.

Then write where the data file will be saved. There should already be a folder with your name under a folder with your PI's name. Ask the mass spectrometry expert from the Reynolds group if you need assistance with this step.

And finally choose an injection volume. **For concentrations at 1.0 mg/mL a direct injection should not require more than 0.1 μ L.** However, if your ion counts are very low, you may increase the injection volume to up to 1.0 μ L.

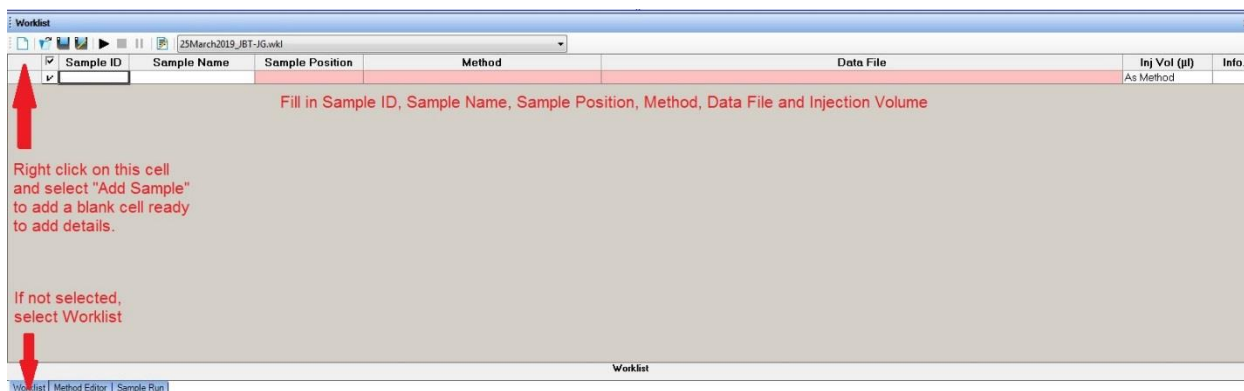


Figure H.11 Worklist setup. Fill in Sample ID, Sample Name, Sample Position, Method, Data File and Injection Volume. Add samples as needed.

2. Once you have a worklist that looks like the one in Figure H.12, you can click the “play” button after you have selected your samples. This will have the instrument begin collecting data. Make sure to save your worklist so that you can access it in the future! The recommended format is “date_initials_PI Initials”.
3. If you realize you have made a mistake, click the stop button found above the “Column Comp.” window. This will stop the current run and the consecutive selected samples.

Once you restart the worklist, you may be asked if you want to override the data files, it is up to you if you wish to do so.

	Sample ID	Sample Name	Sample Position	Method	Data File	Inj Vol (µl)	Inf
1	<input checked="" type="checkbox"/> JBTJG5D	GSNO + CTB	Vial 11	dual_ESI_2neg_CTB.m	D:\MassHunter\Data\Jesus Tepiel\TMBR\JG\March 2019\March 25\GSNO + CTB_5day_r001.d	0.1	
2	<input checked="" type="checkbox"/> JBTJG5D	GSNO + CTB	Vial 11	dual_ESI_2neg_CTB.m	D:\MassHunter\Data\Jesus Tepiel\TMBR\JG\March 2019\March 25\GSNO + CTB_5day_r002.d	0.1	
3	<input checked="" type="checkbox"/> JBTJG5D	GSNO + CTB	Vial 11	dual_ESI_2neg_CTB.m	D:\MassHunter\Data\Jesus Tepiel\TMBR\JG\March 2019\March 25\GSNO + CTB_5day_r003.d	0.1	
4	<input checked="" type="checkbox"/> JBTJG5D	GSNO + GSH + CTB	Vial 21	dual_ESI_2neg_CTB.m	D:\MassHunter\Data\Jesus Tepiel\TMBR\JG\March 2019\March 25\GSNO + GSH + CTB_5day_r001.d	0.1	
5	<input checked="" type="checkbox"/> JBTJG5D	GSNO + GSH + CTB	Vial 21	dual_ESI_2neg_CTB.m	D:\MassHunter\Data\Jesus Tepiel\TMBR\JG\March 2019\March 25\GSNO + GSH + CTB_5day_r002.d	0.1	
6	<input checked="" type="checkbox"/> JBTJG5D	GSNO + GSH + CTB	Vial 21	dual_ESI_2neg_CTB.m	D:\MassHunter\Data\Jesus Tepiel\TMBR\JG\March 2019\March 25\GSNO + GSH + CTB_5day_r003.d	0.1	
7	<input checked="" type="checkbox"/> JBTJG5D	GSNO + CTB	Vial 11	dual_ESI_2pos_CTB.m	D:\MassHunter\Data\Jesus Tepiel\TMBR\JG\March 2019\March 25\GSNO + CTB_5day_POS_r001.d	0.1	
8	<input checked="" type="checkbox"/> JBTJG5D	GSNO + CTB	Vial 11	dual_ESI_2pos_CTB.m	D:\MassHunter\Data\Jesus Tepiel\TMBR\JG\March 2019\March 25\GSNO + CTB_5day_POS_r002.d	0.1	
9	<input checked="" type="checkbox"/> JBTJG5D	GSNO + CTB	Vial 11	dual_ESI_2pos_CTB.m	D:\MassHunter\Data\Jesus Tepiel\TMBR\JG\March 2019\March 25\GSNO + CTB_5day_POS_r003.d	0.1	
10	<input checked="" type="checkbox"/> JBTJG5D	GSNO + GSH + CTB	Vial 21	dual_ESI_2pos_CTB.m	D:\MassHunter\Data\Jesus Tepiel\TMBR\JG\March 2019\March 25\GSNO + GSH + CTB_5day_POS_r001.d	0.1	
11	<input checked="" type="checkbox"/> JBTJG5D	GSNO + GSH + CTB	Vial 21	dual_ESI_2pos_CTB.m	D:\MassHunter\Data\Jesus Tepiel\TMBR\JG\March 2019\March 25\GSNO + GSH + CTB_5day_POS_r002.d	0.1	
12	<input checked="" type="checkbox"/> JBTJG5D	GSNO + GSH + CTB	Vial 21	dual_ESI_2pos_CTB.m	D:\MassHunter\Data\Jesus Tepiel\TMBR\JG\March 2019\March 25\GSNO + GSH + CTB_5day_POS_r003.d	0.1	

Figure H.12 Typical worklist. All the selected samples will be ran when you press play. Make sure to check your sample position, method and data file closely to avoid any instrument errors.

- Once all your samples are ran, a window will pop up that says “Worklist Run Complete” At this point, your all the analytes that were selected have been successfully ran.
- You can add more samples and have the instrument run them if you have more to run. Otherwise, using the main power switch, press “off” to put the instrument in standby.
- DO NOT CLOSE THE DATA ACQUISITION SOFTWARE! IT IS MEANT TO STAY OPEN! IF YOU CLOSE IT BY ACCIDENT, PLEASE LET JESUS T. OR CHRIS A. KNOW SO THAT THEY CAN DO A PROPER SOFTWARE RESTART.**
- For data analysis, please refer to the “M-TOF standard operating procedure for data analysis using MassHunter Qualitative Analysis”

C. Instrument Standby

- Once your samples are done running, to put the instrument on Standby, click the “off” button on the “Main Power Switch” shown in Figure H.5. This will put the instrument on standby mode and you can lock the computer and be done.
- DO NOT SHUT THE COMPUTER OFF**
- DO NOT LOG OFF USER**
- DO NOT SWITCH ACCOUNT**
- ONLY LOCK THE COMPUTER!!**